DILUTE SOLUTION STUDIES OF MOLECULAR WEIGHT DISTRIBUTIONS OF NITROCELLULOSE, MODIFIED LIGNINS AND PMMA GRAFT POLYMERS

by

Emilie J. Siochi

Dissertation submitted to the Faculty of the
Virginia Polytechnic Institute and State University
in partial fulfillment of the requirements for the degree of

DOCTOR OF PHILOSOPHY

in

Materials Engineering Science

APPROVED:

Thomas C. Ward, Chairman

James E. McGrath

Garth L. Wilkes

George Sanzone

James P. Wightman

April, 1989

Blacksburg, Virginia

DILUTE SOLUTION STUDIES OF MOLECULAR WEIGHT DISTRIBUTIONS OF NITROCELLULOSE, MODIFIED LIGNINS AND PMMA GRAFT POLYMERS

by

Emilie J. Siochi

Committee Chairman: Dr. Thomas C. Ward
Materials Engineering Science

(ABSTRACT)

Dilute solution properties of three difficult-to-analyze macromolecular systems were investigated and clarified. Two were notorious for having highly time-in-solution dependent properties, nitrocellulose and lignin, while the third was an ideal model branched methacrylate polymer with which to examine unanswered questions in polymer hydrodynamic behavior.

Gel permeation chromatography with a differential viscosity detector (GPC/DV) was employed to study the dilute solution properties of various polymers, specifically their absolute molecular weight distributions and hydrodynamic behavior. The study was divided into three parts.

The first part focussed on the time dependent change in molecular weight of nitrocellulose. Samples having 12.58% and 13.5% levels of nitration were investigated in THF and EtOAc. GPC/DV, LALLS, FT-IR and intrinsic viscosity experiments revealed that the materials existed as associated molecules in solution which decreased in molecular weight upon storage to extents dependent on the solvent.

The second part was an examination of the hydrodynamic behavior of hydroxypropylated lignins using GPC/LALLS/DV and VPO. These materials were found to increase in molecular weight upon storage in solution due to association. Special precautions had to be taken in running experiments to obtain the correct molecular weights and molecular weight distributions.

The last part involved a fundamental study of PMMA-g-PMMA's having similar molecular weights but containing different levels of branching. Variable temperature GPC/LALLS/DV was employed to obtain molecular weight distributions, branching parameters, average chain dimensions and information on the hydrodynamic behavior of these branched systems. Samples containing up to 40% of long chain branching were found to obey the universal calibration analytic scheme of GPC.

DEDICATION

To my parents, and

ACKNOWLEDGEMENTS

I would like to thank my advisor, Dr. Thomas C. Ward for his guidance, patience, encouragement and enthusiastic support in all phases of this work. It was a blessing to work for someone who understood my need to strike a balance between my work and my family. I had the privilege of learning not only of the complexities of polymer science under the wings of a brilliant man but also of the importance of keeping life's priorities straight at all times.

My thanks are also due to Dr. James E. McGrath and Dr. Garth L. Wilkes, who taught me about other aspects of polymer science which were vital to my work, to Dr. James P. Wightman, who as my Masters advisor gave me valuable lessons in problem solving which I employed in my Ph. D. work and to Dr. George Sanzone for sound advice on the improvement of my dissertation.

I am grateful to Hercules, Inc. who through the Radford Army and Ammunition Plant provided funding and samples for part of this work, to Dr. Wolfgang Glasser for supplying the lignins and to and who took the time to synthesize the model polymers used in the last phase of this work.

I would also like to thank all members of the PolyPchem group, both past and present for providing a stimulating research environment and for being a support network during the trials and tribulations of graduate life. Special thanks go to , who was my first teacher in the experimental side of GPC and to for reducing my instrument down time by sharing his expertise on electronics.

I am pleased to acknowledge the support of the PMIL secretarial staff for their friendship and help with paperwork whenever required.

I thank my daughter, , for helping me keep my perspective and my sanity, especially in the hectic final months of my graduate life. Finally, I thank my husband, , who has supported me in this work and put up with my crazy hours. His love and understanding provided stability in my otherwise roller coaster graduate experience. I could not have completed this work without him. Thank you, .

TABLE OF CONTENTS

LIST OF FIGURES

LIST OF TABLES

CHAPTER 1

INTRODUCTION

As Fujita observed (1):

> "It is misleading to consider that polymer behavior in dilute solutions has been worked out so thoroughly in the past decades that few problems of fundamental importance on this subject remain unsolved or unexplored."

This statement applies to polymers which have been around for a long time as well as the more novel systems having interesting chemical compositions and architectures. In the spirit of this observation, this work is a collection of findings in three areas dealing with different aspects of dilute solution theory. The dissertation is divided into three chapters which are united by the experimental techniques utilized which included conventional methods as well as state-of-the-art instrumentation -- GPC with multidetection capabilities.

In Chapter 2, extensive studies of the molecular weight distribution of nitrocellulose are presented. State-of-the-art GPC was used to explore a more than thirty five year old controversy involving time dependent changes in the solution properties of nitrocellulose.

In Chapter 3, the GPC/DV was applied to novel modified lignins having a three dimensional network structure. A special experimental procedure was required to obtain accurate results.

Finally, in Chapter 4, a fundamental study of some graft homopolymers was conducted to obtain molecular weight distributions, branching parameters, chain dimensions and hydrodynamic behavior information.

It is hoped that the sum of this work will make a meaningful contribution to the area of dilute solution properties of polymers by providing extremely precise experimental results.

REFERENCES

1. Fujita, H., Macromolecules, **21**, 179 (1988).

CHAPTER 2

THE ABSOLUTE MOLECULAR WEIGHT DISTRIBUTION OF NITROCELLULOSE

2.1. INTRODUCTION

Being one of the oldest known polymers, nitrocellulose has been the subject of study for over a century. It was initially used solely for military purposes; however, since the end of World War I, its usage has expanded into the fiber and coatings industries where it has been a mainstay to the present day (1,2). General interest in the molecular weight characterization of nitrocellulose may be classified into two categories. The first and more obvious reason for the relevance of this parameter is that the molecular weight and molecular weight distribution profoundly influence the properties of the product and affect the processability of the material. For instance, the molecular weight, (hence, the viscosity of this material) is one of the most important factors that need to be considered in the determination of non-volatile content in lacquers (2). The second reason is that it is a soluble derivative of cellulose, for which direct molecular weight determination is problematic due to solubility difficulties. Thus, nitrocellulose, barring degradation during nitration, has been utilized as a practical means of indirectly arriving at the molecular weight distribution of the starting cellulose. Very closely tied with this second interest is the focus on the conformation of nitrocelluloses with different degrees of substitution. This piece of information has been a major source of questions related to the methodology of calibration when gel permeation chromatography (GPC) was chosen for molecular weight determination.

In the above context then, the primary aim of this present work was to investigate means of obtaining absolute molecular weights for nitrocellulose by low angle laser light scattering (LALLS) and absolute molecular weight distribution by gel permeation chromatography with a differential viscosity detector (GPC/DV). The DV instrument operates to take advantage of Benoit's universal calibration concept. The results obtained from this fairly new technique shall be compared to those from the more conventional LALLS technique for absolute molecular weight determination.

In trying to do simple measurements of molecular weight determination, difficulty was encountered in data reproducibility over a period of days for the same sample. A closer look at this problem revealed that nitrocellulose systems were characterized by time dependent changes in properties such as molecular weights, molecular weight distributions, second virial coefficients and specific viscosities. Perusal of the nitrocellulose literature will show that this aging phenomenon had been observed as early as 40 years ago. However, no satisfactory mechanism to explain this seemingly anomalous behavior has been unanimously agreed upon by the cellulose community. In this work, the author will attempt to integrate the knowledge of conformation available in literature with results obtained in the absolute molecular weight determination of nitrocellulose. All these data will be discussed and a mechanism for the time dependent changes in the solution properties of nitrocellulose shall be proposed. It is hoped that this work will contribute to a clearer understanding of the solution behavior of nitrocelluloses, as well as clarify the controversy of the true mechanism for aging in nitrocellulose solutions.

2.2. LITERATURE REVIEW

2.2.1. Absolute Molecular Weight Determination of Nitrocellulose

The absolute molecular weight distribution of a polymer is one of the most important parameters which influences its physical properties. It is therefore understandable why the search for a convenient and rapid mode of characterizing this parameter for nitrocellulose (NC) has persisted as a matter of scientific investigation for many years. The two main methods that have been commonly employed were fractionation and more recently, gel permeation chromatography. The evolution of each method as applied to nitrocellulose will be reviewed below.

2.2.1.1. Fractionation

Two ways by which fractionation may furnish fractions in quantities suitable for characterization, as well as molecular weight distribution data on the whole polymer are fractional precipitation and fractional solution. Fractional precipitation is achieved by an incremental decrease in the system's solvent power. This may be accomplished by the addition of a nonsolvent (or precipitant), the elimination of solvent by

evaporation or the lowering of the temperature of the system (3). By this method, the highest molecular weight fraction is obtained first, with each succeeding fraction yielding progressively lower molecular weights. On the other hand, fractional solution involves extraction of fractions by utilizing a series of eluents with increasing solvent power, possibly on a column. Therefore, in contrast to fractional precipitation, the order of fractions obtained is of increasing molecular weight i. e. the lowest molecular weight fraction is obtained first and the highest molecular weight fraction, last (4).

The fractionation methods described above have been utilized in exploratory work done to demonstrate the inhomogeneity of chain lengths and to study the nature of the molecular weight distribution (MWD) curves that result from these procedures (5). A study reported compared results obtained from the two modes of fractionation. Typical curves for the fractionation of nitrated wood pulp are shown in Figure 2.1. Two observations may be noted. Solution and precipitation methods of separation produced characteristically different curves of MWD for the same sample. In the results for the nitrated wood pulp, for instance, fractional solution showed that the highest degree of polymerization was 1500, while the corresponding number by fractional precipitation was 2500. However, both approaches gave self-consistent results based on multiple experiments (6). These differences were obviously critical for the discrepancies meant that results of degree of polymerization determination were method dependent as opposed to sample dependent, which clearly should not be the case. The above data thus bring into question the reliability of the techniques. Which of the two methodologies supplies the correct information?

There appears to be no simple answer to this question since each method has accompanying problems. Fractional solution is difficult because it is influenced by the rate of solvent diffusion into the whole nitrocellulose film or fiber. Since solubility requires solvent diffusion into the sample and the diffusion of dissolved nitrocellulose chains from the inner layers of the solute into the solution, the whole range of chains that are theoretically soluble at a given fractionation step may not actually dissolve. The importance of the role of diffusion rate in the solution process is demonstrated by a difference in ease of solubility as a function of the physical nature of the pulp. This diffusion process is especially crucial in the first phase of

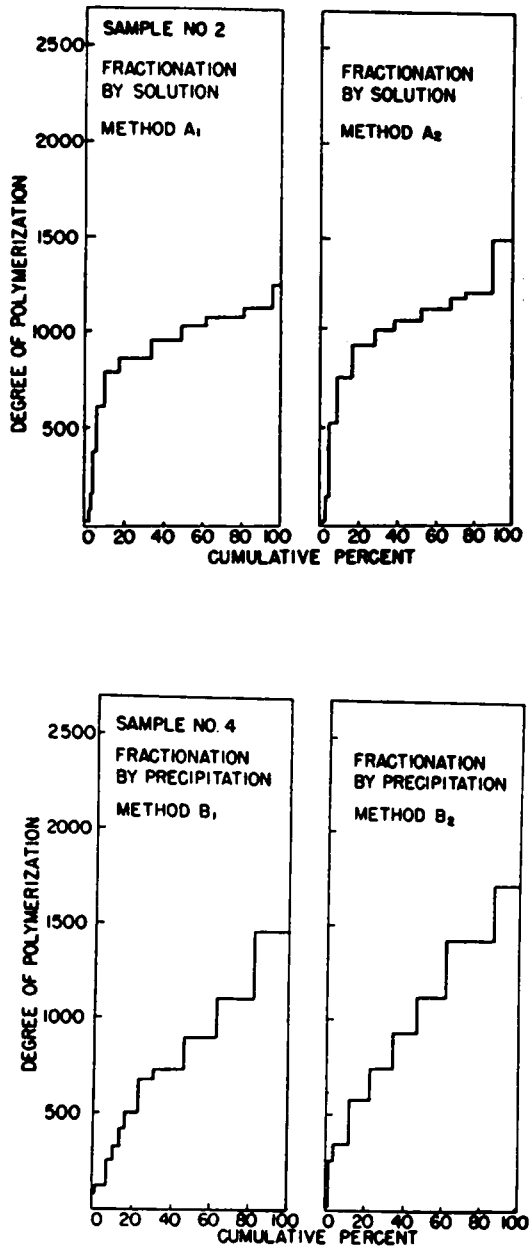

Figure 2.1: Comparison of multiple fractionations of a wood pulp made by the same method and the same worker (a) fractional solution (b) fractional precipitation (7).

the procedure from which the short chain fractions are obtained (7-9). On the other hand, fractional precipitation appears to be selective towards higher molecular weight materials; however, it does not completely precipitate these components from solution. As a result, some of these fragments remain in solution and precipitate with succeeding fractions. All the precipitated fractions therefore contain a certain amount of higher molecular weight species, resulting in the lower molecular weight fractions having increasingly broader polydispersities (10).

In addition to the problems cited above which are characteristic of each method, there are problems common to both techniques. Neither operation yields "clean" fractions (6). These fractionation procedures are time consuming, tedious and are subject to serious experimental errors in sample handling during the various steps involved (6, 11-13). Furthermore, the absolute molecular weight of each of these fractions has to be determined by some other conventional method such as light scattering and osmometry, in order to obtain the information for the MWD. Clearly, depending on the degree of resolution desired, it would take time of the order of a week or two to obtain the required information for each molecular weight distribution if this path were chosen.

Based on the literature in this area, where no alternative to fractionation was available, there appeared to be a preference for the precipitation technique. The complications encountered in the above ways of obtaining a parameter as critical as the MWD have no doubt generated interest in gel permeation chromatography as a means of determining molecular weight distributions. Gel permeation chromatography has the distinct advantage of being a dynamic, continuous method in which it is possible to obtain a chromatogram within a couple of hours (14). In spite of this advantage, the advent of this experiment has brought with it a different set of problems which will be dealt with in the next section.

2.2.1.2. Gel Permeation Chromatography (GPC)

Gel permeation chromatography separates molecules solely according to their effective size in solution, the hydrodynamic volume. It is a type of liquid/solid elution chromatography which typically utilizes columns packed with an inert crosslinked polymer gel. The packing is often made from polystyrene beads

that have been crosslinked. Permeability of the network is regulated by the amount and nature of the diluent used during the polymerization and crosslinking process. Fractionation is achieved by the injection of a dilute polymer solution into a continually flowing stream of solvent. This stream of solvent passes through the bed of highly porous, swollen particles. Typically, a bank of columns containing particles of different pore diameters are connected in series. As the solution flows over the packing bed, molecules having effective sizes smaller than the maximum pore size will penetrate through the gel and are separated. Smaller molecules will require more solvent to elute and will thus be retained longer. The larger molecules elute first because they do not enter as many pores and do not diffuse into them as deeply as the smaller molecules. Thus the separation is entropically driven. Materials having hydrodynamic volumes that are larger than the maximum pore size merely pass through the column in the interstitial volume and elute unfractionated (14-18).

As with any technique, this method has its limitations as well as advantages. Among the shortcomings are first, the amount of sample that may be introduced into the columns is limited because overloading results in a loss of resolution. Secondly, air must be kept out of the system because it creates channels in the columns, rendering them useless. Lastly, the operating temperature is limited to less than 150°C since the gel degrades at temperatures over 150°C. On the other hand, GPC offers several advantages as a fractionation method. Only small samples are required to yield molecular weight distribution information, the analysis time is fairly short, the system is flexible since it allows several different types of samples to be run on the same set of instrumentation, the results obtained from this method are reproducible and lastly, it is inexpensive since the gel is reusable (17,18).

In the application of GPC to nitrocellulose, the problems that surface can be classified as operational problems which are particular to nitrocellulose as far as practical data collection is concerned and as data processing problems. The latter involves the formulation of a method by which raw chromatographic data may be converted to meaningful information on the absolute MWD of the polymer and is the crucial step in the experiment.

2.2.1.2.1. Operational Problems

The two main operational problems in GPC of nitrocellulose involve the appropriate type of column packing and the choice of concentration sensitive detector. The two types of column packing commonly utilized are the Styragel® columns (which consist of crosslinked styrene-divinylbenzene) and passivated silica gel columns. Styragel® appears to be the column packing of choice. They exhibit separation capabilities for molecular weights of nitrocellulose with a degree of polymerization up to 5000, if appropriate experimental conditions were applied (13,19-21). Due to some concern about adsorption of nitrocellulose on the packing, Marx-Figini has tried passivated silica gel columns. No significant advantage was gained by exercising this option (22). In fact, this concern appears unwarranted since Meyerhoff found that clear calibration data could be obtained with Styragel® columns such that comparisons may be made among elution behavior of polystyrene, poly(methylmethacrylate) and nitrocellulose. This is demonstrated in Figure 2.2 where the length of fully extended chain conformation in Angstrom units is plotted against elution volume (19,23).

The second problem in using GPC to analyze cellulose nitrate involves the detector. The two common options are the differential refractive index detector (DRI) and the ultraviolet (UV) detector. Each has its own advantages as well as disadvantages. The solvent that is most commonly employed in nitrocellulose GPC experiments is tetrahydrofuran (THF) because it is compatible with Styragel® column packing and it is a good solvent for nitrocellulose. However, the difference in refractive index between THF and nitrocellulose is of the order of 0.048, making it difficult to use a differential refractive index detector since very high detector stability is required at the maximum sensitivity in order to clearly define the baseline of the chromatogram (13,21). This is an important consideration because the choice of where the chromatogram begins and ends can drastically change the molecular weights determined, especially at the high molecular weight end of the chromatogram. Instead of maximizing sensitivity which is accompanied by higher baseline noise, one can optimize the concentration so that it is high enough to yield a satisfactory signal to noise ratio and yet low enough to avoid undesired effects such as "viscous fingering" and a

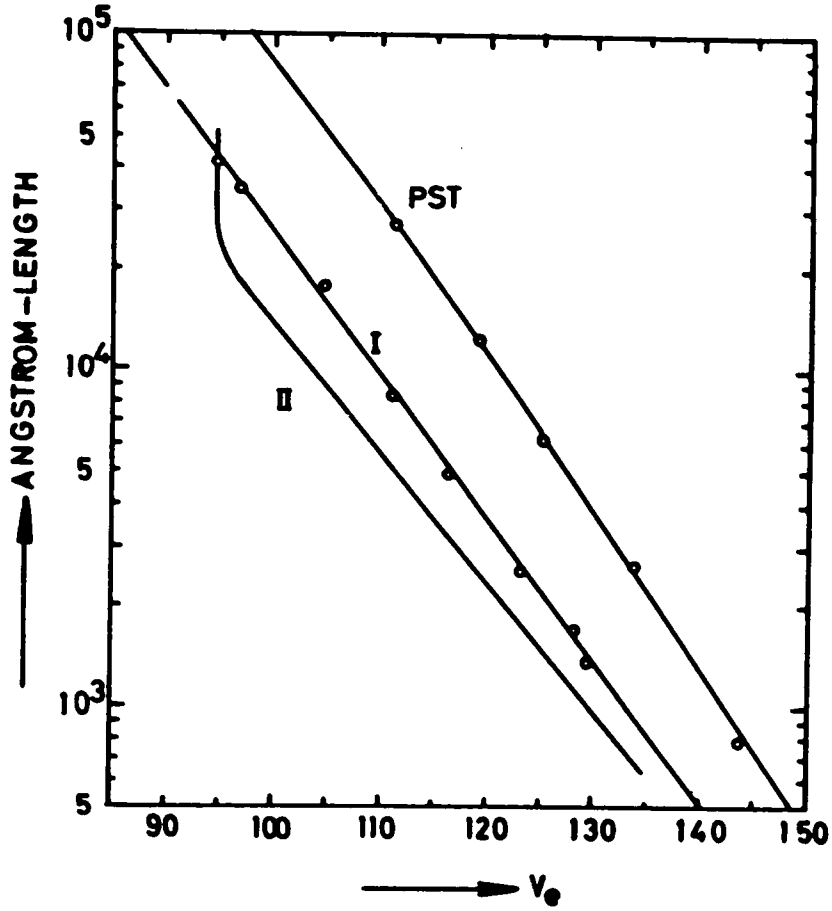

Figure 2.2: Calibration curves generated by nitrocellulose (I & II) and polystyrene (PST) on Styragel columns (22).

dangerous increase in pressure (22). Alternatively, some investigators have utilized an ultraviolet detector. This detector changes absorbance as a function of sample concentration ***and*** the degree of substitution. For it to operate effectively as a concentration sensitive detector thus requires that the sample ran on the chromatograph have a controlled and uniform degree of substitution . This requirement is met only under stringent nitrating conditions which may not be achieved at all times (13,22) .

In summary, most investigators appear to prefer the combination of Styragel® columns and a differential refractive index detector in their work in spite of the electronic difficulties that accompany this decision.

2.2.1.2.2. Calibration Problems

A most important problem in the use of GPC for nitrocellulose characterization is the question of converting the raw data from the chromatogram into meaningful information on absolute molecular weight and MWD (or as many researchers appear to favor -- degree of polymerization and chain length distribution respectively.) The dilemma is twofold. First, applying GPC to nitrocellulose is not a trivial problem because raw chromatographic data are generally converted to molecular weights and MWD by using a calibration curve generated from narrow distribution polymers having well characterized molecular weights. However, narrow MWD nitrocellulose standards are not readily available (24). In order to circumvent this difficulty, several methods were devised in the search for a universal GPC calibration parameter. This led to the second predicament: there was some controversy about what the universal parameter is for the separation mechanism in GPC. The evolution of the understanding of these problems and their solutions shall be detailed below.

2.2.1.2.2.1. Calibration by Molecular Weight

The simplest method of calibration is to generate a plot of molecular weight versus elution volume for standards of well characterized molecular weights. This method assumes that fractions that elute at the same retention volume as the standard have the same molecular weight. Calibration standards that have been used for this purpose may be classified into narrow MWD standards and broad MWD standards.

Narrow distribution standards are the specimens of choice. For nitrocellulose, these are not commercially available and individual researchers resorted to fractionating whole nitrocellulose polymers to provide the required narrow distribution materials. However, fractionation has complications as already mentioned. In addition to those problems, the fractions obtained have been in such small quantities that it was difficult to have sufficient material for molecular weight characterization as well as for use as calibration standards. Preparative scale GPC offers an alternative method of fractionation to obtain narrow distribution standards; however, this operation is tedious because the fractions have to be pooled from several experiments (20,26,27). Because narrow distribution nitrocellulose standards are generally unavailable, several groups have tried to use the more easily accessible polystyrene and poly(methyl methacrylate) standards. However, this practice has not given acceptable results because nitrocellulose molecules are more extended in solution than either of the standards (27). Due to the greater extension of cellulose nitrate chains, the intrinsic viscosity of a cellulosic sample of the same molecular weight as that of a randomly coiled polymer standard would be higher. This results in the switching of calibration curves generated by nitrocellulose and PMMA when passing from molecular weight to intrinsic viscosity as shown in Figure 2.3 (11,19).

Considering that obtaining narrow distribution standards is tedious and laborious, acid hydrolysis and other forms of degradation have been used to obtain broad distribution nitrocellulose standards (26). In fact, several ways have been devised to utilize more easily obtainable broad distribution nitrocellulose fractions as standards.

A method applicable to NC was developed by Cantow et al. (28) who tried to generate a calibration curve by using one polymer sample having a broad, well-characterized MWD. A calibration curve was obtained by comparing values for molecular weights obtained from the integrated normalized GPC chromatogram with the corresponding data for the integral MWD determined separately. The calibration curve generated is shown in Figure 2.4. The curvature was eliminated by making a correction for the effect of concentration on the apparent molecular weight at the low concentration high molecular weight end.

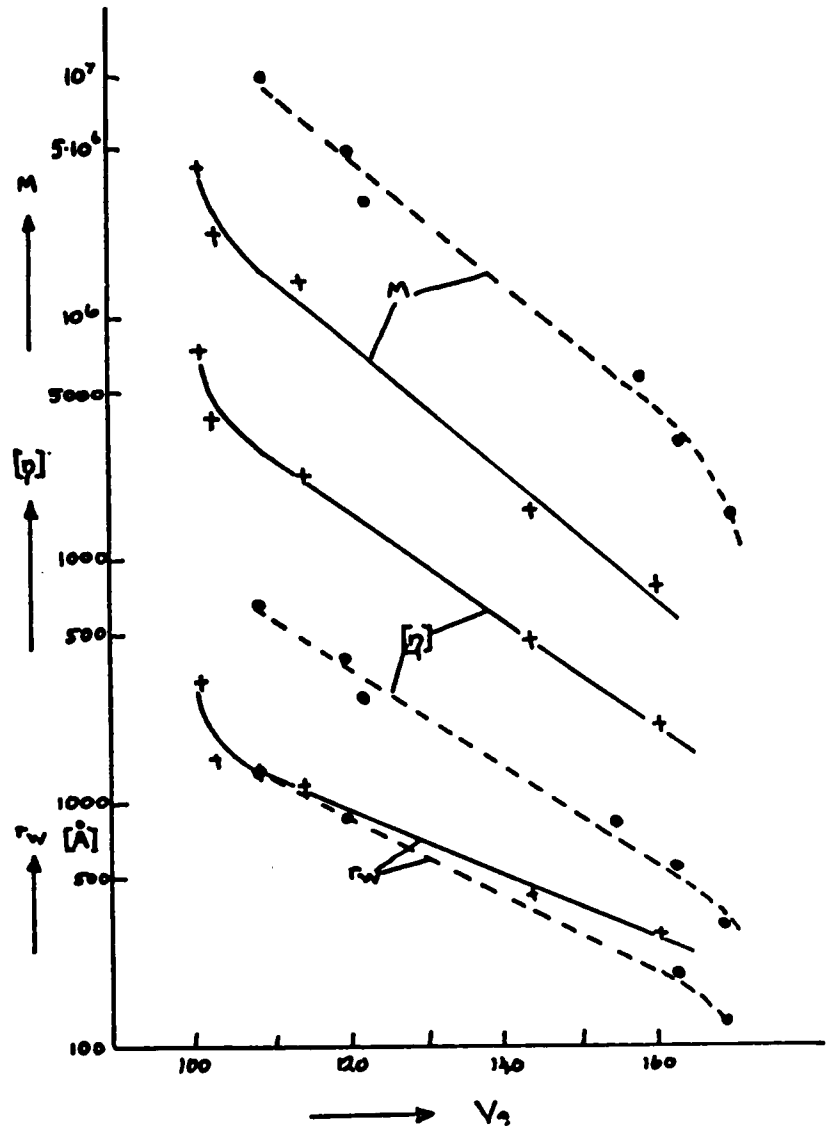

Figure 2.3: Molecular weight, intrinsic viscosity and radius of gyration for trinitrocellulose (+) and PMMA (•) in acetone versus retention volume using four Styragel® columns (20).

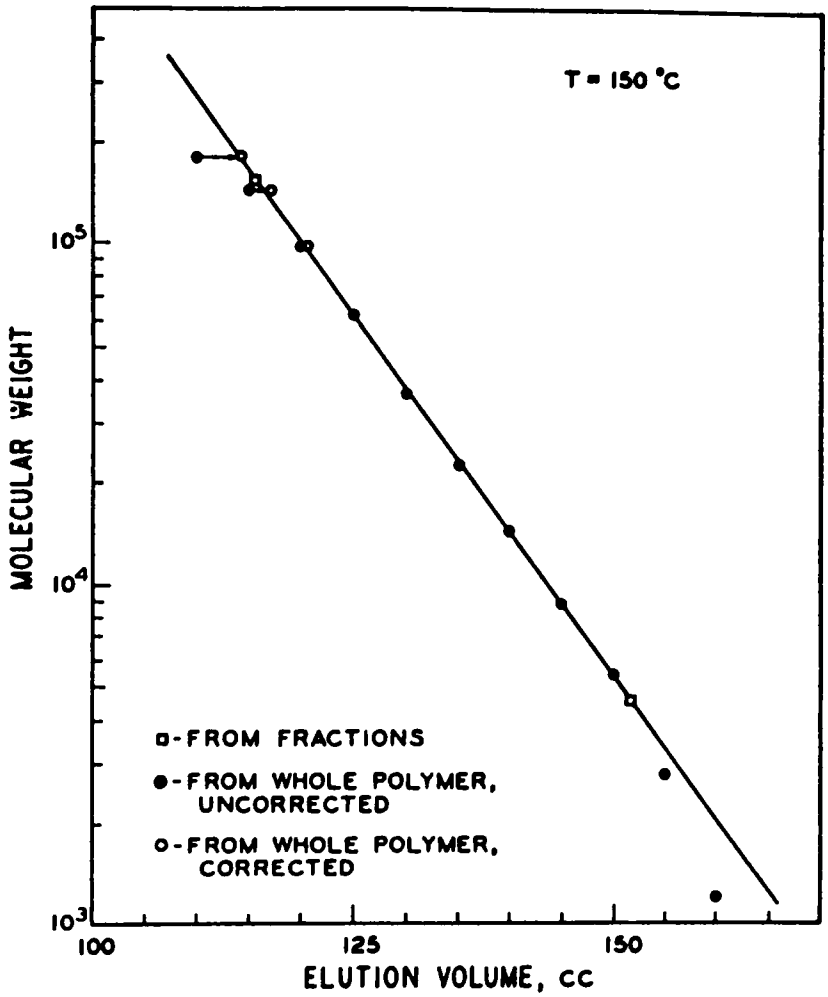

Figure 2.4 GPC calibration with whole polyisobutene demonstrating the influence of the application of a concentration correction (30).

Huang and Jenkins (10) proposed the use of iterative methods to generate a calibration curve. This procedure required two or more broad distribution standards with well characterized weight average and number average molecular weights. They assumed that the calibration curve can be approximated by the equation

$$V = C_1 - C_2 \log M \qquad [2\text{-}1]$$

where V is the elution volume, M is the molecular weight and C_1 and C_2 are constants. This equation generally holds for linear polymers. In order to obtain the calibration curves, they then iteratively varied C_1 and C_2 until the calculated molecular weight matched that which was experimentally determined. Since the experimental results are based on this equation, it is crucial that the two constants are correct. The margin of error in the constants determined here may be reduced by doing the experiment with 5-10 samples to average the experimental errors inherent to molecular weight determination techniques. This calibration method appears to yield reasonable results as evidenced by the close correspondence of molecular weights obtained by viscosity and by GPC in Figure 2.5.

More recently, based on a procedure by Chiantore and Hamielec (29), Goetz et al. (30) utilized one broad MWD standard and a molecular weight calibration plot obtained with narrow distribution standards. The narrow standard calibration curve was transformed to a curve suitable for nitrocellulose by using the chromatogram of a nitrocellulose with known number and weight average molecular weights. Inherent in their procedure is the assumption that GPC separates molecules according to their hydrodynamic volume such that

$$[\eta]_x M_x = [\eta]_{PS} M_{PS} \qquad [2\text{-}2]$$

where $[\eta]$ is the intrinsic viscosity, M is the molecular weight, x represents the sample and PS stands for polystyrene standard. Since

$$[\eta] = KM^a \qquad [2\text{-}3]$$

then

$$K_x M_x^{(a_x+1)} = K_{PS} M_{PS}^{(a_{PS}+1)} \qquad [2\text{-}4]$$

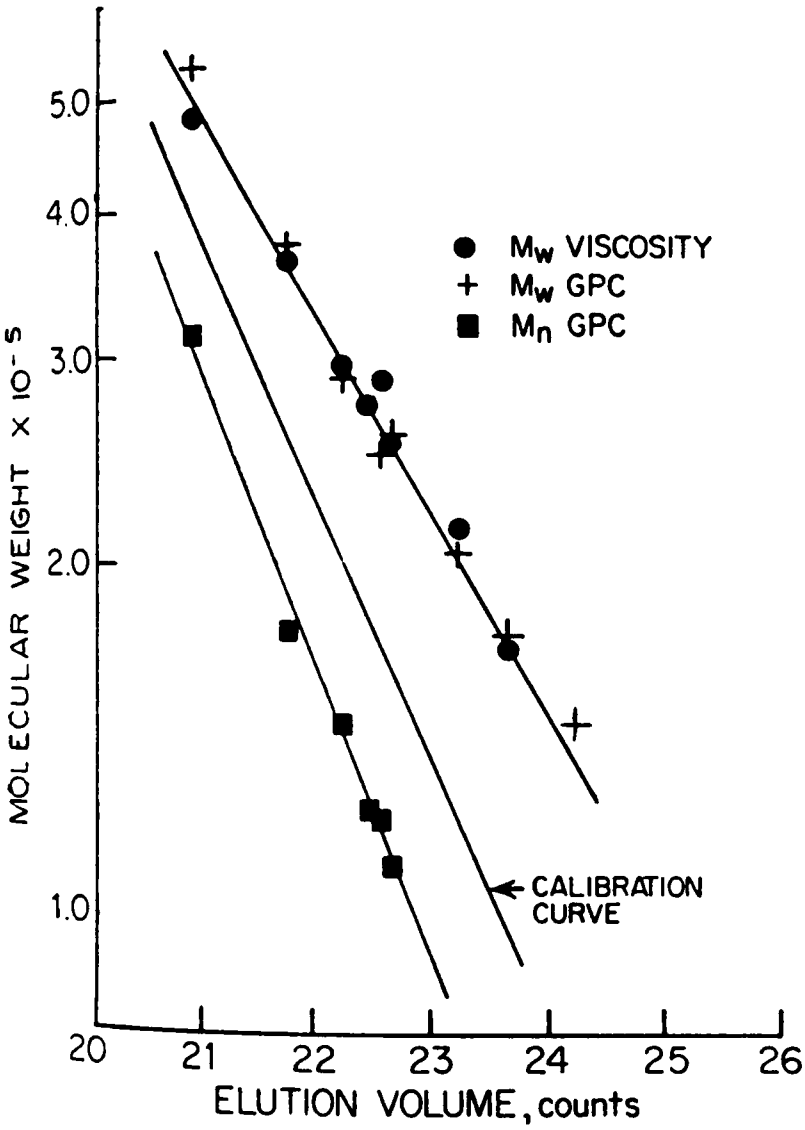

Figure 2.5: GPC calibration curve for cellulose nitrate. Calibration curve: V = 46.10 - 4.5logM (11).

and

$$M_X = \left(\frac{K_{PS}}{K_X}\right)^{\left(\frac{1}{a_x+1}\right)} \cdot C_{PS}(V)^{\left(\frac{a_{PS}+1}{a_x+1}\right)} \qquad [2\text{-}5]$$

If the calibration curve from a narrow standard can be described by M = C(V), then Equation [2-5] may be represented more simply as

$$C_X(V) = \alpha C_{PS}(V)^{\beta} \qquad [2\text{-}6]$$

with α containing the quantity having the ratio of K's and β being the group of terms which makes up the exponent of $C_{PS}(V)$. Equation [2-6] allows the transformation of a calibration curve generated by narrow standards to that for nitrocellulose. Using this equation, α and β were fitted iteratively until the resulting polydispersity value of the broad distribution standard used approached the polydispersity value calculated from the experimentally determined weight and number average molecular weights.

The common requirements in the calibration methods described above are that the standard be of the same structure as the sample to be analyzed and that the $\overline{M}_n$ and $\overline{M}_w$ are known from absolute methods. These requirements are not always easy to satisfy.

2.2.1.2.2.2. Universal Calibration

The pursuit for a universal calibration parameter has generated two factions. One group has based their calibration curve on the length of the extended molecular chain and the other group proposed that the universal calibration parameter should be based on the relationship between the molecules' hydrodynamic volume and the elution volume.

The first method employed what is called a Q factor (11,25). It was assumed that molecules that had the same extended chain length (ECL) would have the same elution volume. Hence, by computing average molecular size from GPC data and a polystyrene calibration curve of ECL versus elution volume, one can presumably calculate average molecular weight by multiplying the computed molecular size by Q where

$$Q = \text{molecular weight/molecular size} \qquad [2\text{-}7]$$

From x-ray measurements, the identity period for trinitrocellulose containing five substituted glucose units was found to be 25.6 Å. The molecular weight of a monomeric glucose trinitrate unit is 297.14 g/mol. These numbers yield a Q factor of 58.0 for cellulose trinitrate (11,23,25,31,32).

The calibration technique that relates elution volume to extended molecular chain length requires only that the standard and the sample have similar chain stiffness; the chains do not have to be extended in solution. This is not true for nitrocellulose and polystyrene (33,34). Evidence from intrinsic viscosity experiments support the hypothesis that the hydrodynamic volume of polystyrene cannot be the same as that of nitrocellulose of the same molecular weight. Comparison of intrinsic viscosity for polystyrene and nitrocellulose has shown that polystyrene is a random coil, while nitrocellulose is stiffer or considered a semiflexible chain. In fact, the characteristic ratio of nitrocellulose is 22, more than twice that of polystyrene which is 10 (33-48).

Chain stiffness effects have been recognized and corrections attempted. Chang (35) suggested that since cellulose trinitrate was a stiff chain and had a larger solvated size, it should possess a lower density in solution. That is, correcting for differences in chain dimensions and monomeric molecular weight of polystyrene and nitrocellulose, the cellulose derivative can have an exclusion volume that is seven times larger than that of a polystyrene molecule with the same molecular weight. Taking this into consideration, an empirical correction was made such that the Q factor was converted to $\overline{Q}$ or effective density factor yielding $Q/\overline{Q} = 5.5$. In spite of this correction, this method of applying universal calibration has not been accepted largely due to the acknowledged difference in chain flexibility between the standards and the cellulosic samples.

A major breakthrough in the development of universal calibration for GPC was achieved when Benoit et al. recognized that the universal separation parameter in GPC was the hydrodynamic volume of the sample. Based on the Einstein viscosity law given by

$$[\eta] = K(V/M) \qquad [2\text{-}8]$$

where [η] is the intrinsic viscosity, K is a constant, V is the hydrodynamic volume of particles and M is the molecular weight, it was suggested that the product [η]M was a direct measure of the hydrodynamic volume of particles and may be used to calibrate chromatograms. Indeed, various samples of different architecture produced a single calibration curve as shown in Figure 2.6, thus confirming Benoit's postulate. This calibration method took into account interactions between the polymer and the solvent, as well as heterocontact interactions present in copolymers. In addition, there was evidence that the calibration curve was independent of the shape of the molecules and was valid both for coils and rigid rods (49). The concept that hydrodynamic volume is the universal separation parameter has been widely accepted, although several groups have tailored it specifically for cellulosic samples by incorporating various corrections.

Meyerhoff (19) claimed that the hydrodynamic volume calibration parameter was not shown to be valid for cellulosics by Benoit. He proposed that for these materials, it was more appropriate to estimate hydrodynamic volume by $[\eta]^{1/3}M^{1/2}$. However, calibration yielded separate lines for PMMA and for cellulose trinitrate, thus invalidating its universality.

Dawkins (33,50) suggested considering an excluded volume effect which would yield:

$$M_2 = \left(\frac{\Phi_2 K_1}{\Phi_1 K_2}\right)^{\left(\frac{1}{a_2+1}\right)} M_1^{\left(\frac{a_1+1}{a_2+1}\right)} \qquad [2\text{-}9]$$

where Φ is the excluded volume effect, K and a are the Mark-Houwink constants and M is the molecular weight. For polystyrene/cellulose trinitrate in THF $\Phi_2/\Phi_1 = 0.58$. This correction allegedly gave better agreement with viscometric results when compared to the Q factor. However, while Benoit's calibration consistently yielded higher molecular weights than viscometric data, Dawkins' added correction resulted in consistently lower molecular weights than those obtained from viscometric data. The best agreement was obtained by comparing viscometric data with the viscosity average molecular weight ($\overline{M}_v$) calculated from GPC data, without including the excluded volume effect. This is achieved by using the equation:

$$\overline{M}_v = [\Sigma w_i M_i^a / \Sigma w_i]^{1/a} \qquad [2\text{-}10]$$

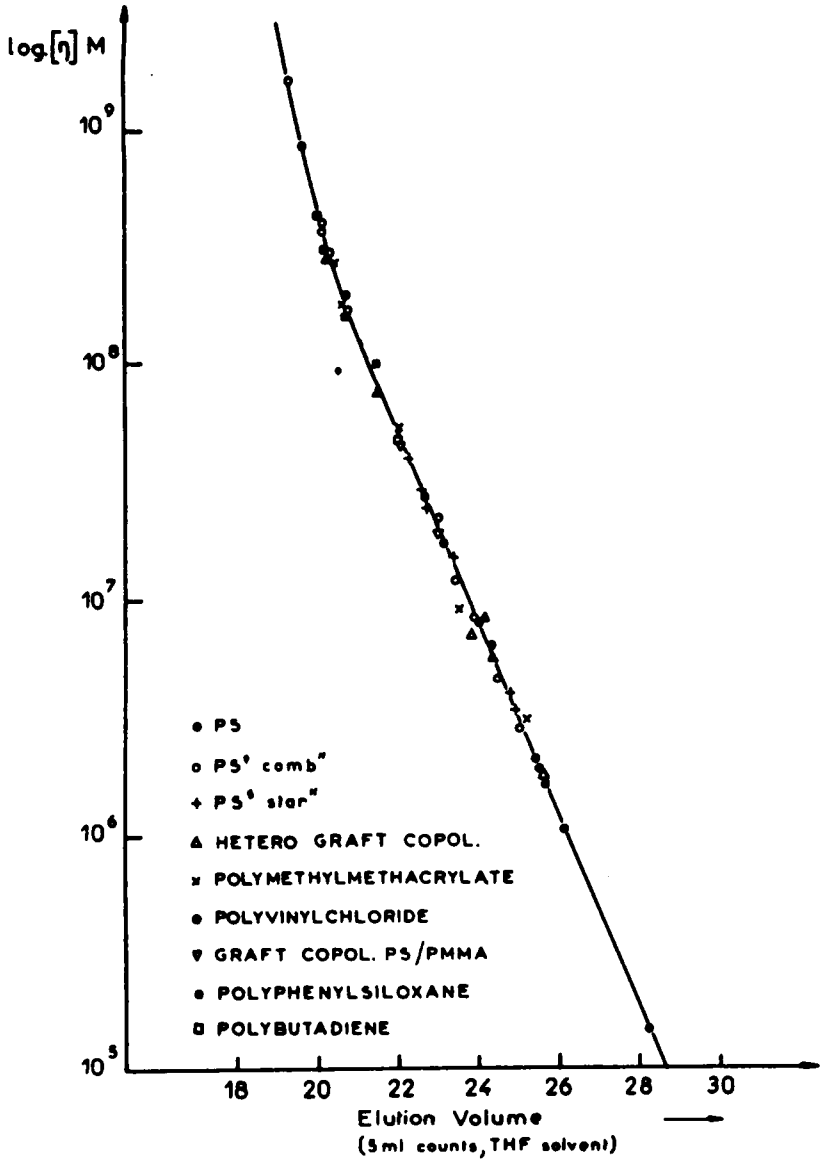

Figure 2.6: Benoit's universal calibration curve generated with polymers of different chemical compositions and architectures (47).

Recognizing that the difficulty in using Benoit's universal calibration curve was not only in the need to determine the intrinsic viscosities of the standards but those of each fraction of the sample as well, Segal et al. tried to eliminate the latter task by using Mark-Houwink constants in the following way:

$$M = (\text{coil size}/K)^{1/a} = ([\eta]M/k)^{1/(1+a)} \qquad [2\text{-}11]$$

where k and a are the Mark-Houwink constants. To obtain the molecular weight of the sample, the coil size of the standard used for the Benoit calibration curve was entered in the equation at the appropriate retention volume. The Mark-Houwink constants of the nitrocellulose were then used to calculate the molecular weight. Caution must be exercised in this regard because a review of the literature has revealed conflicting data on the Mark-Houwink constants. Use of erroneous constants would yield the wrong results. However, barring this complication, M was obtained directly from the calibration curve and intrinsic viscosity measurements of the fractionated nitrocellulose were not necessary (25,34,51,52).

Rudin claimed that Benoit's universal calibration failed in instances where the solute was highly solvated. Benoit had implicitly assumed that the hydrodynamic volume of a solvated polymer species in the GPC columns was that which applied at infinite dilution. This allegedly was not true for highly solvated, high molecular weight fractions for which Rudin's model predicted a smaller hydrodynamic volume when compared to that obtained from the Benoit method. This correction was derived by Rudin and was supposedly superior to Benoit's method for cases of high molecular weight and highly solvated polymers such as nitrocelluloses. However, it was acknowledged that the superiority of this method was marginal or non-existent for polymers of moderate molecular weights and moderate solvent affinity (39). An examination of the calibration plots generated by including the correction revealed that there was little improvement for the nitrocellulose results. This is shown in Figure 2.7 where the deviation from the curves of the data points for NC was of approximately the same amount regardless of the correction.

Marx-Figini (13,20,22) also questioned the validity of Benoit's universal calibration. She found that such plots for polystyrene and fractionated nitrocellulose yielded two separate but parallel lines as shown in Figure 2.8 when their hydrodynamic volume was used as the calibration parameter. However, the curves

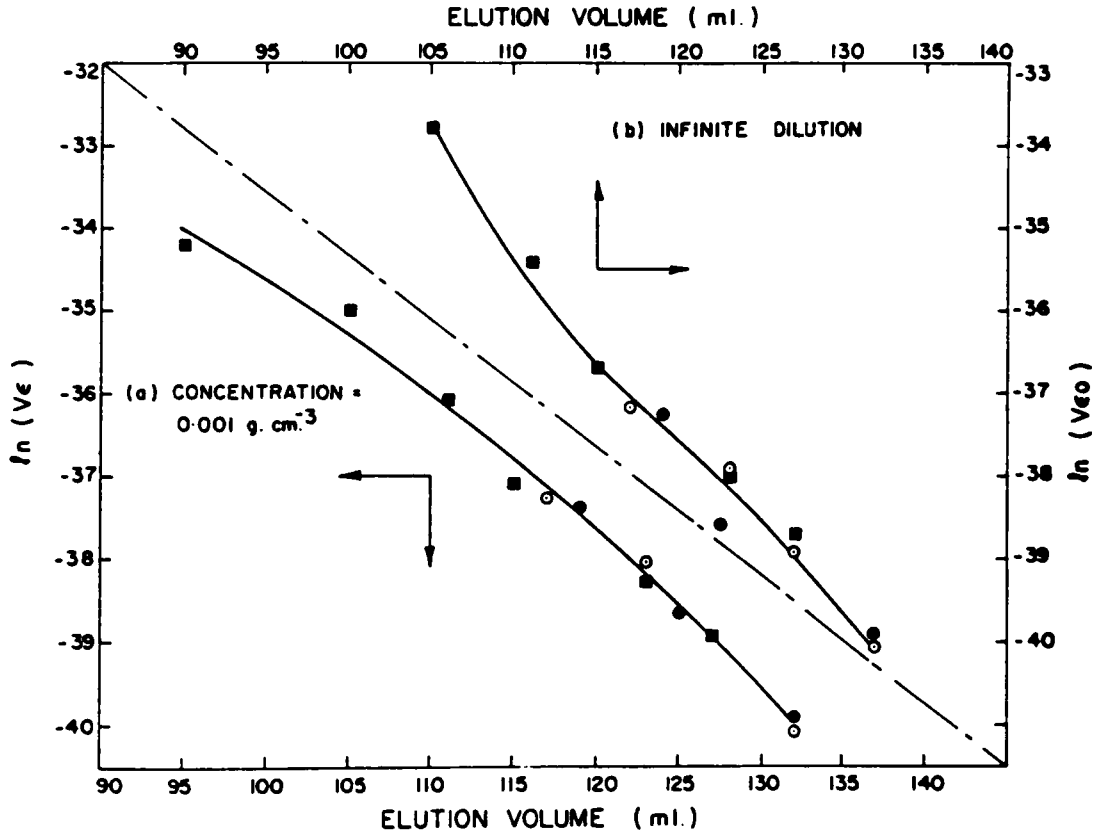

Figure 2.7: Plots of ln(hydrodynamic volume) vs. elution volume for (■) cellulose nitrate, (O) PMMA and (●) polystyrene at (a) 0.001 g/cm^3 concentration and (b) at infinite dilution (50).

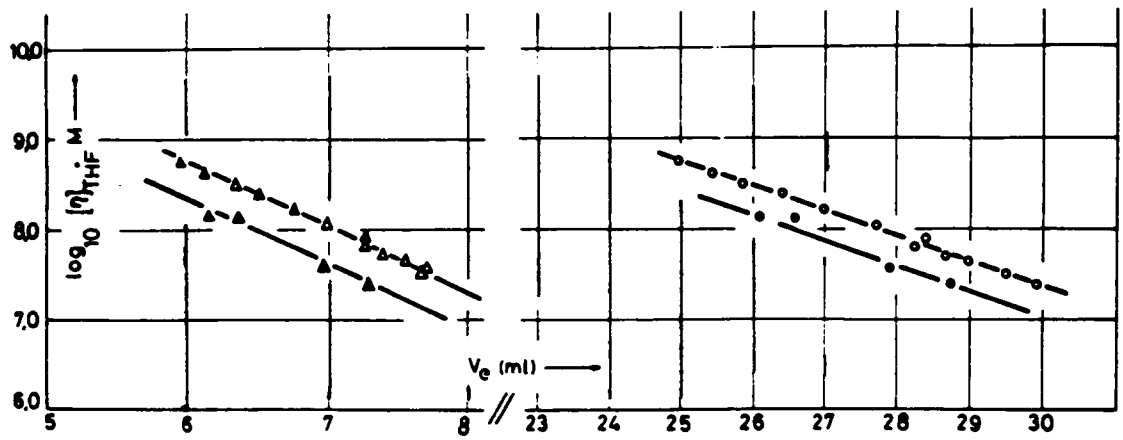

Figure 2.8: Hydrodynamic volume versus elution volume for cellulose trinitrate (Δ,O) and polystyrene (▲,●) in THF. Δ, ▲ done with passivated silica gel columns and O, ● done with Styragel® columns (14).

merged into one when [η] times DP was used as the calibration parameter. This is illustrated in Figure 2.9. Most other researchers in the field, however, have found that nitrocellulose data points lay on the same curve as other narrow distribution standards such as polystyrene (25,33,34,51-53). One can thus presume that the Benoit universal calibration is the simplest and most widely accepted means of converting raw GPC chromatographic data to absolute MWD information.

2.2.1.3. Multidetector GPC

Based on comparisons among results obtained independently by fractionation and by GPC, several investigators have concluded that the two techniques yielded comparable results. However, the application of the two methods in sequence produced more information than either method used independently (13,22,26,27,35,54). On the other hand, an alternative to the use of fractionation and GPC sequentially with a concentration sensitive detector is using GPC with multiple detectors.

The most common multidetector instrument employs a differential refractive index detector in tandem with a LALLS detector. Most LALLS instrumentation currently available commercially utilize a calibration based on instrumental geometric constants. This feature eliminates the need for an external standard and yields an absolute molecular weight, thus circumventing the question of which calibration method to use. However, there seems to be a systematic error present at higher molecular weights (13,55).

More recently, a differential viscosity detector which is based on Benoit's universal calibration has been made commercially available (56,57). The specific viscosity for each polymer fraction as it elutes is determined by a wheatstone bridge-like capillary set-up as shown in Figure 2.10. The differential pressure between the solvent and the solution is measured by a differential pressure transducer as the sample elutes. This quantity is related to the specific viscosity of the fraction eluting by the equation:

$$\text{Differential Pressure}/P_i = \eta_{sp}/4 \qquad [2\text{-}12]$$

where P_i is the inlet pressure and η_{sp} is the specific viscosity. In conjunction with a differential refractive index detector, the differential viscosity detector offers a quick and sensitive on-line method of determining intrinsic viscosity for each eluting fraction of a polymer. This makes the universal calibration method

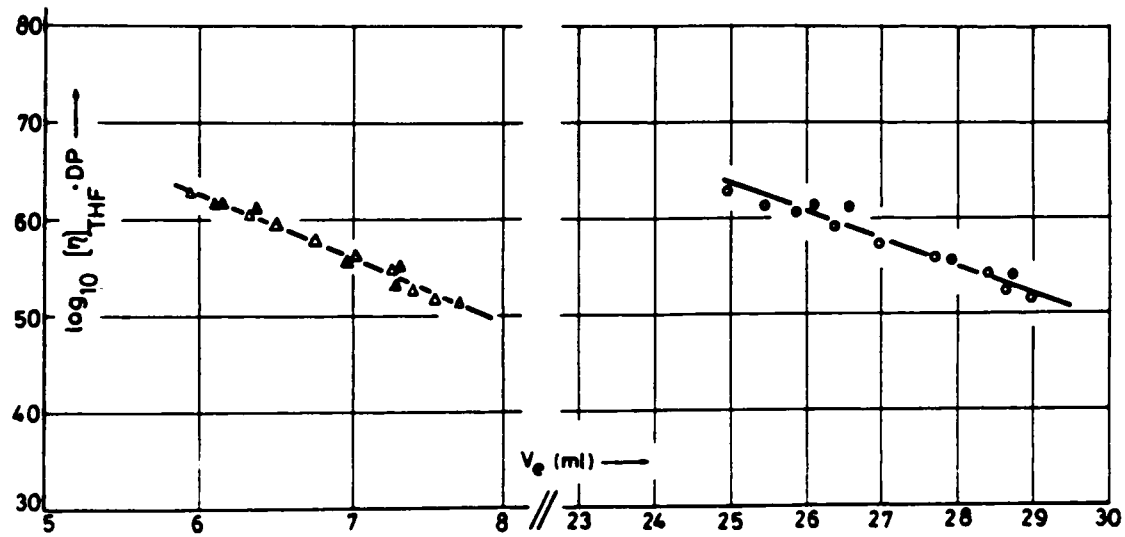

Figure 2.9: Calibration curve generated by expressing hydrodynamic volume as a function of degree of polymerization instead of molecular weight. Legends are the same as in Figure 2.8 (14).

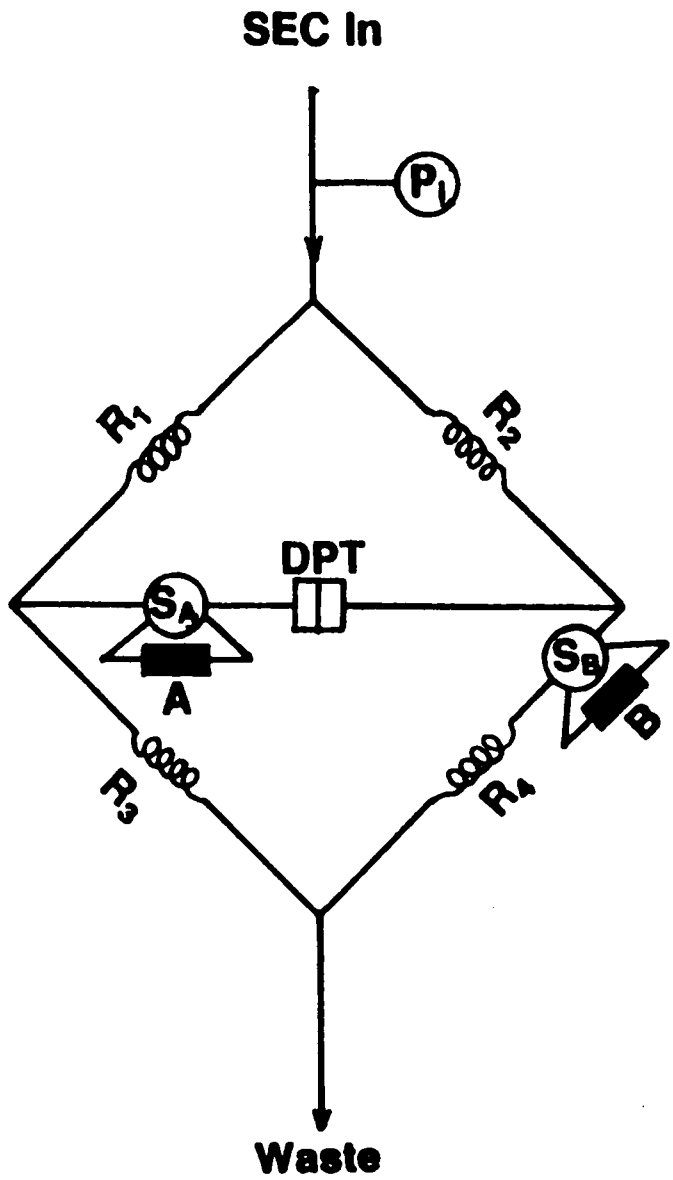

Figure 2.10: Simplified schematic of Viscotek differential viscosity detector (55).

attractive since the labor involved in obtaining data is greatly reduced. In addition to its efficiency, the detector offers the advantage of ease of use. Compared with the GPC/LALLS system which requires a conscientious effort on the part of the operator to eliminate particulate matter in the sample as well as in the GPC system, sample preparation for the GPC/DV is no more complicated than that routinely required for GPC with a single detector.

2.2.1.4. Intrinsic Viscosity Measurements

Intrinsic viscosity experiments provide a quick, easy and inexpensive way to obtain a viscosity average molecular weight, provided the Mark-Houwink constants are known for the particular solvent/polymer system. In addition, the measurements yield conformational information. Although intrinsic viscosity experiments are widely employed to obtain molecular weights, a perusal of the literature reveals that there is some confusion in this matter with regard to NC. A sample of the values available in the more recent literature for NC solutions in THF at 25°C is shown in Table 2.1. A dependence on literature values for these constants requires a knowledge of the degree of polymerization or molecular weight, as well as the level of nitration of the sample. Unfortunately, as is evident from the table, the constants are not always accompanied by such information. Therefore, the problem arises not only from a conflict of data on the same systems but also a lack of knowledge which allows usage of the values published. For investigators who rely on literature values in intrinsic viscosity investigations, these are important issues to address since the correctness of the molecular weight calculated will depend strongly on the accuracy of these constants.

Another motivation for conducting intrinsic viscosity experiments is to obtain information on the conformation of the polymer. The flexibility of the nitrocellulose chain in solution is influenced by several factors. The first factor is the degree of substitution. In cellulose itself, the chain molecules are held to their neighbors by very strong forces due to hydrogen bonding. By substituting the hydroxyl groups with nitro groups, this attraction is reduced to an extent that depends on the degree of substitution. The difference in conformation upon derivatization manifests itself as a change in intrinsic viscosity from that characteristic of a coil to that of a stiffer, more extended chain (36,38,60,61). In fact, as shown in Figure

TABLE 2.1
Mark-Houwink Constants for Nitrocellulose in THF at 25°C

% Nitrogen	Molecular Weight	DP	K x 10^2 (ml/g)	a	Reference
11.88 - 12.13	58000 - 260,000		5.9	0.767	21
	>300,000		0.28	1.0	21
12.0 - 12.6			1.3	0.8	51
13.5 - 13.9		≥2350	2.33	0.84	56
		60 - 6000	3.21	0.84	56
		<1000†	82	1.0	25
		>1000†	446	0.76	25
		≥1000	8.3	0.76	48
		≤1000	0.075	1.14	48
	71,000		1.8	0.84	57
13.8	>300,000		6.1	1.0	58
			2.19	0.89	46
	51,000		0.606	1.014	22

† DP_η

2.11, the intrinsic viscosity of 11.0% nitrocellulose is about half of that of 14% nitrocellulose at the same conditions (61). The second factor that affects the intrinsic viscosity is the solvent. The influence of the solvent is reflected primarily by changes in chain flexibility. This may be due to the modification of the potentials restricting rotations about the ether linkages upon interaction with the solvent (37). In addition, the solvation of hydroxyl groups in incompletely substituted nitrocellulose may also eliminate a potential source of interaction between chains (31,60-65). It has been proposed by Marx-Figini and Schulz that the "goodness" of two solvents be compared by taking the ratio of the intrinsic viscosities obtained in those two solvents. For instance, $[\eta]_{THF}/[\eta]_{EtOAc} = 0.98 - 1.2$ indicating that THF is at least as good a solvent for nitrocellulose as ethyl acetate. Similarly, $[\eta]_{EtOAc}/[\eta]_{Acetone} = 1.28$ (36,40,66,67). Usually, good solvents modify the intrinsic viscosities by further stiffening the chains as solvent power increases. Bad solvents may enhance viscosity by encouraging aggregation (68). Thirdly, intrinsic viscosity is affected by increases in temperature. Nitrocellulose has a large negative $d\ln[\eta]/dT$. This is because the value of the expansion factor, α, decreases with an increase in temperature, suggesting that the elevation of temperature increases chain flexibility (38,41,42,68,69). Finally, intrinsic viscosity for nitrocelluloses is shear rate dependent because of the chain stiffness of the molecules. This dependence may be eliminated by determining the viscosity at different shear rates and extrapolating to zero shear rate. It has also been found that for nitrocelluloses with molecular weights greater than 300,000, there was a substantial effect of the shear rate on viscosity in the range 200 - 2000 s^{-1} (36,70).

Up to this point this review has attempted to examine characterization methods by which solution properties of nitrocelluloses were revealed. The discussion has been limited to the nature of the experimental methods and problems associated with them. The focus will now be shifted to a problem dealing with the nature of the nitrocellulose solutions themselves which makes it difficult to obtain absolute molecular weights regardless of the technique chosen.

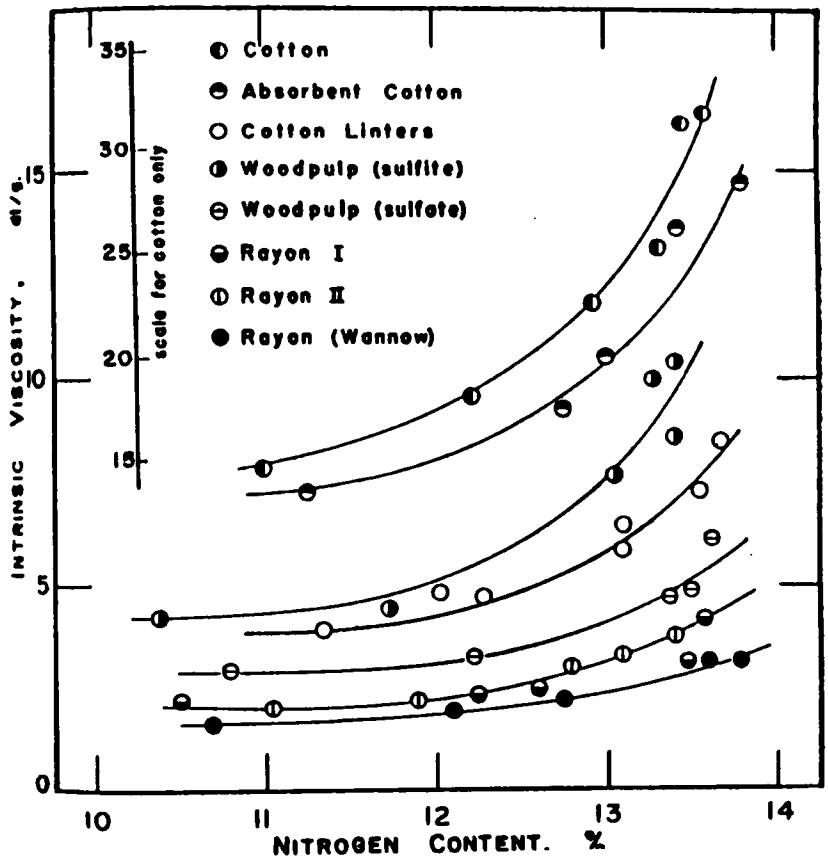

Figure 2.11: Effect of nitrogen content on the intrinsic viscosity of nitrocelluloses (60).

2.2.2. Aging of Nitrocellulose Solutions

Aging in nitrocellulose solutions was recognized quite early in the history of this polymer. It manifested itself as a decrease in specific viscosity of dilute solutions (71-77) as well as in the more concentrated solutions having nitrocellulose contents greater than 10% (78-80). This decrease in viscosity persisted over several days then stabilized. Several theories have been expounded to explain this aging process. A simple, early argument was that the sample had degraded in solution since this had been shown to occur upon exposure to ultraviolet radiation (81,82) or to aggressive thermal treatments (83-85). It was claimed that nitrocellulose degraded in solution due to the presence of residual acids from the nitration process (11,59,71,85,86). Degradation was detected in several cases as a broadening over time of the MWD determined by GPC (24,59). On the other hand, several groups of investigators were proponents of a more complex aging mechanism. The developments of these researchers will be traced below.

Very early, some Russians interpreted the aging of nitrocellulose solutions as resulting from a change in internal structure of the nitrocellulose over time. Specifically, they proposed that the system passed from a gel to a sol in a kinetic process (73-76).

Kanamaru (87) experimented with NC in polar and non-polar solvents. He conducted viscosity experiments in conjunction with x-ray measurements and concluded that the aging of nitrocellulose, especially in polar solvents, was brought about by a decrease in the order of the nitrocellulose crystallites. This loss of order was thought to have been due to solvation by the polar liquids. In relation to solvation, it was suggested that the decrease in viscosity may be due to an equilibrium process between the polar components of the solvent and the nitrocellulose (78).

This view appears to have some basis according to very recent work (88,89) where nitrocellulose was found to retain the supramolecular ordering of the native celluloses from which they were derived. Specifically, it was claimed that spontaneously anisotropic molecular solutions of cellulose nitrate were observed in such solvents as acetone, ethyl acetate, methyl ethyl ketone and 1-pentanol among others (90-92).

A very comprehensive study of aging as evidenced by a decrease in specific viscosity was undertaken by Campbell and Johnson in an effort to pin down mechanisms for aging. They observed that specific viscosity tended to show a rapid decrease over time, then exhibited a very slow decline indefinitely. A selection of their data is shown in Figure 2.12. They tried to remove the solvent and redissolve the samples to the same concentration as the original solutions. This experiment yielded specific viscosities that were the same as or lower than the values observed just before solvent evaporation. In searching for factors that may possibly affect aging, they showed that there was no dependence on concentration, amorphous/crystalline ratio, presence of alkali sensitive linkages or presence of extra stabilization against acid attacks. They demonstrated that ***higher nitrogen containing nitrocellulose showed slower aging*** and that ***higher molecular weight samples aged more rapidly***. Both the rapid and slow aging periods were temperature dependent. Based on the evidence they had, several mechanisms for aging were proposed. These included physical changes including the dispersion of individual molecules, changes in the solvation of the molecules and aggregation. Some of the possible chemical changes proposed were rupture of the main valency linkages between the cellulose nitrate chains and formation or destruction of complexes between nitrocellulose and calcium. Since the rapid initial aging occurred within 300 hours, it was suggested that ***"rapid" viscosity losses were more likely to be physical phenomena.*** On the other hand, ***the long term slow aging was attributed to chemical changes*** (71).

Moving away from viscosity studies, Spurlin noticed that plots of reduced osmotic pressure against concentration sometimes showed an upward or downward curvature at the more dilute concentrations. This is illustrated in Figure 2.13. He speculated that this may be due to interchain interactions, as cellulosics were known to contain localized regions which tended to be attracted to each other, especially in hydroxyl containing solvents (60,65,93).

If the above attractions occurred on a large scale, it may be possible to observe gelation phenomena. This was the case for dilute solutions of nitrocellulose in ethanol. These solutions underwent reversible association upon heating, forming an irregular network which liquefied on cooling (41,72). In fact,

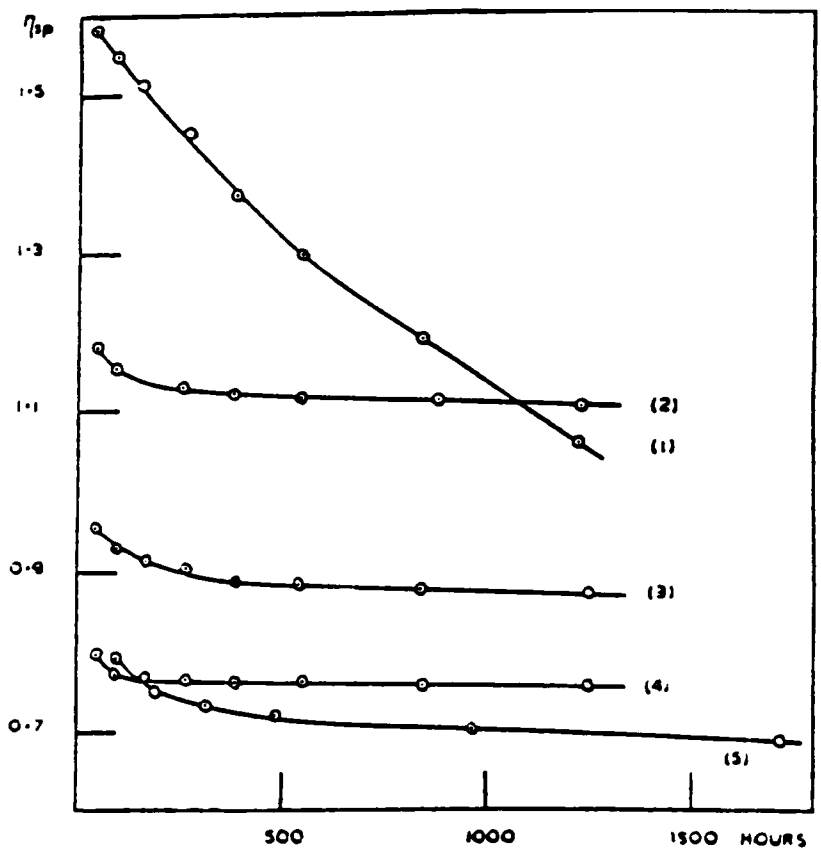

Figure 2.12: Typical aging curves of different samples of cellulose nitrate having a concentration of 0.2 wt/v % at 20°C (71).

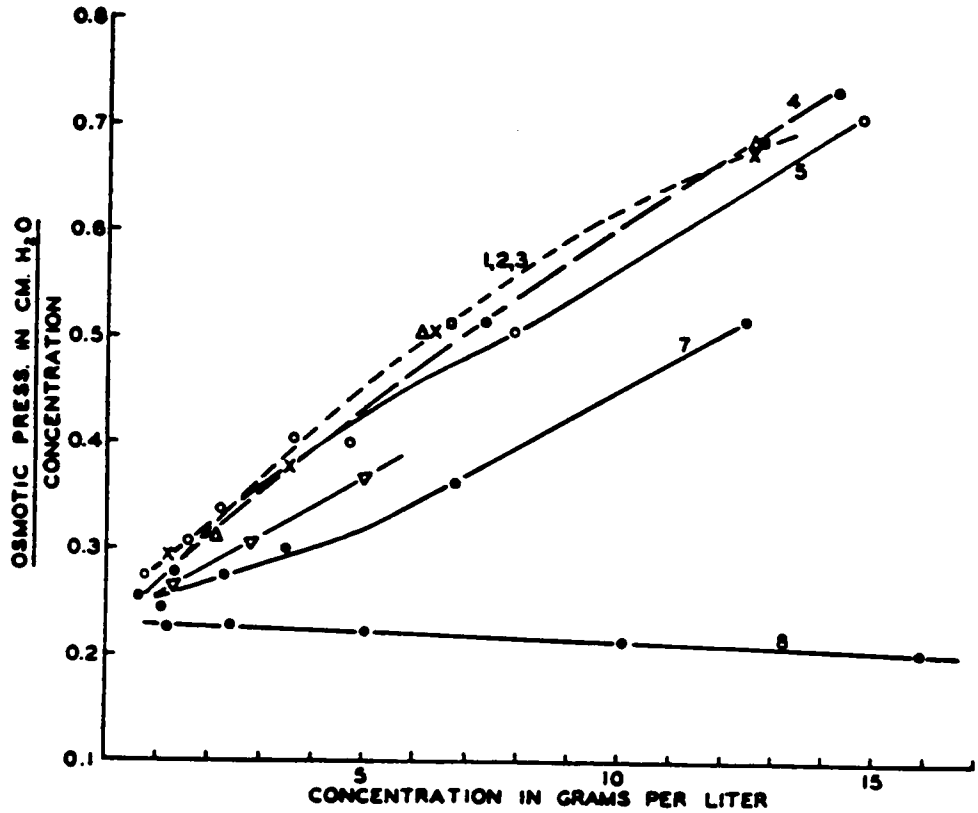

Figure 2.13: Curvature in osmotic pressure plots for cellulose nitrate 1. Ethyl benzoate +11% ethanol 2. Methyl salicylate + 20% methanol 3. Acetophenone + 3% ethanol 4. Cyclohexanone + 5.8% ethanol 5. Acetone 6. Acetic acid 7. Methanol 8. Nitrobenzene (95).

supramolecular gels were known to form in other solvents. A micrograph in Figure 2.14 shows that the gel structure was spherulitic in nature. Intrinsic viscosity measurements indicated that they were rather compact clusters with large radii of gyration. To explain these phenomena, it was postulated that the gel particles were residual unreacted cellulose crystallites (94).

More recently, light scattering studies on moderately concentrated nitrocellulose solutions indicated the presence of microgels after centrifugation (95). The presence of these gels was manifested by an angular dependence of scattered light as shown in Figure 2.15. The anomaly was reduced but not eliminated by centrifugation. As further evidence, the microgel content was seen as a high molecular weight peak on a GPC/LALLS chromatographic signal as shown in Figure 2.16. This peak was not visible on the concurrent differential refractive index detector trace, indicating that the species was present as a small percentage of the sample injected. However, this microgel was sufficient to cause blockage of the filter used for sample preparation (21,27,96).

Finally, more details on the characteristics of the gel were obtained by sedimentation studies (97). These results indicated that the aggregates resembled highly branched polymers more than swollen gels. The gel had a few effective branch points brought about by a number of interchain hydrogen bonds acting cooperatively. Infrared spectroscopy revealed a high absorbance in the range characteristic of hydrogen-bonded hydroxyl groups. Renitration of the incompletely substituted nitrocellulose reduced intrinsic viscosities and reduced curvature in the Zimm plot, such that it was characteristic of unassociated cellulose chains. These results implied that incompletely nitrated materials tended to aggregate by interchain hydrogen bonding. Elimination of the hydroxyl groups removed the source of hydrogen bonding, thus breaking the aggregates up into single chains.

The literature review given above demonstrates that the cellulose community has established a number of experimental methods for obtaining MWD data, with difficulty. However, there is still a need to address the nature of nitrocellulose itself which made characterization a problem. Specifically, there is no unanimous acceptance of the possible mechanism for aging. Instead, this complication appears to be

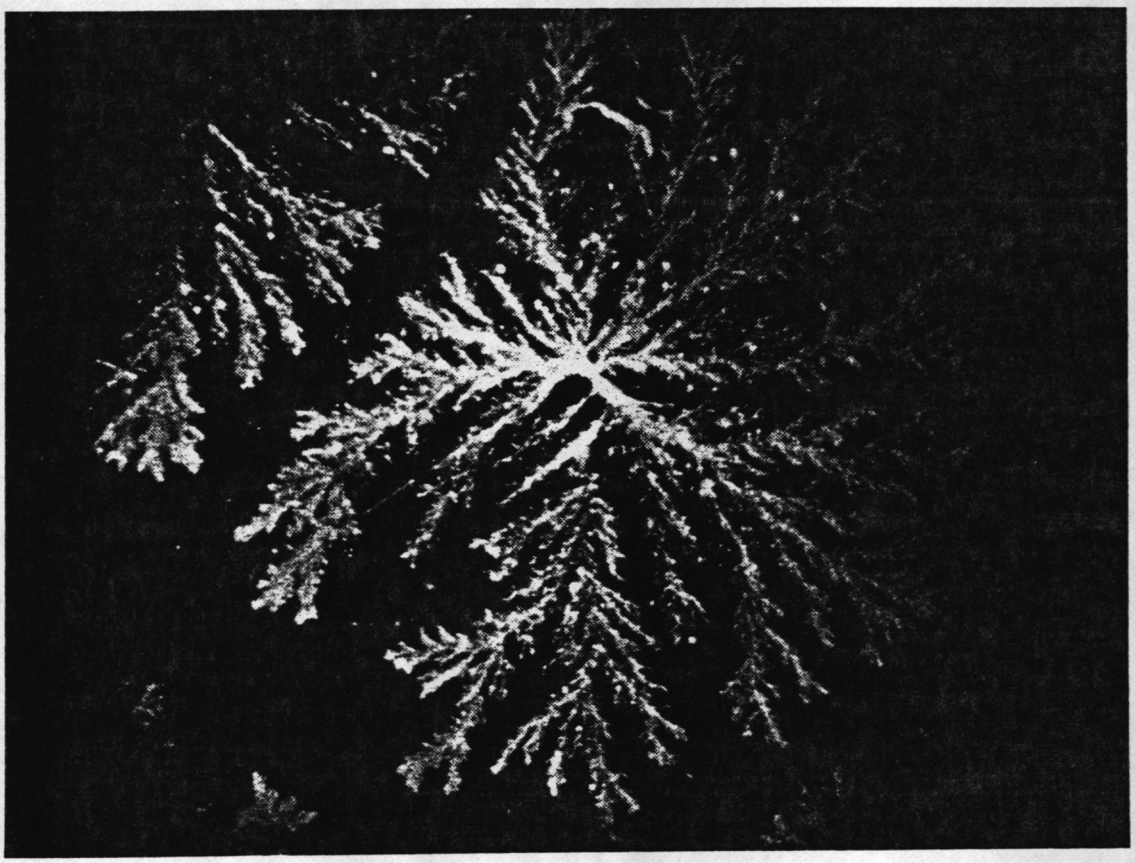

Figure 2.14: Spherulitelike cellulose nitrate gel with a diameter of about 0.5 mm (96).

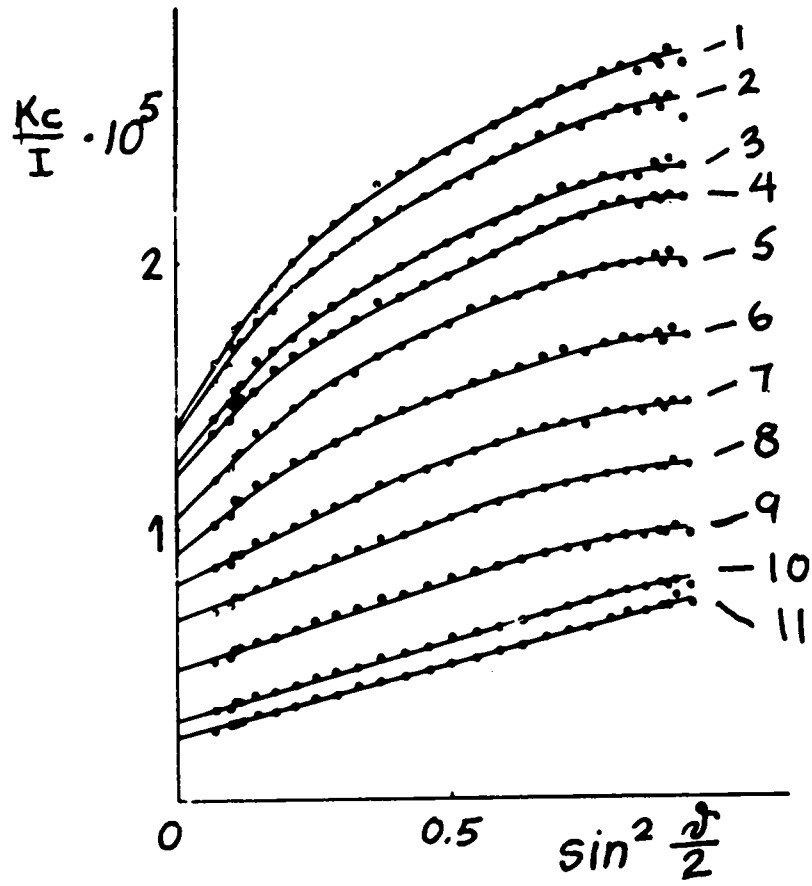

Figure 2.15: Zimm plot for cellulose nitrate with a molecular weight of 780,000, 1 - 11 are fractions of increasing molecular weights (97).

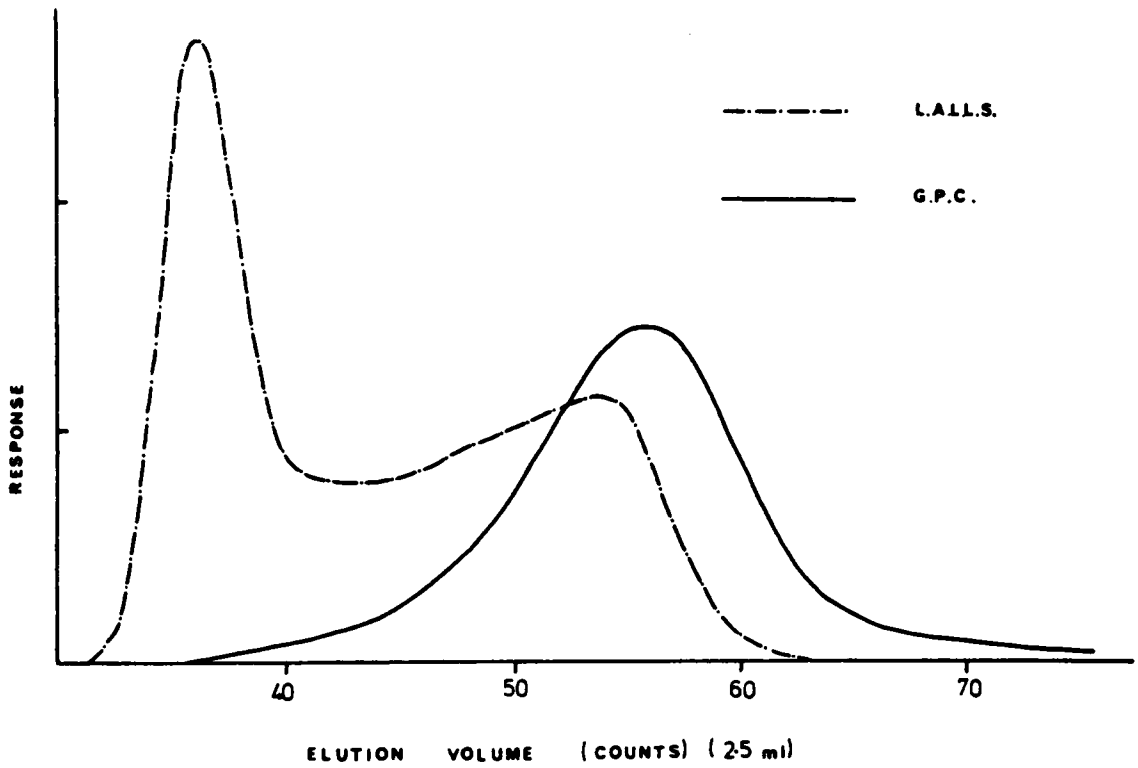

Figure 2.16: Output from GPC/LALLS analysis of cellulose nitrate (22).

ignored in most of the more recent studies. However, this omission does not detract from the fact that the phenomenon still presents a very critical issue because aging results in molecular weights that are dependent on how soon after sample preparation the measurements were conducted. Because this is so, even with the existence of fast, easy and sensitive methods for absolute molecular weight determination, there is question as to which molecular weight on what day is truly representative of a sample. Hopefully, the work to be presented here will contribute to answering this question.

2.3. EXPERIMENTAL

2.3.1. Materials

Through the Radford Army and Ammunition Plant, Hercules, Inc. provided 12.58% and 13.5% nitration level nitrocelluloses. The percentages translate roughly to average degrees of substitution 2.53 and 2.80 respectively (31). These materials were nitrated cotton linters obtained from Buckeye Cellulose Corp. Phenolphthalein indicator and stability tests were used to ensure the absence of residual acid after nitration. These specimens were stored under water in polyethylene bottles. Just before solution preparation, approximately 10 grams of sample was washed several times with absolute ethanol. Most of the alcohol was removed by suction filtration. The moist sample was then dried in a vacuum oven at 60 - 65°C for two hours and used immediately afterwards.

The solutions for all the experiments conducted were made with Burdick and Jackson HPLC grade unstabilized tetrahydrofuran (THF), non-spectrograde tetrahydrofuran (THF/NS) with 250 ppm of butylated hydroxytoluene (BHT) as antioxidant and ketone-free ethyl acetate (EtOAc).

2.3.2. Specific Refractive Index Increment (dn/dc) Measurements

Solutions having 0.4%, 0.6%, 0.8%, 0.9% and 1.0% of 12.58% and 13.5% nitrocellulose were prepared in the three solvents at room temperature. The concentrations were determined by weighing out the sample and the solvent. The solvent weight was converted to volume by using densities. These values were determined by weighing out 10 ml portions of the solvents in 10 ml volumetric flasks and dividing the weight by 10 to obtain the parameter of interest in units of g/ml. After the solutions were prepared,

they were shaken overnight on an orbital shaker at 225 rpm, then used the next morning. They were stored in amber bottles to prevent degradation due to ultraviolet radiation exposure (81,82). Specific refractive index increment measurements were made at 27°C using a Chromatix KMX-16 laser differential refractometer with a laser operating at 633 nm. Five repetitions were made and the average taken. The measurements were repeated on different aliquots from the same sample bottles up to 17 days after sample preparation.

2.3.3. Static Light Scattering Measurements

The solutions of 12.58% and 13.5% nitrocellulose in THF, THF(NS) and EtOAc used for the LALLS experiment were prepared in the same manner as that used for the dn/dc above. Concentrations used for the measurements varied with the nitrogen level of the material and the solvent used. Typically, a series of six solutions ranging in concentration from 0.5 to 4 mg/ml were required. The solutions were filtered through a 0.2 μm Acrodisc CR filter fed by a syringe and again just before it entered the sample cell. This dual filtering was found necessary for the solvents used above because particulate matter interfered significantly in the scattering measurements -- the solvents themselves were low scattering media. This is evidenced by a Rayleigh scattering factor of 4.4×10^{-6} cm^{-1} for all three solvents compared to 14.1×10^{-6} cm^{-1} for toluene (98,99). The static measurements were carried out on a Chromatix KMX-6 LALLS photometer which was equipped with a 2 mW He-Ne laser operating at 633 nm. The temperature in the sample chamber was 27°C. The experiments were conducted at a 6 - 7° forward scattering angle and repeated over a period of 17 days for different aliquots taken from the same set of solutions.

Data were processed by plotting $Kc/\overline{R}_\theta$ against concentration where K is an optical constant given by:

$$K = (2\pi^2 n_o^2/\lambda_o^4 N_A)\,(1 + \cos^2\theta)\,(dn/dc)^2 \qquad [3\text{-}1]$$

where

n_o = solvent refractive index

λ_o = scattering wavelength -- 633 nm

N_A = Avogadro's number

θ = observation angle

dn/dc = refractive index increment

For the conditions utilized in the experiments equation [3-1] reduced to:

$$K = (4.079 \times 10^{-6}) (n_o^2) (dn/dc)^2 \quad [3\text{-}2]$$

where the values for the solvent refractive indices are 1.4034 for THF and 1.3669 for EtOAc. These values were based on extrapolation from values measured at other wavelengths. The refractive indices available in literature were generally obtained at 23°C. In order to convert these numbers to those needed under the experimental conditions, a correction was carried out by assuming that the refractive index decreased at a rate of 0.0004/°C (100,101).

$\overline{R}_\theta$ is the excess Rayleigh scattering. This was obtained by measuring Rayleigh scattering for the polymer solution and for the solvent as follows. The scattered intensity was set close to 1000 mV on the LALLS meter. The appropriate attenuators were then inserted to obtain a transmitted intensity of greater than 250 mV. The ratio of the scattered intensity over the transmitted intensity was taken and multiplied by the solid angle which is an instrument constant. This parameter was a function of the forward scattering angle, cell path length (15 mm) and solvent refractive index. The constants were tabulated in Appendix A3 of the KMX-6 manual and are characteristic of each particular instrument (102). $\overline{R}_\theta$ is the difference between the Rayleigh scattering of the solution and the Rayleigh scattering of the solvent. The intercept of the $Kc/\overline{R}_\theta$ versus concentration graph was the inverse of the absolute weight average molecular weight, $\overline{M}_w$ and the slope was twice the second virial coefficient, A_2.

2.3.4. Gel Permeation Chromatography

Polymer Laboratories narrow distribution polystyrene standards with peak molecular weights 1,350, 3,250, 9,000, 34,500, 68,000, 127,000, 194,000, 500,000, 1,840,000 and 2,950,000 g/mol were dissolved in HPLC grade THF. These were used to construct the universal calibration curve required to determine absolute molecular weights and molecular weight distributions of the nitrocellulose samples (49).

Approximately 0.2% solutions of 12.58% and 13.5% nitrocellulose solutions were prepared in HPLC grade THF as in the procedure described for dn/dc measurements. These samples were filtered through a 0.5 μm Millipore filter prior to analysis on a Waters 150C ALC/GPC equipped with a differential refractive index detector and a Viscotek Model 100 differential viscosity detector connected in parallel. The conditions for the chromatography experiment were: flow rate 1.0 ml/min, sensitivity 256, scale factor 80, injection volume 200 μl, Ultrastyragel® columns with pore diameters of 500 Å, 10^3 Å, 10^4Å, 10^5Å and 10^6Å. The run time was 64 minutes per sample. Temperature was set at 30°C both for the GPC and the viscosity detector. Experiments were repeated over 21 days for different aliquots from the same samples.

2.3.5. Intrinsic Viscosity Measurements

The solutions used for intrinsic viscosity experiments had concentrations of approximately 0.05%, 0.1%, 0.15%, 0.2%, 0.3%, 0.4%, 0.6%, 0.8%, 0.9% and 1.0% wt/vol. The experiments were conducted using a Cannon Ubbelohde capillary viscometer immersed in a water bath held at 30°C. Measurements were taken on different aliquots from the same solutions over a period of 17 days.

2.3.6. Infrared Spectroscopy

Infrared spectra of the samples were taken on a Nicolet 5DXB FT-IR spectrophotometer equipped with an MCT detector. The samples were films cast on a KBr salt plate from various concentrations of solutions given in Table 2.2. The solutions were prepared as described above. Where special treatments were included prior to the experiment, these are specified in Table 2.2. The experiments were carried out on the films cast from the aged solutions for a total of 21 days. All spectra were taken after 100 scans at a gain of 1.

2.3.7. Redissolving of Dried Nitrocellulose Films

The solutions used for the above experiments were allowed to evaporate slowly until no detectable smell of solvent was present. Slow evaporation was achieved by covering the bottles with aluminum foil punctured with tiny needle holes and storing them in the hood. Evaporation in air generally took 10 - 14 days depending on the amount of solution remaining in the bottles. Except for the 12.58% nitrocellulose

TABLE 2.2
Conditions for FT-IR Experiments

SAMPLE	CONCENTRATION x 10^3 (g/ml)	PRETREATMENT
12.58% NC/THF	1.020	Sonicated after 15 days of storage
	3.999	
	8.053	
	9.877	2 - 3 drops of nitric acid added to about 4 mls of sample after 15 days of storage
	10.188	Redissolved 6 months after solvent was evaporated
12.58% NC/EtOAc	1.040	Sonicated after 15 days of storage
	4.077	
	9.967	2 - 3 drops of nitric acid added to 4 mls of sample after 15 days of storage
13.5% NC/THF	2.095	
	4.093	
	9.992	2 - 3 drops of nitric acid added to 4 mls of sample after 15 days of storage
13.5% NC/EtOAc	1.499	
	6.084	
	10.160	2 - 3 drops of nitric acid added to 4 mls of sample after 15 days of storage

in THF samples, all other dried samples were redissolved to the same concentration as the original solutions after 14 days. This was done for 12.58% nitrocellulose in THF 6 months after the solvent evaporated. In addition, for the THF(NS) solutions, the evaporated samples were dried in the vacuum oven at room temperature for two hours before redissolution. The solutions were shaken at 225 rpm on an orbital shaker for 1 - 5 hours depending on the concentration. This was necessary because it was found that the dried films went into solution much sooner than the original fibrous material did. Intrinsic viscosity, dn/dc and IR experiments were conducted as soon as no detectable solute was visible. The samples were then stored and measurements were repeated for up to a week.

2.4. RESULTS AND DISCUSSION

2.4.1. Specific Refractive Index Increment

The specific refractive index increment is a quantity that is determined by using a differential refractometer operating at the same wavelength and temperature as the LALLS. The dn/dc was calculated by taking the average values of $\Delta n/c$ for the series of five solutions used in the experiment. Uncertainties in the results were a consequence of the propagation of errors based on the reproducibility of the measurements and the accuracy of the concentrations. Details of error analysis are given in the appendix. Results indicated that for the nitrocellulose solutions, dn/dc changed over time and there appeared to be some dependence of $\Delta n/c$ on concentration.

The values of dn/dc for 12.58% and 13.5% nitrocellulose in the three solvents used are given in Tables 2.3 and 2.4 respectively. These data are plotted in Figures 2.17 and 2.18 in order to make analysis of trends easier. The results for 12.58% NC in Figure 2.17 indicate that for the THF solution, the dn/dc changed by 19% between the sixth day and the 13th day, but remained constant prior to and subsequent to that time span. The trend for the stabilized THF was not as clear. It appeared that even if the refractive indices of the two solvents were the same, the dn/dc was always higher in THF(NS) than in THF. Furthermore, the dn/dc in THF(NS) fluctuated wildly during the whole experiment. In contrast to this behavior, the dn/dc for the EtOAc solution remained constant throughout the same time span with a maximum change of only 2.5%.

TABLE 2.3
Specific Refractive Index Increments of 12.58% Nitrocellulose

SOLVENT	DAY	dn/dc x 10^2 (ml/g)	UNCERTAINTY x 10^4 (ml/g)
THF	1	7.075	1.633
	3	7.390	1.405
	6	7.213	1.268
	8	7.504	1.248
	9	7.626	1.337
	13	8.593	1.487
	15	8.469	1.414
	17	8.548	1.408
THF(NS)	1	8.868	1.394
	3	8.704	1.361
	4	9.267	1.437
	7	8.200	1.254
	9	9.031	1.359
	11	8.786	1.430
	15	8.835	1.344
	17	11.105	1.714
EtOAc	1	9.976	1.819
	3	10.006	1.831
	5	9.983	1.785
	8	10.066	1.697
	9	10.006	1.802
	11	9.991	1.668
	15	9.841	1.663
	17	9.808	1.617

TABLE 2.4
Specific Refractive Index Increments for 13.5% Nitrocellulose

SOLVENT	DAY	dn/dc x 10^2 (ml/g)	UNCERTAINTY x 10^4 (ml/g)
THF	1	7.941	1.325
	3	8.129	1.280
	5	8.244	1.294
	8	8.523	1.470
	10	8.748	1.428
	12	9.094	1.555
	14	9.318	1.543
	17	9.546	1.534
THF(NS)	1	11.282	1.816
	3	8.662	1.440
	5	9.011	1.470
	8	8.394	1.364
	9	8.767	1.464
	11	7.970	1.274
	15	9.539	1.538
	17	8.397	1.355
EtOAc	1	9.939	1.539
	3	9.961	1.554
	5	9.973	1.665
	8	9.960	1.704
	10	9.990	1.596
	12	9.968	1.608
	15	9.971	1.622
	17	9.968	1.561

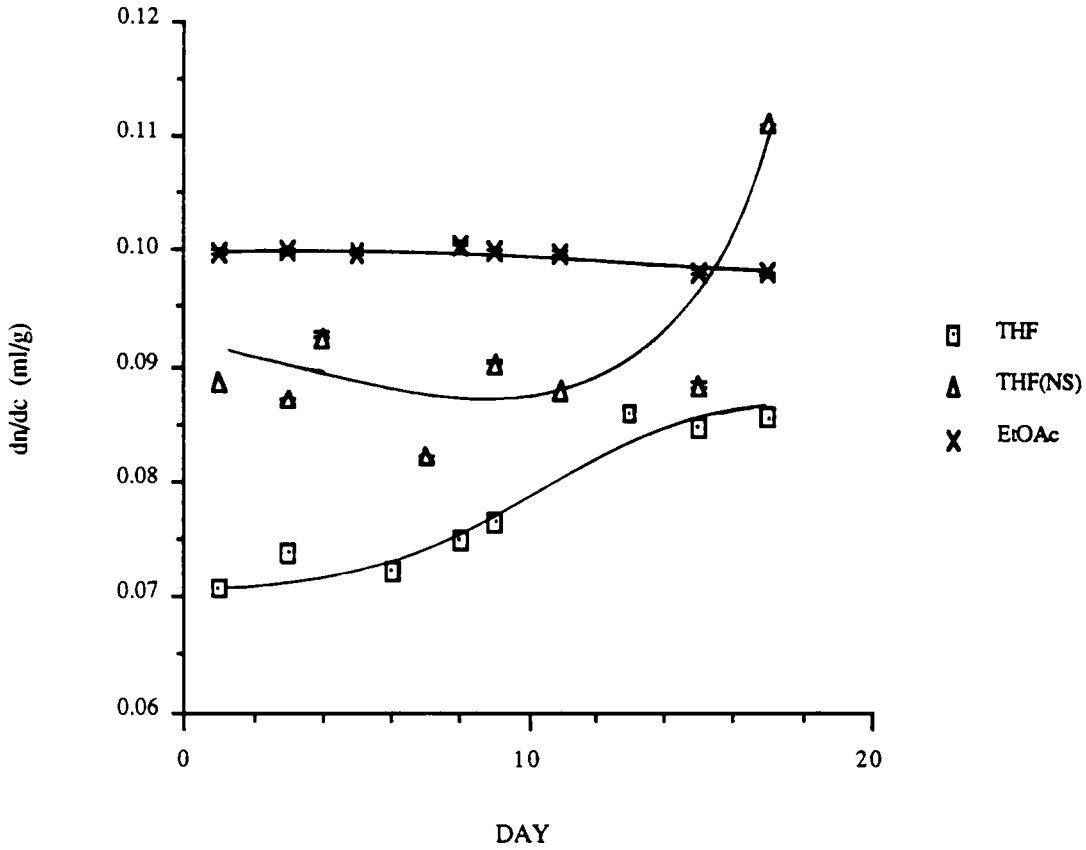

Figure 2.17: Time dependent change in dn/dc of 12.58% nitrocellulose in three solvents.

Figure 2.18 is a composite of the dn/dc results for 13.5% nitrocellulose. For the THF solution, the dn/dc values increased monotonically. As in the case of the 12.58% nitrocellulose, there was no clear trend for the THF(NS) solutions. In contrast to the less nitrated analog however, there were some days when the dn/dc values for the THF(NS) solutions almost coincided with that for the THF solutions. This was expected in view of the fact that both the stabilized and unstabilized THF have the same refractive index. Again, for the EtOAc solution, the dn/dc was unchanged over the three weeks of the experiment.

At this point, the results for the stabilized THF solutions are not clear. One can only speculate that since the sole difference between this solvent and the unstabilized THF was the presence of antioxidant, this compound was the source of the discrepancy. Perhaps, due to solvent evaporation, the BHT concentration was changing over the half hour that it took to gather the data. However, if this were so, the $\Delta n/c$ values would not have been as reproducible as they were.

Sidestepping the above issue for the moment, the author wishes to look into the noticeable difference in trends between the results for the THF solutions and the EtOAc solutions. The results for both levels of nitration suggest that the trends observed here were due to a dependence on the solvent. Based on some solubility parameter experiments (103), it was established that THF had a closer solubility parameter match with and hence was a better solvent for the nitrocelluloses than EtOAc. These results are shown in Table 2.5. The above information implies that the solvent dependence of the results may be related to degree of solvation. Using the knowledge obtained from the work of several investigators (36,38,63), one may speculate that the slight difference in trends for the results of the 12.58% and 13.5% NC was due to the difference in the conformation of molecules with different levels of nitration. Due to extensive hydrogen bonding, the less nitrated molecule was more coiled and thus less accessible to solvation. On the other hand, the 13.5% NC molecule which resembled a semirigid rod, was more extended in solution due to decreased hydrogen bonding potential, and was therefore more accessible to the solvent molecules. Perhaps, the changes in dn/dc were an evidence of this phenomenon which is understandably time dependent. With this in mind, the more drastic changes observed in the THF solutions may have been a reflection of the

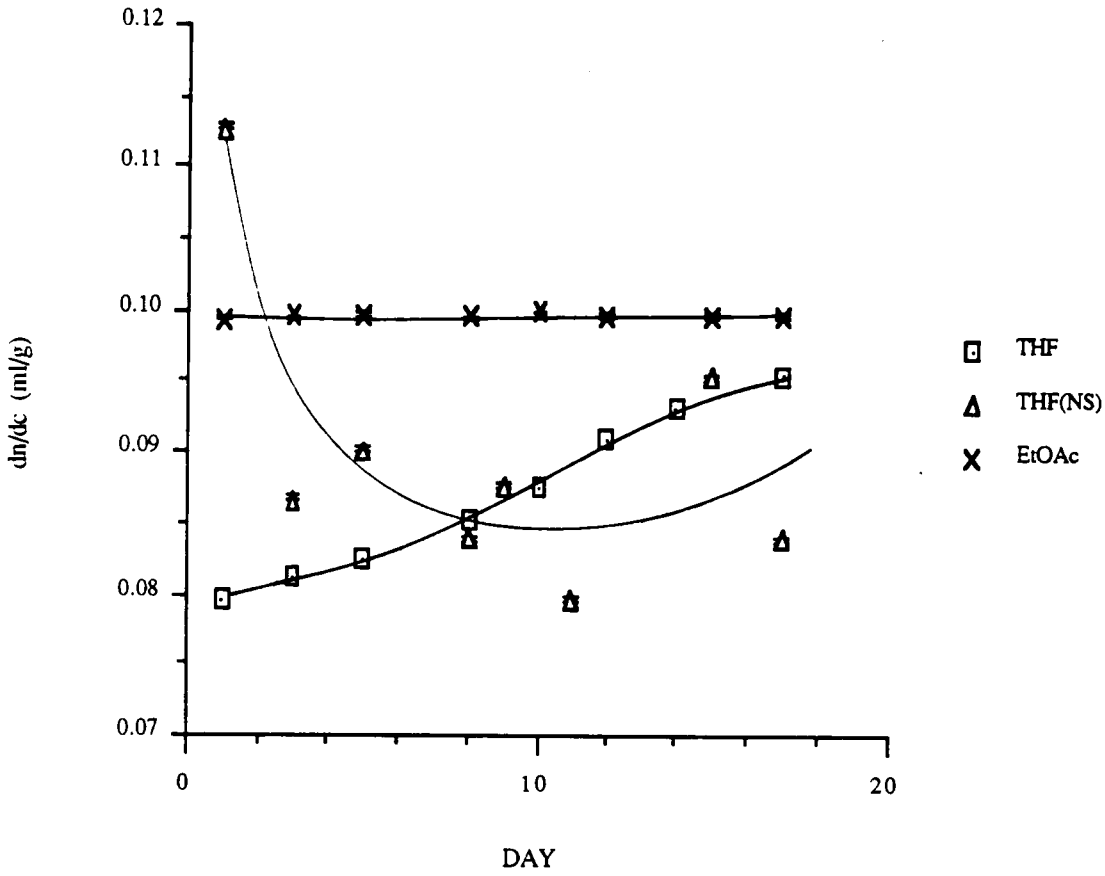

Figure 2.18: Time dependent change in dn/dc of 13.5% nitrocellulose in three solvents.

TABLE 2.5
Solubility Parameters

MATERIAL	δ $(cal/cm^3)^{1/2}$
12.58% Nitrocellulose	12.4
13.5% Nitrocellulose	11.4
Tetrahydrofuran	9.5
Ethyl Acetate	9.0

greater physical changes imparted to the solute as a result of greater solvation by the better solvent, THF, compared to the poorer solvent EtOAc.

Having examined the trends in the time dependent variations in dn/dc, the author now wishes to scrutinize the Δn/c results more closely. Figures 2.19-2.26 reflect not only the shifts in Δn/c values brought about by time, but the accompanying changes as a function of concentrations as well. Care was taken to show all data with the same scale in order to facilitate comparison of results between days. Focussing on the results for 12.58% NC/THF as shown in Figure 2.19, one may observe that the shape of the plot remained generally the same for the first six days. Over the course of the second week, while the values of the solutions having concentrations greater than and equal to 0.6% changed very slightly, the Δn/c for the 0.4% solution increased drastically. In the calculation of dn/dc, the data for 0.4% was excluded whenever the deviation of the value of this point from the mean was four times greater than the average deviation of the rest of the data points (106). After the solvent was slowly evaporated and the samples redissolved six months later, the values of Δn/c for the 0.6% solutions were higher than those obtained just before the solvent was evaporated. These data are shown in Figure 2.20. Unfortunately, there was not enough solution of the 0.4% concentration left for this phase of the experiment.

The results from the same experiment done on 12.58% NC/THF(NS) are shown in Figure 2.21. The scatter in the data was greater in this solvent than in the pure THF. This characteristic persisted for nine days. It was only on the 11th day that the expected independence from concentration of the Δn/c values was observed. The role played by the antioxidant was not clear. In the determination of dn/dc, the same criterion for data rejection in the THF solution was used here.

Completing the series of 12.58% NC is Figure 2.22 which shows the results obtained from EtOAc solutions. The results were more internally consistent than for the THF solutions. That is, any shifts up or down of the values occurred across the whole concentration range. This is in contrast to the results of THF shown previously, in which the concentration and time dependence of the changes were more apparent.

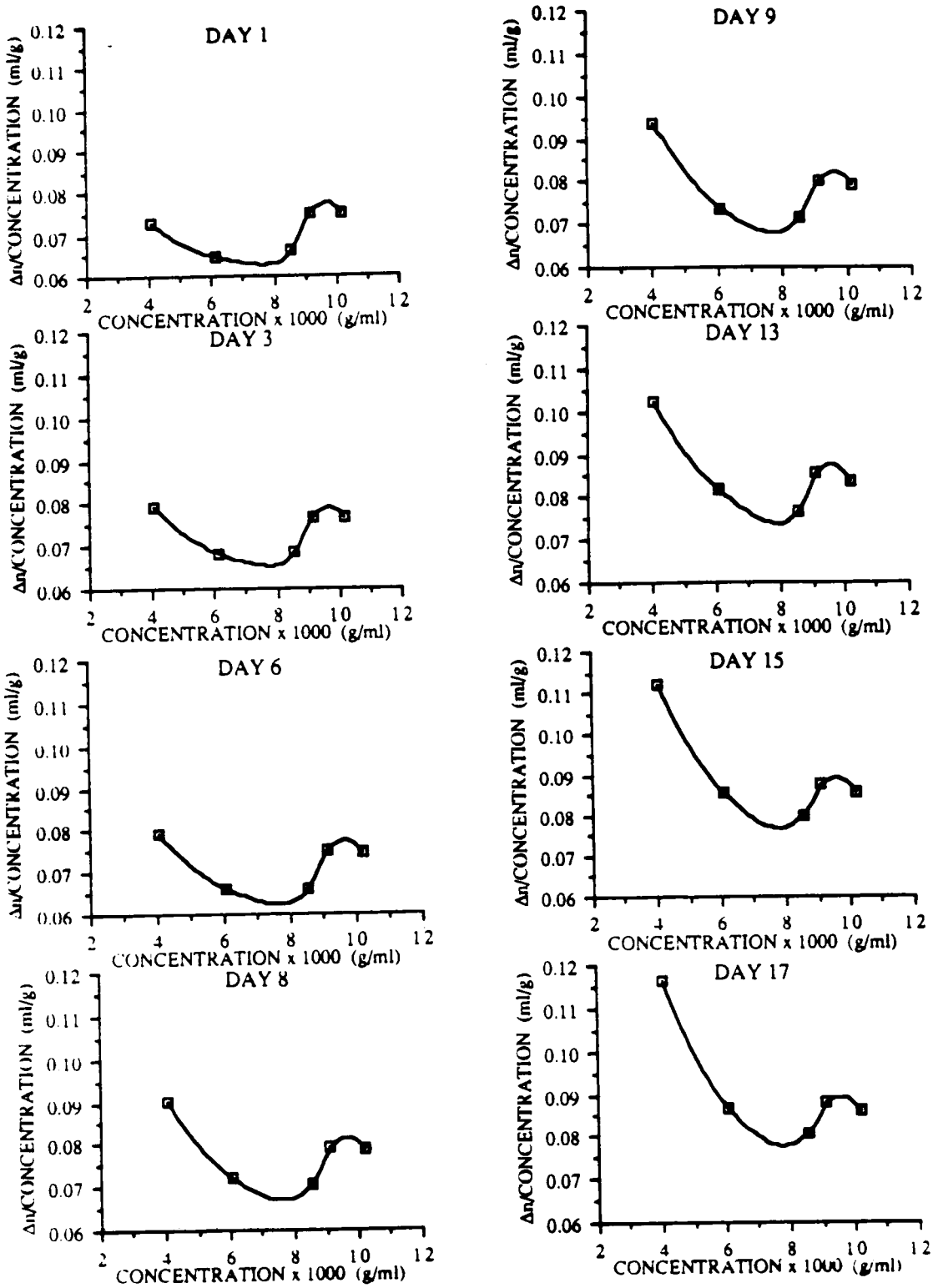

Figure 2.19: Concentration and time dependent changes in Δn/concentration for 12.58% NC/THF.

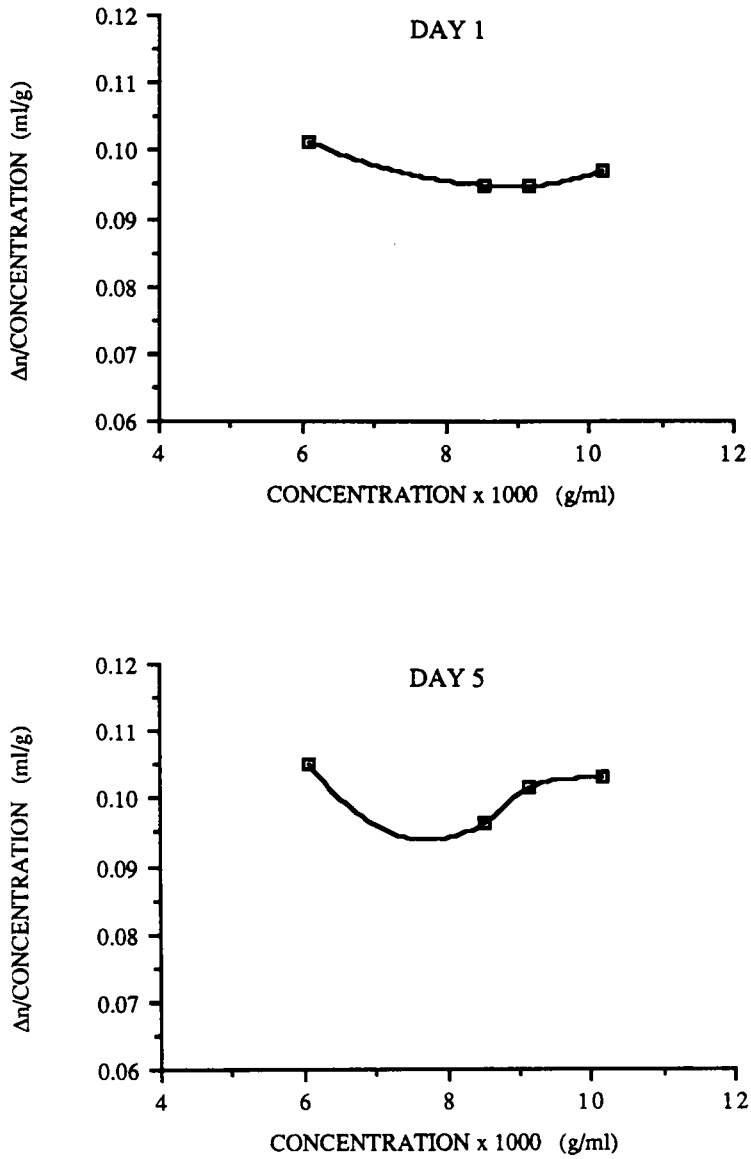

Figure 2.20: Concentration and time dependent changes in Δn/concentration for redissolved 12.58% NC/THF.

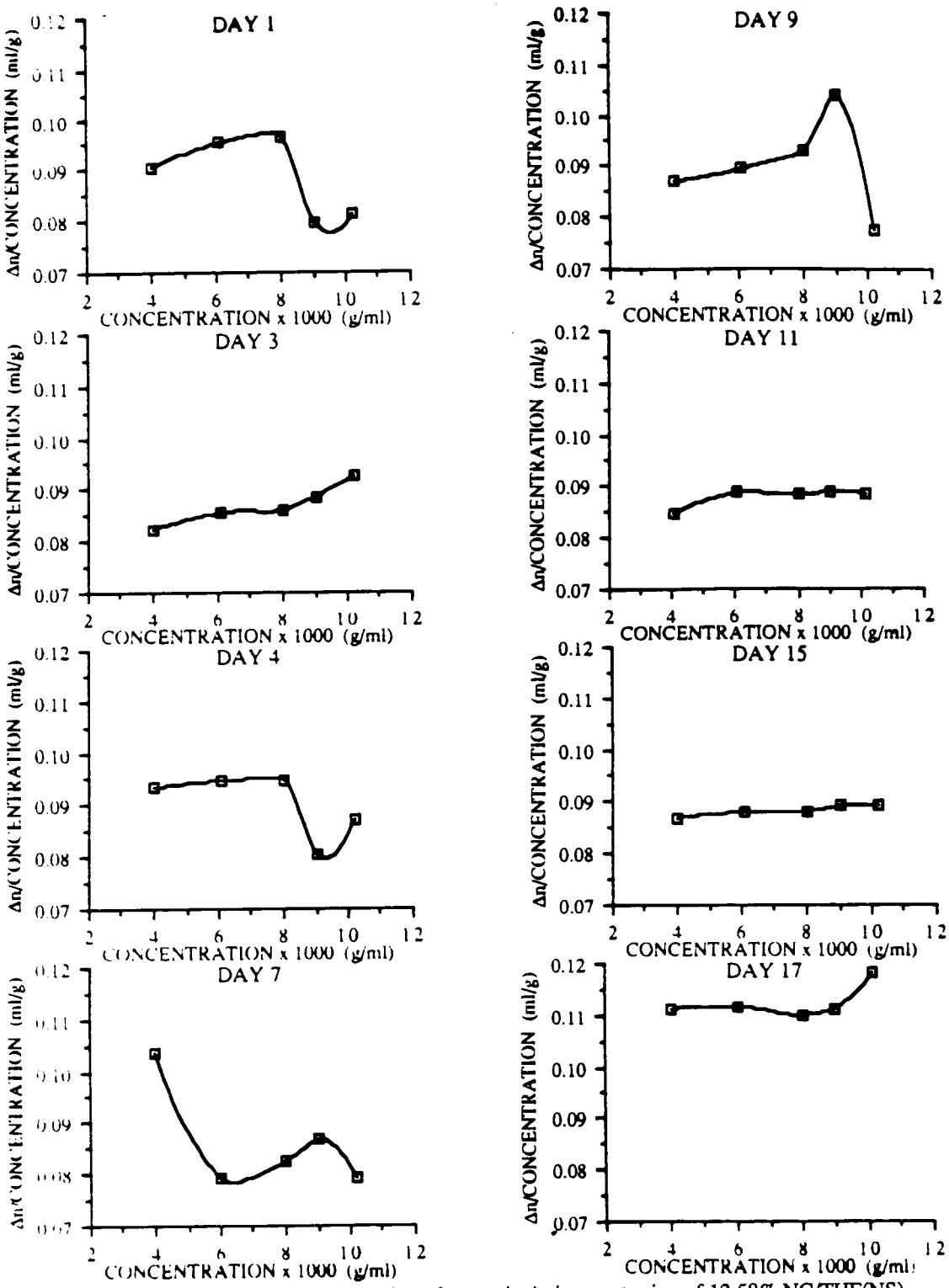

Figure 2.21: Concentration and time dependent changes in Δn/concentration of 12.58% NC/THF(NS).

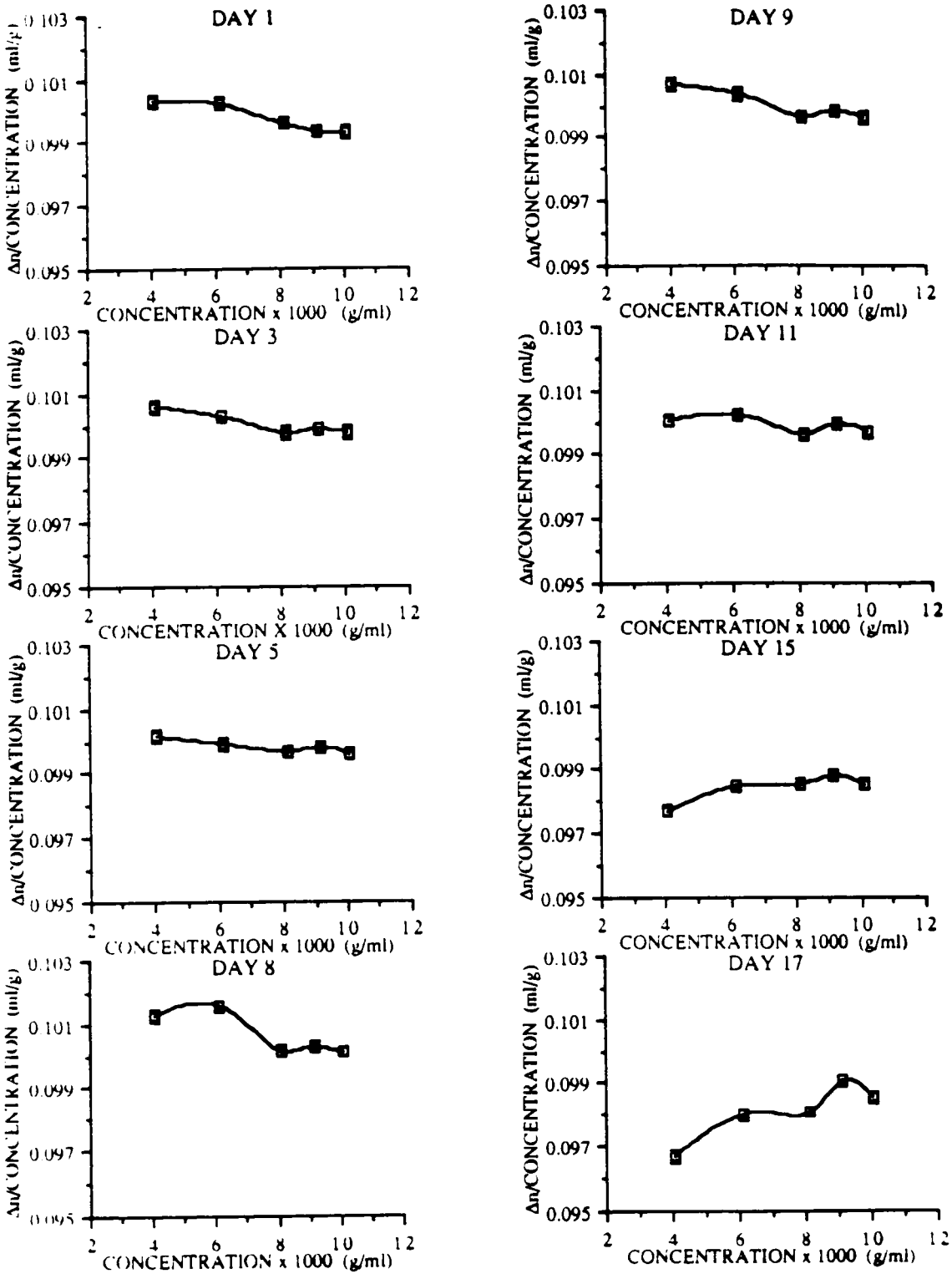

Figure 2.22: Concentration and time dependent changes in Δn/concentration of 12.58% NC/EtOAc.

Moving on to the 13.5% NC series, the results for 13.5% NC/THF are shown in Figure 2.23. The $\Delta n/c$ versus concentration plots showed no concentration dependence in the first eight days of the experiment. This was what would typically be expected. Any changes that took place over time occurred almost uniformly across the whole concentration range used. However, from the tenth day onwards, there appeared a hint of the trend seen for 12.58% NC/THF where the $\Delta n/c$ of the more dilute solutions changed more rapidly than those at the higher concentrations.

Figure 2.24 shows the analogous experiment in THF solutions containing BHT. The data obtained on the third, fifth, eleventh and seventeenth day were what would typically be expected. On the other days, the shape of the graph was distorted by the deviation from expected behavior of one concentration The identity of the anomalous concentration was not the same from day to day. Whether the BHT had a detrimental effect on solvation that resulted in this problem can only be speculated on. The lack of a clear pattern in the results made it difficult to gauge if the trends seen in the unstabilized THF solutions were due to degradation of the nitrocellulose chains by THF through peroxide formation or to some other mechanism.

Finally, Figure 2.25 is a summary of the results for 13.5% NC/EtOAc. The graphs for this system revealed an interesting trend. Even as all the concentrations yielded an almost constant value of $\Delta n/c$ over time, the $\Delta n/c$ for the 0.8% solution continuously increased in value such that by the eighth day, the graph showed a clear maximum at this concentration. What is more intriguing is that after the solutions were evaporated and redissolved, this maximum persisted. This is shown in Figure 2.26. The presence of this maximum after redissolution may suggest that there existed an "equilibrium" structure that did not quite disappear even after the sample was dried and redissolved.

The discussion of the dn/dc results here was for the most part, speculative. Their significance is not fully understood as yet. It is possible that the interpretation arose from reading too much into the data. Perhaps the trends observed may be understood more as the other data are collected and discussed and all the results are tied together more neatly.

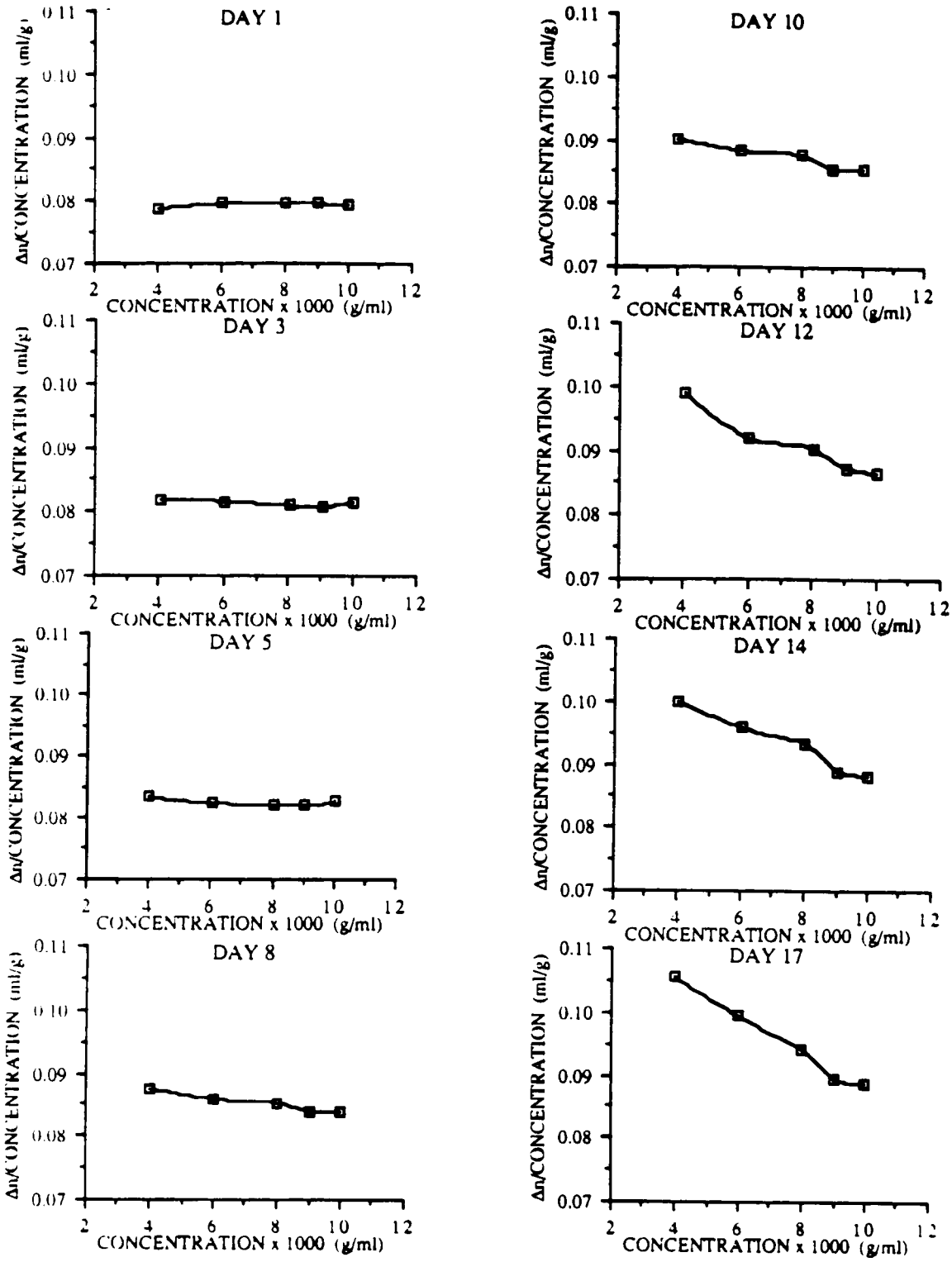

Figure 2.23: Concentration and time dependent changes in Δn/concentration for 13.5% NC/THF.

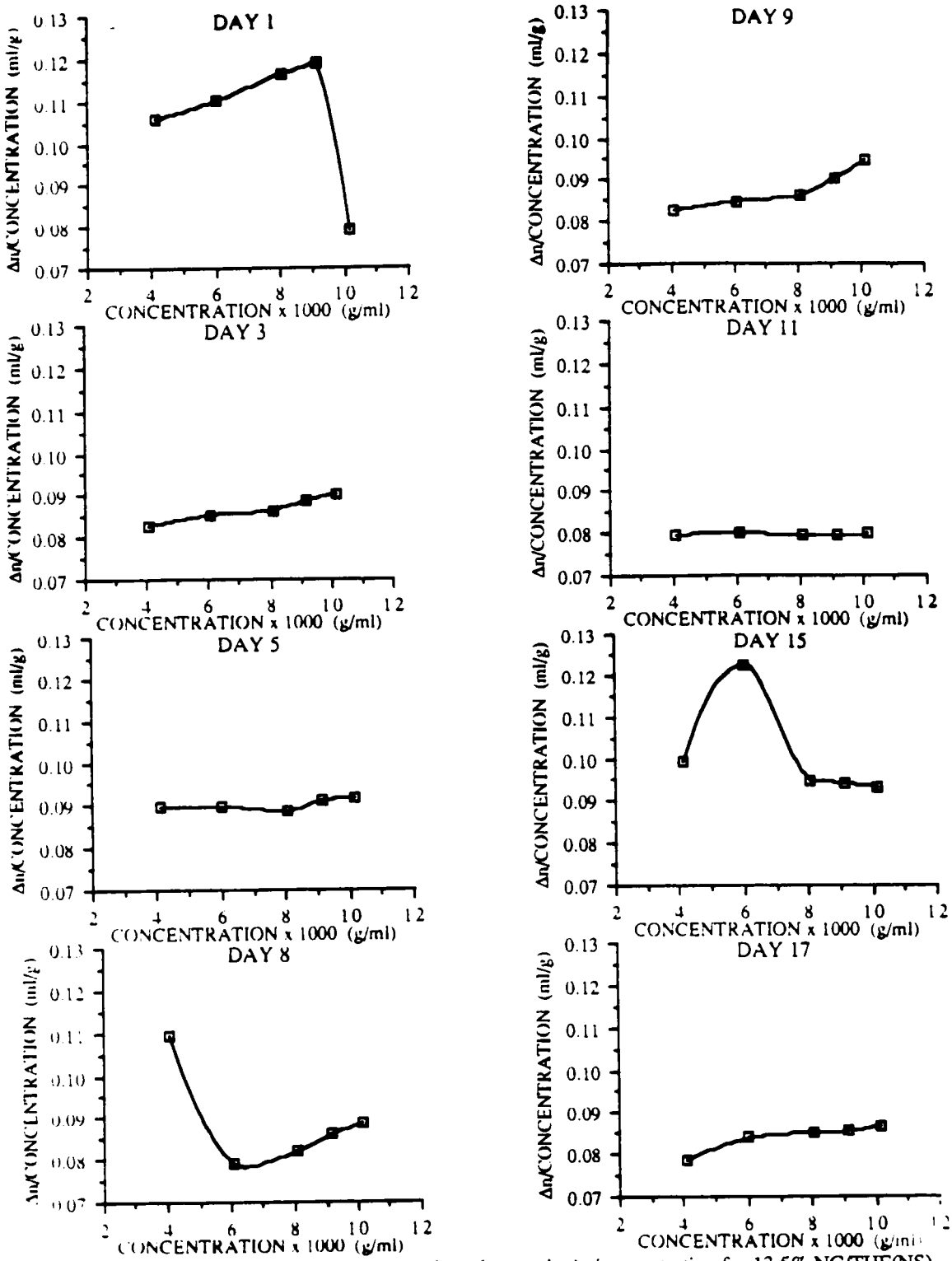

Figure 2.24: Concentration and time dependent changes in Δn/concentration for 13.5% NC/THF(NS).

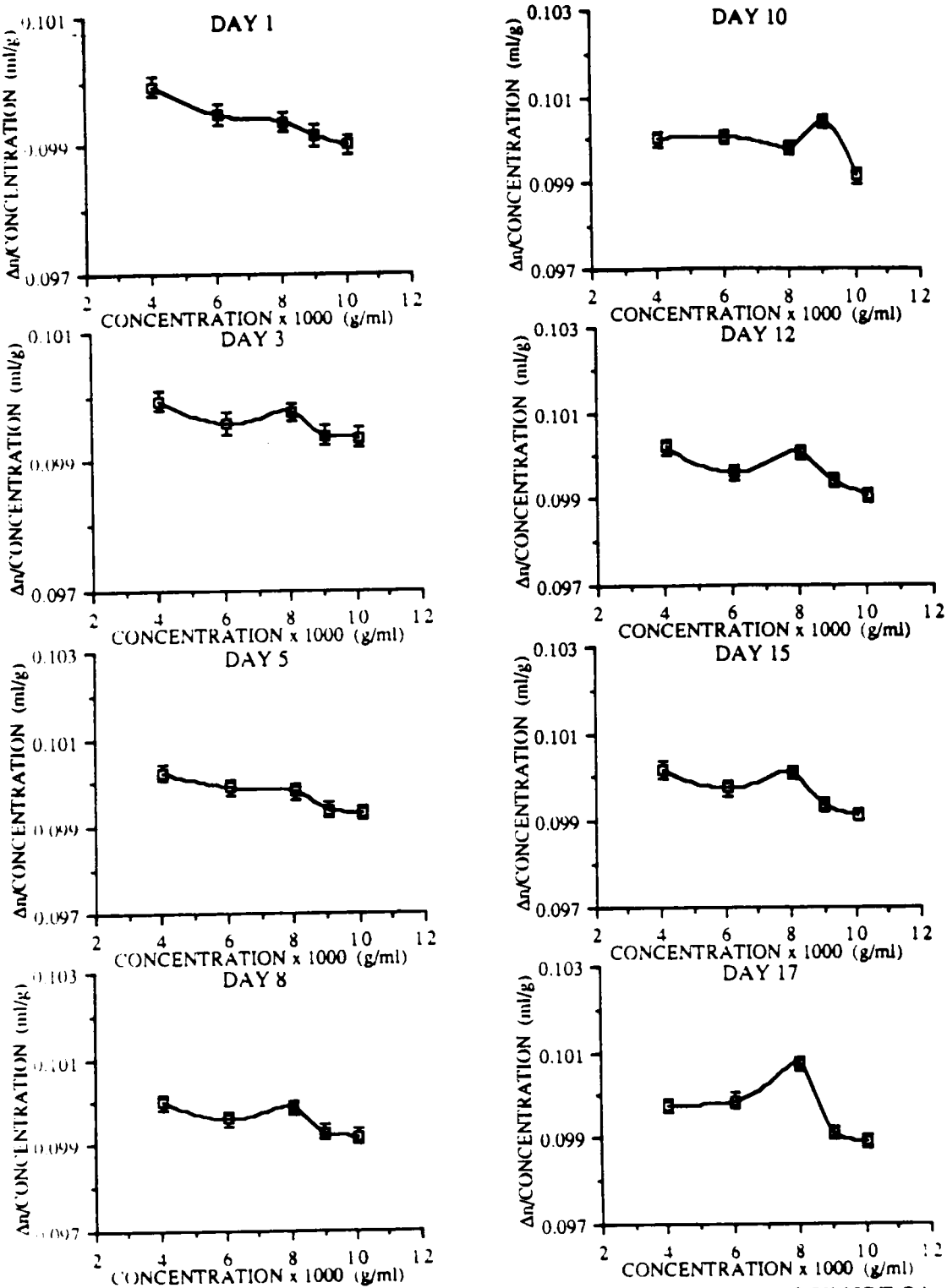

Figure 2.25: Concentration and time dependent changes in Δn/concentration for 13.5% NC/EtOAc

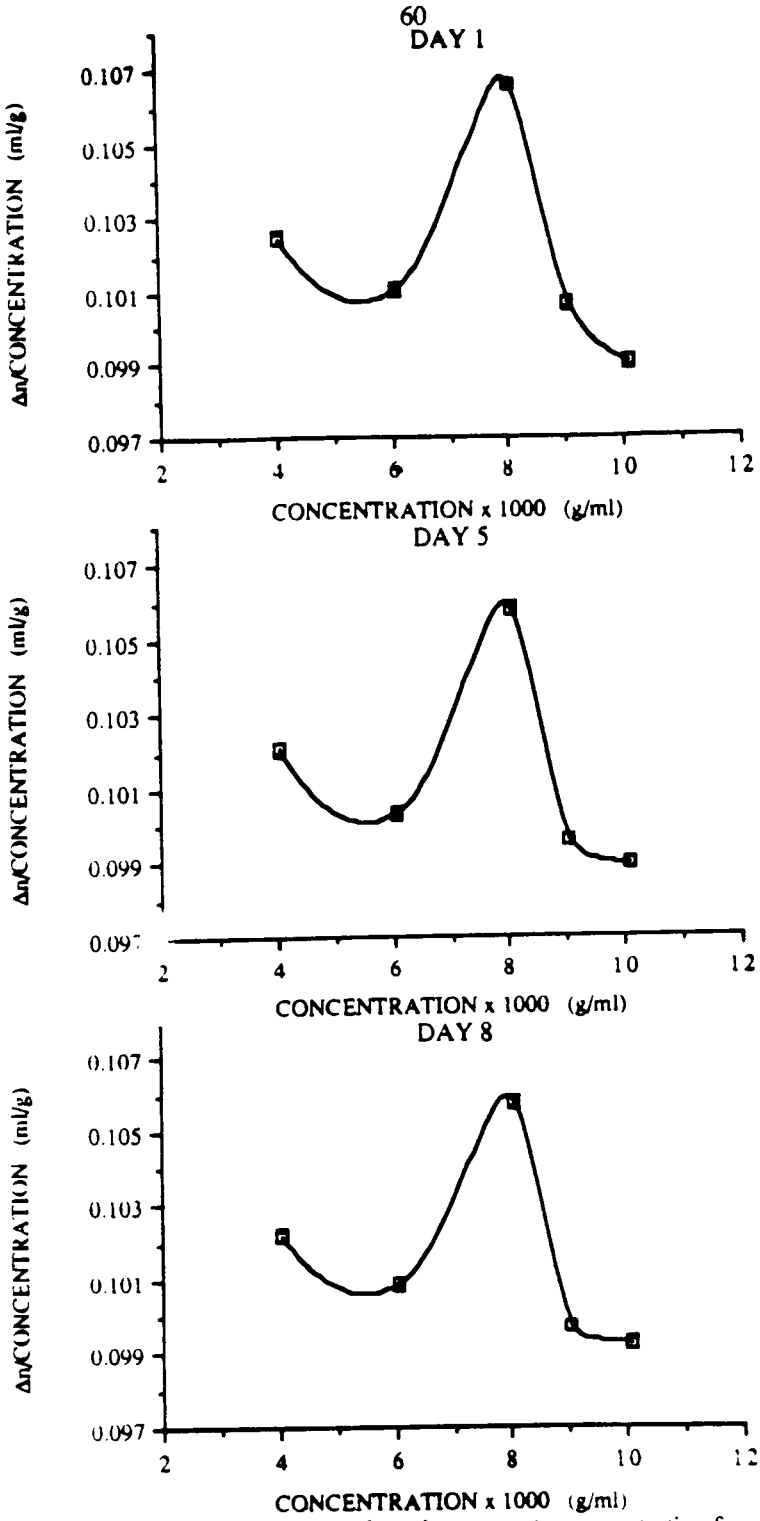

Figure 2.26: Concentration and time dependent changes in Δn/concentration for redissolved 13.5% NC/EtOAc.

2.4.2. Low Angle Laser Light Scattering

The results obtained from the static LALLS experiment are shown in Tables 2.6 and 2.7 for 12.58% and 13.5% nitrocellulose respectively. They include changes in absolute weight average molecular weight, $\overline{M}_w$, and second virial coefficient, A_2, over time for the systems examined. A composite of the molecular weight results for 12.58% NC in the three solvents utilized is shown in Figure 2.27. Details of the error analysis are given in the appendix.

It is interesting to note that for the THF solutions, the molecular weights obtained for the two types of THF did not follow the same trends until the sixth day, at which time the results were practically identical. The difference in results on the first four days of the experiments reflected the large difference in values of the dn/dc for the BHT containing solvent and the unstabilized THF. The precipitous drop in molecular weight on the 17th day may again be attributed to the effect of the behavior of the dn/dc on the molecular weight calculations for the stabilized solution. From the sixth day on to the 15th day, there was a similarity in the trends for both solvents -- both showed a slight decrease in molecular weight over time -- about 25% for THF and 15% for THF(NS). The decrease in molecular weight may be a result of several things. It is proposed here that the two mechanisms that may be responsible for this phenomenon are: (1) degradation by chain scission, and (2): a time dependent dissociation of aggregated NC molecules by solvation. The fact that the trend was seen in both cases weakens the argument that the decline in molecular weight was a result of degradation by chain scission through attack of any peroxide present in the unstabilized THF.

The results for the EtOAc solution were different in that the molecular weight was lower on the first day. This may be a result of EtOAc being a poorer solvent for NC. This being so, a longer time was required to dissolve the solute. The lower molecular weight may then be a consequence of having the incompletely dissolved higher molecular weight material filtered out during the LALLS experiment. The results for the third day tests were more in line with what was seen for the THF solutions. Just as for the

TABLE 2.6
LALLS Results for 12.58% Nitrocellulose

SOLVENT	DAY	$\overline{M}_w$ (g/mole)	ERROR (g/mole)	$A_2 \times 10^4$ (mol cm^3/g^2)	ERROR x 10^5 (mol cm^3/g^2)
THF	1	238398	6289	4.770	2.380
	3	227679	5403	7.273	2.150
	6	221797	5276	6.876	2.199
	8	214058	5746	8.303	2.537
	9	201291	4060	8.219	2.189
	13	163872	4198	11.526	3.256
	15	192997	5604	13.481	3.410
	17	173281	4759	12.051	3.342
THF(NS)	1	173041	4118	10.445	3.028
	3	194428	4391	10.693	2.458
	4	173380	3863	12.432	2.875
	7	219249	6963	9.971	3.094
	9	186887	5090	12.556	3.495
	11	186604	5204	10.434	2.957
	15	183711	4379	11.350	2.953
	17	112827	2925	17.853	5.038
EtOAc	1	94192	2568	-2.839	1.295
	3	287551	8115	6.485	4.164
	5	255030	5189	6.273	2.264
	8	253449	5164	5.767	2.109
	9	246444	5395	5.940	2.654
	11	259841	5875	6.526	2.508
	15	255336	5915	5.961	2.421
	17	264953	5896	6.664	2.250

TABLE 2.7
LALLS Results for 13.5% Nitrocellulose

SOLVENT	DAY	$\overline{M}_w$ (g/mole)	ERROR (g/mole)	$A_2 \times 10^4$ (mol cm^3/g^2)	ERROR $\times 10^4$ (mol cm^3/g^2)
THF	1	182014	12599	12.996	1.352
	3	129000	4318	5.962	1.039
	5	163038	8857	12.820	1.200
	8	115456	4558	7.783	1.340
	10	118244	5199	11.210	1.833
	12	97920	3210	10.324	1.330
	14	95614	3883	9.867	1.541
	17	92798	3843	10.420	1.757
THF(NS)	1	77238	3215	18.804	1.380
	3	131323	3449	11.276	0.504
	5	128833	3598	13.607	0.485
	8	131844	3009	9.628	0.374
	9	135884	4479	11.214	0.488
	11	145638	2944	7.913	0.293
	15	118252	4024	15.678	0.599
	17	144577	4869	10.900	0.340
EtOAc	1	227295	9705	11.781	1.506
	3	192990	6466	0.723	1.447
	5	291424	13826	23.866	1.019
	8	190164	5134	9.075	0.823
	10	184564	5766	10.400	1.017
	12	169964	4768	5.837	0.945
	15	181384	6188	5.945	0.883
	17	179275	4141	6.497	0.573

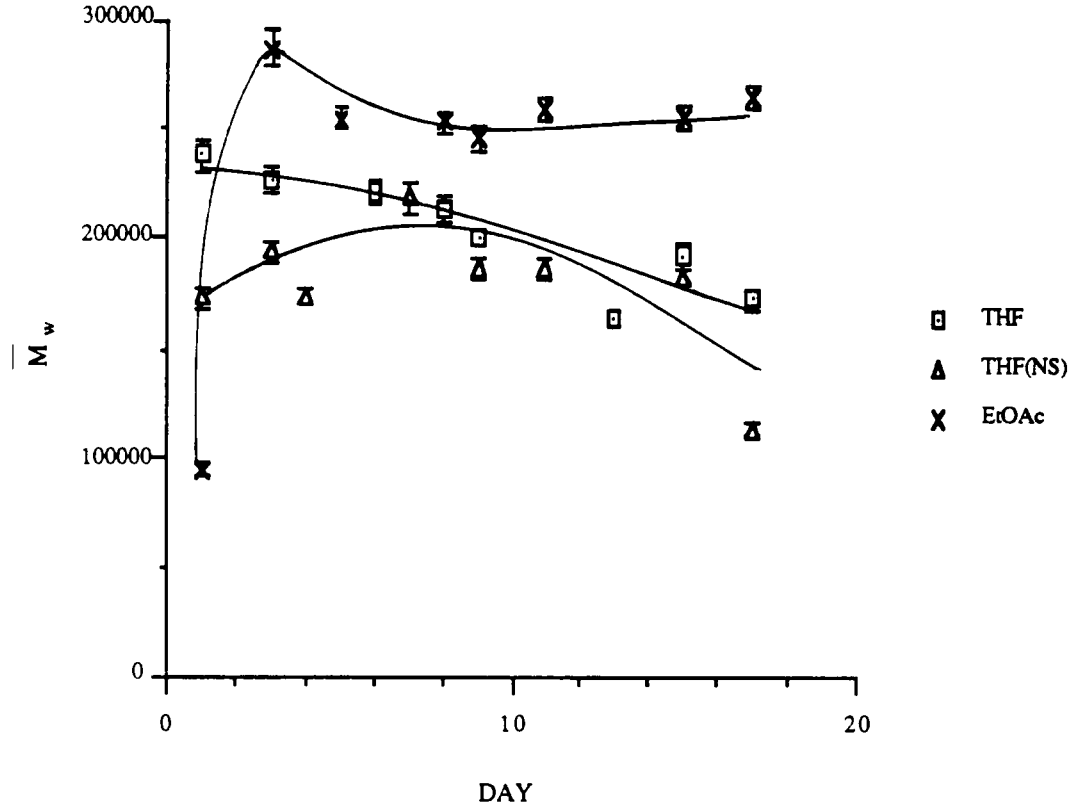

Figure 2.27: Change in $\overline{M}_w$ determined by LALLS over time for 12.58% nitrocellulose.

THF solutions, there was a slight decrease in molecular weight after the fifth day. This was of the order of about 11%. The values remained constant after that.

In all solvents, it is clear that the molecular weight dropped to an "equilibrium" value after a few days in solution. A clue as to what could physically be happening to cause the observed changes may be extracted by looking at the accompanying changes in second virial coefficient in these solutions. These results are shown in Figure 2.28. One may notice that the values of A_2 for the EtOAc solutions were always lower than those for the THF solutions and especially poor initially. Since A_2 is an indication of solvent polymer interactions, this suggests that THF with or without the BHT was a better solvent fo NC than EtOAc. This postulate is consistent with the solubility parameter results quoted earlier.

The value of A_2 for the EtOAc solution was negative on the first day. This is a clue pointing to the aggregation of the nitrocellulose molecules in this inferior solvent. The quantity became positive on the third day and remained relatively constant afterwards while those for THF tended to increase. Putting these results together with those obtained from the molecular weight measurements, it is proposed that nitrocellulose molecules associate in solution and the decrease in molecular weight with time was caused by an increase in solvent/polymer interaction. That is, over time, in an environment of a good solvent, these clusters of molecules are broken up by the increased solvation. If this were so, then liquids with greater solvent power would yield smaller "clusters" at equilibrium. This model is consistent with the finding that one obtains lower molecular weights with good solvents compared to poor solvents. At the same time, it explains the increase in A_2 observed for the better solvent systems.

The results for molecular weight determination of the 13.5% NC series are shown in Figure 2.29. In this case, the results for the THF solutions and THF(NS) solutions were similar to those seen for the 12.58% NC in that the molecular weight agreed only after a few days in solution. The molecular weight in THF consistently decreased until it reached an "equilibrium" value that was about 45% lower than the value on the first day. In contrast to 12.58% NC, the molecular weight in EtOAc started out being highest on the first day of the experiment. Just as in the case of the less nitrated analog, the EtOAc solution yielded

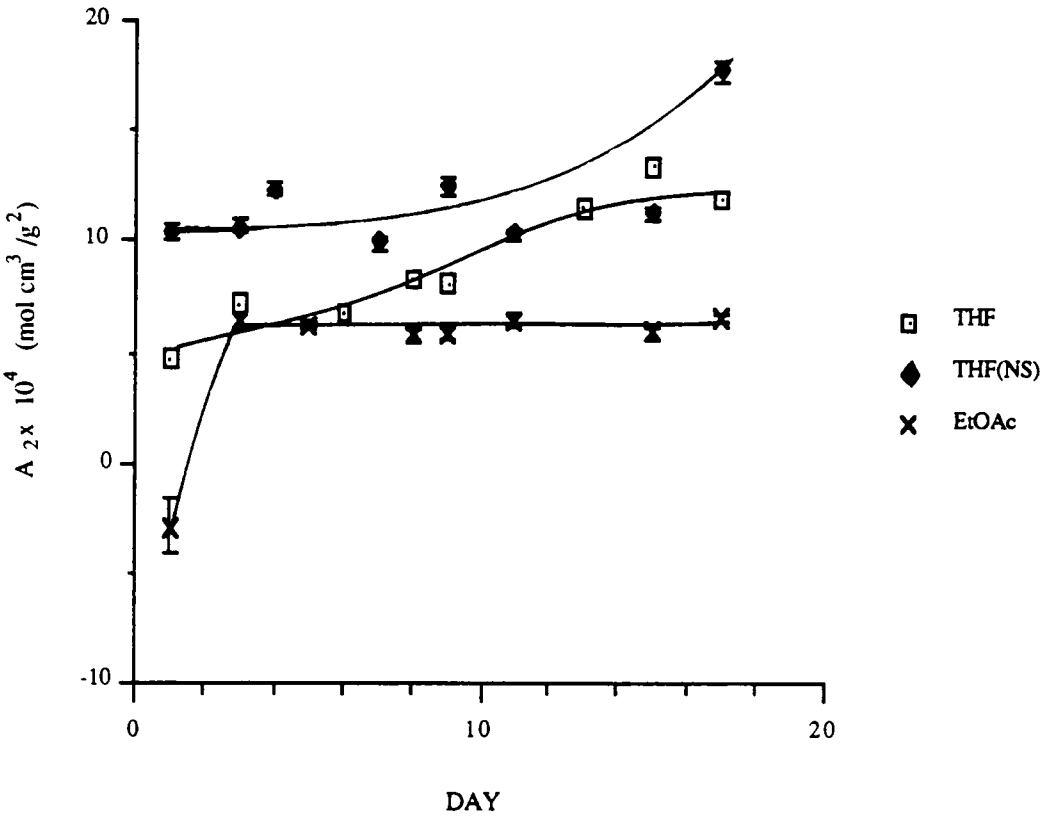

Figure 2.28: Change in second virial coefficient over time for 12.58% nitrocellulose.

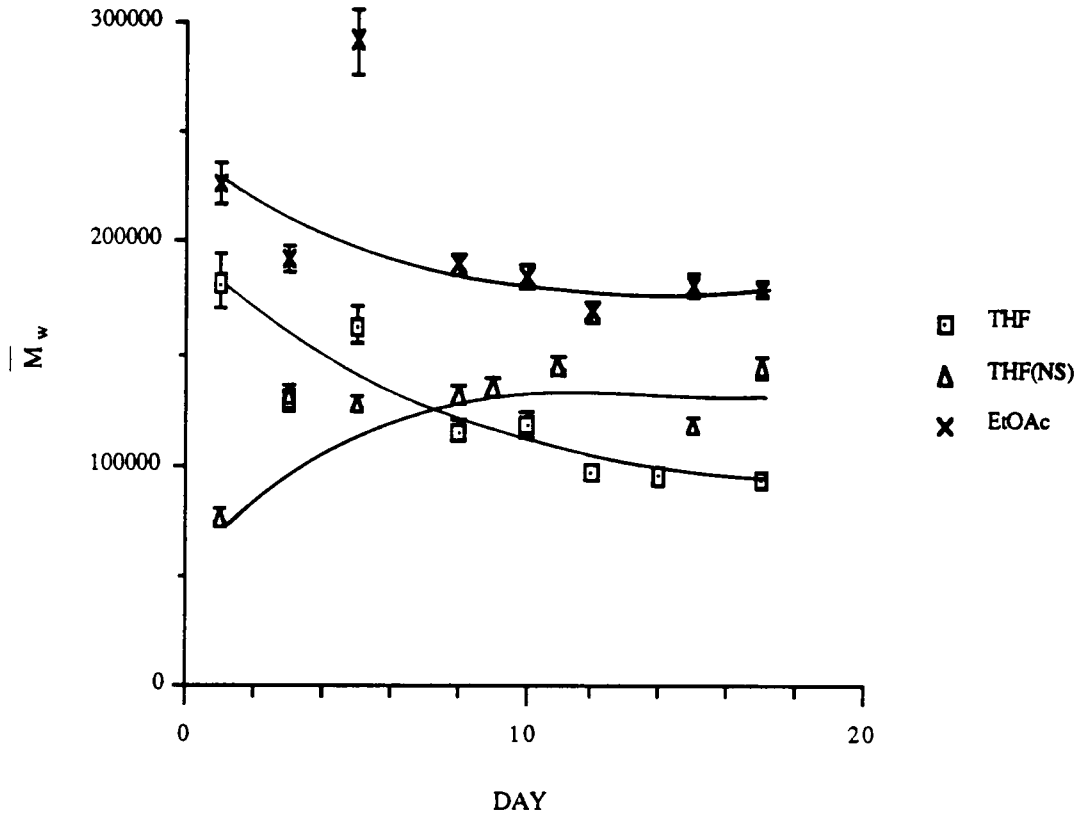

Figure 2.29: Change in molecular weight determined by LALLS over time for 13.5% nitrocellulose.

higher molecular weights than the THF solutions throughout the whole experiment. The equilibrium value was about 20% lower than the original value and plateaued more rapidly than the other systems. Again, this was perhaps a manifestation of the greater degree of chain extension known to exist in the more highly nitrated analog of NC. The greater degree of nitration resulted in a decreased number of hydroxyl groups which were responsible for association brought about by hydrogen bonding. Once more, since EtOAc was a poorer solvent, the molecular weight determined in this solvent was greater than that obtained in THF. The value of $\overline{M}_w$ in this solvent also remained relatively constant over the days in which the experiments were conducted. This was a reflection of the inability of the poorer solvent to break up the higher molecular weight aggregates.

The A_2 for the three systems now under discussion are shown in Figure 2.30. The overlap in error bars precludes the extraction of any sensible trends. Perhaps this lack of distinguishability in solvent/polymer interaction was a result of the greater extension in the chains of the more nitrated analog. With greater chain extension, the solvation process was aided, therefore, the effect of the solvation was diminished. It was not completely obliterated however, as evidenced by the dependence of the molecular weights on the solvent.

The proposed model for what may be occurring in the 12.58% NC systems holds here. An added dimension may be injected if one takes into consideration the possibility of better alignment possible in the more extended chains. This may result in the formation of crystallites in solution initially. In a parallel argument as that put forth for the 12.58% solutions, solvation may destroy this order, resulting in species with lower apparent molecular weights.

One may also entertain the possibility that the changes discussed above were brought about by degradation via chain scission during storage. Certainly, this would explain the more pronounced decrease in $\overline{M}_w$ in THF, since peroxides that may have been present can very well have initiated degradation. For the moment, this phenomenon cannot be completely eliminated. Further experiments which will be discussed

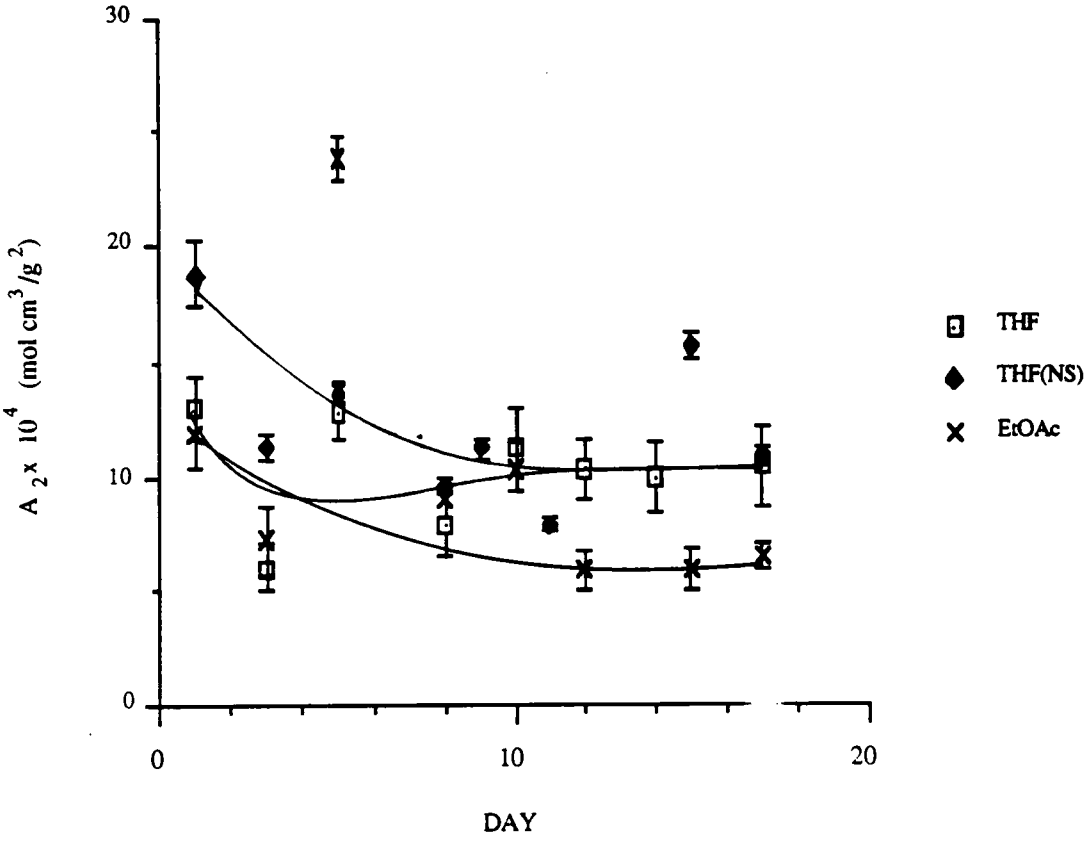

Figure 2.30: Change in second virial coefficients over time for 13.5% nitrocellulose.

subsequently contribute to this issue. Before those data are presented, further evidence on changes in molecular weight on aging will be presented.

2.4.3. Gel Permeation Chromatography

Gel permeation chromatography was used to determine molecular weight changes of nitrocellulose. Because the universal calibration was employed, absolute molecular weights were obtained. These numbers may be directly compared to the absolute values obtained independently by the static LALLS measurements. Due to solvent/column packing compatibility, the investigation was constrained to the use of unstabilized THF.

Duplicate runs were made for each sample on a given day. The results from this experiments are given in Table 2.8. The changes in weight average molecular weight of 12.58% NC/THF are shown in Figure 2.31. The error bars are the standard deviations in the results. The molecular weight dropped by about 40% in the course of two weeks. In addition to this, the ***values of $\overline{M}_w$ obtained here were within 1% of those obtained by LALLS for the first day of the experiment.*** The disparity increased to 12% on the 18th day. The trends were similar for both methods in that the decrease in molecular weight was gradual over the first week, most rapid in the second week, then slowed down again by the third week.

Figure 2.32 is the analogous result for 13.5% NC/THF. Once again, the trend shown here is in agreement with that obtained by the LALLS. The numerical agreement in results between LALLS and GPC/DV was not as good for 13.5% NC as it was for 12.58% NC. ***The variation on the first day was of the order of 12%.*** This disparity increased to 55% by the 18th day. The discrepancy may have been brought about by the more extended conformation for the 13.5% NC which makes it resemble a rigid rod. Perhaps the universal calibration was not applicable to this polymer as it approached optimum solvation over time. The acceptable agreement of results in the course of the experiment for the less nitrated analog may indicate that even with solvation of 12.58% at its optimum, the chain was not fully extended.

TABLE 2.8
Weight Average Molecular Weights From GPC

SAMPLE	DAY	$\overline{M}_w \times 10^{-5}$ (g/mole)	DEVIATION $\times 10^{-3}$ (g/mole)
12.58% NC	1	2.408	4.879
	3	2.392	0.566
	5	2.486	37.340
	7	2.022	5.940
	14	1.504	3.606
	18	1.529	0.000
	21	1.312	3.465
13.5% NC	1	2.042	18.170
	3	1.870	2.051
	5	1.790	5.657
	7	1.662	4.384
	14	1.508	4.031
	18	1.434	7.778
	21	1.382	12.450

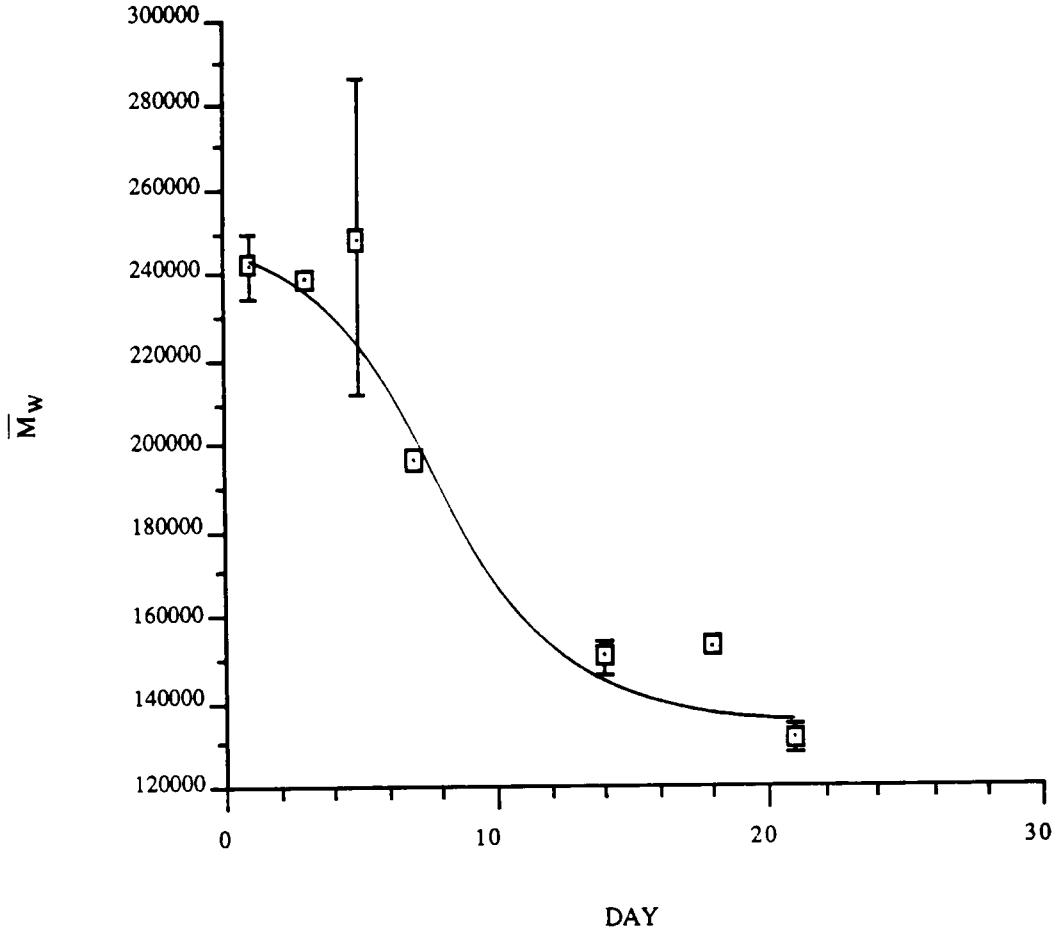

Figure 2.31: Change in weight average molecular weight determined by GPC over time for 12.58% nitrocellulose.

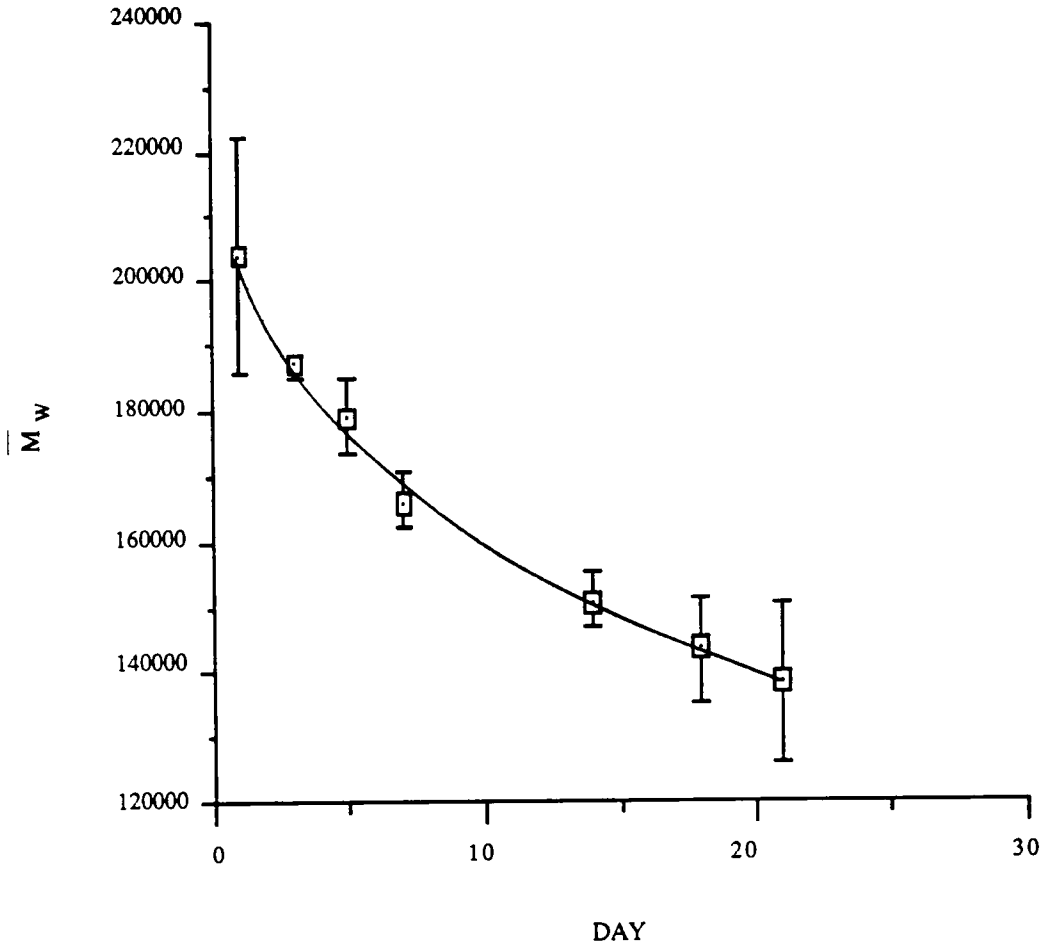

Figure 2.32: Change in weight average molecular weight determined by GPC over time for 13.5% nitrocellulose.

In confirming the results obtained by static LALLS, the above findings demonstrated the validity of the universal calibration method as applied to 13.5% nitrocellulose in the initial stages of the experiment and throughout this time period for the 12.58% nitrocellulose. This is in agreement with what most investigators have found in more tedious ways, since most researchers ignored the presence of this time dependent phenomenon (25,33,34,39,51-53). The consistency of results obtained from the two methods of molecular weight determination allows a claim that the results shown in Figures 2.33 and 2.34 are changes in the absolute molecular weight distributions of 12.58% and 13.5% NC respectively. The areas under the curve did not stay the same as expected because only every tenth collected datum was used in the construction of the plot. The same area would have been obtained had every point been used. ***In both cases, the distribution narrowed over a period of 21 days.*** The change in the polydispersity per week is given in Table 2.9 for the data shown in Figures 2.33 and 2.34. A simple calculation would show that the polydispersity of 12.58% NC decreased by 22% over 21 days and that for 13.5% by 29% over the same time period. Furthermore, the narrowing occurred as a result of the higher molecular weight end moving towards lower molecular weights, while the lower molecular weight end remained mostly unchanged. This result was in agreement with the proposed model that the observed shifts in molecular weight were due to a physical change occurring during aging. That is, the molecules initially existed as aggregates when dissolved. These clusters were slowly broken up as a result of better solvation by the solvent molecules. The shift only in the high molecular weight end was consistent with the postulate that aggregated molecules were present in solution initially. These clusters were broken up resulting in a general decrease in molecular weight. Meanwhile, the low molecular weight end remained stationary because these molecules were already at an "equilibrium" state. A slight increase in the concentration of lower molecular weight material was visible over time. These two facts would be consistent with the formation of smaller molecules as a result of dissociation of aggregates by solvation and the absence of degradation by chain scission.

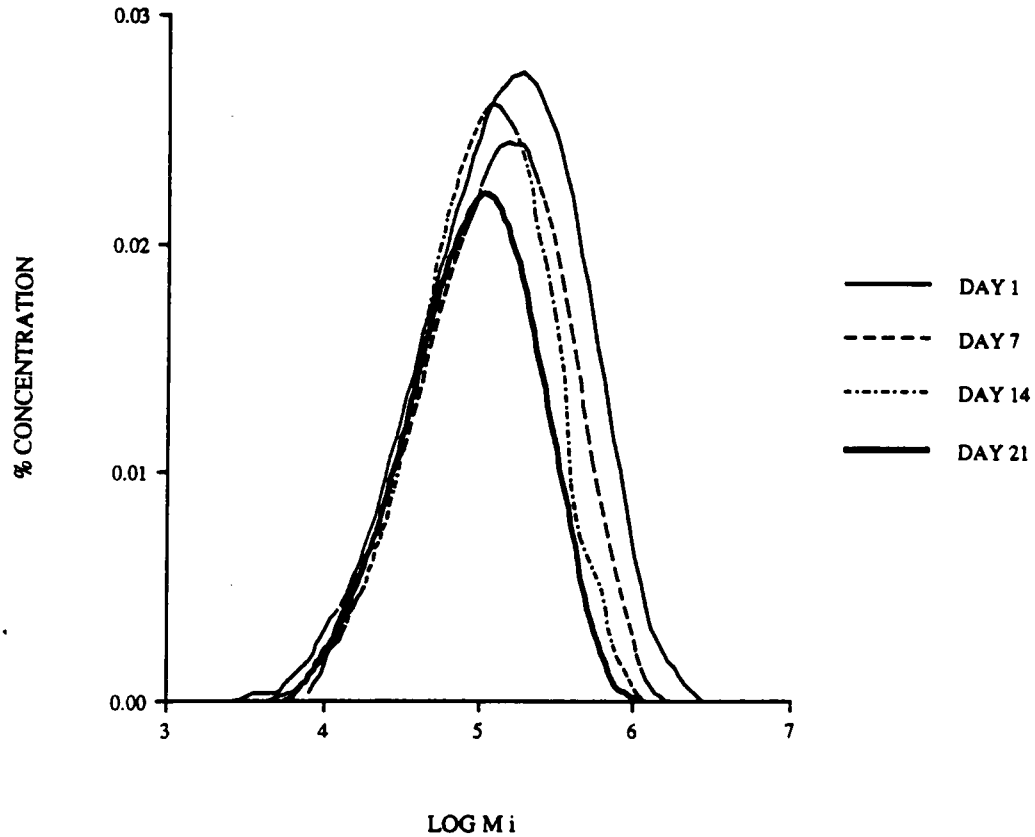

Figure 2.33: Change in molecular weight distribution of 12.58% nitrocellulose over time.

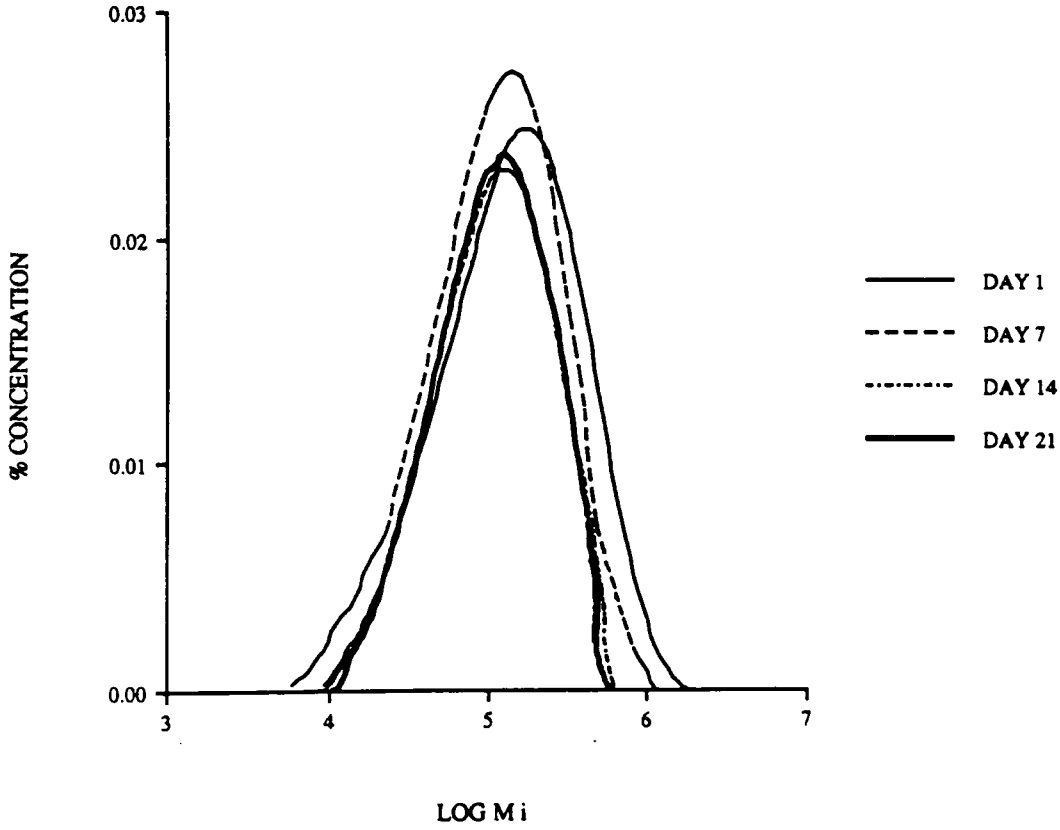

Figure 2.34: Change in molecular weight distribution of 13.5% nitrocellulose over time.

TABLE 2.9
Time Dependent Changes in Polydispersity of Nitrocellulose

SAMPLE	DAY	POLYDISPERSITY
12.58% NC	1	2.437
	7	2.275
	14	2.219
	21	1.913
13.5% NC	1	3.198
	7	2.808
	14	2.367
	21	2.292

For the sake of argument, one may again postulate that degradation was the mechanism for the changes observed. Looking at the data on absolute MWD one may argue that the larger molecules would be more susceptible to chain scission than the smaller molecules. However, this contention suffers in that if chain scission were random, then it should occur in the shorter chains as well as in the longer chains, though not as often. This being the case, the entire distribution should have shifted to lower molecular weights to reflect the loss of longer chains and the formation of lower molecular weight fragments. This complete shift was not visible in the results shown. Although the evidence here appear to lean towards the postulate that the decrease in molecular weight was due to dissociation, one may not say that they are absolutely conclusive. This provided the impetus for further experiments.

2.4.4. Infrared Spectroscopy

In an attempt to understand what may be happening at the molecular level, IR experiments were conducted on solutions exposed to various treatments. However, only qualitative information was expected; therefore, no attempts were made to monitor film thicknesses. The analysis thus boiled down to a comparison of the presence or absence of absorbances at various wavenumbers with changes in peak intensities not taken into consideration.

2.4.4.1. Infrared Spectroscopy of Aged Samples

Figure 2.35 contains the spectra taken for films made from a 1% solution of 12.58% NC/THF. The peak designations are given in Table 2.10. The spectra were ***identical*** over the 22 day period, thus indicating that no change in chemical structure occurred in this period. The solvent was evaporated slowly and the dried films were redissolved one week later. In addition, a separate experiment was conducted where the dried films stood for approximately six months before redissolution. A comparison of the spectra from these two samples is shown in Figure 2.36. The films that did not age for six months after evaporation showed the same spectra as before they were redissolved. However, the spectra obtained from films made with the samples redissolved six months after evaporation had an absorbance at 1770 cm^{-1} wavenumbers. This absorbance is characteristic of a carbonyl group. The carbonyl group could very well have resulted

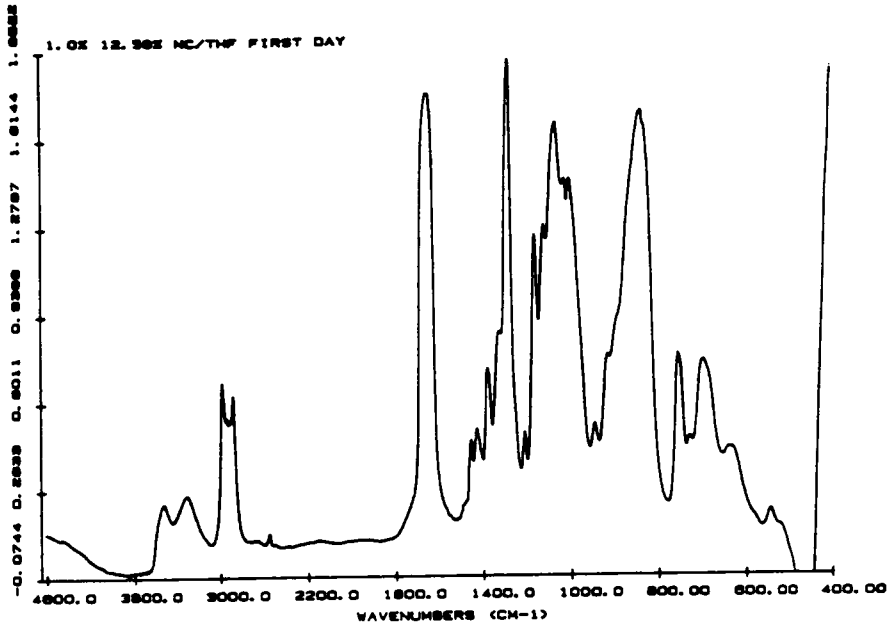

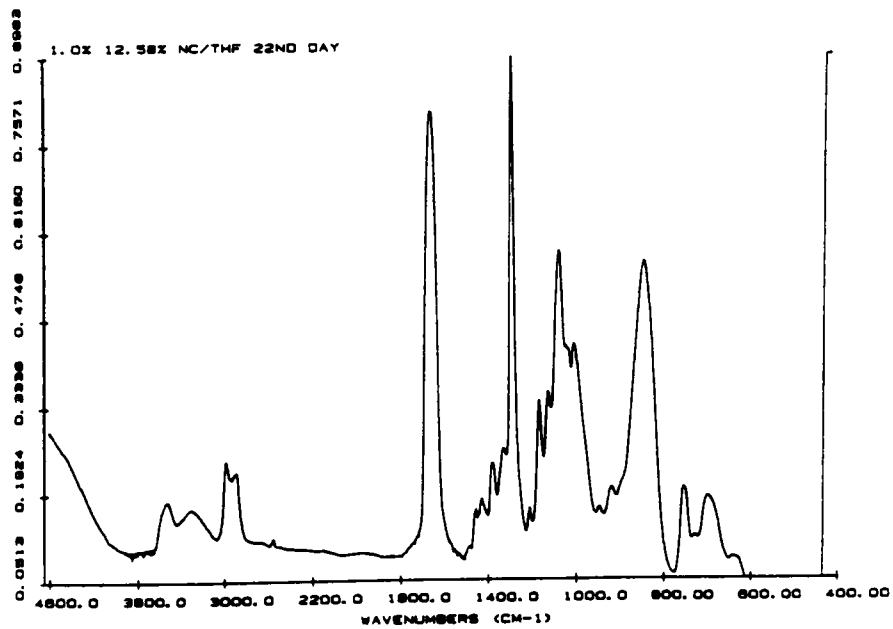

Figure 2.35: Infrared spectra of films made from aged 1.0% NC/THF solutions.

TABLE 2.10
Peak Designation for Infrared Spectra of Nitrocellulose (86,107)

WAVENUMBER (cm^{-1})	FUNCTIONAL GROUP
3566 - 3534	Intermolecularly bonded hydroxyl
3312	Weakly intramolecularly bonded hydroxyl
1770	Carbonyl group
1729	Carboxyl group from ester
1425 - 1278	Symmetrical vibration of NO_2
1163 - 1007	Asymmetrical C--0--C stretching
835	N--O linkage π bond stretching
753 - 695	NO_2 bending vibrations

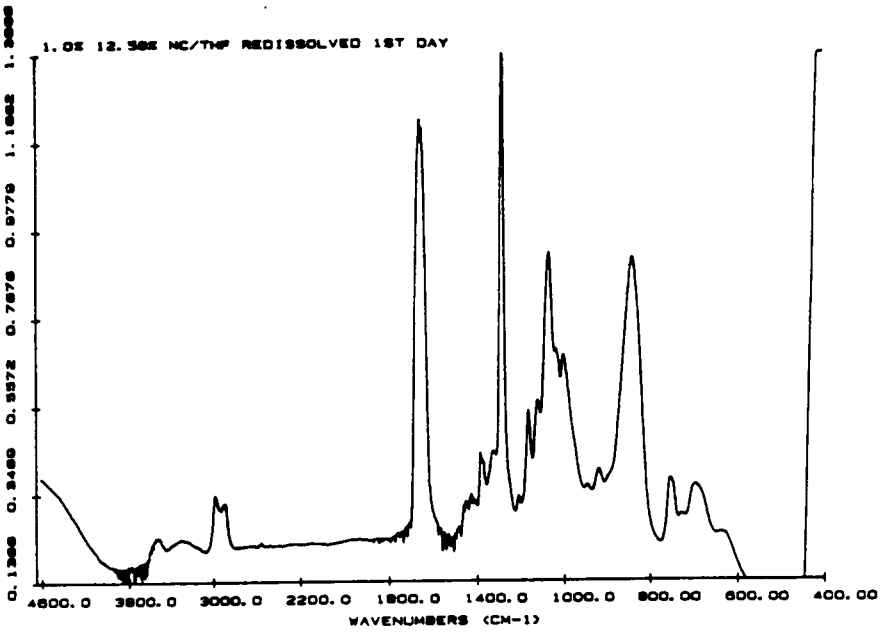

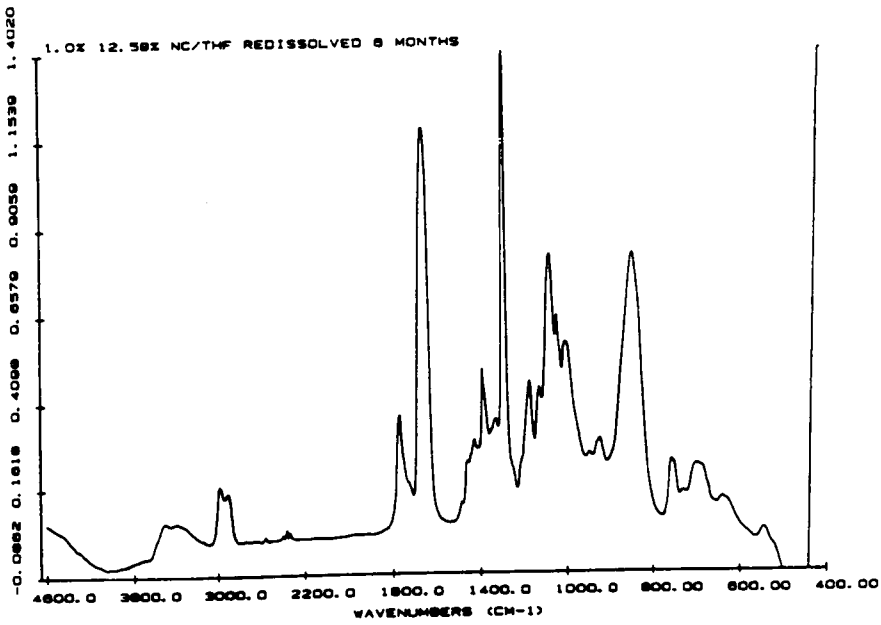

Figure 2.36: Infrared spectra of films made from redissolved 12.58% NC/THF.

from degradation by chain scission between the anhydroglucose units of the nitrocellulose (85). These results suggest that there was ***no chemical degradation significant enough for IR detection over a period of about 40 days.*** However, sometime between 40 days and six months, chemical degradation did occur.

Figure 2.37 contains a comparison of spectra taken from a film made from a 1% solution of 12.58% NC/EtOAc. The spectra were taken over a three week period where films were made from solutions standing quiescent during that time. The IR peak designations are given in Table 2.10. One of the differences between these spectra and the ones obtained for the THF solutions is the shoulder appearing on the absorbance at 1729 cm^{-1} wavenumbers. Since it represents the ester functionality and was absent from the spectra taken of films cast from the THF solutions, it is believed to be due to residual solvent. In addition, a broad peak appeared at 3550 cm^{-1} which is in the realm of intermolecularly bonded hydroxyl groups. The absorbance here due to weak intramolecular hydroxyl bonding was absent. The spectra for the films did not change over the 22 day period. The same results were obtained after the solvent was evaporated and the films were redissolved to their concentration before evaporation. It thus appears that ***no chemical change*** occurred over this time for 12.58% NC/EtOAc.

Figure 2.38 contains a comparison of the IR spectra obtained of films made from 1% solutions of 13.5% NC/THF on different days. The designations for the absorbances are given in Table 2.10. The spectra looked identical up to the 15th day. On the 22nd day, however, one can notice the beginnings of a peak at 1770 cm^{-1} wavenumbers where the carbonyl group is expected to absorb. This peak persisted even after evaporation and redissolution of the sample as shown in Figure 2.39.. It thus appears that ***13.5% NC in THF may start to degrade after a 15 - 20 day aging period.***

Finally, the IR spectra taken of films made from 1% solutions of 13.5% NC/EtOAc are shown in Figure 2.40. The peak designations are similar to those given for films made from 12.58% NC/EtOAc given in Table 2.10. Like the results for 12.58% NC/EtOAc, the spectra for 13.5% NC/EtOAc revealed

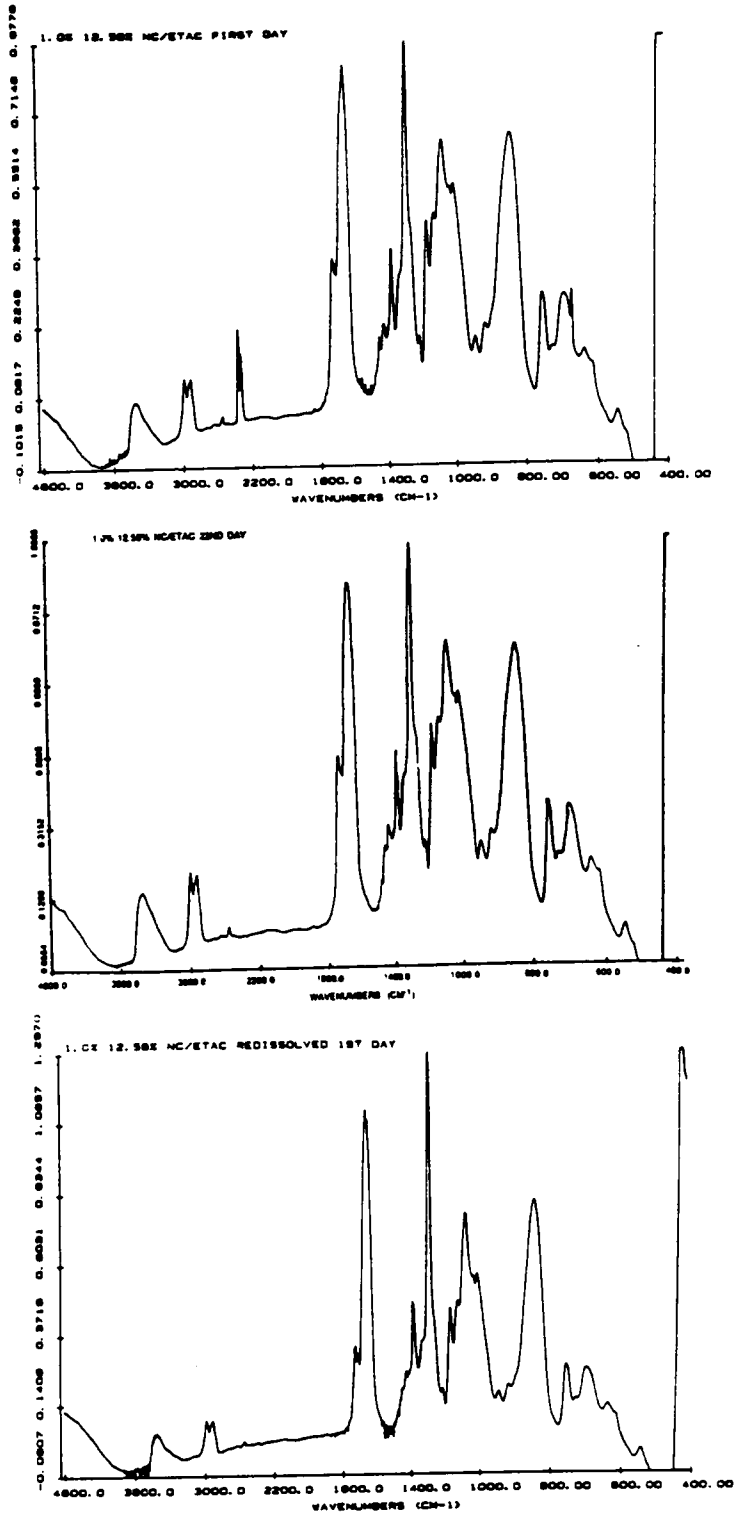

Figure 2.37: Infrared spectra of films made from aged 1.0% NC/EtOAc solutions.

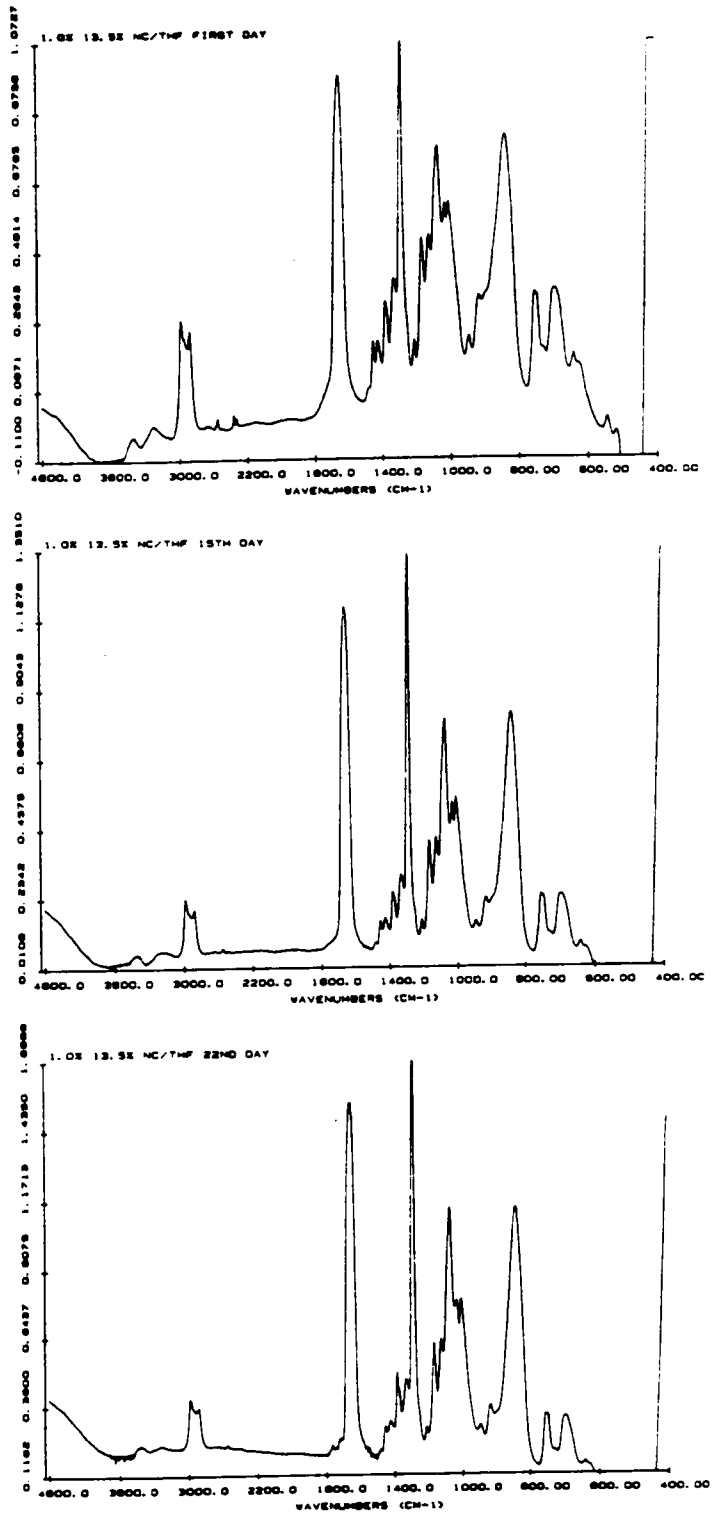

Figure 2.38: Infrared spectra of films made from aged 13.5% NC/THF solutions.

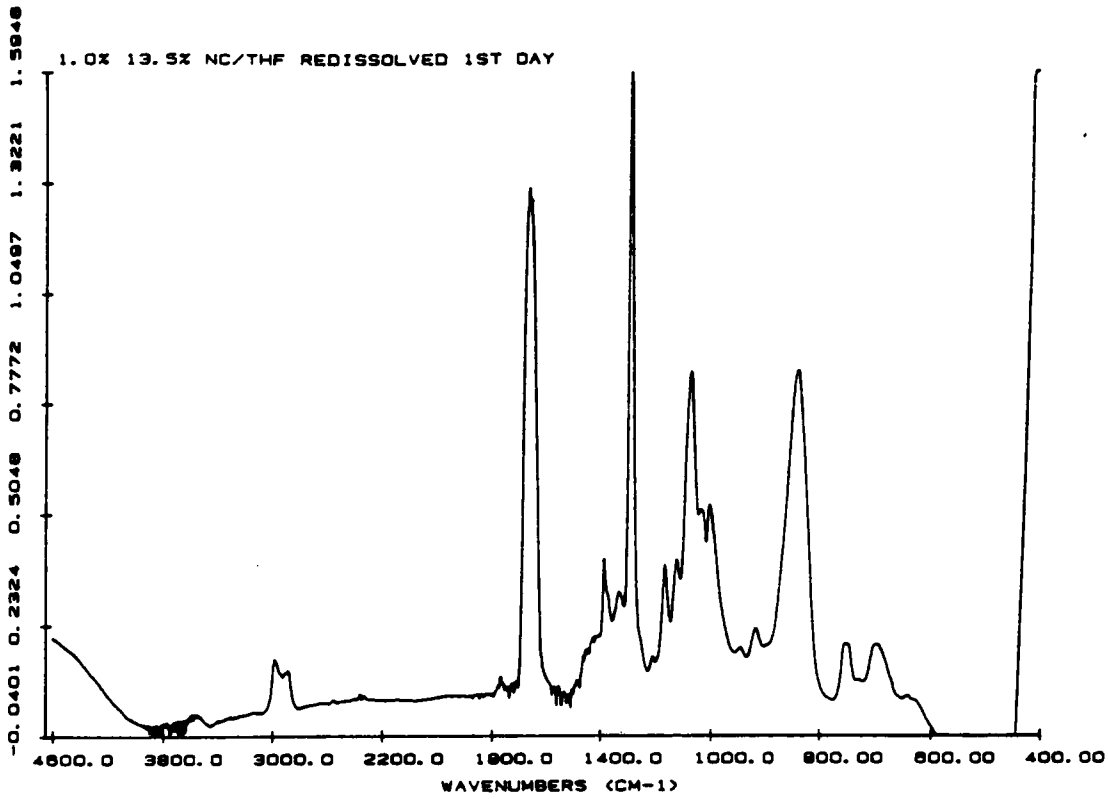

Figure 2.39: Infrared spectrum of film made from redissolved 1.0% solution of 13.5% NC/THF.

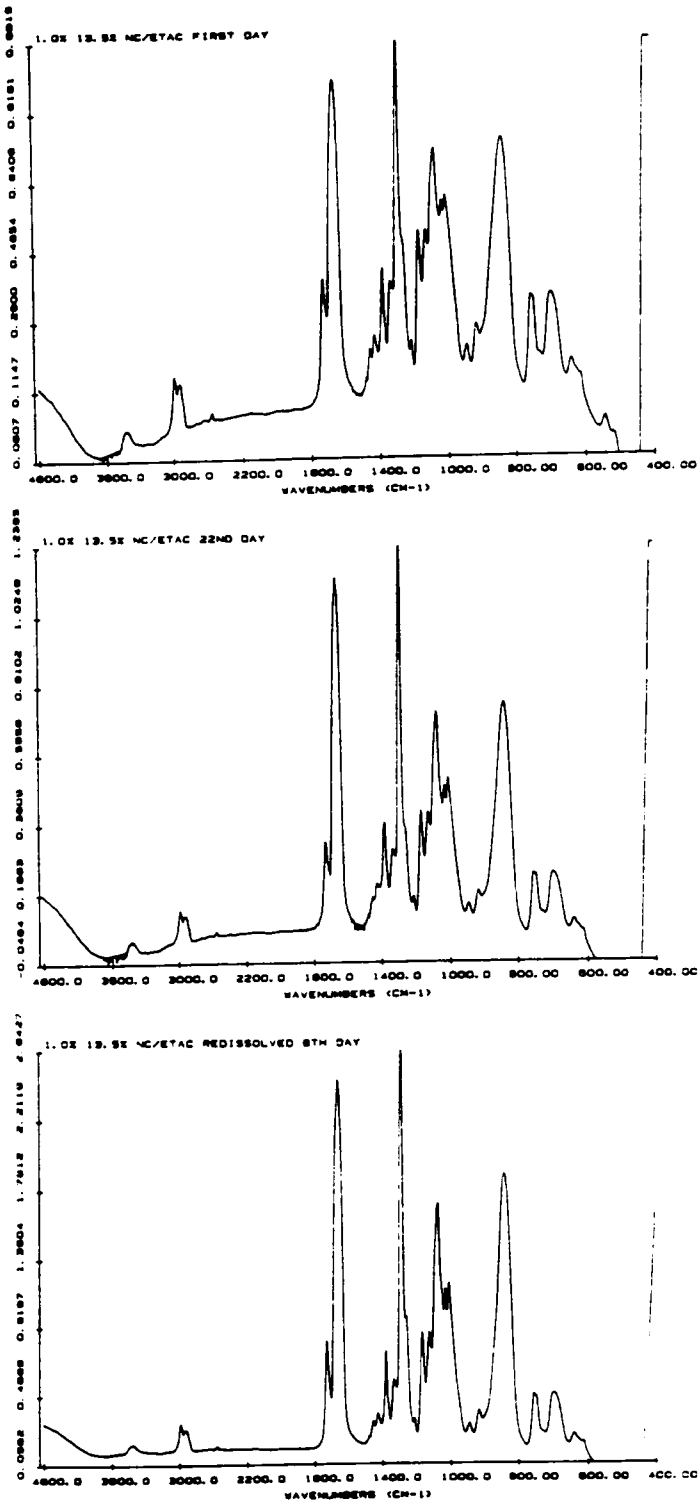

Figure 2.40: Infrared spectra of films made from aged 1% 13.5% NC/EtOAc solutions.

that ***no chemical degradation occurred over the approximately 40 day period*** of the investigation which included aging, evaporation and redissolution of the sample.

The IR results for the untreated (no physical or chemical aggressors) solutions of 12.58% and 13.5% NC in EtOAc and THF revealed that no significant chemical degradation was detectable over the three weeks except for the 13.5% NC/THF system. This weakens the argument for using degradation by chain scission to explain the decrease of molecular weights observed in the GPC and the LALLS experiments. However, this does not absolutely eliminate degradation as a mechanism because it is possible that very little chain scission was required to cut molecular weights to the extents observed; this little amount of chain scission may not be detectable by IR.

2.4.4.2. Infrared Spectroscopy of Sonicated Samples

Figure 2.41 is the set of spectra obtained for films made from sonicated 1.0% 12.58% NC/THF solutions. Sonication initially did not appear to alter the structures of the NC. However, after 15 days, a small peak at about 1770 cm^{-1} started to be apparent. This wavenumber corresponds to an aldehyde absorption. It thus appears that sonication of films from THF solutions caused degradation by chain scission. The spectrum shown in Figure 2.42 does not exhibit a significant increase in the carbonyl peak intensity after evaporation of the solvent and redissolution.

Spectra taken from films made with sonicated 0.1% NC/EtOAc solutions are shown in Figure 2.43. The most significant difference in absorbances was seen in the spectra for the first day where the two peaks at about 1278 and 1376 cm^{-1} reversed in intensity after sonication. After aging for one week, the spectra reverted to what it looked like for the untreated solutions. Additional sonication appeared to increase the resolution of the symmetric NO_2 absorption to a certain extent. More sonication 15 days after initial treatment resulted in an absorbance at around 1770 cm^{-1} where a carbonyl group is expected to absorb. The tiny peak persisted after solvent was evaporated and the sample was redissolved. Evaporation of the solvent and redissolution yielded a film whose spectrum resembled that obtained before evaporation. It appears that sonication of samples made from 0.1% 12.58% NC/EtOAc solutions did not suffer degradation by chain

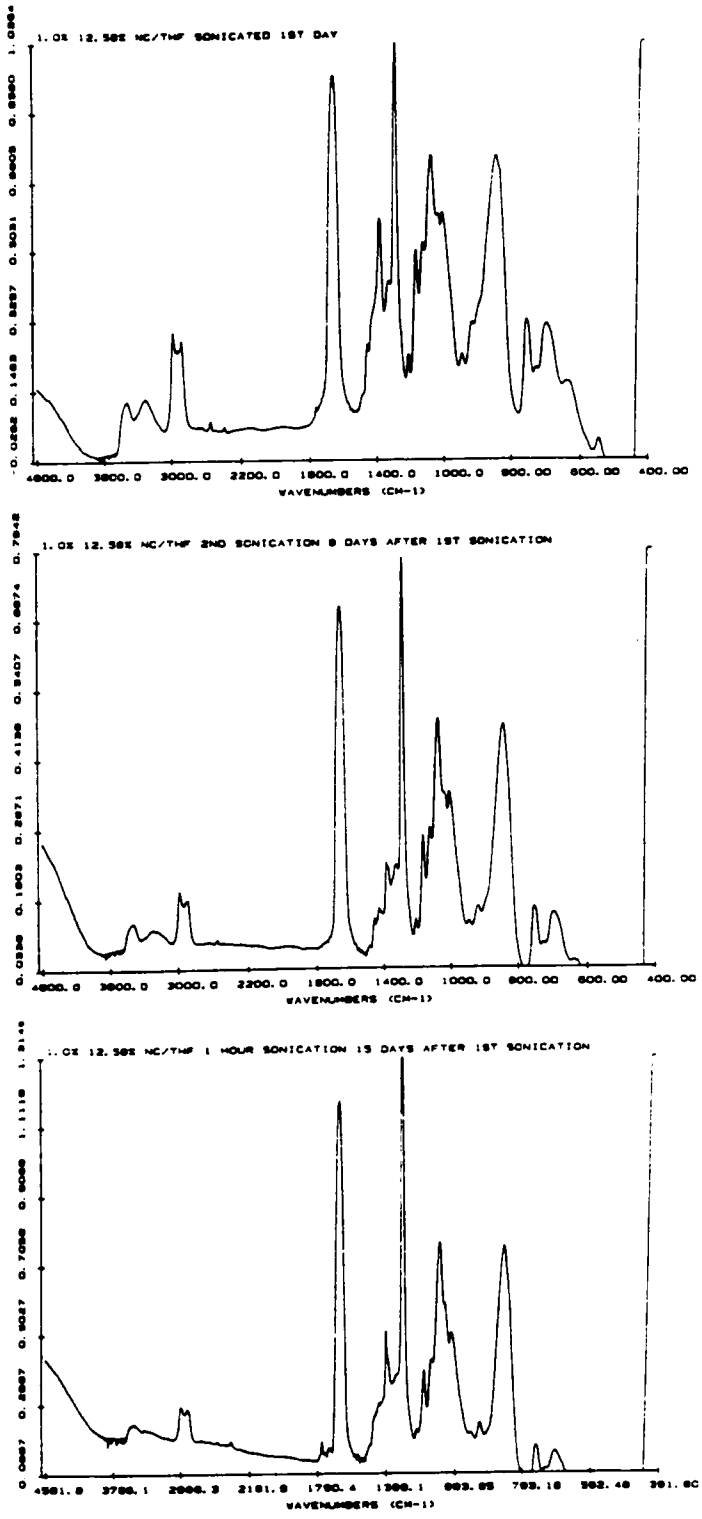

Figure 2.41: Infrared spectra of films made from sonicated 1.0% 12.58% NC/THF.

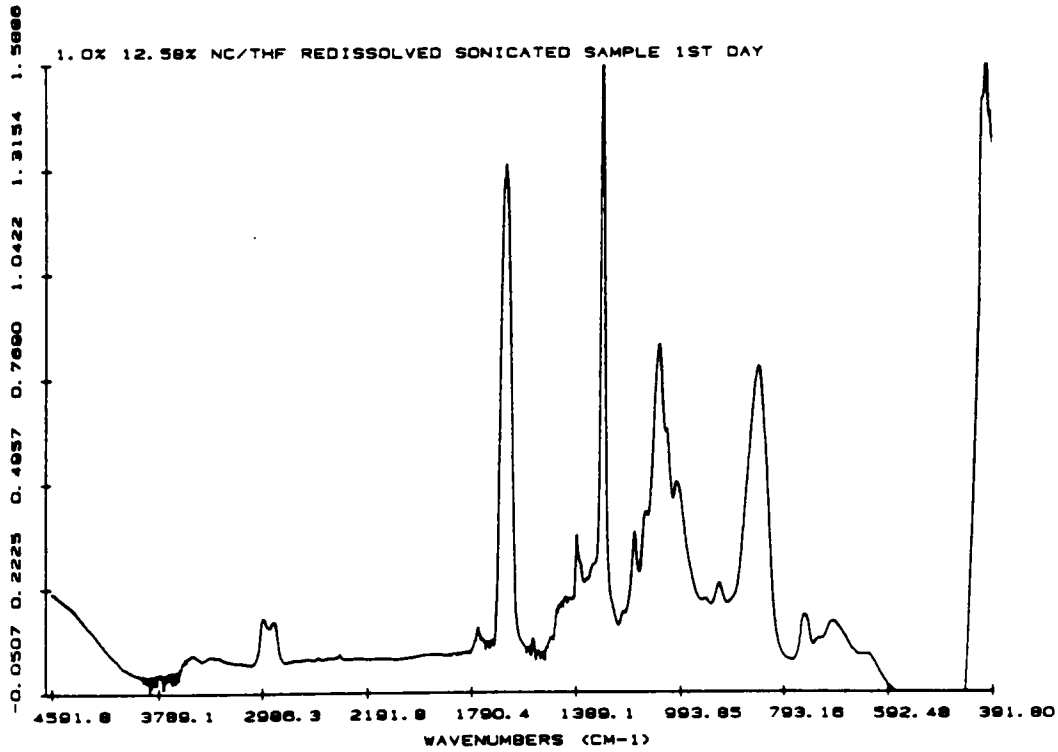

Figure 2.42: Infrared spectra of films made from redissolved sonicated 1.0% 12.58% NC/THF.

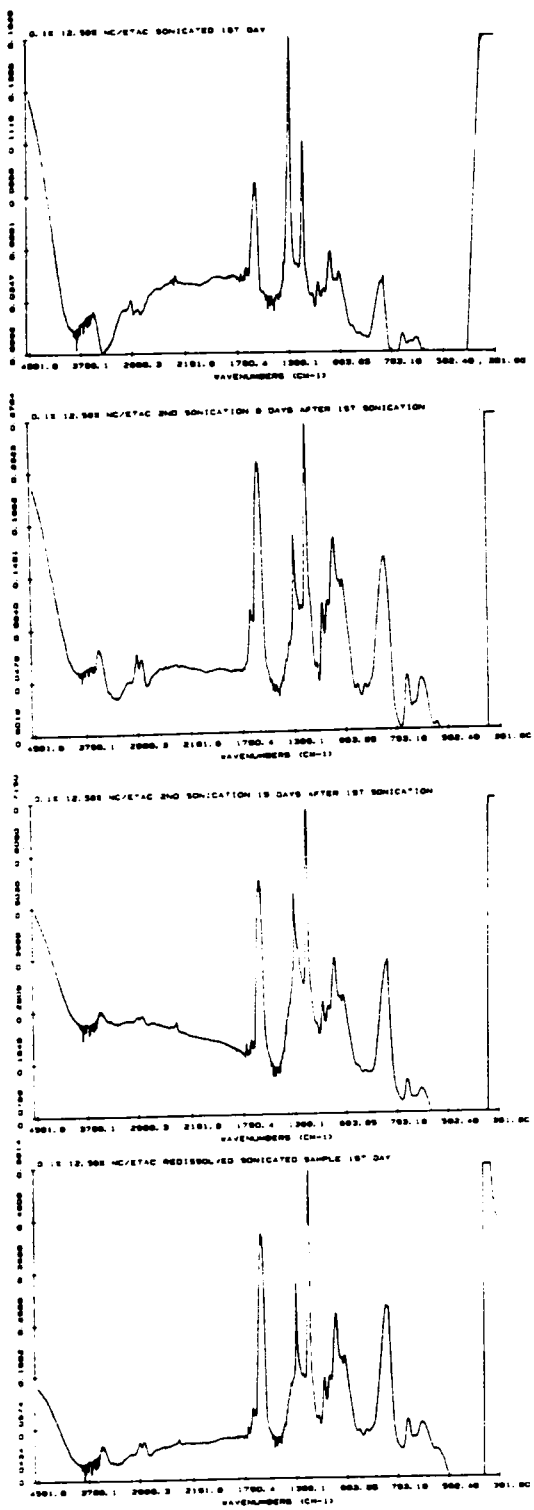

Figure 2.43: Infrared spectra of films made from sonicated 0.1% 12.58% NC/EtOAc.

scission immediately. However, excessive sonication, which was accompanied by an increase in the solution temperature to about 65°C probably accelerated the degradation process.

These results suggest that NC in THF was more vulnerable to degradation. Whether this was due to chain extension leading to better solvation or the presence of peroxides in the solvent was not entirely clear from the evidence collated so far. However, from these results one may learn that sonication is not a viable method to accelerate the approach to the equilibrium state of solvation.

2.4.4.3. Infrared Spectroscopy of Nitric Acid Doped Samples

The spectra for films from 12.58% NC/THF nitric acid doped solutions taken immediately after doping are shown in Figure 2.44. Again, there was an absorption at around 1770 cm^{-1} wavenumbers and the symmetric NO_2 absorption peaks resembled the ones obtained in the sonicated samples. After the films were redissolved, the spectra from the sample cast from the soluble portion was noticeably weaker, though still identical to the ones obtained before solvent evaporation. In addition, a clear, insoluble film was present. The spectra of products of redissolution are shown in Figure 2.45. Except for the more intense peaks in the hydroxyl region, the spectrum was the same as that obtained for the samples before evaporation, though the peaks here were broader and less resolved. This may be an indication that in addition to chain scission, the nitric acid stripped off the nitro groups causing the nitrocellulose to revert back to a less nitrated and more insoluble derivative. This effect was not observed in the results for 12.58% NC/THF after a six month storage period. If the relative intensity of the carbonyl peak were an indication of degradation initiated by nitric acid, this may be interpreted as: the process requires a long time to reach the levels seen in the case of the 12.58% NC/THF samples, which were stored for six months after solvent evaporation before redissolution.

The spectra obtained for films from 12.58% NC/EtOAc heavily doped with concentrated nitric acid are shown in Figure 2.46. The solution had a strong acetic acid smell. The shoulder at 1729 cm^{-1} that appeared in the absence of nitric acid practically disappeared and was replaced by a peak at 1770 cm^{-1}. This indicates immediate degradation by chain scission as was expected. The changing of relative intensities at

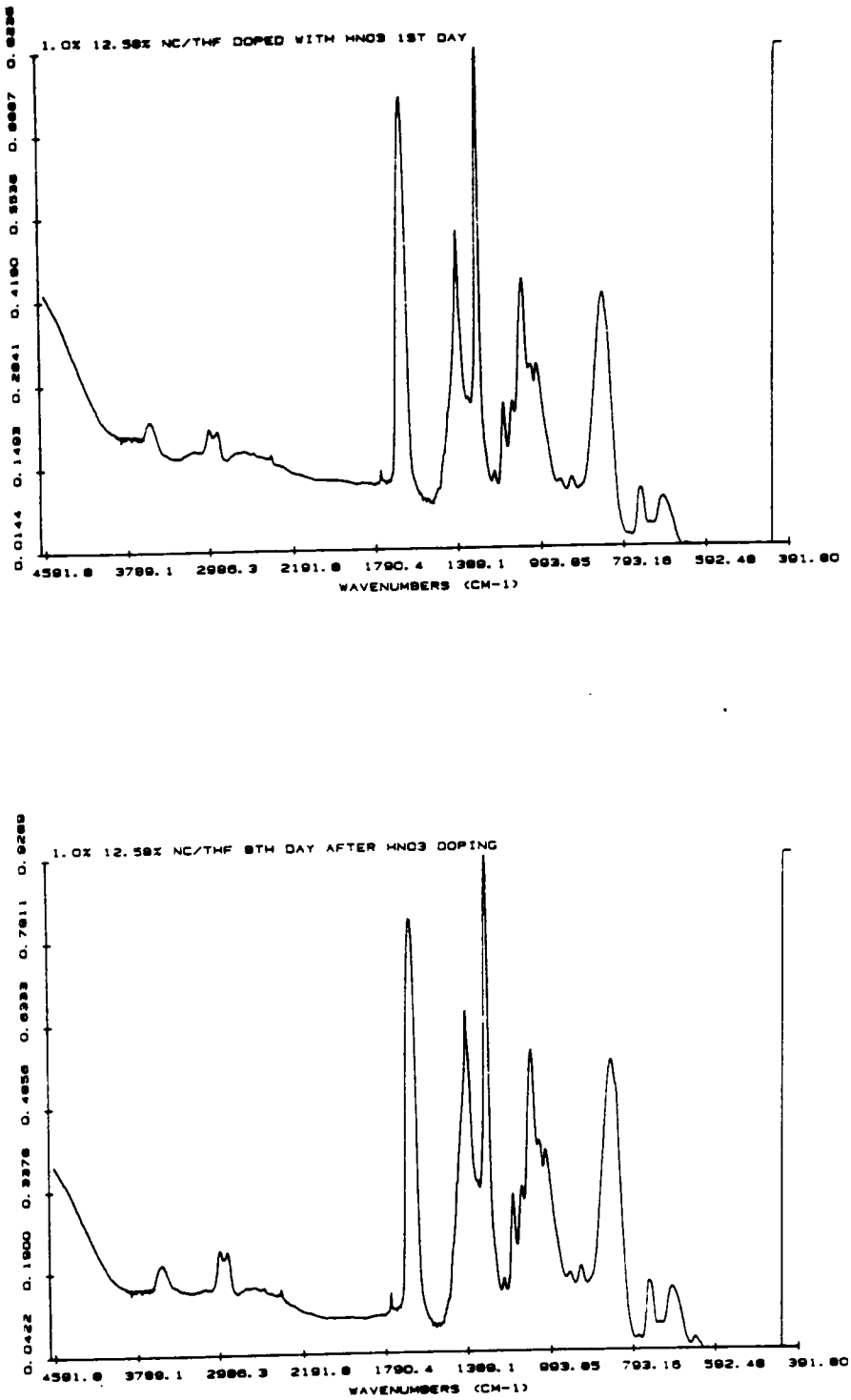

Figure 2.44: Infrared spectra of films made from 1.0% 12.58% NC/THF doped with nitric acid.

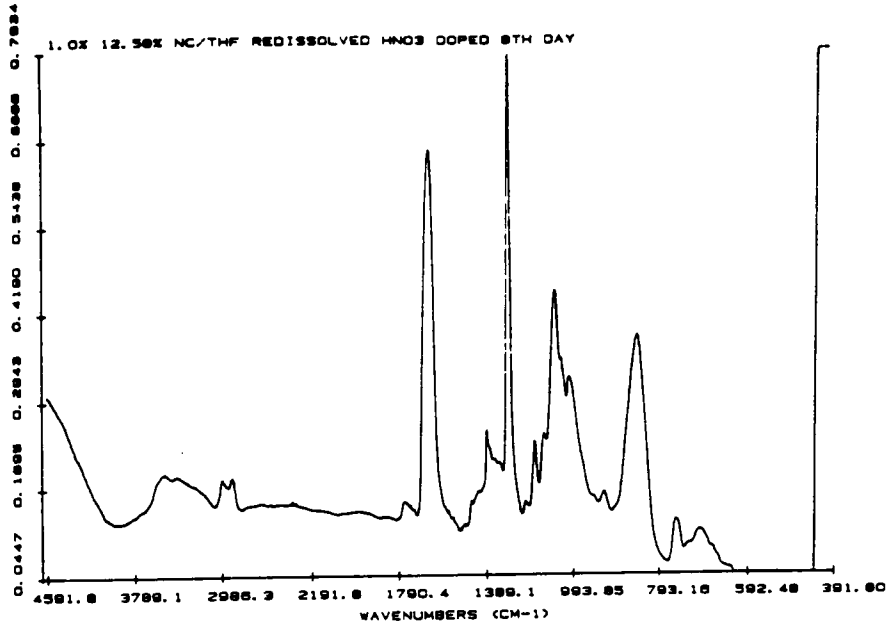

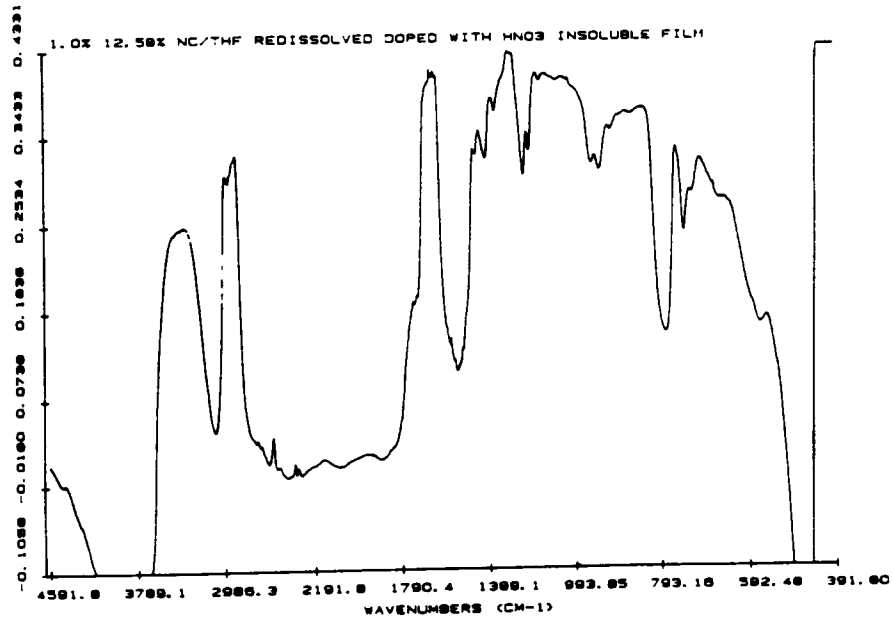

Figure 2.45: Infrared spectra of insoluble film and film cast from redissolved acid doped 1.0% 12.58% NC/THF.

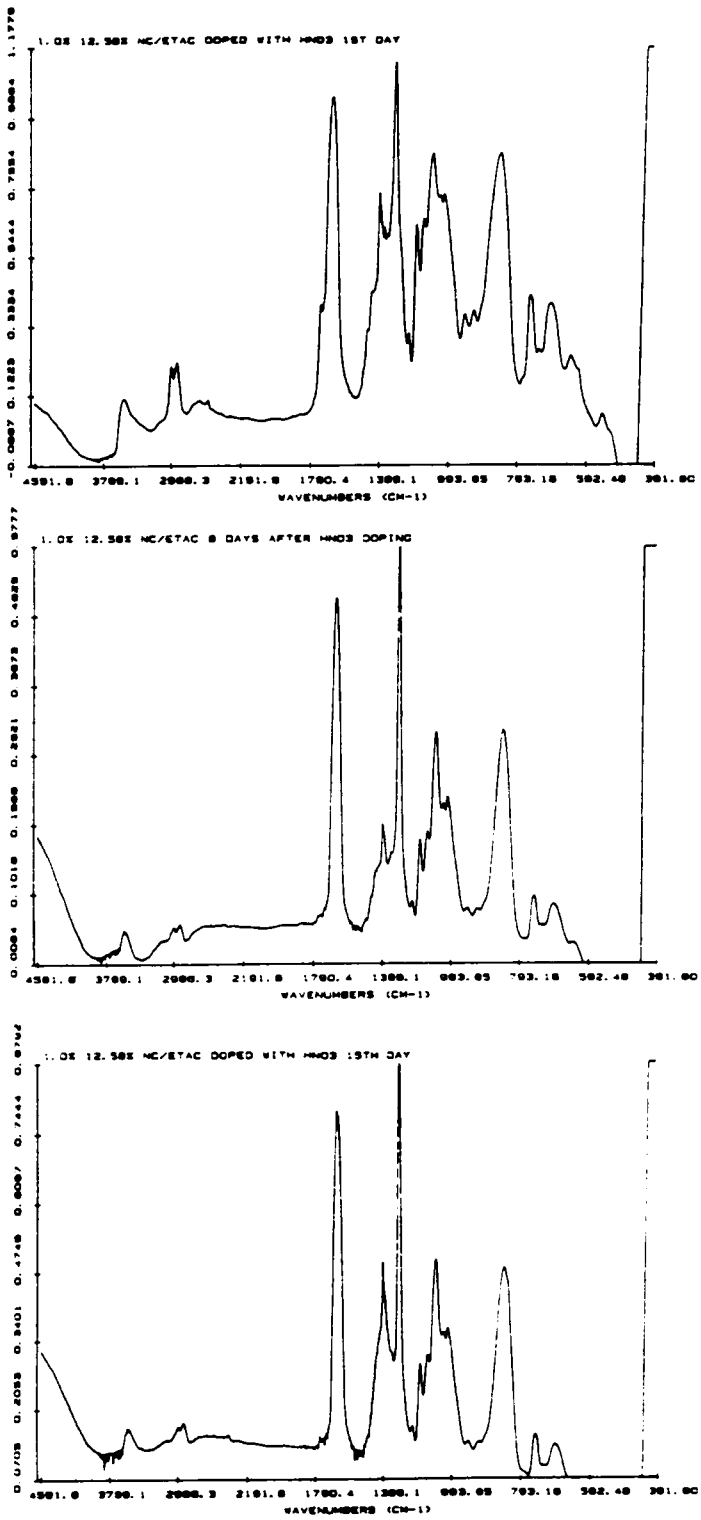

Figure 2.46: Infrared spectra of films made from 1.0% 12.58% EtOAc doped with nitric acid.

about 1278 and 1376 cm^{-1} happened once more. This phenomenon may or may not be related to degradation by chain scission. Its similarity to the occurrence of the same behavior after sonication is striking. After the solvent was evaporated and the sample was redissolved, the solution was noticeably less viscous. The spectra of the film made from this solution was very weak and had more intense peaks where the hydroxyl absorption was supposed to occur. In addition, an insoluble film was formed which refused to go into solution even after a considerable length of time. The spectra obtained of this film is shown in Figure 2.47. It looks similar to the one from NC except for a much more intense absorption at 3452 cm^{-1} and 2900 cm^{-1}. Again, this may be due to a reversion to cellulose by denitration which would be consistent with the fact that the film was now insoluble.

The spectra for films cast from 1% 13.5% NC/THF nitric acid doped solutions are shown in Figure 2.48. The peak at 1770 cm^{-1} was visible after a couple of hours and the doublet at 1278 and 1376 cm^{-1} was very intense. This appears to support previous evidence that the 13.5% NC/THF combination was the most susceptible to degradation. Again, aside from THF being a good solvent, 13.5% NC is a more extended chain than 12.58% NC, thus allowing better access of solvent molecules to the solute. It appears that the sooner the molecule is solvated, the greater is its vulnerability to oxidizing species which cause degradation by chain scission. Upon evaporation of solvent and redissolution, a more pronounced peak appeared at 1770 cm^{-1} and an insoluble film was formed. Again, the spectrum of the insoluble film was similar to that obtained from the other solutions above.

Finally, the spectra for films obtained from casting 1% 13.5% NC/EtOAc nitric acid doped solutions onto KBr plates are shown in Figure 2.49. Again the peak at around 1729 cm^{-1} wavenumbers was hardly visible and the NO_2 absorbances looked different from what was normally obtained in untreated solutions. Over time, the peak at about 1770 cm^{-1} became more pronounced, signifying the occurrence of degradation by chain scission with the addition of nitric acid. Upon evaporation of the solvent and redissolving the film, the solution was much less viscous. The film made from this solution yielded a spectrum with more pronounced hydroxyl absorption and an overall weaker absorbance. An insoluble film was also obtained.

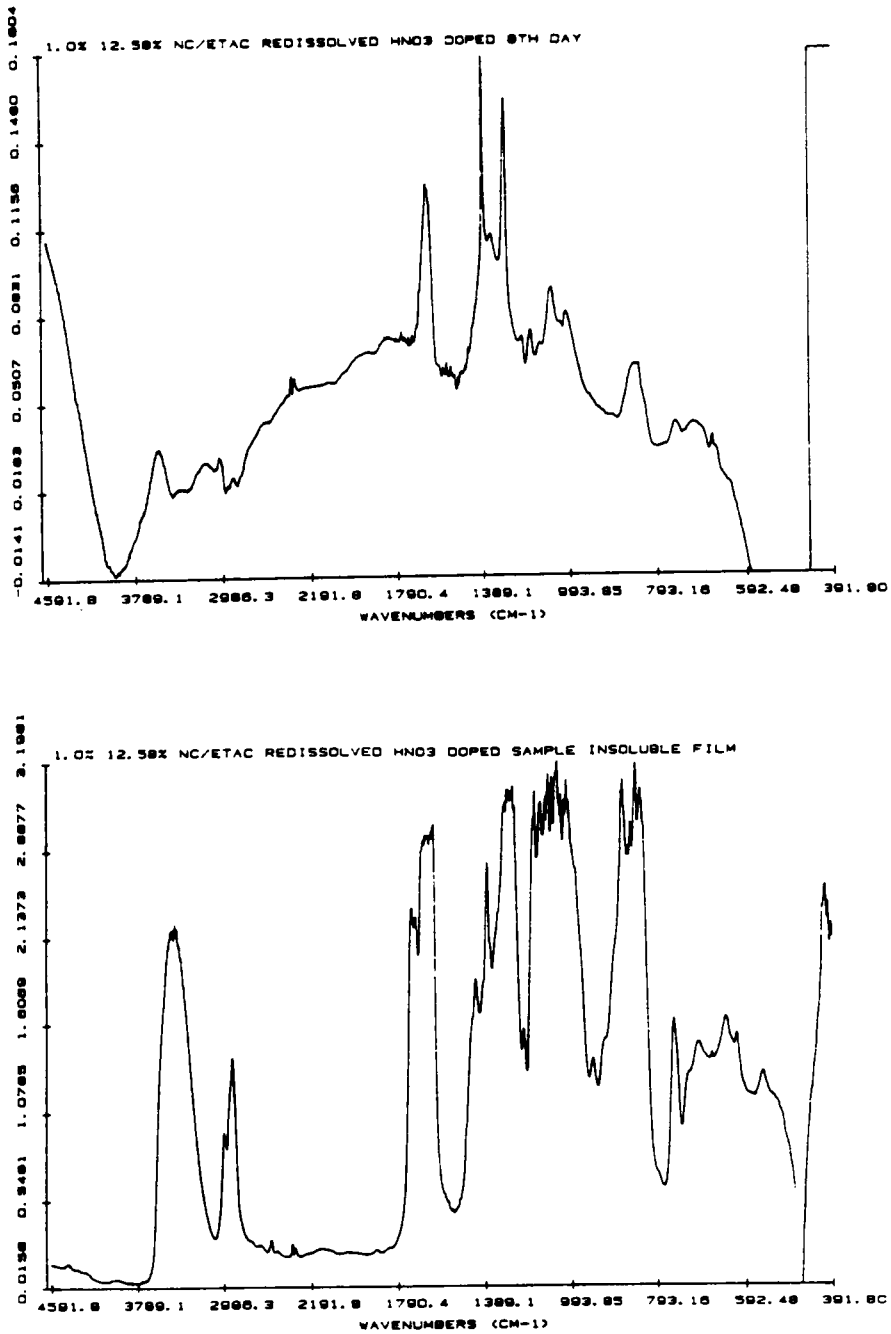

Figure 2.47: Infrared spectra from insoluble film and film cast from redissolved 1.0% 12.58% NC/EtOAc doped with nitric acid.

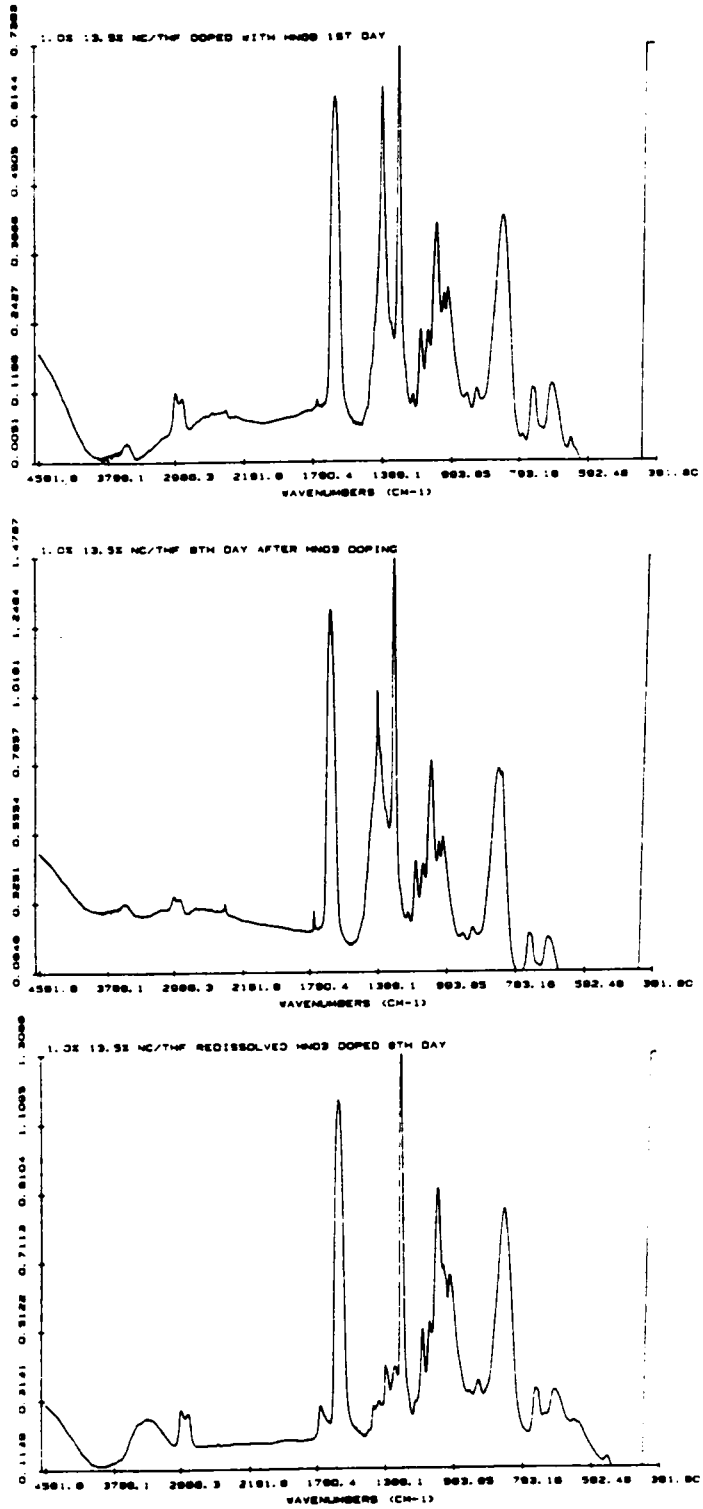

Figure 2.48: Infrared spectra of films made from nitric acid doped 1.0% 13.5% NC/THF.

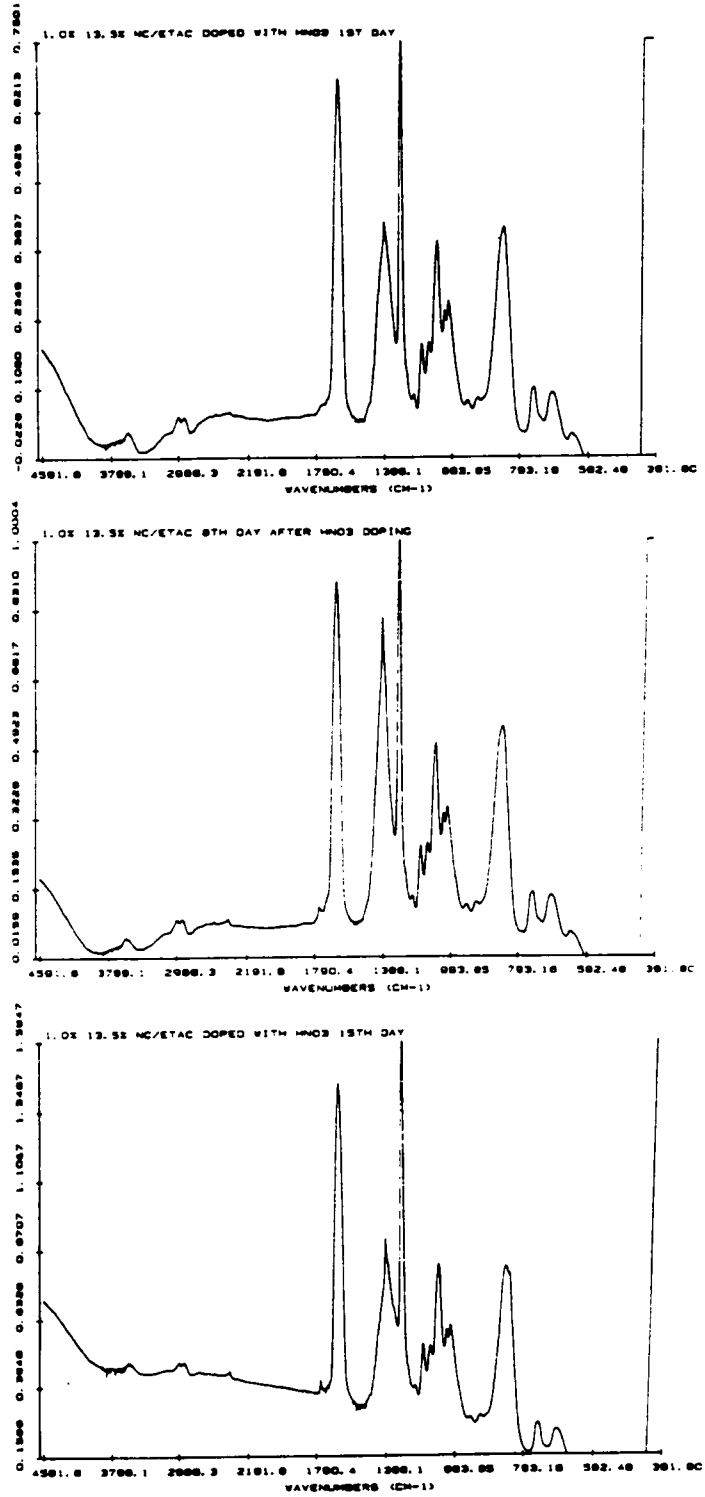

Figure 2.49: Infrared spectra of films made from nitric acid doped 1.0% 13.5% NC/EtOAc solutions. the results.

This spectrum was similar to that obtained in Figure 2.47, which indicates that the two films were most likely the same species.

The above results showed that acidification of NC solutions accelerated the degradation process. The effect of the nitric acid was also immediate, with visible degradation occurring within a couple of hours of the addition of the acid. Another effect of the presence of acid was the formation of insoluble material after redissolution. The results here strengthen the premise for the aging mechanism proposed in the previous section -- no degradation by chain scission occurred up to at least 15 days of aging. Contrary to the formation of insoluble material after redissolution if denitration occurred, the samples were dissolved with greater ease the second time around. The association/dissociation mechanism is in better agreement with these results.

2.4.5. Intrinsic Viscosity

The tests that yielded the most conclusive results regarding aging were the intrinsic viscosity experiments. This is consistent with the weighting of the flow times in that experiment more toward changes in the high molecular weight fraction of the distribution in an averaging fashion. The error bars in the graphs are the standard deviations in the reproducibility of the experiments.

2.4.5.1. 12.58% NC/THF

The specific viscosities of 12.58% NC/THF solutions were measured over 17 days. The solvent was then evaporated slowly and the dried films were stored in their original amber bottles for six months before being redissolved to their original concentrations. The viscosities were thus measured six months after the original samples were dried. The reduced viscosity plot is shown in Figure 2.50. An inset of the more dilute concentrations is also shown to demonstrate the presence of a slight maximum at 0.4%. The presence of this maximum was typical in reduced viscosity plots for associated macromolecules (70,108,109). A closer look at viscosity was taken by examining the concentration as well as time dependent changes in specific viscosity. A composite of these graphs is shown in Figure 2.51.

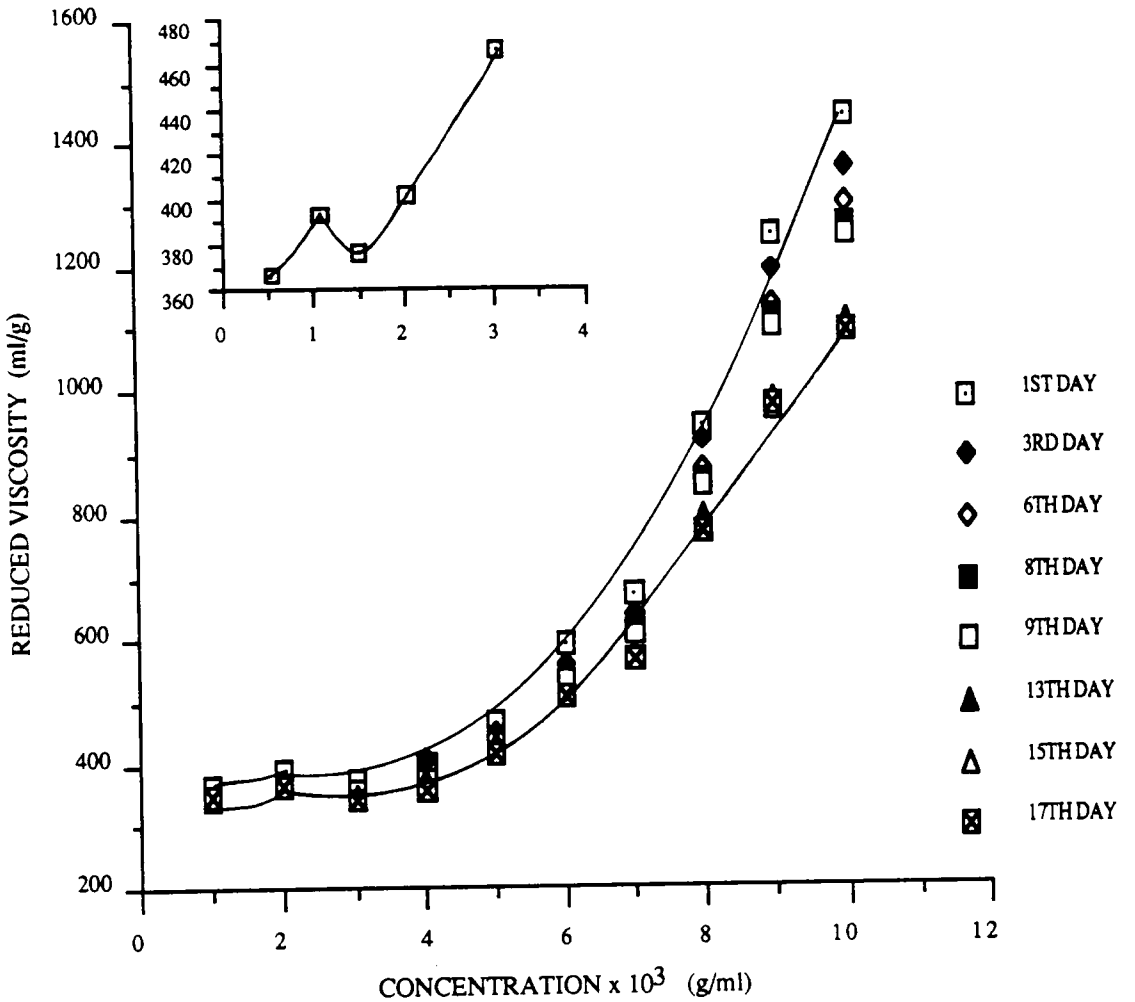

Figure 2.50: Reduced viscosity plot for 12.58% nitrocellulose in unstabilized THF.

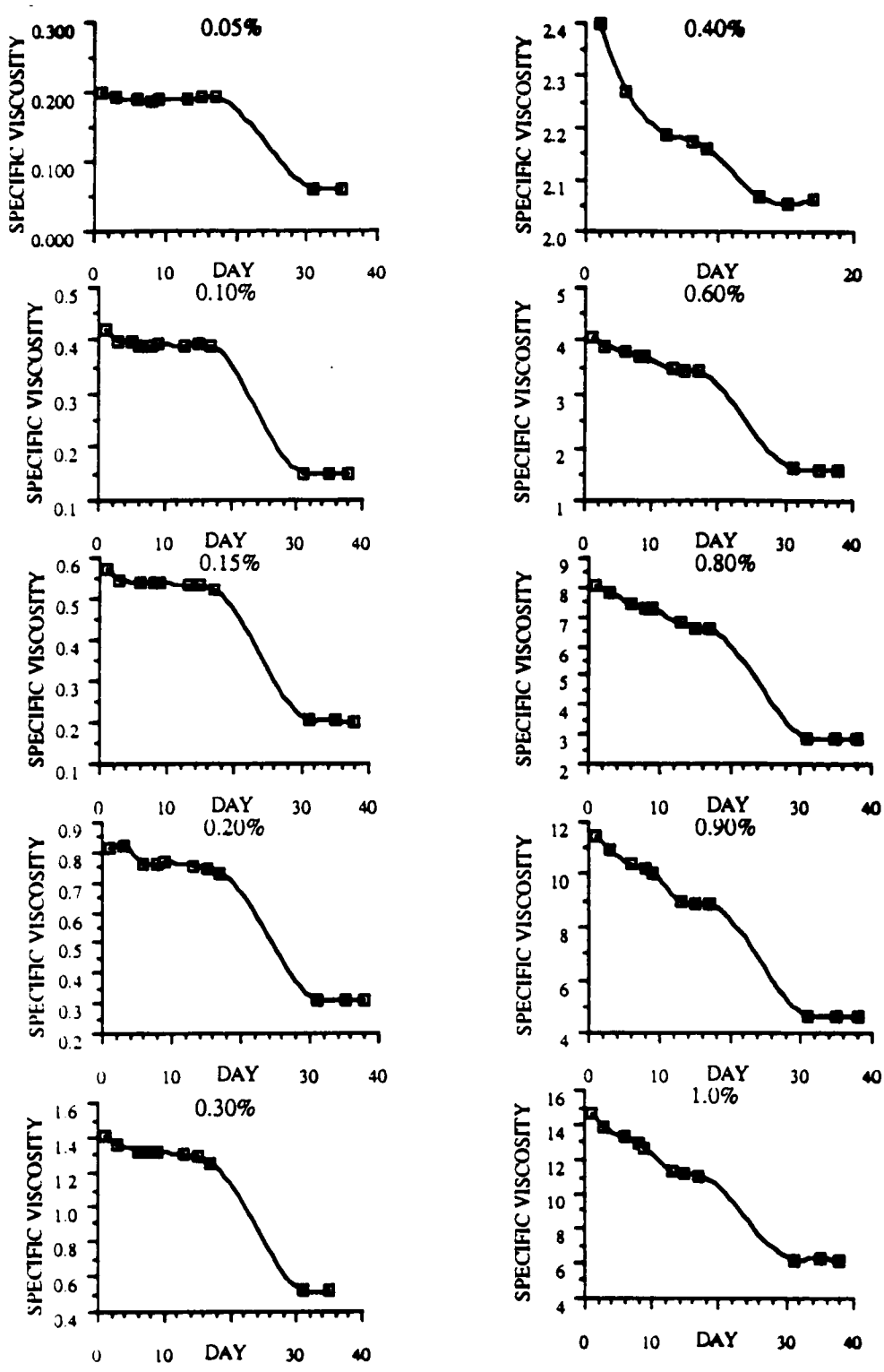

Figure 2.51: Concentration and time dependent changes in specific viscosity for 12.58% NC/THF.

Examination of the data taken before redissolution revealed a dependence on concentration. The viscosities of the more dilute solutions tended to level off at an "equilibrium" value soon -- in four days. On the other hand, the viscosities of the more concentrated solutions decreased continuously for about ten days before reaching a steady value. This may be explained by an ease of solvation in more dilute solutions where there are fewer molecules compared to greater difficulty in achieving optimum solvation in the presence of more molecules for the concentrated solutions.

The data taken for the redissolved samples are also shown in Figure 2.51. They are represented by data from 30 days of initial solution and beyond. The specific viscosities for the samples here were roughly a third of what they were originally. In addition, one does not see the change in rate of aging; rather, the values were constant over a week. These differences may be accounted for by degradation due to chain scission of the NC molecules. Indeed, this was proven by the IR spectra taken of these samples as already discussed.

2.4.5.2. 12.58% NC/THF(NS)

In order to insure that the loss of viscosity and molecular weight of 12.58% NC/THF was not due to degradation from peroxide formation in the THF, stabilized THF solutions were also studied. The reduced viscosity plot is shown in Figure 2.52. Although it was fairly linear at lower concentrations, the graph started to curve upward at concentrations greater than 0.3%. Furthermore, the viscosity decrease was more pronounced for the higher concentrations. The concentration and time dependent changes of specific viscosity are detailed in Figure 2.53. For the more dilute solutions, there was no clear trend. There was some scatter in the data for the 0.05% solutions. The 0.15% solutions showed continuously decreasing viscosities while the viscosity of the 0.2% solution leveled off at about the eighth day before decreasing at a different rate after the tenth day. The other concentrations showed decreases in viscosity similar in pattern to those seen in the unstabilized THF solutions with the viscosities tending to level off after the tenth day. These results demonstrated that the decrease in viscosity in the unstabilized THF solutions was not due to degradation from peroxides.

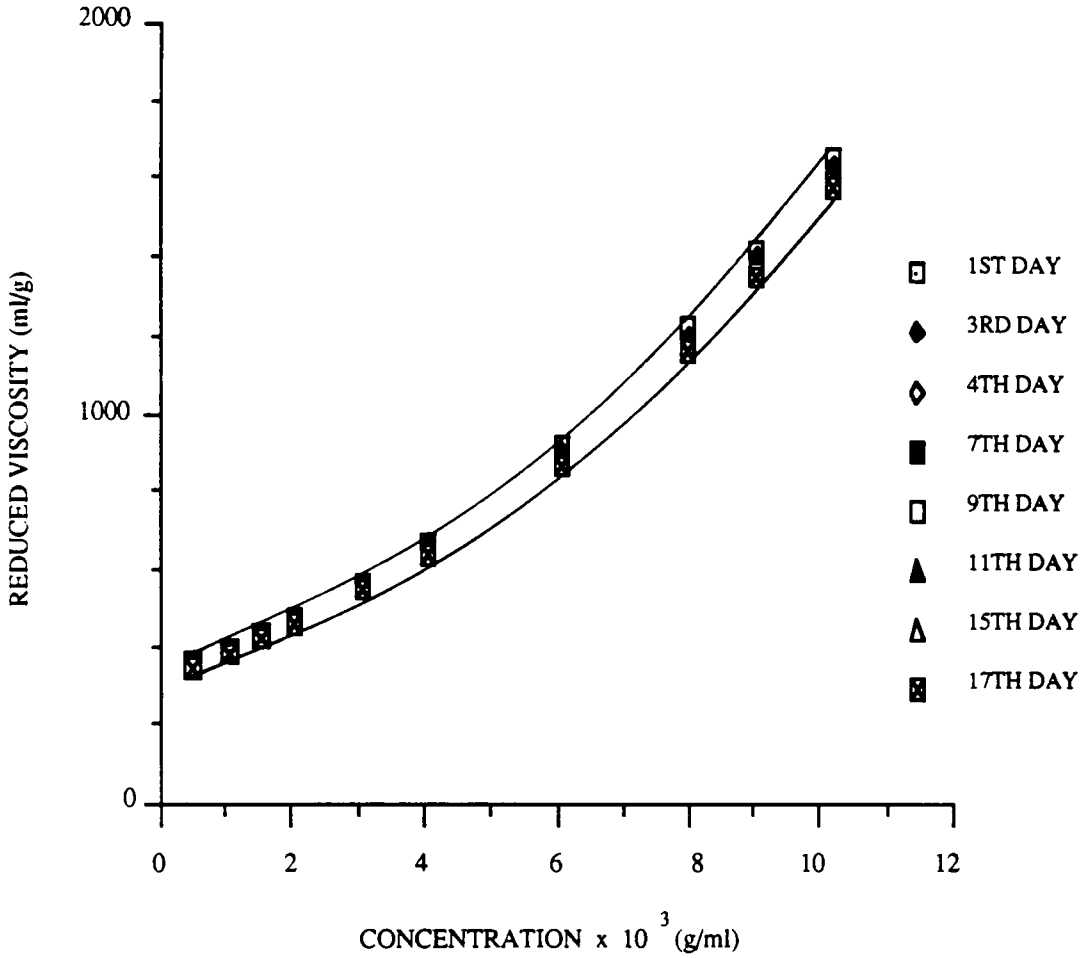

Figure 2.52: Reduced viscosity plot for 12.58% nitrocellulose in stabilized THF.

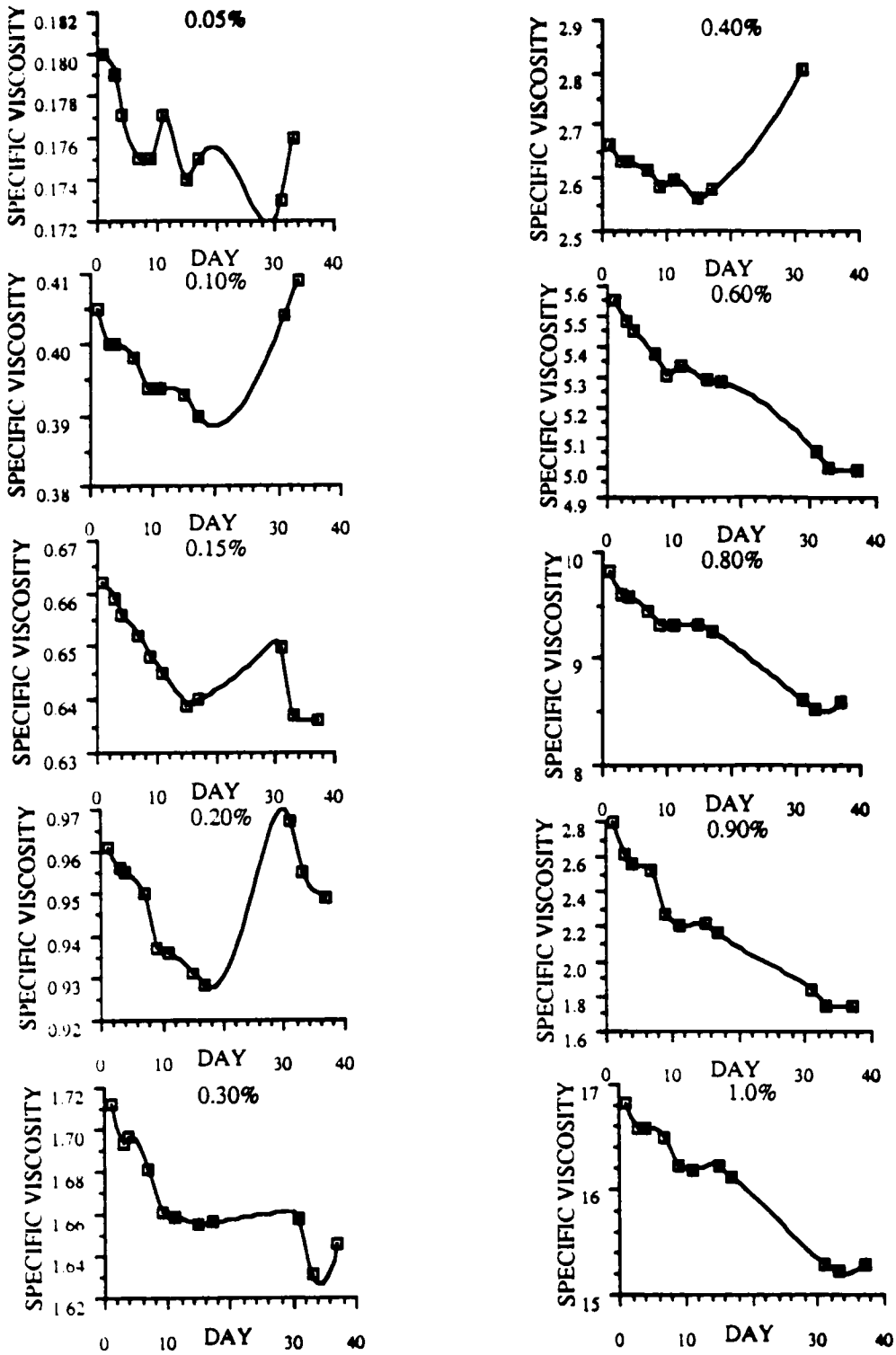

Figure 2.53: Concentration and time dependent changes in specific viscosity of 12.58% NC/THF(NS).

After the solvent was evaporated slowly and the samples redissolved to their original concentrations, the viscosities recovered to close to their original values for the 0.1% and 0.2% solutions, while the viscosity for the 0.15% solution recovered to one-half the original value. The decrease in viscosity a few days later occurred at a faster rate than that seen in the original solutions. All other concentrations revealed a decrease in viscosity from that on the 17th day. Unlike the results for the unstabilized THF solutions, the viscosities showed slight decreases where they did not go back to their original values. Interestingly enough, the viscosity increased slightly for some of the solutions on the third day after redissolution. For this system, there was a deviation from the trend seen earlier. Where the viscosities of the more concentrated solutions usually returned to close to the viscosity immediately after sample preparation, and while those for the more dilute solutions did not, the opposite was seen in this case. In taking note of the variations in experimental conditions, it is suggested that time and extent of agitation were factors which affected the dissociation. The more concentrated solutions were agitated a 100 rpm higher than the lower concentrations. This may have accelerated the dissociation process, causing the investigator to miss the point at which the viscosity had gone back up. The length of time after redissolution and measurement of viscosity also appeared to be a factor. The longer the difference between the two steps, the smaller the possibility of recovery.

Considering the fact that the viscosities were recovered in the more dilute solutions and the fact that the rate of loss in viscosity was fairly rapid in the redissolved samples, the absence of recovered viscosity in the more concentrated solutions may be attributed to a time factor. One can only speculate that the samples were in solution too long so that even if the viscosities were indeed recovered, by the time the measurements were carried out, the viscosities were already at some value much lower than where they should have been. In any case, the fact that the viscosities of some went back up and that there was a decrease in viscosity afterwards, was in agreement with the trends observed for the unstabilized solutions. These results indicate that ***peroxide degradation was not the cause*** of the decrease in viscosity in the unstabilized THF solutions.

2.4.5.3. 12.58% NC/EtOAc

The reduced viscosity plot for 12.58% NC/EtOAc is shown in Figure 2.54. A curvature in the plot was apparent even at the lower concentrations. This departure from linearity for such a plot is an indication of some association present in solution (69,105,106). Another observation that may be noted is that the viscosity decreased over time with the loss being more prominent for the more concentrated solutions.

Examining the change in time dependence of specific viscosity for the different concentrations revealed new facts. The trends observed are shown in Figure 2.55. The only solution which showed a relatively constant viscosity over an extended period of time was that at 0.05% until its viscosity dropped about 20% on the 14th day. The 0.1% to 0.8% solutions showed decreased viscosities at about the same rate, if the slopes are a good indication. The decrease occurred at a slightly lower rate for 0.9% - 1% solutions. The data points corresponding to greater than 30 days were obtained from samples made after the solvent from the original solutions were evaporated slowly. Most interestingly, for 0.1%, 0.4%, 0.8%, 0.9% and 1.0% concentrations, the viscosities of the redissolved samples were greater than or equal to the viscosities of the solutions which aged for approximately 17 days. On the third day after redissolution, the viscosities dropped once more before leveling off. It is significant to note that the rate of decrease was greater for the redissolved samples than those of the initially dissolved solutions. The fact that the viscosities for some concentrations were partially recovered indicates that ***degradation by chain scission was not the major mechanism causing the decrease in viscosity initially***, otherwise, the NC would have to repolymerize to recover the viscosity. The steeper slope which is an indication of the rate of decrease in viscosity suggests that in evaporating the solvent and redissolving the dried film, the physical nature of the NC changed in a way that allowed easier solvation by the solvent molecules. This is consistent with the observation of greater ease of dissolution of the films formed after solvent evaporation compared to the dried nitrocellulose fibers utilized in the original solutions. One explanation for this may be that residual solvent was present since the samples were not dried in the oven before redissolution. The residual solvent may also explain why the viscosity was not fully recovered or not regained at all for most of the samples.

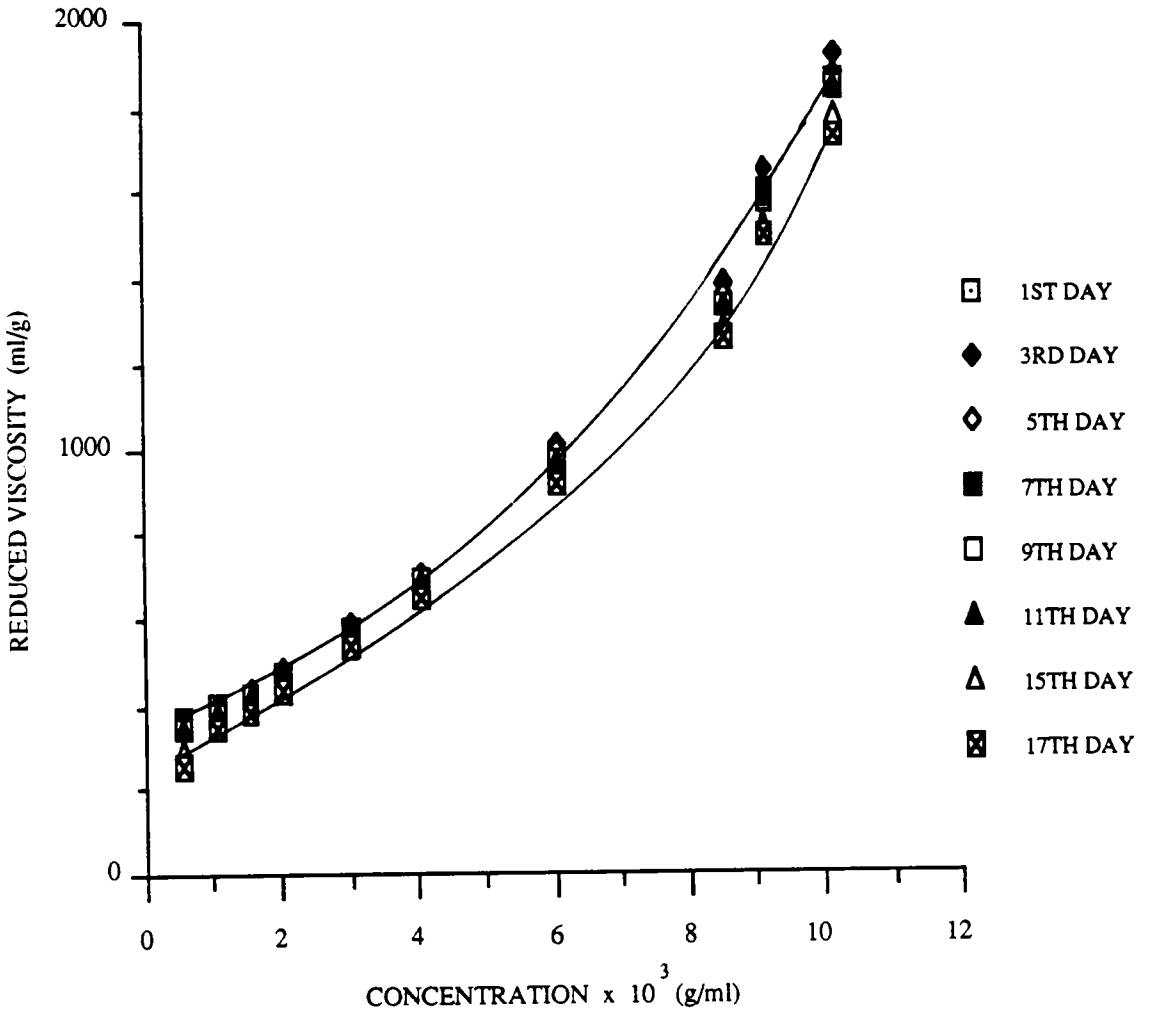

Figure 2.54: Reduced viscosity plot for 12.58% nitrocellulose in ethyl acetate.

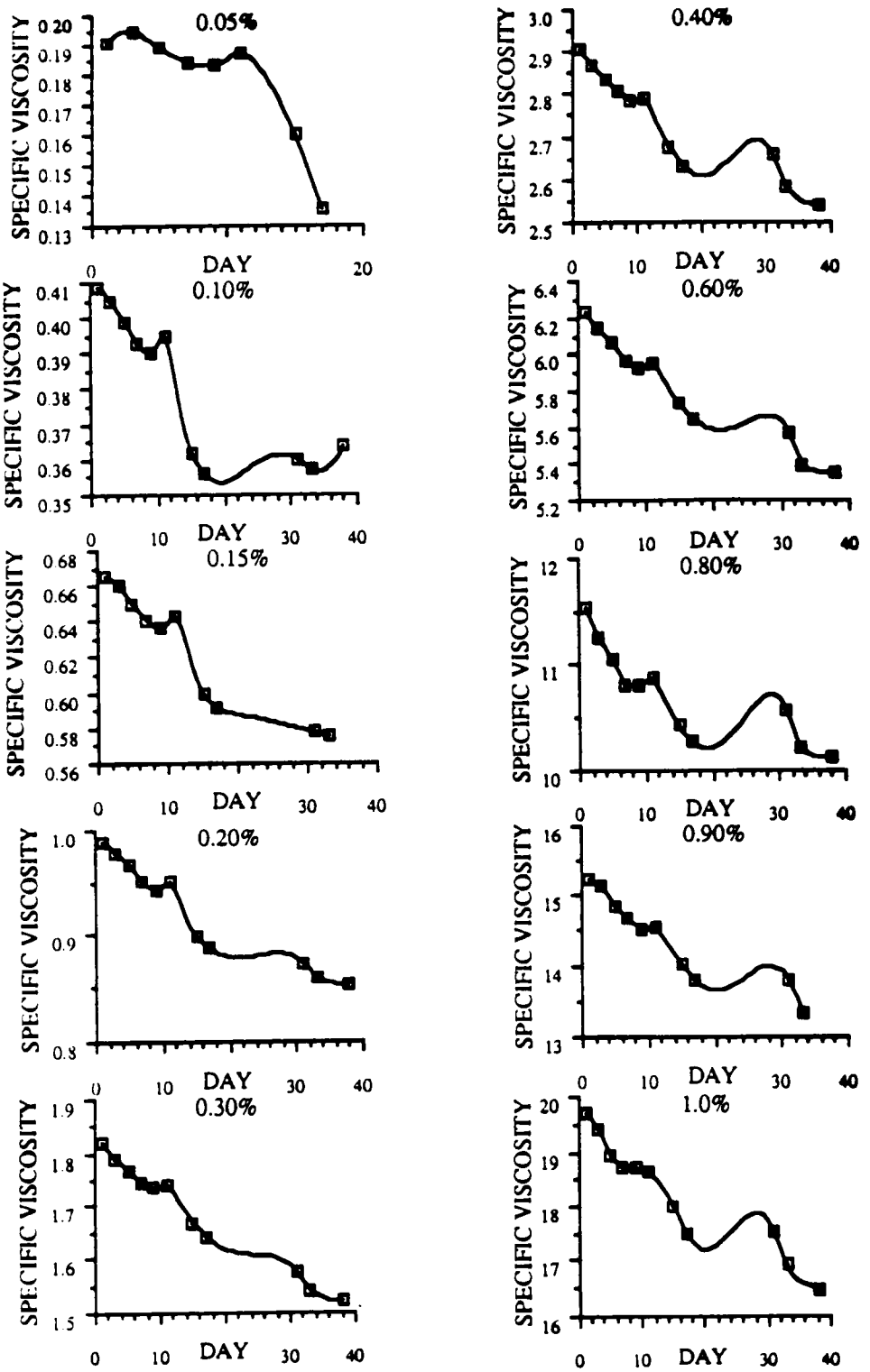

Figure 2.55: Concentration and time dependent changes in specific viscosity of 12.58% NC/EtOAc.

These results were not in agreement with those obtained by Campbell and Johnson (71) where the viscosities of their redissolved samples were always lower than before the solvent was evaporated. The difference in techniques employed in the experiment may be the key to this dilemma. While Campbell and Johnson utilized vacuum to quickly drive the solvent away, the samples used here were allowed to dry very slowly. The more gradual technique may be more favorable to an equilibrium of association and dissociation being established if such events were occurring.

2.4.5.4. 13.5% NC/THF

The reduced viscosity plot for 13.5% NC/THF is shown in Figure 2.56. The plot was characteristic of associated molecules once again with a slight maximum visible at about 0.2%. There was a very dramatic difference in the decrease of reduced viscosity at concentrations greater than 0.6%, compared to the 12.58% NC/THF. This points to a concentration dependent mechanism for the change. Again, this may be explained by association/dissociation of molecules. The chances of more molecules being closer together, given conformation, increasing the possibility of association are greater at higher concentrations. The opposite is expected for the more dilute solutions.

A closer examination of specific viscosities is shown in Figure 2.57 for the whole range of concentrations utilized. The more dilute solutions showed a plateau in the specific viscosity developing after the tenth day in solution. As concentration increased the plateau length shortened and subsequently disappeared completely at 0.3%. Upon evaporation of the solvent and redissolution of the sample to the original concentration, the viscosity was always lower than the last measured value. The values obtained were anywhere from 16 - 25% less than the original and in most cases continued to decrease slightly afterwards. This pattern deviated from that seen in the clearly degraded 12.58% NC/THF where the viscosities were 60 - 70% less than the original and remained constant over the next week. This indicates that the 16 - 25% decrease in viscosity was not due to degradation in spite of the absence of viscosity recovery.

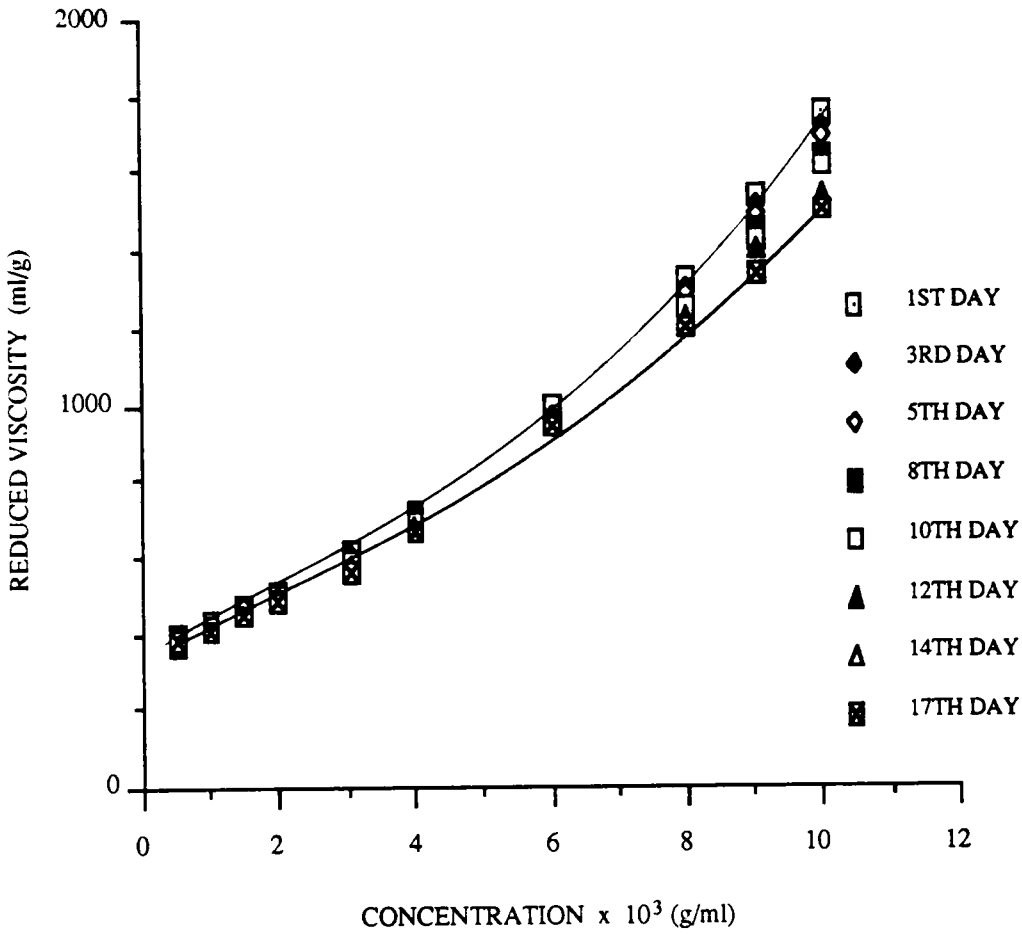

Figure 2.56: Reduced viscosity plot of 13.5% nitrocellulose in unstabilized THF.

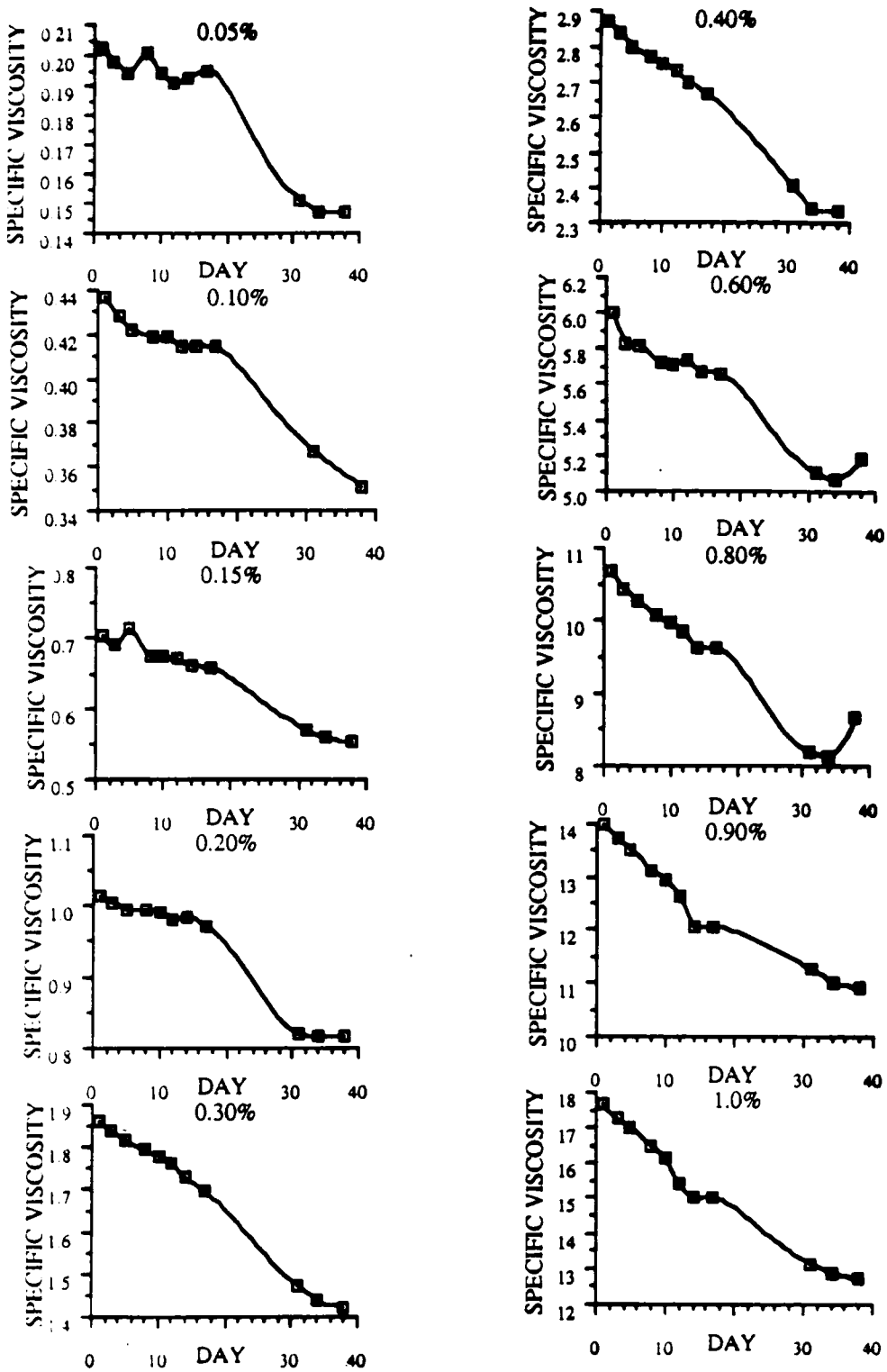

Figure 2.57: Concentration and time dependent changes in specific viscosity for 13.5% NC/THF.

2.4.5.5. 13.5% NC/THF(NS)

In order to confirm that the behavior observed above was duplicated even in stabilized systems, NC solutions in THF(NS) were studied. The reduced viscosity plots are shown in Figure 2.58. Again, there was a curvature in the plot. The inset, which is a magnified view of the plot at lower concentrations reveals that there is a definite maximum at 0.15% concentration. Again, the shape of the viscosity plot indicates that there was association of molecules present in solution. A closer look at changes in specific viscosity as a function of time and concentration is given in Figure 2.59. There was consistently a plateau region of viscosity in all the concentrations. This may be an indication of the quality of the solvent in that it was able to achieve an equilibrium dissociated state regardless of the solution concentration. Oddly enough, for concentrations greater than or equal to 0.6%, there was quite a bit of scatter present. A look at the redissolved samples shows that only 0.9% and 1.0% solutions behaved normally i. e. the viscosities rose back slightly then rapidly dropped. In most other solutions, the viscosities continued to increase over time, which was the opposite of what was expected. One likely explanation may be that the initial redissolved solution was not a true solution and thus was more dilute. Having removed some of this, then the undissolved sample that remained went into solution with less solvent so the solution became more concentrated than was thought and the calculated viscosity rose. Having five other sets of solutions behaving the opposite way, however, renders doubt to this possibility.

2.4.5.6. 13.5% NC/EtOAc

Finally, the last system studied was 13.5% NC/EtOAc. The reduced viscosity plot for this system is shown in Figure 2.60. Once more, there was a slightly noticeable maximum at about 0.15% concentration which is indicative of the presence of associated molecules in solution (69,105,106). Just like all other systems discussed, the viscosity decrease was more pronounced at the higher concentrations than for the more dilute solutions.

Figure 2.61 is a composite of the specific viscosity results which demonstrate the concentration and time dependence of the change in specific viscosity. In most cases, the viscosity decreased continuously

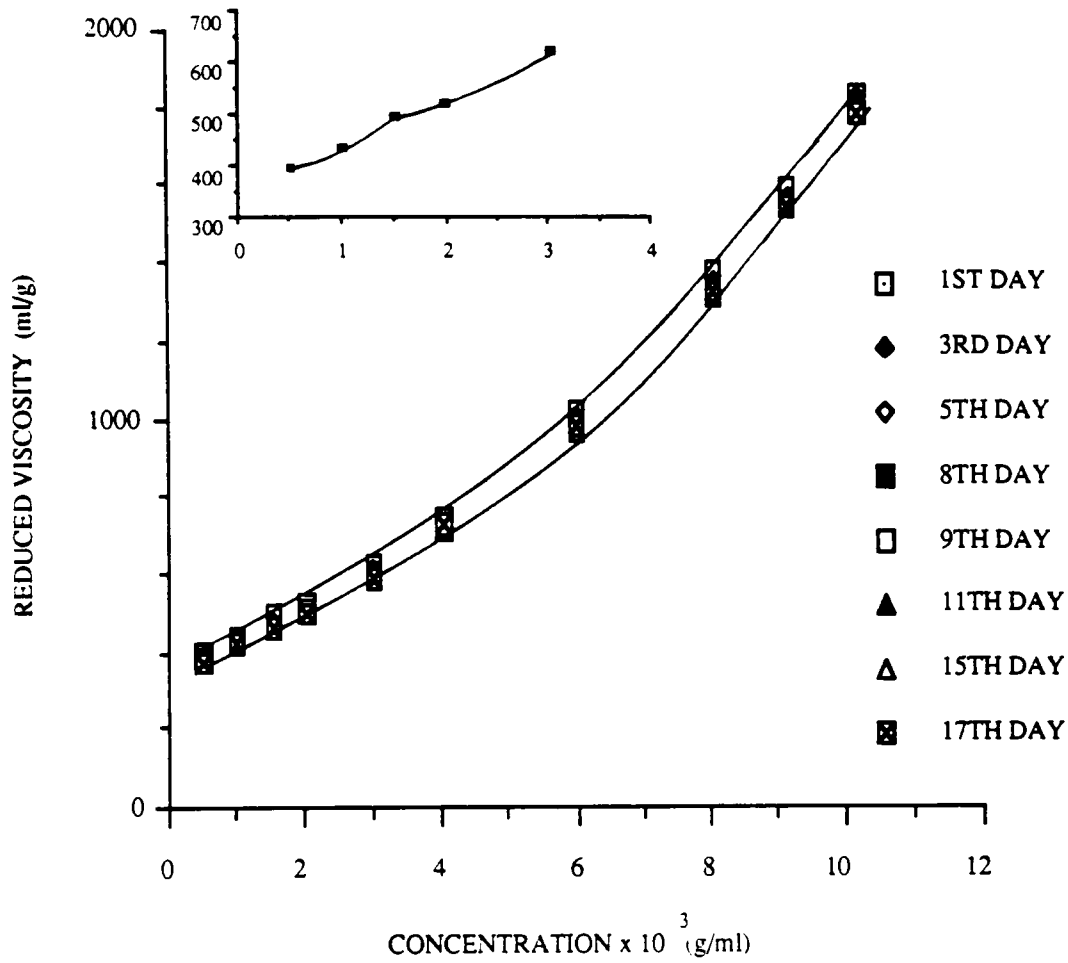

Figure 2.58: Reduced viscosity plot for 13.5% nitrocellulose in stabilized THF.

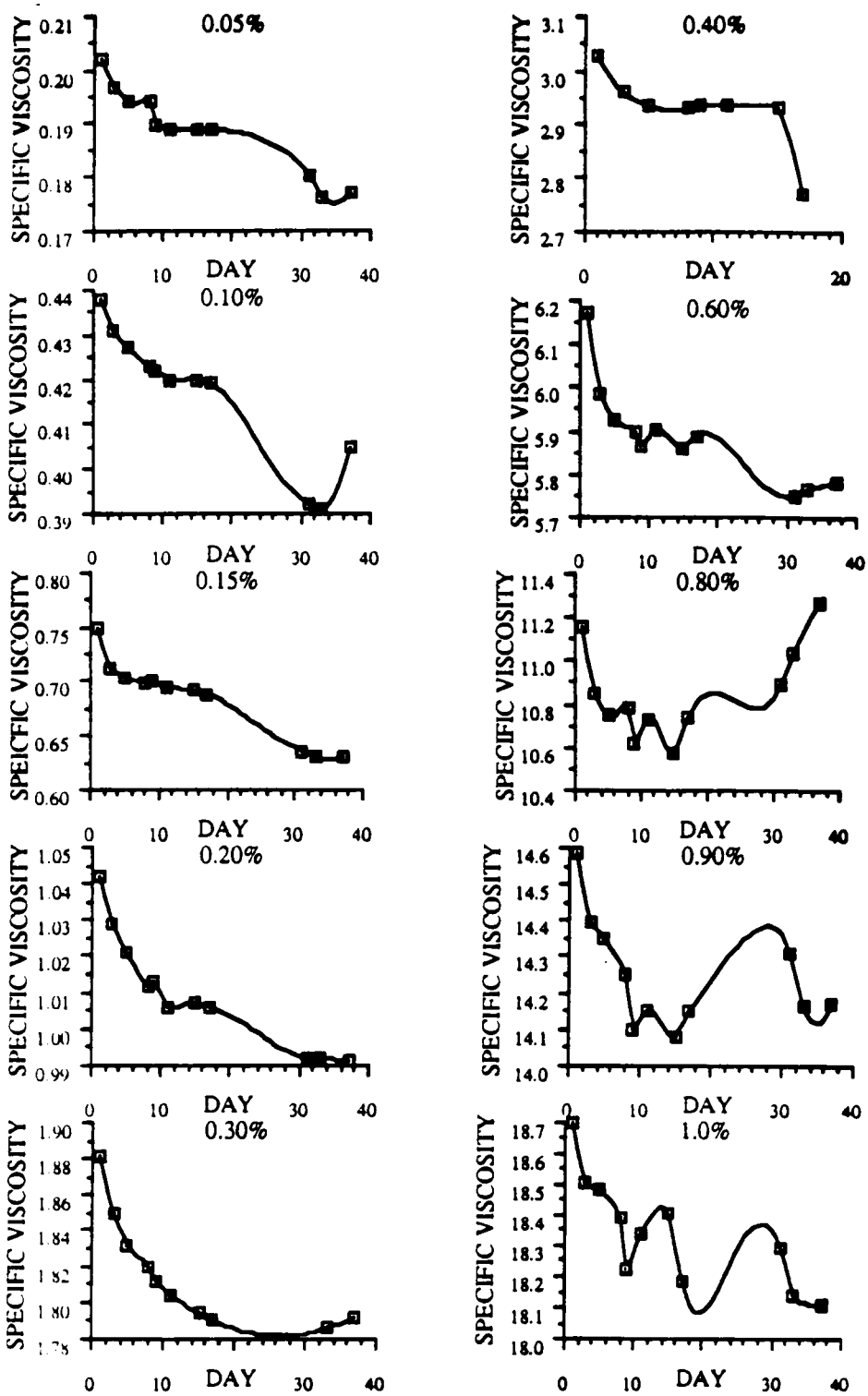

Figure 2.59: Concentration and time dependent changes in specific viscosity for 13.5% NC/THF(NS).

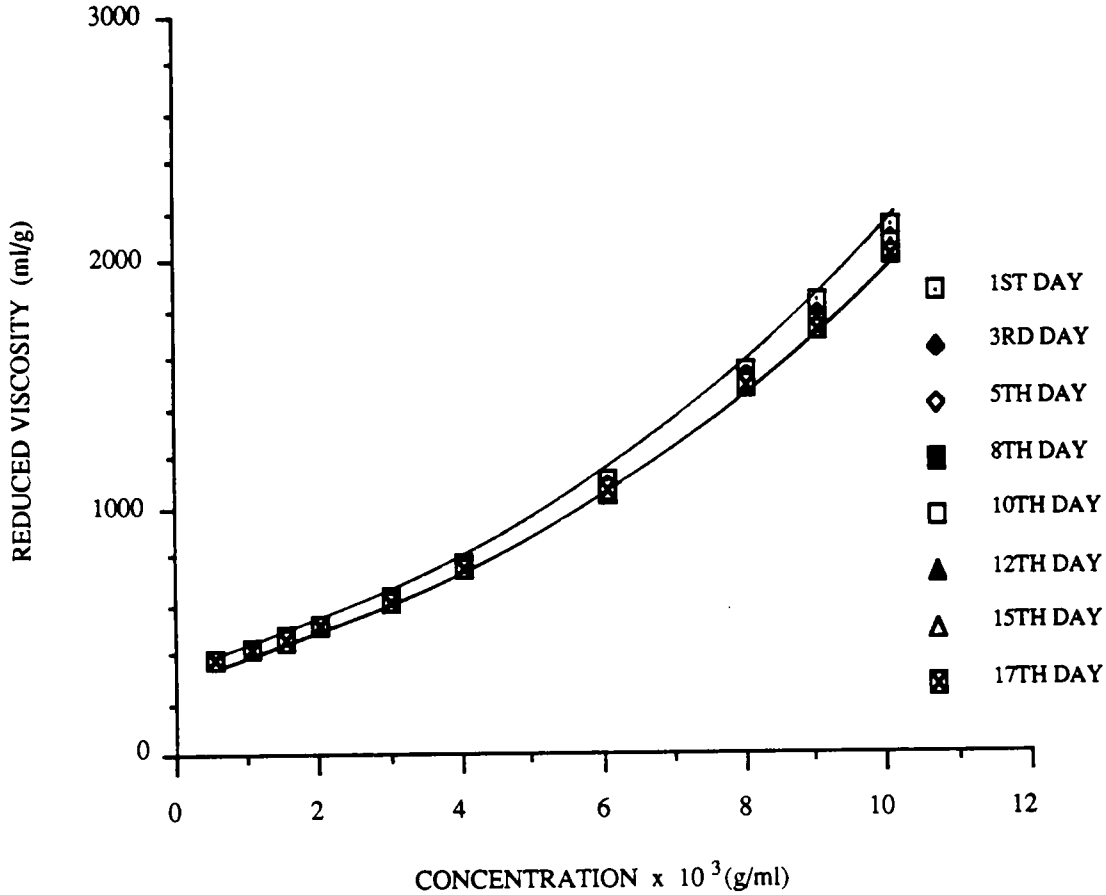

Figure 2.60: Reduced viscosity plot of 13.5% nitrocellulose in ethyl acetate.

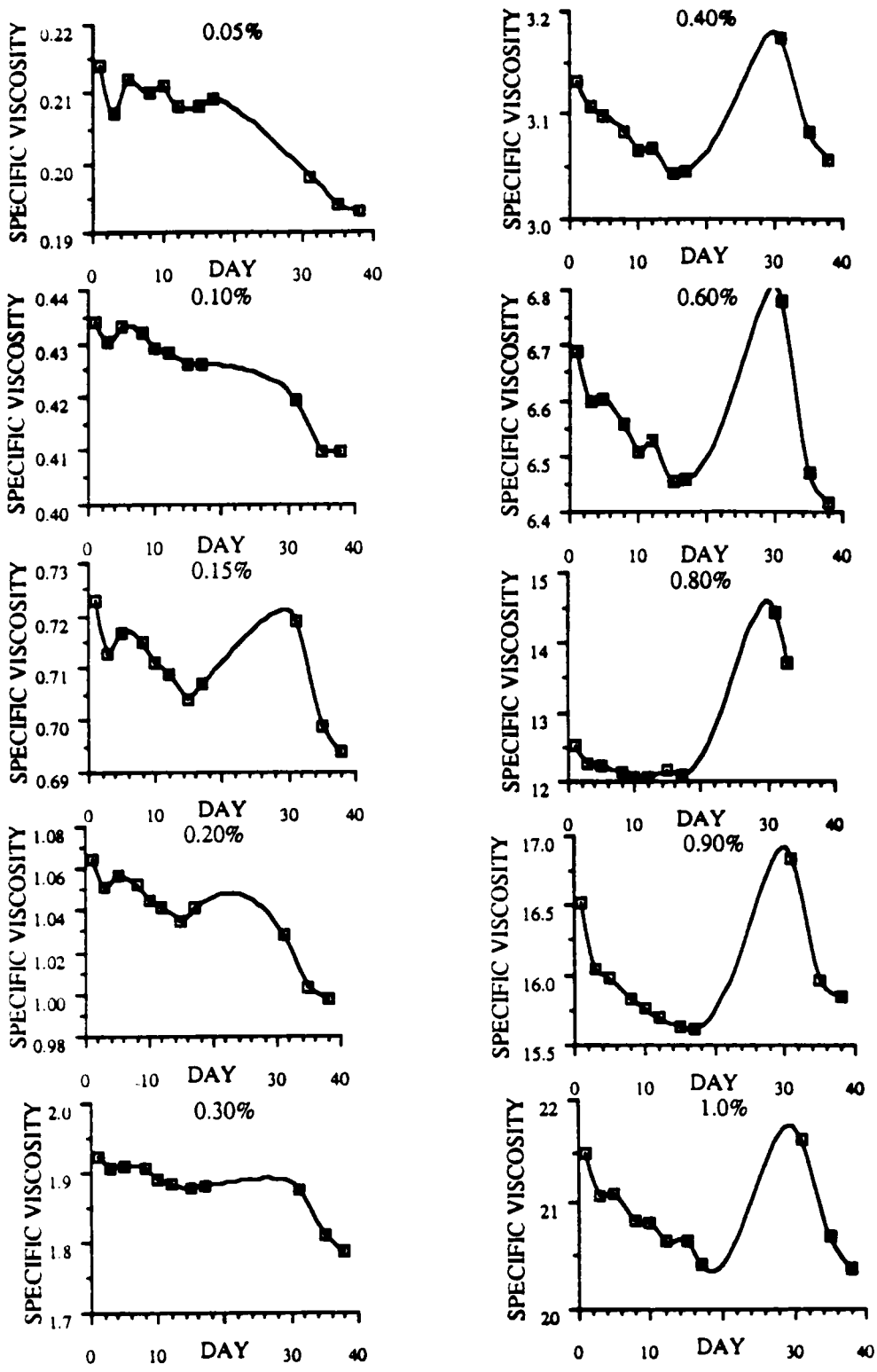

Figure 2.61: Concentration and time dependent changes in specific viscosity for 13.5% NC/EtOAc.

with time. The exceptions were in the 0.05% and 0.10% solutions where the values leveled off after around the tenth day of aging. The more interesting results were those for 0.15%, 0.4%, 0.6%, 0.8% 0.9% and 1.0%. The viscosities of these solutions were either fully or almost fully regained. This is important because it ***is conclusive evidence that the decrease in viscosity was not due to degradation***. Degradation by chain scission would result in shorter chains which have to repolymerize as the solvent was evaporated in order to yield the results seen above. On the other hand, if the mechanism for decrease in viscosity were some sort of equilibrium between associated and dissociated molecules, then the loss of solvent may result in reassociation, thus yielding viscosities that were the same as the original viscosities ***immediately*** upon redissolution. However, the faster rate of decrease after redissolution is evidence that even after reassociation there was a difference in physical structure of the nitrocellulose compared to the originally fibrous sample. It is possible for the macromolecule did not recoil to as tight a conformation as in the original sample so that the solvent molecules have easier access for optimum solvation after redissolution. Whether the associated molecule is gel-like or liquid crystal-like may be conformation dependent. There has been evidence for liquid crystal like structures in concentrated solutions for the trinitrate derivative of cellulose (88-92). Perhaps, the more highly coiled 12.58% NC would a form gel structure by hydrogen bonding since it has more underivatized hydroxyl groups along the chain, while the more extended 13.5% nitrocellulose would be more susceptible to alignment leading to crystallite formation or liquid crystal related structures.

2.5. SUMMARY AND CONCLUSIONS

The main objective of this investigation was to determine the absolute molecular weight and molecular weight distribution of nitrocellulose. Before this objective could be achieved however, the aging of nitrocellulose solutions had to be understood. In order to achieve this secondary objective several experiments were carried out to examine the effect of nitration level and solvent power on this phenomenon. Specifically, the two cellulose nitrates studied had nitration levels of 12.58% and 13.5%. The solvents used were tetrahydrofuran -- both stabilized and unstabilized -- and ethyl acetate.

The LALLS experiment revealed a decrease of molecular weights over time in all three solvents. The molecular weights in EtOAc were always higher than those in THF. This decrease in molecular weights was accompanied by systematic changes in the specific refractive index increments and second virial coefficients. The second virial coefficient in EtOAc was lower than that in THF. In addition, this quantity remained relatively constant for the EtOAc over a three week period but changed over the same time span for THF solvent.

The GPC experiment exposed the same trend of decrease in molecular weights over time. The values of weight average molecular weight obtained by this method agreed closely with those measured by LALLS for the 12.58% nitrocellulose, but began to differ for the 13.5% nitrocellulose. The agreement was better at the earlier stages of the investigation, with the disparity increasing as the aging time lengthened. Although the discrepancies were within tolerable limits for the 12.58% system, they reached unacceptable levels for the 13.5% system. This may be a hint that at some point, the universal calibration was not valid for the more rodlike nitrocellulose analog.

In addition to this information on molecular weights, the GPC results also showed that the absolute molecular weight distributions for both nitration level nitrocelluloses narrowed as aging continued. The significant changes in polydispersity occurred within two weeks of sample preparation, then became insignificant afterwards. Interestingly enough, the narrowing of MWD was achieved by a shift only in the higher molecular weight end of the distribution to lower molecular weights, with the lower molecular weight end remaining stationary. A slight increase of the concentration of lower molecular weight species accompanied this horizontal shift. This behavior was interpreted to mean that the aging phenomenon was brought about by the dissociation of clusters of solute which did not immediately dissolve initially, thus yielding higher initial apparent molecular weights. These aggregates were broken up as the solution aged, leading to the decrease in the measured apparent molecular weights. If the mechanism for dissociation was solvation, the role of solvent power may then explain the trends seen in the second virial coefficients as well as the difference in molecular weights obtained in the different solvents. Due to the preponderance of

views leaning towards degradation by chain scission as the mechanism for aging, two other experiments were carried out:

(1) Infrared spectra of films cast from aged solutions were taken. These results revealed no evidence of chain scission for all systems up to two weeks. Beyond this time, 13.5% NC/THF was the only combination of polymer/solvent that exhibited some degradation. The solvent was evaporated and the dried sample was redissolved. There was no degradation apparent for systems that were undegraded before this step. However, some degradation was evident in the 12.58% NC/THF which was stored for six months prior to redissolution. Sonication and nitric acid doping were found to accelerate this degradation process.

(2) Finally, the specific viscosities of these systems were followed during storage of solutions. In all cases, this quantity systematically decreased with "equilibrium" values reached for the dilute solutions but not for the concentrated solutions. The plots of the reduced viscosities exhibited maxima related to the presence of associated molecules in solution. After the solvent had been evaporated, and new solvent was added, the specific viscosities of some of the systems ***reverted to their original values***. The subsequent ***rate*** of decrease in viscosity was significantly faster after the redissolution.

Based on the findings summarized above, it may be concluded that the aging of nitrocellulose solutions is a complex phenomenon which is a result of a two stage process. The early aging appears to be due physical changes in the structure of nitrocellulose brought about by the solvent requiring time to achieve optimum solvation. This depends on NC production conditions, nitration level and native cellulose, as well as solvent and temperature. Before this stage is reached, some association is present, resulting in higher ***apparent*** molecular weights. Kinetically, as the solvent penetrates these clusters, the aggregates are broken up into smaller species. The nitration level and solvent power are important factors in such an aging. The more nitrated analog reached optimum solvation sooner than its less nitrated counterpart. This procedure was also aided by greater solvent affinity for the polymer. It appears that the initial stage was completed within 14 days. Based on this time, the absolute molecular weight and MWD measured are those

obtained ***at this point.*** It was shown that the GPC/DV which is based on a universal calibration concept was a viable method for the less nitrated cellulose, while more caution should be taken when applying this method to the more highly nitrated analog.

The slow ***long term aging*** of nitrocellulose may indeed be attributed to chemical changes such as degradation by chain scission. Exactly when this stage starts or overlaps with the initial physical changes occurring was not clear in the study. Once again, it was established that nitration level and solvent power influence the point at which this stage begins.

REFERENCES

1. Wint, R. F. and Shaw, K. G., in *ACS Symposium Series 285 (Applied Polymer Science)*, Tess, R. W. and Poehlein, G. W. (eds.), 2nd Ed., American Chemical Society, Washington, D. C. 1985, p.1073.

2. Reveley, A., in *Cellulose and its Derivatives Chemistry, Biochemistry and Applications*, Kennedy, J. F., Phillips, G. O., Wedlock, D. J. and Williams, P. A. (eds.), Wiley, New York, 1985, p. 211.

3. Akira, K., in *Polymer Fractionation*, Cantow, M. J. R. (ed.), Academic Press, New York, 1967, p. 43.

4. Elliott, J. H., in *Polymer Fractionation*, Cantow, M. J. R. (ed.), Academic Press, New York, 1967, p. 67.

5. Conrad, C. M., Ind. Eng. Chem., **45**, 2511 (1953).

6. Mitchell, R. L., Ind. Eng. Chem., **45**, 2526 (1953).

7. Demougin, P., Compt. Rend., **196**, 408 (1933).

8. Park, G. S. and Said, M. M., in *Cellulose and its Derivatives Chemistry, Biochemistry and Applications*, Kennedy, J. F., Phillips, G. O., Wedlock, D. J. and Williams, P. A. (eds.), Wiley, New York, 1985, p. 337.

9. Reiser, V., Masura, V. and Kozmal, F., Cellulose Chem. Technol., **1**, 51 (1967).

10. Huang, R. Y. M. and Jenkins, R. G., Tappi, **52**, 1503 (1969).

11. Segal, L., J. Polym. Sci. C, **21**, 267 (1968).

12. Segal, L., J. Polym. Sci., Polym. Lett., **4**, 1011 (1966).

13. Marx-Figini, M., Das Papier, **36**, 577 (1982).

14. Waters Associates Inc. Technical Publication B40, 1981.

15. Moore, J. C., J. Polym. Sci. A, **2**, 835 (1964).

16. Moore, J. C. and Hendrickson, J. G., J. Polym. Sci. C, **8**, 233 (1965).

17. Maley, L. E., J. Polym. Sci. C, **8**, 253 (1965).

18. Altgelt, K. H. and Moore, J. C., in *Polymer Fractionation*, Cantow, M. J. R. (ed.), Academic Press, New York, 1967, p. 123.

19. Meyerhoff, G., J. Chromatogr. Sci., **9**, 596 (1971).

20. Marx-Figini, M. and Soubelet, O., Polym. Bull., **11**, 281 (1984).

21. Cunningham, A. F., Heathcote, C., Hillman, D. E., Paul, J. I., in *Chromatographic Science Series Vol. 13, (Liquid Chromatography of Polymers and Related Materials II)*, Marcel Dekker Inc., New York, 1980, p. 173.

22. Marx-Figini, M. and Soubelet, O., Polym. Bull., **6**, 501 (1982).

23. Meyerhoff, G. and Jovanovic, S., J. Polym. Sci. Polym. Lett., **5**, 495 (1967).

24. Stalder, C., Stahli, C. and Herren, C., PFW SIG BP 1945 (1985).

25. Segal, L., in *Advances in Chromatography, Vol. 12*, Giddings, J. C., Grushka, E., Keller, R. A. and Cazes, J. (eds.), Marcel Dekker Inc., New York, 1975, p. 31.

26. Alexander, W. J. and Muller, T. E., Sep. Sci., **6**, 47 (1971).

27. Holt, C., Mackie, W. and Sellen, D. B., Polymer, **19**, 1421 (1978).

28. Cantow, M. J. R., Porter, R. S. and Johnson, J. F., J. Polym. Sci. A-1, **5**, 1391 (1967).

29. Chiantore, O. and Hamielec, A. E., J. Liq. Chromatogr., **7**, 1753 (1984).

30. Goetz, H., Elgass, H. and Huber, L., J. Chromatog., **349**, 357 (1985).

31. Segal, L., Timpa, J. D. and Wadsworth, J. I., J. Polym. Sci. A-1, **8**, 25 (1970).

32. Ouano, A. C., Barrall, E. M. II, Broido, A., Javier-Son, A. C., in *Advances in Chemistry Series, Vol 125*, ACS, Washington D. C., 1973, p. 187.

33. Ouano, A. C., Broido, A., Barrall, E. M. and Javier-Son, A. C., Polym. Pre., **12**, 859 (1971).

34. Segal, L., Timpa, J. D. and Wadsworth, J. I., J. Polym. Sci. A-1, **8**, 3577 (1970).

35. Chang, M., Tappi, **55**, 1253 (1972).

36. Enoksson, B., Chemica Scripta, **4**, 43 (1973).

37. Flory, P. J., Spurr, K. Jr. and Carpenter, D. K., J. Polym. Sci., **27**, 231 (1958).

38. Moore, W. R. and Edge, G. D., J. Polym. Sci., **47**, 469 (1960).

39. Rudin, A. and Hoegy, H. L., J. Polym. Sci. A-1, **10**, 217 (1972).

40. Timpa, J. D. and Segal, L., J. Polym. Sci. A-1, **9**, 2099 (1971).

41. Newman, S., Krigbaum. W. R. and Carpenter, D. K., J. Phys. Chem., **60**, 648 (1956).

42. Mikesova, J. and Quadrat, O., Collec. Czech. Chem. Commun., **40**, 2461 (1975).

43. Kamide, K. and Saito, M., Makromol. Chem., Rapid Comm., **4**, 33 (1983).

44. Dayan, S., Maissa, P., Vellutini, M. J. and Sixou, P., Polym. Comm., **23**, 800 (1982).

45. Aharoni, S. J., Macromolecules, **16**, 1722 (1983).

46. Staikos, G. and Dondos, A., Eur. Polym. J., **19**, 555 (1983).

47. Saito, M., Polymer J., **15**, 213 (1983).

48. Immergut, E. H. and Eirich, F. R., Ind. Eng. Chem., **45**, 2500 (1953).

49. Grubisic, Z., Rempp, P. and Benoit, H., J. Polym. Sci. Polym. Lett., **5**, 753 (1967).

50. Dawkins, J. C., Maddock, J. N. and Coupe, D., J. Polym. Sci., Part A-2, **8**, 1803 (1970).

51 Wadsworth, J. I., Segal, L. and Timpa, J. D., Polym. Pre., **12**, 854 (1971).

52. Wadsworth, J. I., Segal, L. and Timpa, J. D., in Advances in Chemistry Series Vol. 125 (Polymer Molecular Weight Methods), ACS, Washington D. C., 1973, p. 178.

53. French, D. M. and Nauflett, G. W., J. Liq. Chromatogr., **4**, 197 (1981).

54. Brewer, R. J., Tanghe, L. J., Bailey, S. and Burr, J. T., J. Polym. Sci. A-1, **6**, 1697 (1968).

55. Wirsen, A., Makromol. Chem., **189**, 833 (1988).

56. Haney, M. A., J. Appl. Poly. Sci., **30**, 3023 (1985).

57. Haney, M. A., J. Appl. Poly. Sci., **30**, 3037 (1985).

58. French, D. M., Nauflett, G. W. and King, G. M., Report No. NOLX 81, Ordinance Laboratory, U. S. Navy, June 1974.

59. Cosgrove, J. D., Head, B. C., Lewis, T. J., Graham, S. G. and Warwicker, J. O , in *Cellulose and its Derivatives Chemistry, Biochemistry and Applications*, Kennedy, J. F., Phillips, G. O., Wedlock, D. J. and Williams, P. A. (eds.), Wiley, New York, 1985, p. 143.

60. Spurlin, H. M., in *High Polymers V: Cellulose and Cellulose Derivatives*, Ott, E. (ed.), Interscience, New York, 1943, p. 853.

61. Lindsley, C. H. and Frank, M. B., Ind. Eng. Chem., **45**, 2491 (1953).

62. Marx-Figini, M. and Schulz, G. V., Makromol. Chem., **54**, 102 (1962).

63. Scherer, P. C. and Crookston, N. J., J. Polym. Sci, **14**, 129 (1954).

64. Campbell, H. and Johnson, P., J. Polym. Sci., **4**, 247 (1949).

65. Brown, W. J., Tappi, **49**, 367 (1966).

66. Marx-Figini, M., Cellulose Chem. Technol., **18**, 549 (1984).

67. Marx-Figini, M., Die Angew. Makromol. Chem., **72**, 161 (1978).

68. Paul, C. W. and Cotts, P. M., Polym. Pre., **27**, 215 (1986).

69. Elias, H. G., in *Order in Polymer Solutions*, Solc, K. (ed.), Gordon & Breach Science Publishers, London, 1976, p. 209.

70. Immergut, E. H., Ranby, B. G. and Mark, H. F., Ind. Eng. Chem., **45**, 2483 (1953).

71. Campbell, H. and Johnson, P., J. Polym. Sci., **5**, 443 (1950).

72. Campbell, H. and Johnson, P., J. Polym. Sci., **3**, 735 (1948).

73. Morozov, A. A. and Pamfilov, A. V., J. Gen. Chem. USSR, **8**, 175 (1938).

74. Morozov, A. A. and Pamfilov, A. V., J. Gen. Chem. USSR, **7**, 2154 (1937).

75. Morozov, A. A., Pamfilov, A. V. and Shikher, A. G., J. Gen. Chem. USSR, **8**, 572 (1938).

76. Morozov, A. A. and Pamfilov, A. V., J. Gen. Chem. USSR, **9**, 759 (1939).

77. Chedin, J., J. Chem. Phys., **44**, 141 (1947).

78. Scheiber, J., Farbe und Lack., **147**, 139 (1940).

79. Goldman, I. O., Kino Fotokhim. Prom., **3**, 30 (1938); CA **32**, 8769.

80. Rogovin, Z. A. and Glazman, S., J. Gen. Chem. USSR, **8**, 498 (1938).

81. Claesson, S. and Wettermark, G., Arkiv For Kemi, **17**, 355 (1961).

82. Claesson, S., Palm, G. and Wettermark, G., Arkiv For Kemi, **17**, 579 (1961).

83. Carignan, Y. P. and Turngren, E. V., J. Ballist., **6**, 1374 (1982).

84. Fowler, A. H. K., H. S. Munro and Clark, D. T., in *Cellulose and its Derivatives: Chemistry, Biochemistry and Applications*, Kennedy, J. F., Phillips, G. O., Wedlock, D. J. and Williams, P. A. (eds.), Wiley, New York, 1985, p. 245.

85. Isler, J. and Flegier, D., in *Cellulose and its Derivatives: Chemistry, Biochemistry and Applications*, Kennedy, J. F., Phillips, G. O., Wedlock, D. J. and Williams, P. A. (eds.), Wiley, New York, 1985, p. 329.

86. Wehr, W., Kolloid Z., **88**, 185 (1939).

87. Kanamaru, K., Kolloid Z., **87**, 191 (1939).

88. Viney, C. and Windle, A. H., in *Wood and Cellulonics, Industrial Utilization, Biotechnology, Structure and Properties*, Kennedy, J. F., Phillips, G. O. and Williams, P. A. (eds.), Ellis Horwood, New York, 1987..

89. Viney, C. and Windle, A. H., J. Mater. Sci. Lett., **5**, 516 (1986).

90. Gray, D. G., in *J. Appl. Poly. Sci, Applied Polymer Symposium 37, Proceedings of the Ninth Cellulose Conference*, Sarko, A. (ed.), John Wiley & Sons, New York, 1983, p. 179.

91. Aharoni, S. M., Polym. Pre., **22**, 116 (1981).

92. Gray, D. G., Farad. Discuss. Chem. Soc., **79**, 257 (1985).

93. Spurlin, H. M., in *High Polymers V: Cellulose and Cellulose Derivatives*, Ott, E. (ed.), Interscience, New York, 1943, p. 910.

94. Schurz, J. and Tritthart, H., Polymer, **7**, 475 (1966).

95. Dautzenberg, H., J. Polym. Sci. C., **39**, 123 (1972).

96. Segal, L. and Timpa, J. D., Tappi, **52**, 1669 (1969).

97. Holt, C., Mackie, W. and Selen, D. B., Polymer, **17**, 1027 (1976).

98. Stuting, H. H., Chromatix Instruments Operator's Guide, LDC/Milton Roy, Florida, 1981.

99. Johnson, B. L. and Smith, J. in *Light Scattering from Polymer Solutions*, Huglin, M. B. (ed.), Academic Press, New York, 1972, p. 27.

100. Skoog, D. A. and West, D.M., *Principles of Instrumental Analysis*, Holt, Rinehart & Winston, New York, 1971.

101. Lange's Handbook of Chemistry, Dean, J. A. (ed.), 12th ed., McGraw-Hill, New York, 1979.

102. Chromatix KMX-6 Low Angle Laser Light Scattering Photometer Operating Manual for LALLS Serial No. 337.

103. Balcells, E., to be published.

104. Silverstein, R. M., Basler, G. C. and Morri, T. C., *Spectrometric Identification of OrganicCompounds*, 4th ed., John Wiley & Sons, New York, 1981.

105. Elias, H. G., *Macromolecules 1 Structure and Properties*, 2nd ed., Plenum Press, New York, 1984, p. 353.

106. Elias, H. G., in *Light Scattering from Polymer Solutions*, Huglin, M. B. (ed.), Academic Press, New York, 1972, p. 397.

CHAPTER 3

THE ABSOLUTE MOLECULAR WEIGHT DISTRIBUTION OF HYDROXYPROPYLATED LIGNINS

3.1. INTRODUCTION

Lignin is a biopolymer which ranks second in natural abundance only to cellulose. Due to its profusion, variety and properties, the potential for technological applications is tremendous (1,2). Before these latent possibilities may be realized however, it is necessary to understand the structure/property relationships for this type of material. At the heart of this requirement is the need to determine absolute molecular weights and molecular weight distributions for lignins.

A literature review will reveal that the usual methods for molecular weight determination include the use of vapor phase osmometry or ultracentrifugation. These techniques involve the tedious fractionation of this highly polydisperse polymer in order to obtain its molecular weight distribution. With the relatively recent advent of gel permeation chromatography (GPC), most investigators have turned to this instrument for lignin characterization due to its ease of use and short analysis time. However, the GPC molecular weights and hence molecular weight distributions typically obtained thus far have only been relative quantities since the calibration method commonly used was based on the molecular weights of polystyrene standards, which are structurally and topologically very different from lignins. In an attempt to obtain absolute numbers while bypassing the use of calibration standards with substantially different chemical structures, Kolpak et al. have resorted to a dual detection system for GPC which utilized both a differential refractive index (DRI) detector and a low angle laser light scattering (LALLS) detector (3). However, the use of GPC/LALLS to study lignins has complex problems associated with it that make its application to lignin analysis difficult.

About twenty years ago, Benoit et al. demonstrated that GPC separates molecules according to their hydrodynamic volume, which may be calculated by taking the product of intrinsic viscosity and molecular weight (4). In order to obtain absolute molecular weights, it is thus necessary to calibrate the instrument

based on molecular size and not molecular weight as is the usual practice. To take advantage of Benoit's universal calibration curve, one must be able to measure the intrinsic viscosity of the standards and the samples as they elute from the chromatograph. In this connection, a number of on-line viscosity detectors have been developed recently (5-16). Their use is still limited however since most of these detectors were one-of-a-kind models. In fact, only one (15,16) is commercial. Aside from the fact that viscosity detectors are not readily available, there is another reason for their lack of use in lignin research. There appears to be a reluctance to apply the universal calibration concept to lignins because of the prevalent belief that lignins have a three dimensional network structure which invalidates the procedure. However, no research has appeared to provide support for this viewpoint.

It is the objective of this investigation to show the feasibility of using GPC with a differential viscosity detector (GPC/DV) for the analysis of lignin molecular weights and molecular weight distributions. This was achieved by simultaneous use of the DRI as the concentration sensitive detector, the LALLS and the DV. VPO was used to provide reference values for the average molecular weights obtained.

In the course of the work, some anomalies due to the acknowledged association of lignin macromolecules were encountered (17-24). This added aspect of lignin behavior shall also be explored and emphasized as important. Hydroxypropylated lignins were the actual materials investigated.

3.2. LITERATURE REVIEW

3.2.1. Occurrence of Lignins

Lignin is an amorphous, aromatic biopolymer second in natural abundance only to cellulose. It is composed of phenylpropane units linked primarily through ether bonds and constitutes 15-40% of the dry weight of wood. Lignin concentration is highest in the middle lamella region where it serves to hold the wood fibers together. Aside from acting as a matrix for the cellulose fibers, the other functions of lignin include providing a means of conducting solutes over extended distances, energy storage, resistance to biodegradation and to stress brought about by changes in water balances and humidity (1,2,21,23-29).

3.2.2. Uses of Lignins

A combination of the abundance of lignins, its versatility due to the variation in sources and the recent interest in renewable resources have opened up research into the potential uses of lignins in many fields (17,27,30,31). Possible applications of lignins include its utilization as a prepolymer for engineered materials (30-32); specifically, it is touted as a phenol replacement in the synthesis of thermosetting resins (1,33-39) as well as thermoplastics (40). It has been employed as a particulate filler and reinforcing agent in rubber (1,2,25). Lignins may also be degraded to generate acids for methane production. These acids may subsequently be converted into hydrocarbons, thus making petroleum-like materials in a matter of hours instead of waiting on a geological time scale (41).

Where limitations existed in the potential of lignins for utilization in solid systems, efforts have been made to modify the pure material. These methods included derivatization by hydroxyalkylation and carboxylation to produce lignins that may be used in the formation of polyurethanes with a wide range of properties (33-35,42,43). Lignins have also been blended with polyurethane based sealants to make materials with improved properties (44). Finally, lignin has been used as a backbone, onto which 2-propenamide was grafted. The resulting material proved to be useful as a filtrate and control agent in mud drilling (1,25,29,45,46).

The above uses are but a few examples of the possible applications of lignins. The potential for its usage in a wide variety of fields will be aided by an understanding of the relationship between its structure and the properties of the end use materials. Due to this knowledge, several groups have delved into the chemical structure of lignins (47-51), its architecture (52,53) and its conformation (54-59). In all the above endeavors, a major analytical aid has been the determination of absolute molecular weights and molecular weight distributions of the lignins.

3.2.3. Molecular Weight Determination of Lignins

Methods previously used to obtain molecular weights of lignins and its derivatives include vapor phase osmometry (3,19,31,32), ultracentrifugation (20,21,54,58,60) and gel permeation chromatography

(1,3,17,19-22,27,35,37,49,50,55,59,61,-66). Each method has advantages and disadvantages as discussed below.

3.2.3.1. Vapor Phase Osmometry (VPO)

Vapor phase osmometry reveals absolute number average molecular weights. However, the method can be very time consuming. Furthermore, proper calibration of the instrument is critical to success since a constant necessary for data reduction is molecular weight dependent. A multistandard calibration method which circumvents this possible source of error has been devised in our laboratory by Dr. Jean-Noel Gorce.

3.2.3.2. Ultracentrifugation

Although ultracentrifugation is a standard method for absolute molecular weight determination, its application to lignins is fraught with difficulties. It has been documented that the wide polydispersity of lignins results in unique problems when ultracentrifugation was used for molecular weight determination. First, the molecular weight obtained seems to be strongly dependent on the speed of the centrifuge (58). Secondly, it was shown that fractions of lignin in the low molecular weight end of the distribution were chemically different from those at the high molecular weight end (20). This presents a problem since only one specific refractive index increment (dn/dc) is used throughout the experiment; this parameter varies with chemical structure, therefore, the assumption of constant dn/dc would yield erroneous results.

3.2.3.3. Gel Permeation Chromatography (GPC)

Gel permeation chromatography appears to be the most popular technique for the determination of lignin molecular weights and molecular weight distributions, no doubt due to its ease of use and convenience (17,19-22,31,32,35,37,46,55,61-75). Typical GPC analyses utilized columns based on crosslinked dextran or polystyrene crosslinked with divinylbenzene. There has been, rarely, usage of silica gel columns. Analyses tended to be carried out with aqueous sodium hydroxide systems or with organic solvents such as dioxane, tetrahydrofuran or dimethylformamide with LiCl or LiBr. The columns may be calibrated either by using narrow molecular weight distribution polystyrene standards, lignin model compounds or narrow fractions of lignin samples whose molecular weights were determined by

ultracentrifugation. In most cases, polystyrene standards have given reasonable values of molecular weights; however, it was found that these standards were not suitable for molecular weight determination of lignin derivatives. For these modified lignins, derivatized lignin model compounds were more appropriate (68). Caution must be exercised in assigning molecular weights using this type of calibration because this method yields ***apparent*** and not ***absolute*** molecular weights.

3.2.3.4. GPC Multidetection

The detector typically used for GPC analysis is the concentration sensitive detector, usually an ultraviolet or a differential refractive index detector. An early attempt at using multidetection in GPC was made by Kolpak et al. (3). These authors used GPC with both a DRI and a low angle laser light scattering (LALLS) detector. The lignin solutions were highly colored and the concentrations used absorbed a significant amount of the incident light. A correction, particularly significant with more concentrated solutions, was applied for static LALLS measurements to obtain second virial coefficients for GPC/LALLS. Also, the lignins were shown to fluoresce, although the fluorescence was claimed to be minimal at 633 nm, the analysis wavelength. This is illustrated in Figure 3.1 (3). A filter was installed to remove this extraneous radiation. In spite of these precautions however, the number average molecular weight obtained by LALLS was found to be about three times greater than that obtained by VPO. This may be related to a very recent finding that a third factor, related to beam polarization, needs to be considered in the experiment. This approach reportedly reduces the molecular weights obtained by 30-40% (76,77).

3.2.4. Association of Lignins

There is quite a bit of evidence that lignins associate in solution. Most of the work done in this area involved kraft lignins and organosolv lignins. The first evidence for association of lignins appeared in the work by Benko in 1964 (18). Some of his observations on molecular weight determination include: a) Kraft lignins tend to have higher apparent molecular weights with decreasing solution pH. b) Solvents such as formamide tend to cause rather than diminish the extent of association present in aqueous solvents. c) For milled wood and kraft lignins, either a slow dissociation or chemical reaction was seen in the initial

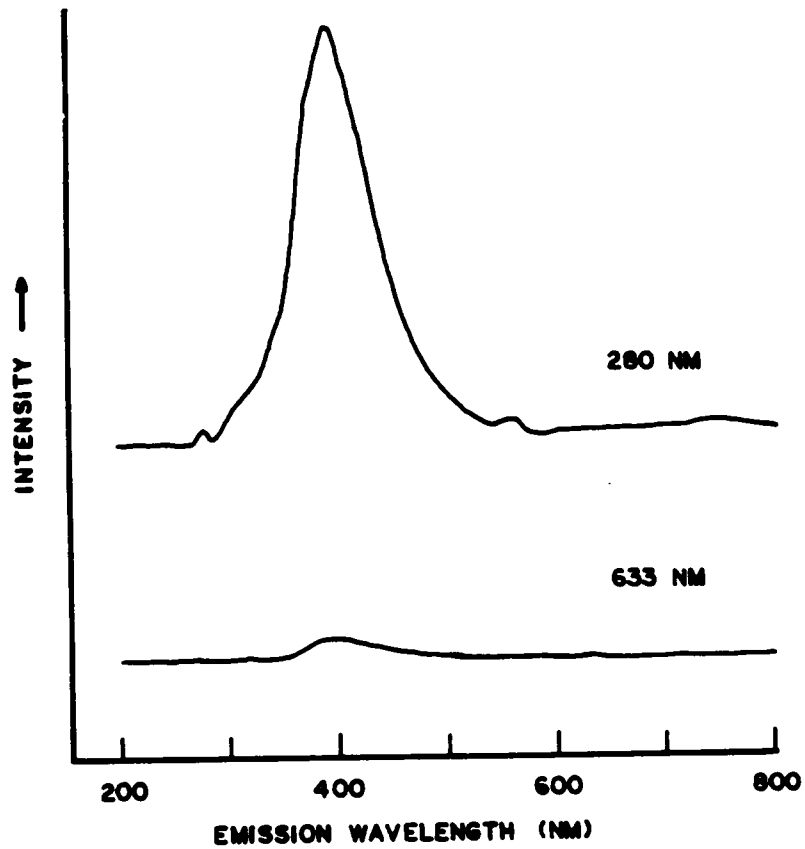

Figure 3.1: Fluorescence spectra for a kraft lignin in THF; excitation wavelengths are 280 nm and 633 nm (3).

phase of the experiment; however, the ***apparent*** molecular weights increased over time. d) Heating in a sodium carbonate solution lowered the apparent molecular weight.

Additional proof of lignin association surfaced in VPO experiments by Brown (19). The apparent molecular weight values obtained from DMSO and DMF were significantly lower than those in dioxane. The molecular weight decrease in the respective solvents, were accompanied by an increase in the second virial coefficients. This assocation phenomenon was reduced as the solvent power increased. Hydrogen bonded complexes of lignin with the highly polar solvents were postulated.

The association of the lignin molecules has been revealed by multimodal peaks in GPC chromatograms (17). Also the reduced viscosity plots for these kraft lignins exhibited rather pronounced curvature even for samples that were supposed to be dissociated, as in Figure 3.2. The reduced viscosity data have clear maxima. The maxima and curvature are both signs of association (78-80). It was also found that without the addition of NaOH to the solution, intrinsic viscosity increased over time. Subjecting solutions to elevated temperatures resulted in a faster increase in intrinsic viscosity which was thermally irreversible; however, the addition of NaOH induced dissociation of the aggregates. This is demonstrated in Figure 3.3. It was suggested that long range van der Waals forces played an important role in lignin association (17).

McCarthy et al. discovered that addition of LiCl or LiBr to the GPC eluant effected a change from the bimodal chromatographic peak which resulted from molecular association to a single broad peak (see Figure 3.4). It was proposed that the salt shielded dipoles in the individual molecules thus preventing association. Further studies showed that when the fractions from the bimodal molecular weight distribution of lignins were collected and rechromatographed, the materials from the higher and lower end of the distribution were chemically different though not vastly different in molecular weights (20).

The effect of solvent type was emphasized in further work by McCarthy et al. (21). They demonstrated that apparent molecular weight distributions obtained using organic solvents were multimodal, extending to very high molecular weights as seen in Figure 3.5. On the other hand, those obtained by alkaline aqueous eluants tended to be a broad envelope of components with some detailed information in the lower molecular

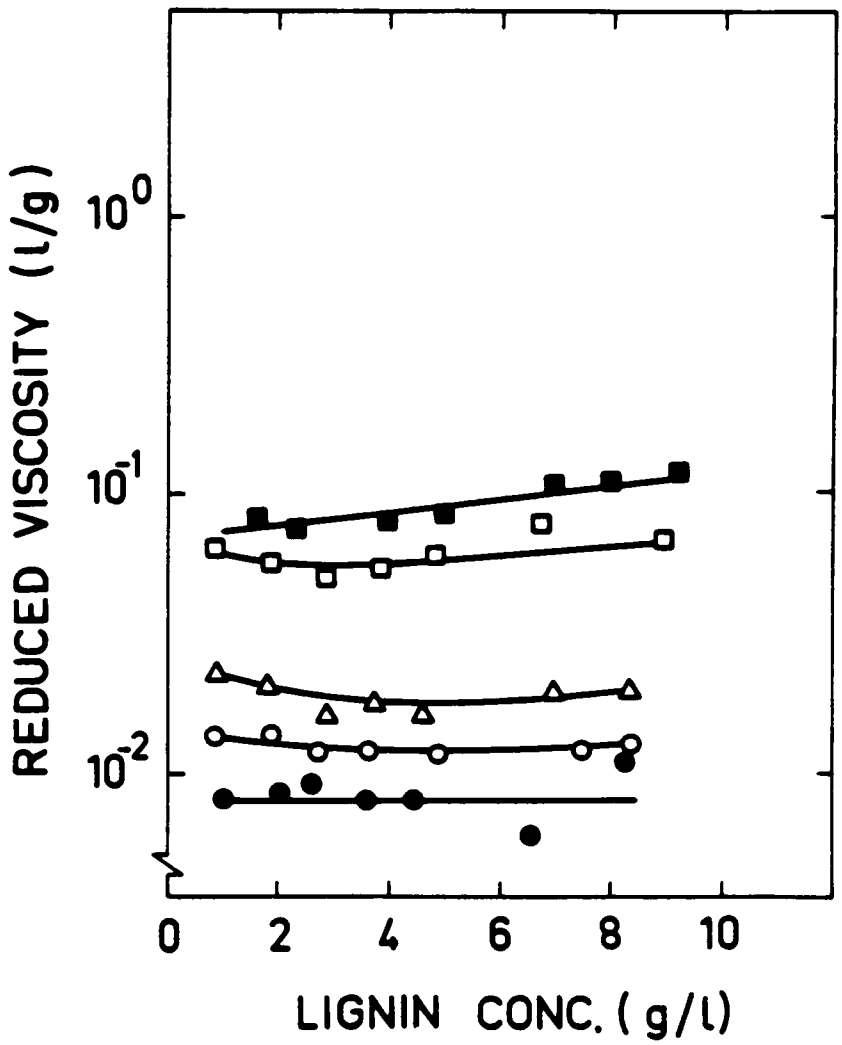

Figure 3.2: Reduced viscosity plots of kraft lignin with different degrees of dissociation: ●= 1.0, o = 0.7, Δ = 0.4,□= 0.2,■= 0 (17).

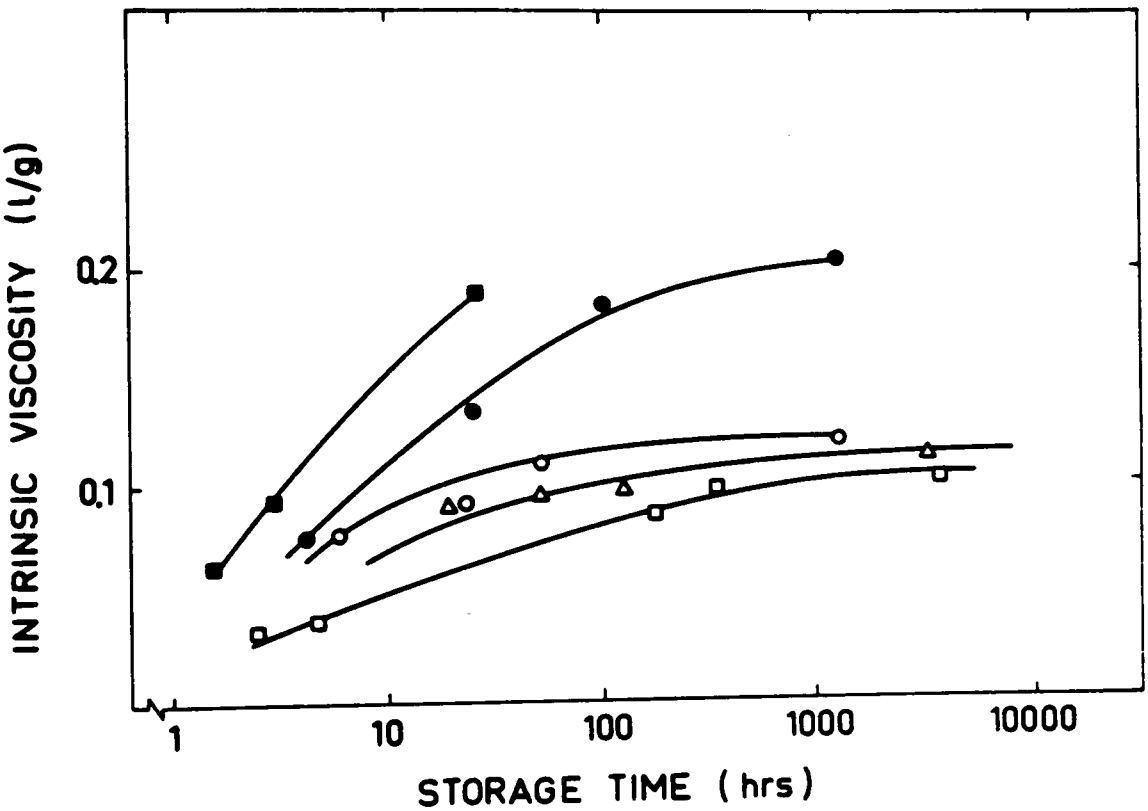

Figure 3.3: Intrinsic viscosity change as a function of storage at different temperatures: ■35.5°C,● 27.5°C, o 20.0°C, Δ 14.5°C,□11.0°C (17).

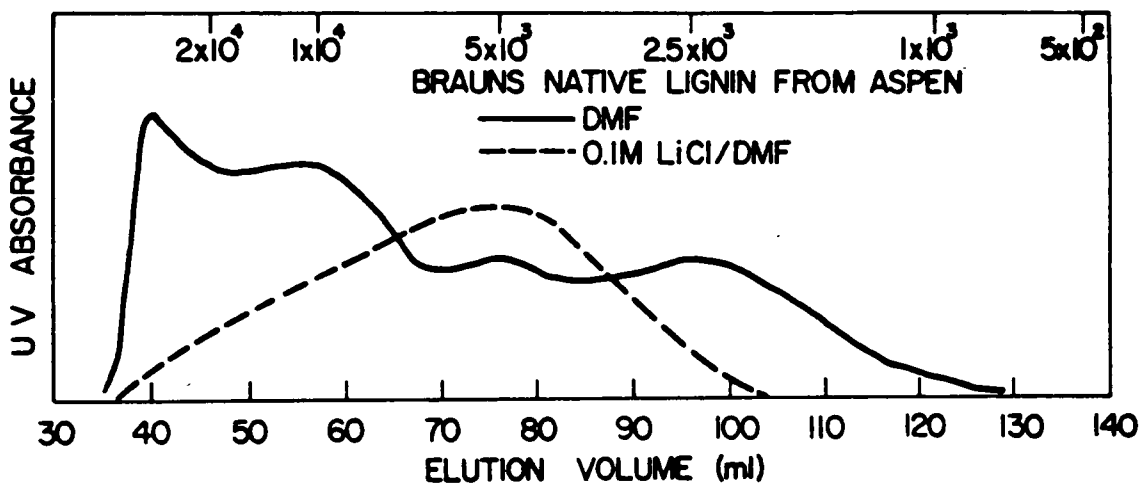

Figure 3.4: Gel chromatogram of aspen lignin on Sephadex LH-60 with DMF and DMF/0.1 M LiCl (20).

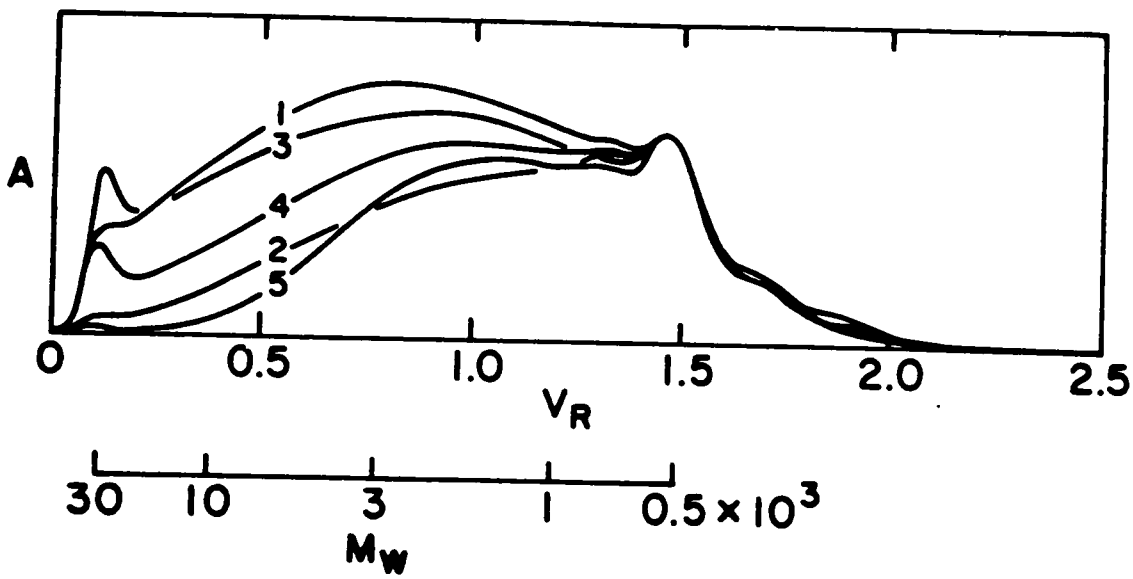

Figure 3.5: Elution profiles of organosolv lignins in Sephadex G75/0.10 M aqueous NaOH (1) red alder (2) western cottonwood (3) wheat straw (4) trembling aspen (5) bagasse (21).

weight region as shown in Figure 3.6. In the organic solvents, the molecular weights of the the associated complexes could be up to three orders of magnitude higher than those for the individual components. Again, a time effect was evident as molecular weight increased after some storage time. A rather intensive study was conducted to look into the effects of zwitterions and counterions on the association mechanism. The two step proposed mechanism based on this study was that the reaction initially involves a rapid equilibrium between the associated complexes and the dissociated components. The interaction between these two materials was proposed to be highly specific in the sense that high molecular weight species prefer to interact with the low molecular weight materials. The equilibrium was disturbed by the zwitterion in the direction of dissociation. The second step was a slow change which may be conformational in nature. In this step, the dissociated species were postulated to convert to a form which made reassociation inaccessible. McCarthy et al. proved hydrogen bonding was not involved by showing that exhaustive methylation and acetylation of the lignins did not significantly affect the amount of high molecular weight species present. Based on the available data, the proposed cause for association was the existence of some intermolecular orbital interaction of the HOMO-LUMO type (21-24).

Utilization of THF by some researchers recently revealed that bimodality of the chromatograms due to the solvent was not evident. However, there was evidence for an increase in apparent molecular weights over time as illustrated in Figure 3.6 (3,50,68,81).

3.3. EXPERIMENTAL

3.3.1. Materials

Hydroxypropyl (HPL) derivatives of four lignins were studied. The first sample was the HPL derivative of an organosolv red oak lignin. This was obtained by reacting a red oak organosolv lignin with propylene oxide according to a procedure described by Wu and Glasser (33). The organosolv pulping experiment was performed at an industrial pilot plant using aqueous methanol and 1% sulfuric acid as pulping medium. The reaction product with propylene oxide was isolated from homopolymer by liquid/liquid extraction with hexane from acetonitrile solution and it was precipitated in water.

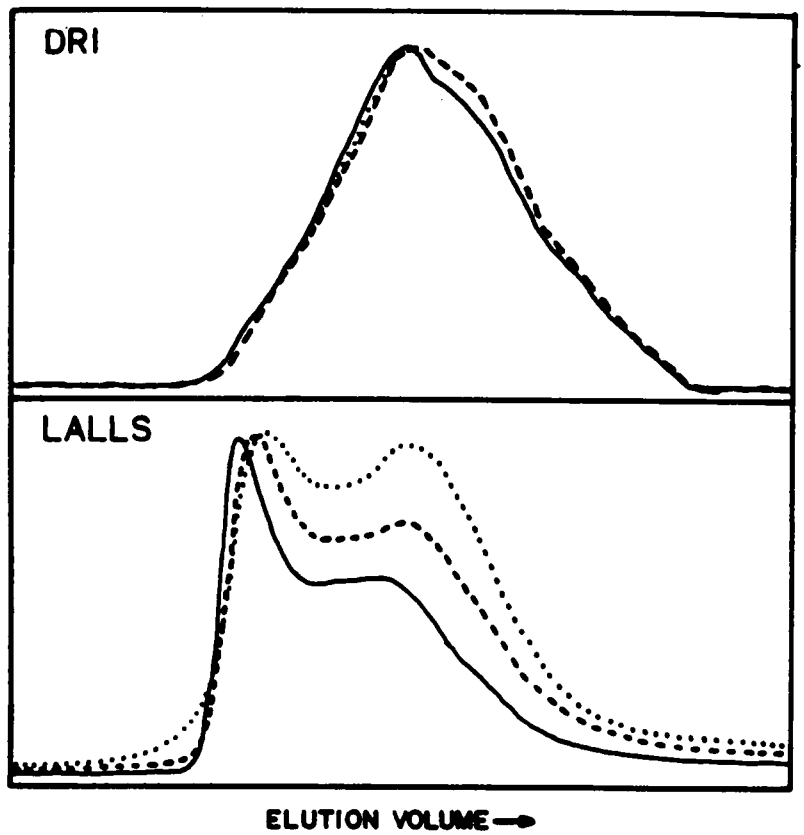

Figure 3.6: Aging of kraft lignin in THF evident in DRI and LALLS chromatograms (. . . .) 0.3 h, (---) 3.3 h, (___) 24h (3).

The second sample was designated as RO:PO. This was a different batch of the red oak HPL above, produced in larger quantity to allow preparative fractionation.

The third sample was aspen organosolv lignin HPL, made from a lignin supplied by the Biological Energy Corporation of Valley Forge, PA. This lignin was isolated from aspen by pulping with aqueous ethanol and a trace of sulfuric acid followed by hydroxypropylation (33).

The last sample was a hydroxypropyl derivative of a Westvaco hardwood kraft lignin. A kraft lignin supplied by Westvaco, Charleston, SC was isolated from a commercial kraft cook of mixed hardwood species by acidification of the spent pulping liquor, then hydroxypropylated (33).

3.3.2. Vapor Phase Osmometry

Vapor phase osmometry was conducted on a Wescan Model 233 at 30°C on the first day and the third day of sample solution preparation. The lignin solutions were made up with HPLC grade tetrahydrofuran (THF). On the first day of sample preparation, injections were completed within half an hour of solution. Number average molecular weights were obtained by multistandard calibration.

3.3.3. Specific Refractive Index Increment (dn/dc) Measurements

The solutions made from the four HPL's varied from a pale golden yellow to almost brown in color depending on the concentration. This was important in the selection of the concentration range to utilize in the dn/dc determination. Typically, it is desirable to pick a minimum concentration for which the deflection on the meter of the Chromatix KMX-16 laser differential refractometer is at least 2000. This was not possible for the lignins because at these "ideal" concentrations, the absorbance of the incident beam by the solutions was significant enough so that the transmitted power reaching the detector was inadequate. The solution to this problem involved a two-step process. First, the refractometer was calibrated so that the maximum concentration of the salt solution used for the standard calibration procedure caused the refractometer meter to deflect to 2000. Secondly, UV-Vis absorbance of the solutions at 633 nm were measured over a range of concentrations in order to determine the conditions at which the solutions had an absorbance of 0.1. These experiments were conducted on a Perkin-Elmer 552 Spectrometer at 633 nm with

a path length of 1 cm. The results of this experiment are given in Table 3.1. Based on these findings, the concentrations used for the experiment were chosen such that they had absorbances which were substantially below 0.05. All measurements were taken at 27°C. The specific refractive index increments were determined immediately after the solutions were made and then again on the third day after sample preparation.

3.3.4. Static Low Angle Laser Light Scattering

The concentrations of the solutions used for the light scattering experiments were chosen based on the UV-Vis absorbance experiment conducted for the dn/dc measurement. The requirement that the absorbance of the solutions used for the static light scattering experiment be lower than 0.1 was even more critical here than in the refractive index increment experiment because a large amount of absorbance would result in a significant reduction of the elastic scattering intensity, yielding erroneous results. The solutions were filtered through a 0.2 μm Acrodisc CR filter as they came out of the syringe pump at the rate of 0.15 ml/min and again just before they entered the sample cell. This dual filtering was found necessary for the THF solutions because particulate matter interfered significantly in the scattering measurements, since THF is a low scattering medium, having a Rayleigh scattering factor of 4.4×10^{-6} cm^{-1}. The static measurements were carried out on a Chromatix KMX-6 LALLS photometer which was equipped with a 2 mW He-Ne laser operating at 633 nm and an interference filter after the solution to remove any radiation due to fluorescence. The temperature in the sample chamber was 27°C. The experiments were conducted at a 6 - 7° forward scattering angle immediately after sample preparation. They were repeated on the third day after sample preparation for different aliquots taken from the same set of solutions. No polarization corrections were applied. Data were analyzed by the standard methods found in the KMX-6 manual.

3.3.5. Gel Permeation Chromatography

Polymer Laboratories narrow distribution polystyrene standards with peak molecular weights of 1250, 2150, 3250, 5000, 9000, 34,500, 68,000 and 170,000 g/mole were dissolved in HPLC grade THF. These

TABLE 3.1
UV-Vis Absorbance of Lignin/THF Solutions at 633 nm

LIGNIN	CONCENTRATION (g/L)	ABSORBANCE	ε (cm^2/g)
Red Oak	0.997	0.019	44.375
	2.541	0.087	
	5.052	0.203	
	7.582	0.324	
	9.912	0.408	
RO:PO	0.966	0.032	32.202
	1.509	0.044	
	2.053	0.064	
BB-HPL	0.954	0.051	55.935
	1.455	0.080	
	2.061	0.113	
Westvaco	1.100	0.045	33.011
	1.520	0.059	
	2.009	0.075	

were used to construct the universal calibration curve required to determine absolute molecular weights and molecular weight distributions with the differential viscosity detector.

Approximately 2.5 mg/ml solutions of the lignins were prepared in HPLC grade THF. These samples were analyzed on a Waters 150C ALC/GPC equipped with a differential refractive index detector and having a parallel connected Viscotek Model 100 differential viscosity detector and a Chromatix KMX-6 as in Figure 3.7. Six columns ranging from 100 Å to 10^6 Å pore diameter were mounted in series in the chromatograph and maintained at 30°C.

The scheme for GPC sample management is given in Figure 3.8. On the first day, duplicate runs for each sample were made at time "t" within five minutes of sample preparation. This sample was designated as A1(t). Four hours later, a second chromatogram was taken on the same stock of solution and designated as A1(t+4). The same stock solutions were retested in the same fashion three days later with these duplicate runs four hours apart. The first of these solutions will be designated as A3(t) and the duplicate as A3(t+4). This entire set of experiments was carried out again on new solutions in order to evaluate reproducibility. The new tests will be referred to as B1(t), B1(t+4), B3(t), and B3(t+4) with the annotations having the same meaning as explained above.

3.4. RESULTS AND DISCUSSION

3.4.1. Vapor Phase Osmometry

A non-traditional calibration curve was used in the determination of the molecular weights of the lignins by VPO and is shown in Figure 3.9. The points correspond to polystyrene standards with molecular weights of 5000, 2150, 1250 and to sucrose octaacetate which has a molecular weight of 678.6 g/mole. In order to obtain the molecular weight of an unknown sample, a plot of ΔV (voltage change of the solution of concentration c which is related to the temperature increase to compensate for the lower vapor pressure of the solvent in the solution) versus the corresponding concentration is made. The slope of this line (linear) yields $\Delta V/c$ so that the number average molecular weight may be determined from the calibration curve by interpolation.

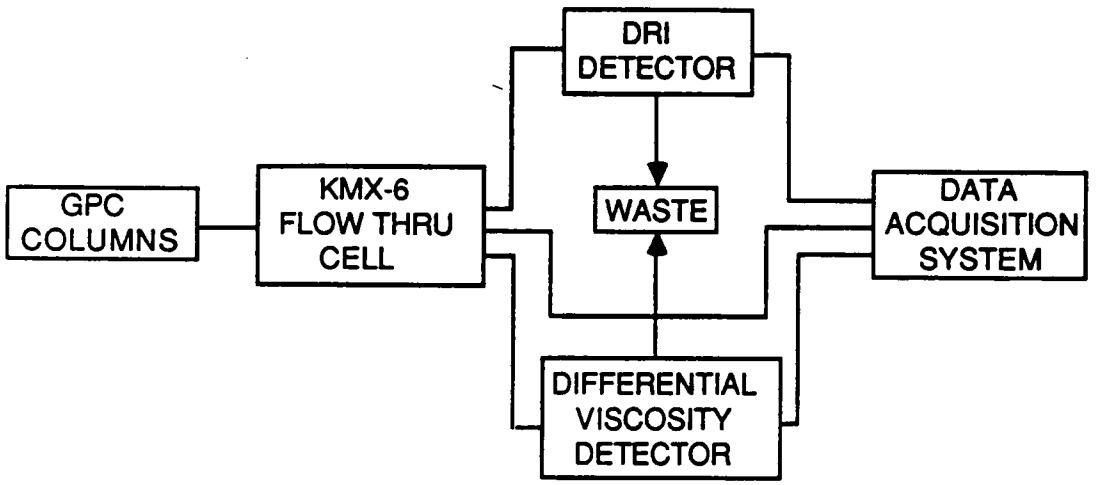

Figure 3.7: GPC multidetector set-up.

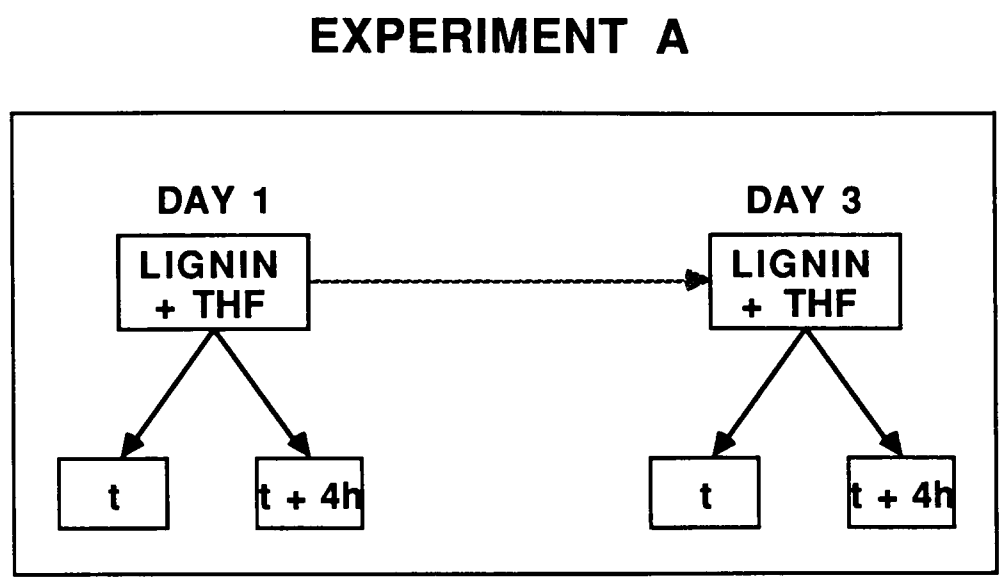

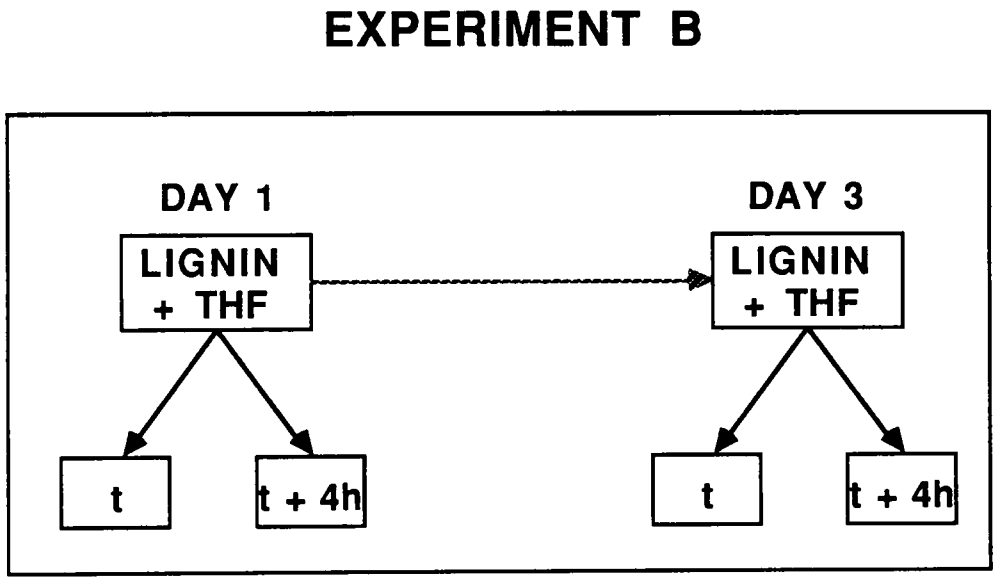

Figure 3.8: GPC sample management scheme.

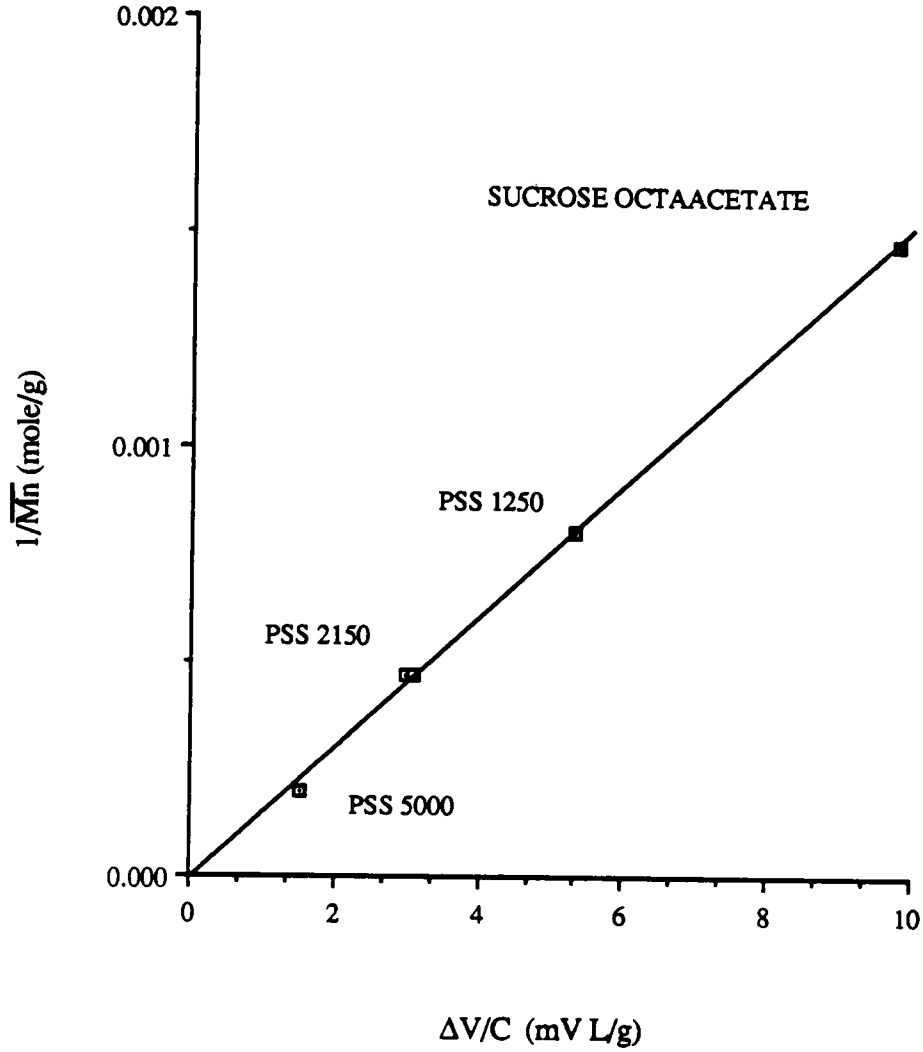

Figure 3.9: VPO calibration curve.

A typical ΔV versus concentration plot for red oak is shown in Figure 3.10. In all of these experiments, the data were linear as in Figure 3.10. The intercept of all of the ΔV vs. c graphs for the first day experiments were lower than those data on the third day. Except for RO:PO, the ΔV at zero concentration was close to zero, as expected. Another common feature for all experiments was a decrease in slope of these ΔV vs. c analyses on the third day compared to the first day tests. This was an indication of an increase in ***apparent*** molecular weights over time. The change in values of ΔV was greater for the more dilute concentrations. A summary of the results is given in Table 3.2. The apparent number average molecular weights obtained from the third day investigations were consistently about 20% higher than found on the first day for the same solution. The findings obtained in this experiment are in agreement with observations on the association that lignins are known to undergo (17-24).

Further proof of HPL association was revealed from graphs of ΔV/concentration against concentration as shown in Figure 3.11 for the red oak sample. The slope of such graphs is proportional to the second virial coefficient of the solution, which is an indication of solvent-polymer interaction. In all cases, the data from the first day experiments were linear when treated as in Figure 3.11. The slopes of such plots for red oak and for RO:PO were slightly negative while those for aspen and Westvaco hardwood were slightly positive. There was a dramatic difference in second virial coefficients obtained from the third day experiments. First, the points were better fitted to higher order equations and second, the slope of the $\Delta V/c$ vs. c lines for the more dilute solutions were highly negative. This behavior is typically indicative of association in solution. In this case, the apparent higher molecular weights were due to association which was aided by a diminished interaction between the macromolecule and the solvent.

As previously indicated, the number average molecular weights, $\overline{M}_n$, obtained by VPO will be used as reference values for the GPC experiment. The $\overline{M}_n$ reproducibility was excellent as long as the time dependent changes described above were taken into consideration.

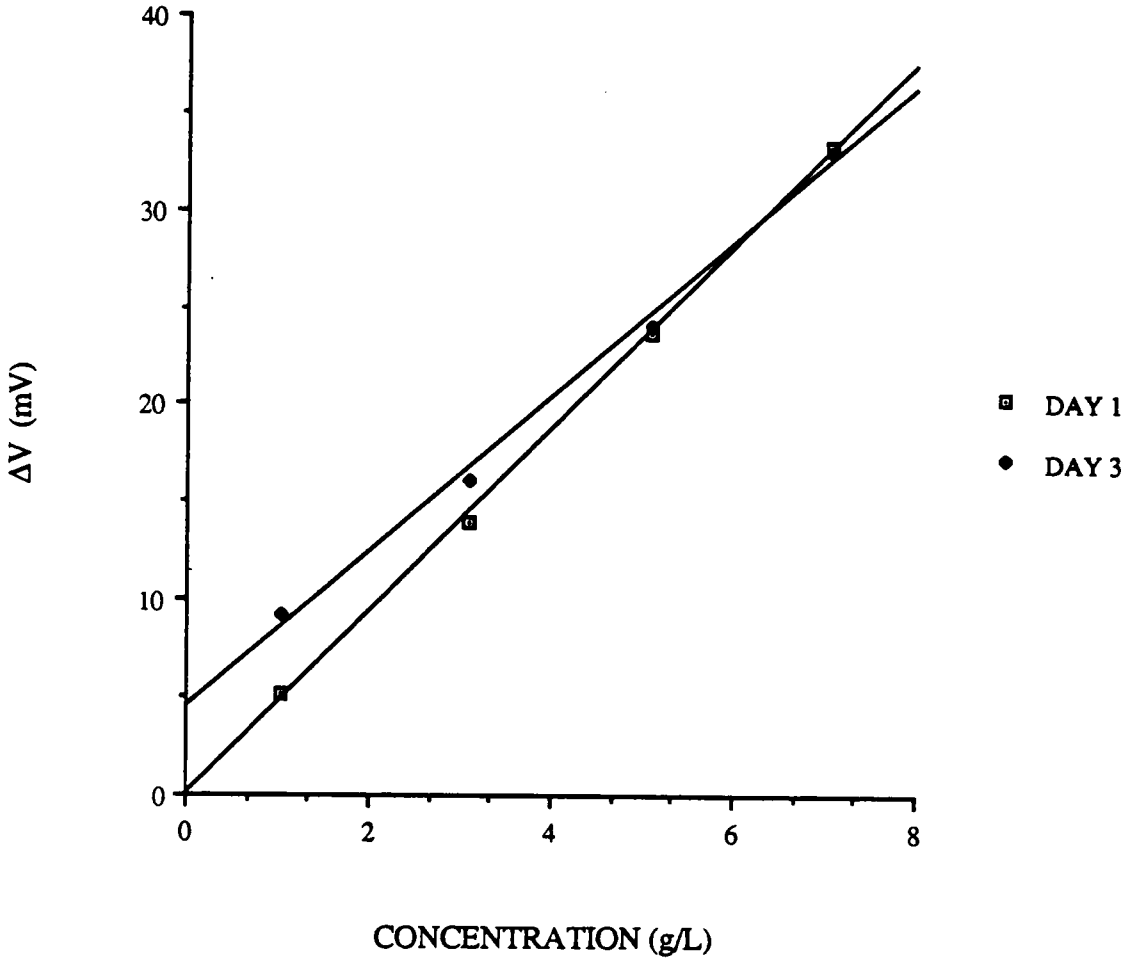

Figure 3.10: ΔV versus concentration plot for red oak HPL lignin.

TABLE 3.2
$\overline{M}_n$ from Vapor Phase Osmometry

SAMPLE	DAY	SLOPE	INTERCEPT	CORRELATION	$\overline{M}_n$ (g/mole)	% DIFFERENCE
Red Oak	1	4.697	-0.030	0.9996	1416	17.3
	3	3.962	4.519	0.9978	1684	
RO:PO	1	5.982	0.367	0.9994	1108	19.5
	3	4.929	12.348	0.9986	1348	
Aspen	1	4.775	-1.621	0.9982	1393	19.3
	3	3.946	6.492	0.9997	1691	
Westvaco	1	4.441	-1.226	0.9994	1499	21.0
	3	3.614	5.071	0.9963	1850	

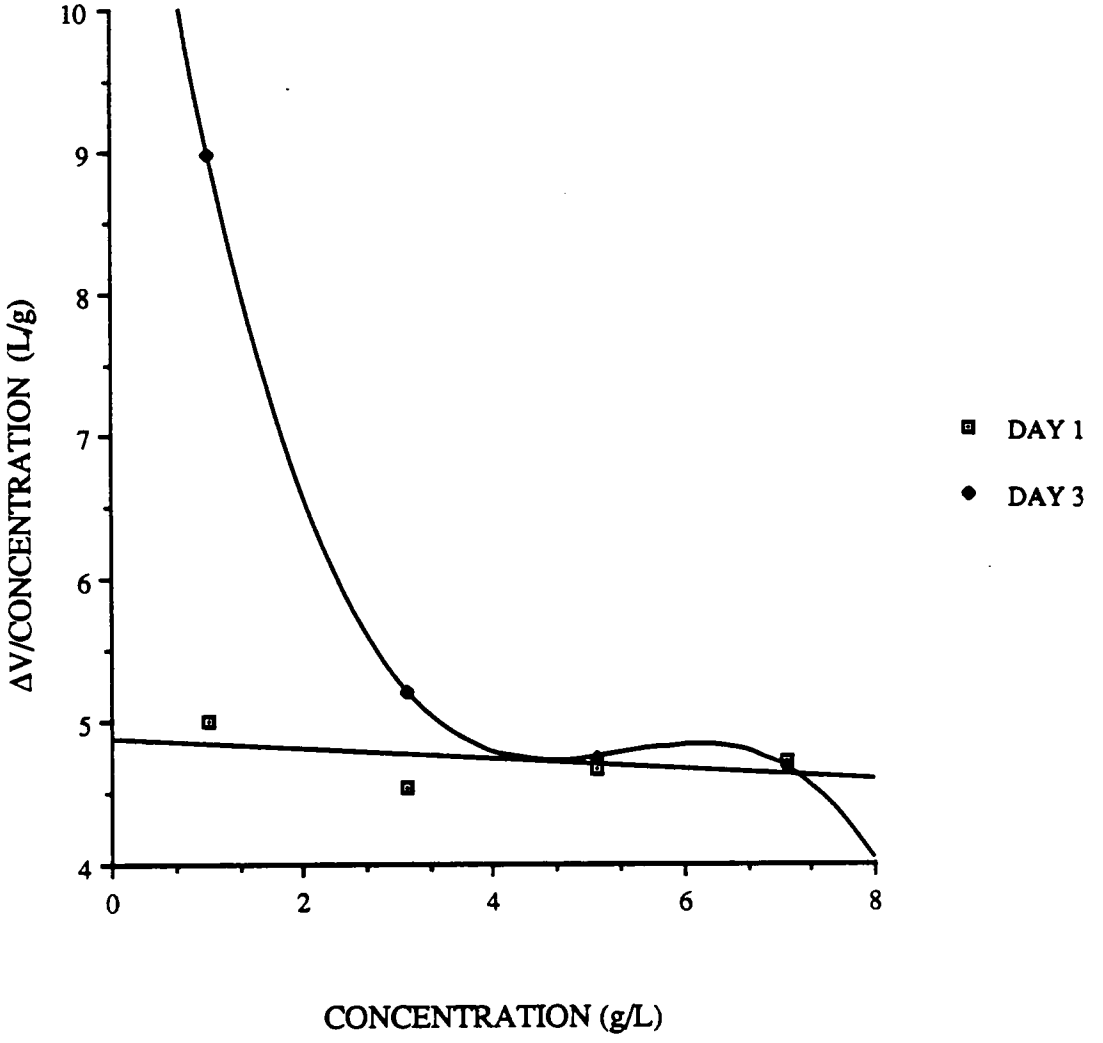

Figure 3.11: ΔV/concentration versus concentration plot for red oak HPL lignin.

3.4.2. Specific Refractive Index Increment (dn/dc)

The specific refractive index increments measured on the first day and the third day of sample preparation are shown in Figures 3.12-3.15. A zero slope should result for ideal solutions. Results for red oak HPL are given in Figure 3.12 where Δn/concentration was plotted against concentration. The most notable feature of these graphs is that the Δn/c values obtained on the third day experiments were much higher than those obtained on the first day. The error bars represent the standard deviation in five repetitions for the experiment. For all the data, there was no overlap of error bars so the changes noted were real.

The corresponding results for RO:PO are shown in Figure 3.13. The features of this graph were similar to Figure 3.12. Figure 3.14 contains a plot of Δn/concentration versus concentration for the aspen HPL. The results for the first day had a slope of approximately zero. On the third day however, there was a significant increase in the magnitude of the Δn/c. The Δn/concentration values for the more dilute solutions were higher than those of the more concentrated solutions. Finally, the results for Westvaco kraft lignin HPL are shown in Figure 3.15. As in the case of aspen HPL, there was no concentration dependence of Δn/concentration on the first day of experiments. However, there was clear curvature in the plot by the third day after the solution preparation, with values of Δn/concentration being much higher on the third day than on the first.

In view of the concentration dependence discovered for most samples, the dn/dc values used were obtained by taking the intercept of the Δn/concentration versus concentration plots. A summary of the dn/dc values for all samples on the two days of analysis is given in Table 3.3. The lack of precision was aggravated by the small quantities weighed out for the dilute solutions required in the experiment. This table contains a column indicating the percent difference in the values for both days. Except for the red oak solutions, the differences in dn/dc between the first day and the third day experiments were significant. This would considerably affect the molecular weights calculated by static LALLS since this quantity is squared in the calculations.

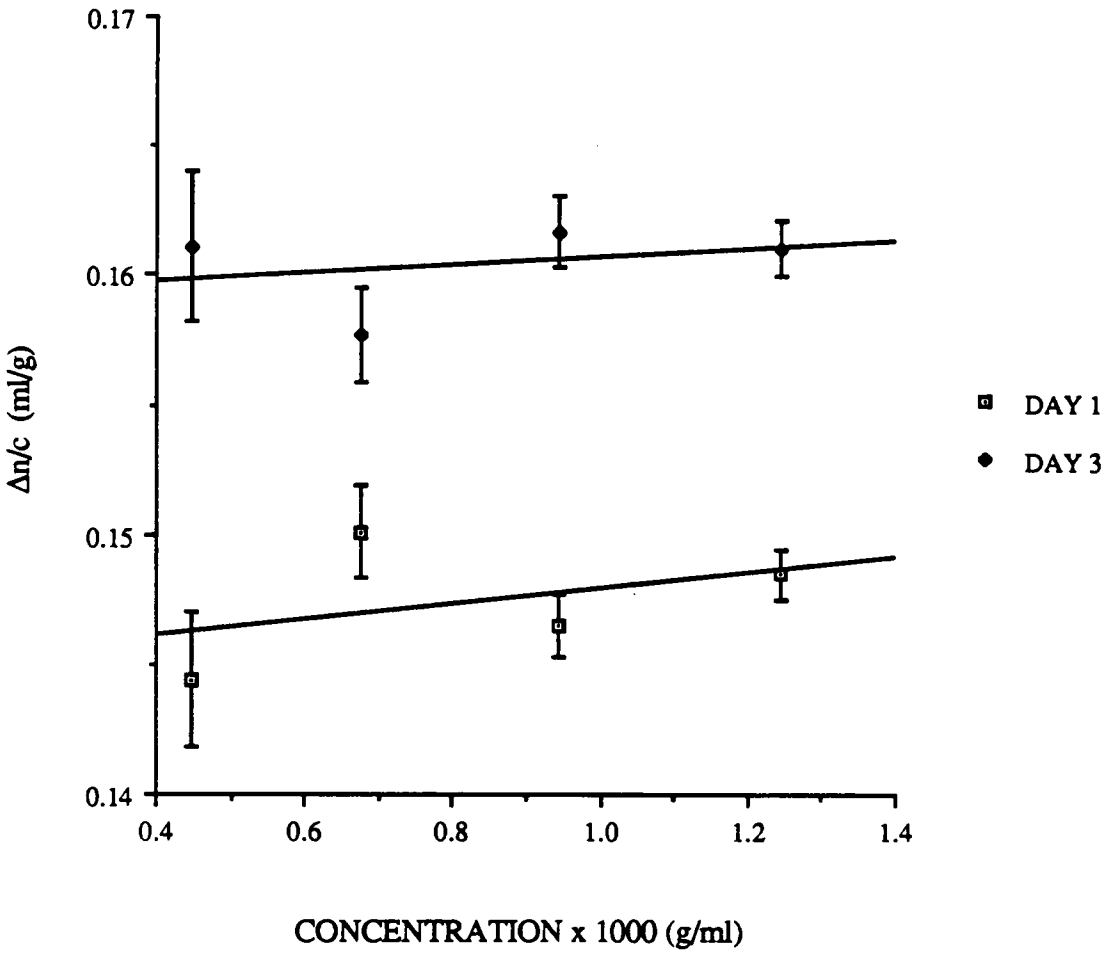

Figure 3.12: Δn/concentration versus concentration plot for red oak HPL lignin.

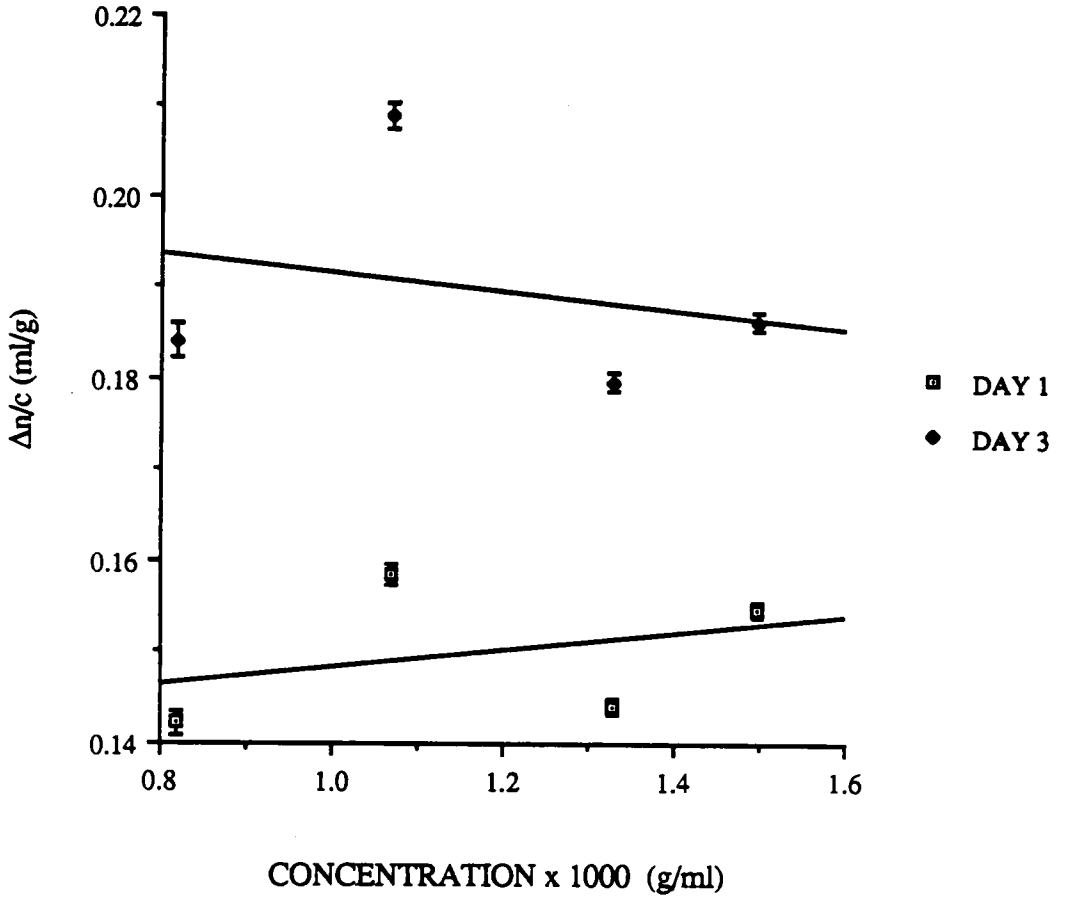

Figure 3.13: Δn/concentration versus concentration plot for RO:PO lignin.

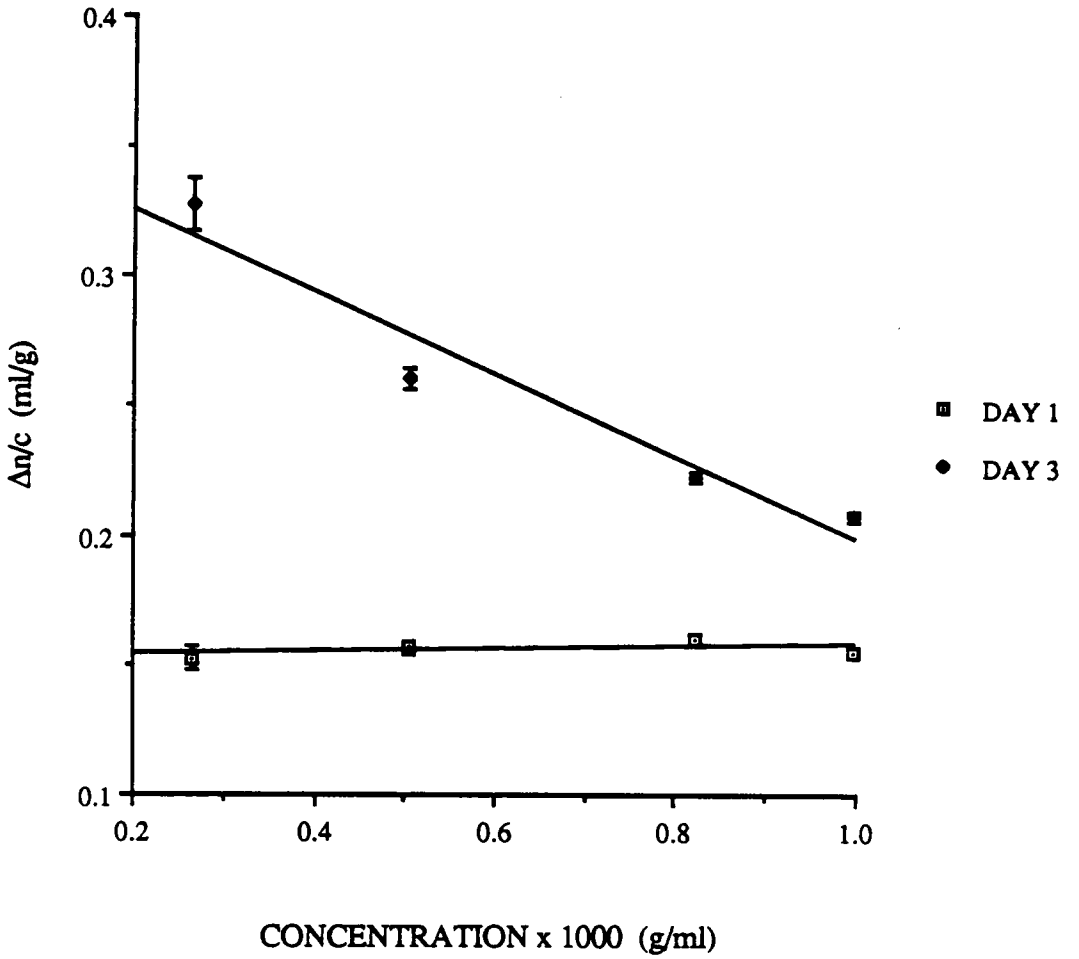

Figure 3.14: Δn/concentration versus concentration plot for aspen HPL lignin.

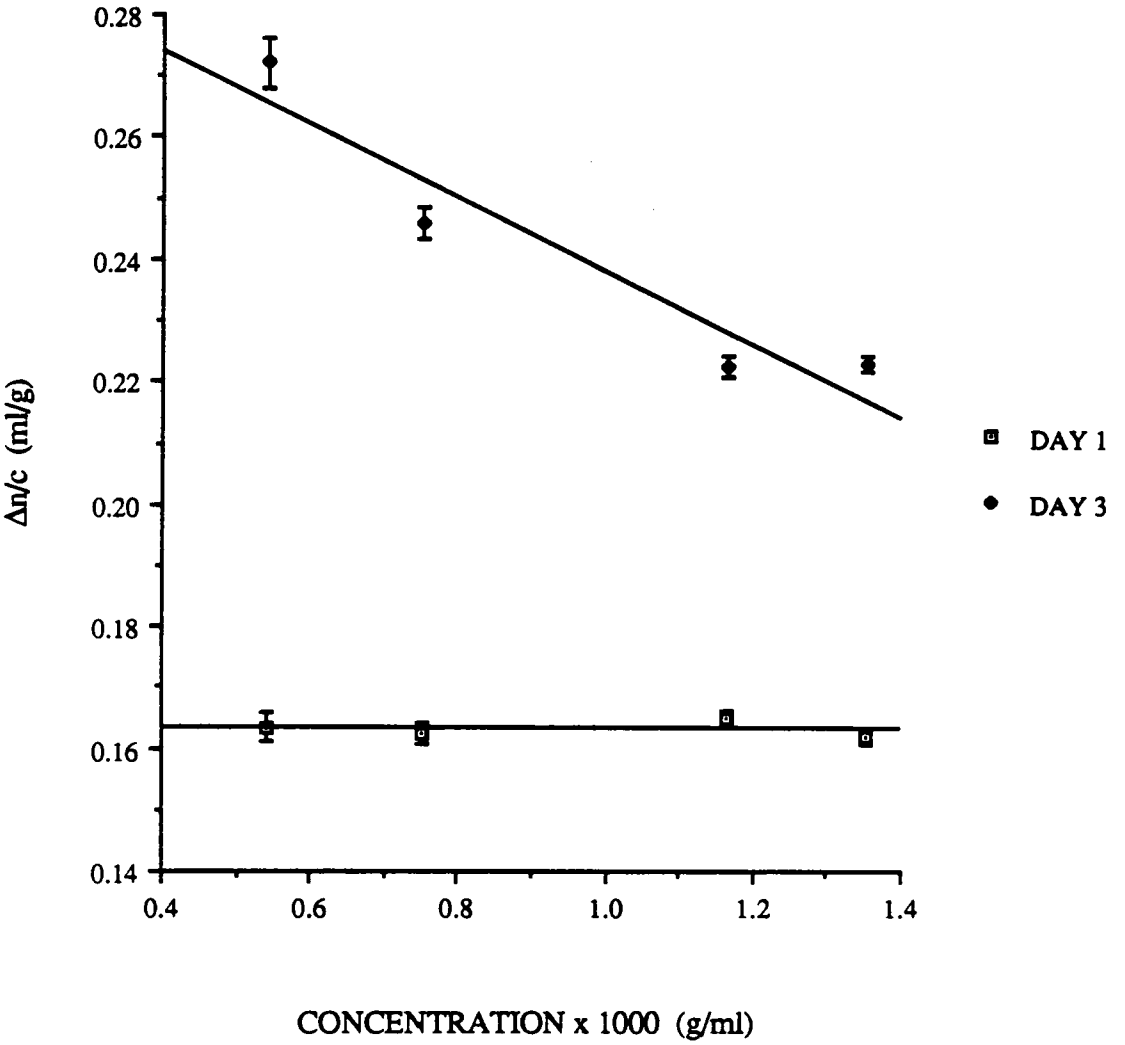

Figure 3.15: Δη/concentration versus concentration plot for Westvaco hardwood kraft lignin HPL.

TABLE 3.3
Specific Refractive Index Increments for HPL Lignins

SAMPLE	DAY	dn/dc (ml/g)	ERROR	% DIFFERENCE
Red Oak	1	0.145	0.016	9.2
	3	0.159	0.017	
RO:PO	1	0.139	0.026	37.0
	3	0.202	0.033	
Aspen	1	0.152	0.017	80.0
	3	0.358	0.030	
Westvaco	1	0.163	0.023	58.6
	3	0.298	0.026	

3.4.3. Static Low Angle Laser Light Scattering (LALLS)

The results for static LALLS are shown in Figure 3.16 for aspen HPL. This static experiment was done in order to get a second virial coefficient for each solution investigated. The second virial coefficient may be calculated as one half of the value of the slope of a plot of $Kc/\overline{R}_\theta$ versus concentration. Typically, one obtains a linear plot. However, none of the HPL solutions exhibited such behavior. All the analyses had some curvature to them both on the first day and on the third day experiments. Although there was some reproducibility in the shape of the curves for all samples, there was no clear pattern to the deviations from ideality. Thus, it was impossible to measure the absolute weight average molecular weight from the static LALLS investigations. In any case, the more important parameter here was the second virial coefficient which was necessary for the GPC/LALLS experiment. Since it was obvious that an accurate value may not be obtained due to the complex nature of these solutions, the data from VPO were used instead. This was a reasonable course of action since the same solvent and temperature were used in both the VPO and the GPC experiments. The static LALLS results are cited above to indicate to other workers the problems with solutions that contain materials which can associate and to suggest the following alternative.

The equation appropriate in the VPO calculations is:

$$\frac{\Delta V}{c} = K\left(\frac{1}{\overline{M}_n} + A_2 c\right) \qquad [3\text{-}1]$$

where ΔV is the voltage change brought about by the temperature rise to compensate for the lower solvent vapor pressure in the solution, c is the concentration, A_2 is the second virial coefficient, $\overline{M}_n$ is the number average molecular weight and K is an instrument constant. K is the intercept of the plot of $\Delta V/c$ versus c for the calibration standards. There is a clear dependence of K on molecular weight as shown in Figure 3.17. The K used to calculate the second virial coefficient of the lignins was that obtained for a polystyrene standard with a molecular weight of 1250 g/mole. This choice was based on the VPO results which

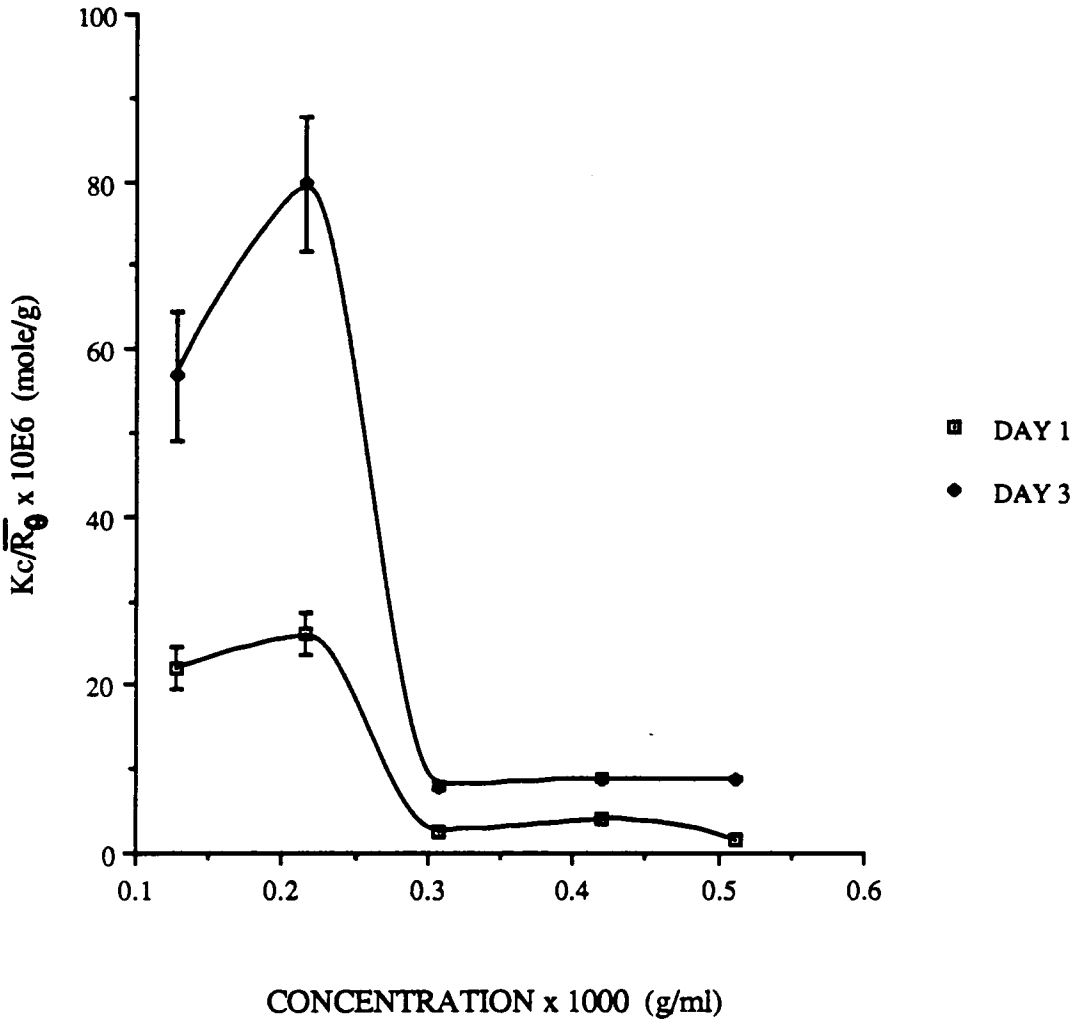

Figure 3.16: $Kc/\overline{R_\theta}$ versus concentration plot for aspen HPL lignin.

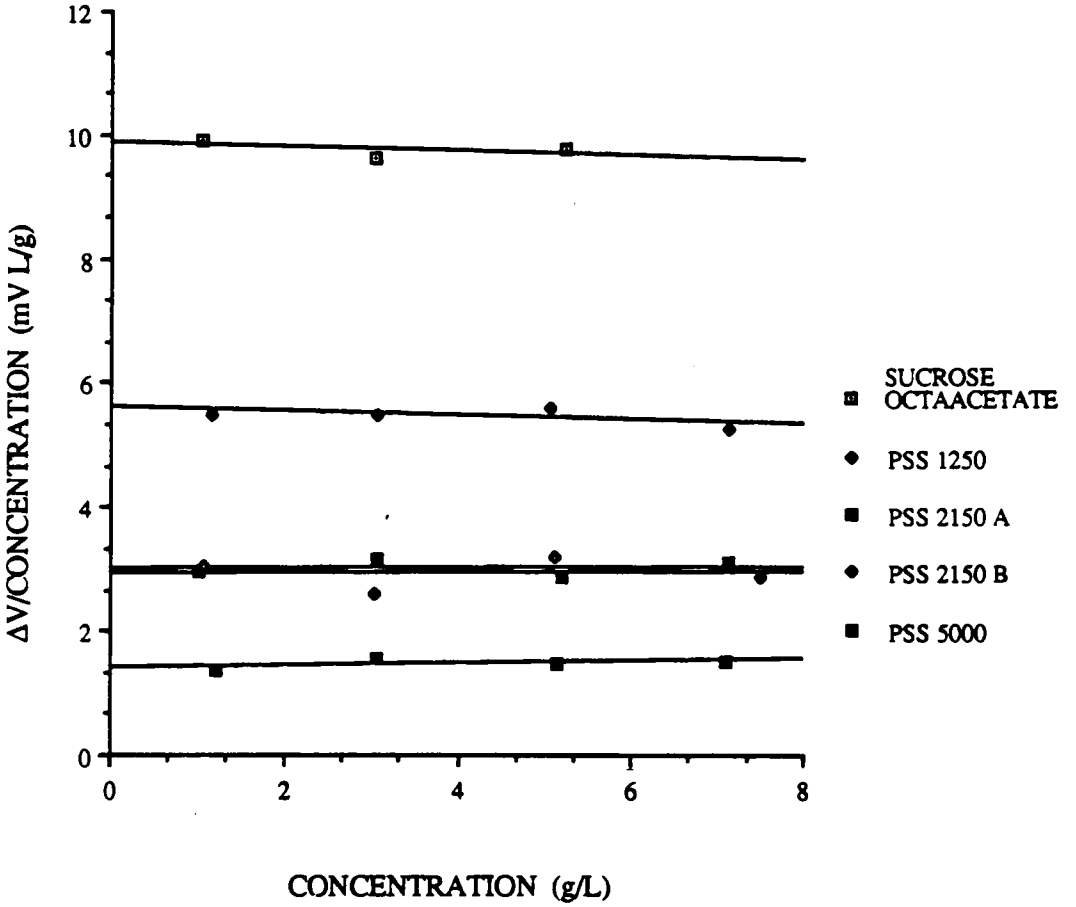

Figure 3.17: ΔV/concentration versus concentration plot for calibration standards.

indicated that the molecular weight of this standard was closest to those of the HPL samples. The values of A_2 calculated for the first day experiments are given in Table 3.4. These values were used for both the first day and third day experiments in GPC/LALLS, since those are the data points which may be plotted to yield a straight line from which a slope may be calculated. This was deemed to be an acceptable procedure in view of the nature of the $\Delta V/c$ plots for the work on the third day as illustrated in Figure 3.11.

3.4.4. GPC/LALLS

3.4.4.1. Red Oak

An example of the data taken by GPC/LALLS for red oak HPL is shown in Figure 3.18. Figure 3.18a is the data taken for red oak A1(t) and Figure 3.18b is the chromatogram for the same sample run four hours later (red oak A1(t+4)). The bold trace is from the differential refractive index (DRI) detector and the finer trace is from the LALLS signal. The higher noise level in the LALLS signal is due to the low sensitivity of this instrument in the detection of polydisperse low molecular weight polymers.

The time dependent change in absolute molecular weight distribution for red oak is shown in Figure 3.19a for red oak A1(t) and A1(t+4). The distribution for red oak A1(t) became significantly more skewed toward the high molecular weight side four hours after solution preparation. A duplicate run made under the same conditions is shown in Figure 3.19b. These samples are designated as B1(t) and B1(t+4). Although the skew toward the high molecular weight material after four hours is not as great as in the previous sample A, there was a clear movement in the same direction. These data indicate that the time scale for association is relatively short.

Figure 3.20 contains a comparison of the absolute molecular weight distributions obtained for red oak A1(t), A1(t+4), A3(t) and A3(t+4). The molecular weight distribution appears to be constantly changing over time. On the first day red oak A1(t+4) contained more high molecular weight material than A1(t), but on the third day, A3(t) had more low molecular weight species than A1(t+4). The distribution shifted toward higher molecular weights once more for A3(t+4). The absolute molecular weight averages for this sample are shown in Table 3.5. Although the values of molecular weights were not exactly reproducible

TABLE 3.4
A_2 Calculated from VPO Results

SAMPLE	$A_2 \times 10^3$ (mole cm^3/g^2)
Red Oak	-6.327
RO:PO	-15.35
Aspen	-1.123
Westvaco	20.23

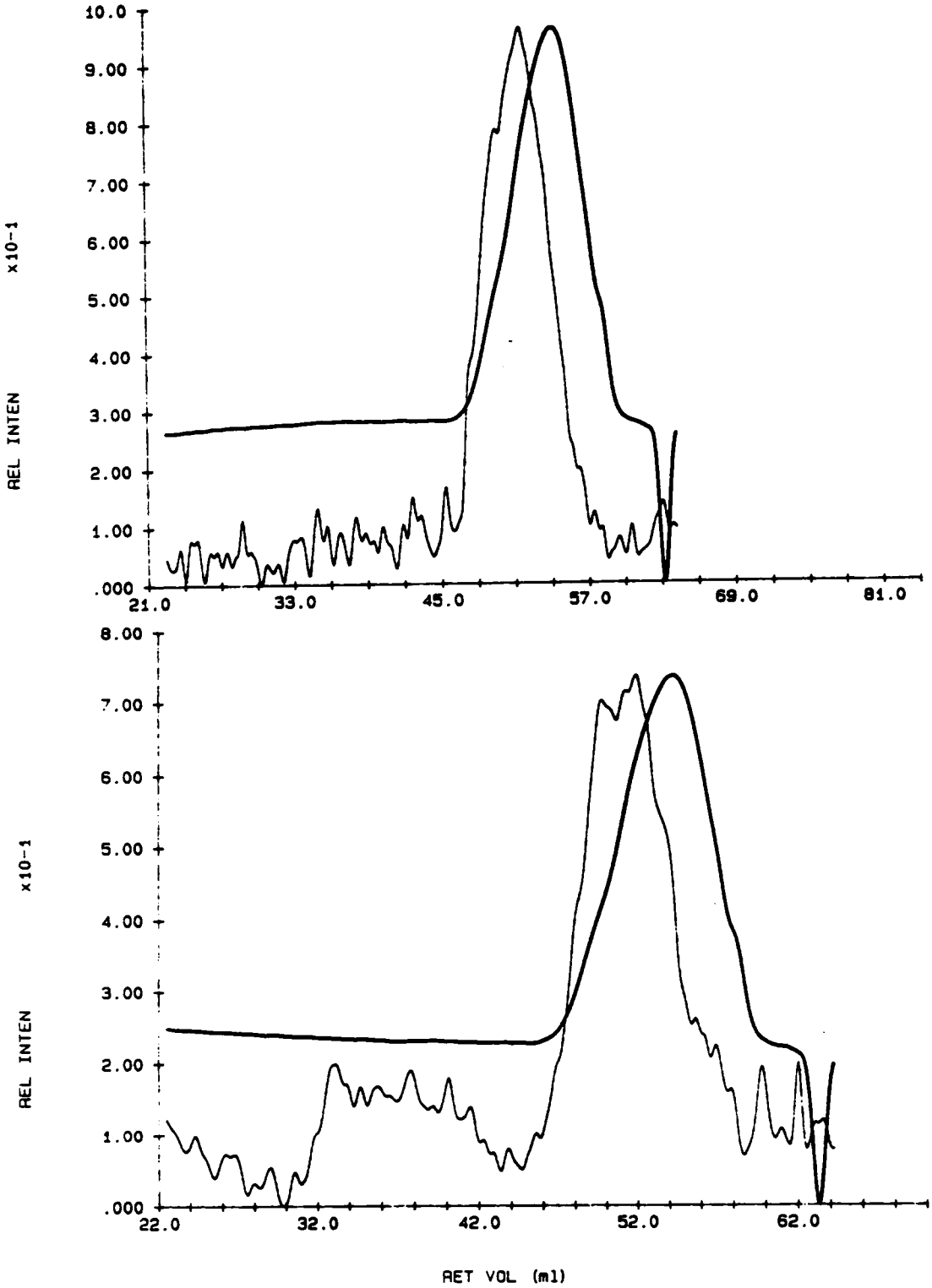

Figure 3.18: GPC/LALLS dual chromatogram for a) red oak A1(t) and b) red oak A1(t+4).

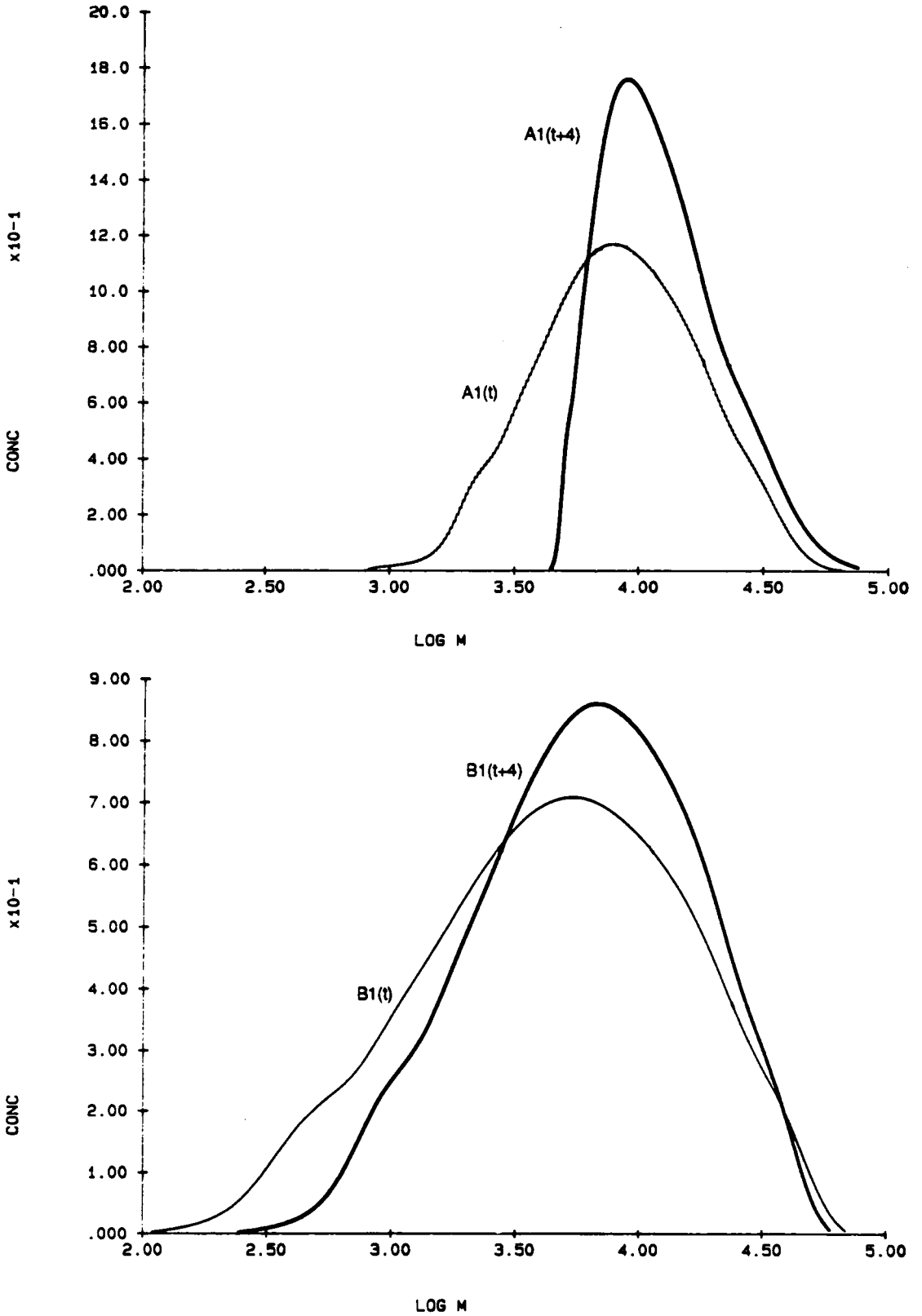

Figure 3.19: Absolute molecular weight distributions for a) red oak A1(t) and red oak A1(t+4) b) red oak B1(t) and B1(t+4).

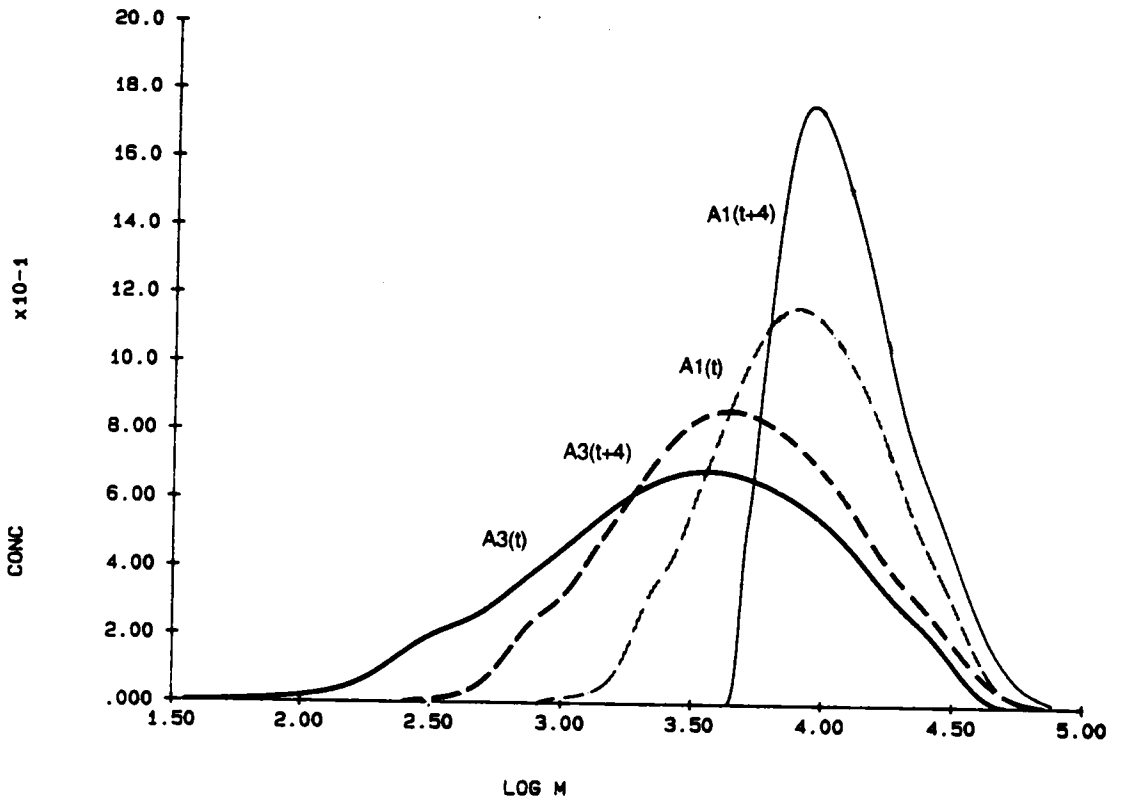

Figure 3.20: Absolute molecular weight distributions for red oak A.

TABLE 3.5
Results from GPC/LALLS

SAMPLE	SET	DAY	TIME	$\overline{M}_n$ (g/mole)	$\overline{M}_w$ (g/mole)	POLYDISPERSITY
Redoak	A	1	t	6708	11500	1.72
	B	1	t	2710	11170	4.12
	A	1	t+4	9441	12320	1.30
	B	1	t+4	4371	11690	2.68
	A	3	t	1701	7565	4.45
	B	3	t	4906	10120	2.06
	A	3	t+4	3185	8265	2.59
	B	3	t+4	2658	6400	2.41
RO:PO	A	1	t	5433	11470	2.11
	B	1	t	9326	14760	1.58
	A	1	t+4	5968	12570	2.11
	B	1	t+4	5300	11980	2.26
	A	3	t	2459	4470	1.82
	B	3	t	1578	3826	2.42
	A	3	t+4	1312	4095	3.12
	B	3	t+4	3534	4055	1.15
Aspen	A	1	t	4004	24070	6.01
	B	1	t	6470	22540	3.48
	A	1	t+4	6560	23310	3.55
	B	1	t+4	5311	22140	4.17
	A	3	t	2205	3311	1.50
	B	3	t	2190	3501	1.60
	A	3	t+4	1004	3813	3.80
	B	3	t+4	822	3426	4.16
Westvaco	A	1	t	3711	17120	4.61
	B	1	t	12430	21810	1.76
	A	1	t+4	6322	19460	3.08
	B	1	t+4	3714	17320	4.66
	A	3	t	2386	4741	1.99
	B	3	t	858	4872	5.68
	A	3	t+4	2139	5350	2.50
	B	3	t+4	1608	2518	1.57

between sets of experiments, the trends were consistent for the first day of the experiment; the molecular weights increased within four hours of sample preparation. On the third day, the trend between the two sets of samples were reversed. For set A, the molecular weights increased with time, while they decreased for set B. The dispersity generally decreased within the day. The complex nature of the associations that are occurring within these solutions was again illustrated by the GPC/LALLS results. The fact that the average values of $\overline{M}_n$ obtained are in general larger than those from the VPO experiment is attributed to the lack of a polarization correction in the experiments. However, the general time dependence of the results is correct and the most important point of these GPC/LALLS experiments.

3.4.4.2. RO:PO

In Figure 3.21 are shown the molecular weight distribution of RO:PO on the first day and on the third day of sample preparation. It appears that the RO:PO molecular weight increased slightly on the first day then decreased continuously afterwards as seen in the data for RO:PO A3(t) and A3(t+4). However, as in the case of red oak, this trend was not reproduced with a second set of experiments. All average molecular weights are displayed in Table 3.5. It is obvious that for experiment set B, the molecular weights were lower on the third day compared to those on the first day. However, in contrast to the first set of solutions, the molecular weights of RO:PO B3(t+4) were higher than those of RO:PO B3(t). Also in contrast to red oak, the molecular weights of RO:PO were generally lower on the third day than on the first day of solution preparation. These differences were unexpected because RO:PO is supposed to be identical to red oak, yet, the association pattern seems to be different.

3.4.4.3. Aspen

The absolute molecular weight distributions for aspen (experiments A) are shown in Figure 3.22. The results for A1(t), A1(t+4), A3(t) and A3(t+4) are all overlaid in one plot. The amount of lower molecular weight species in A1(t) decreased over time, while the amount of the higher molecular weight species increased as seen in the shift of the distribution, e. g., A1(t+4). After two days of storage, aspen A3(t+4), was found to have a considerably greater amount of low molecular weight species.

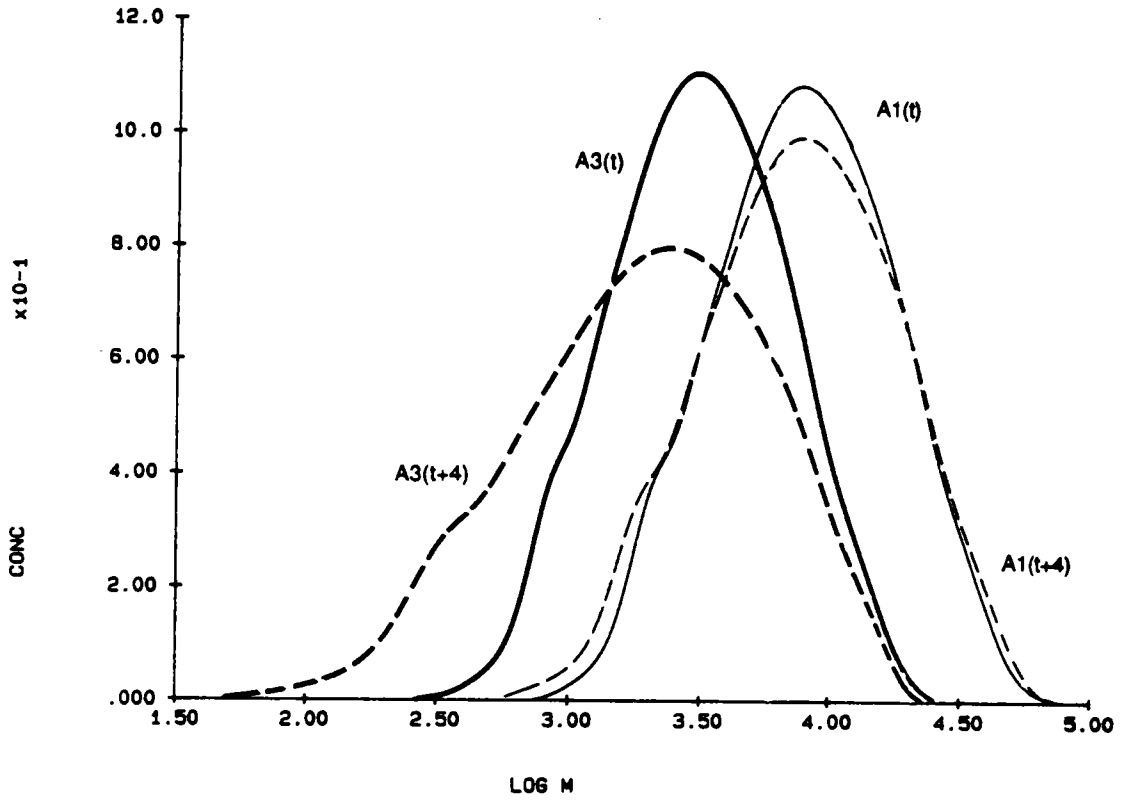

Figure 3.21: Absolute molecular weight distributions for RO:PO A.

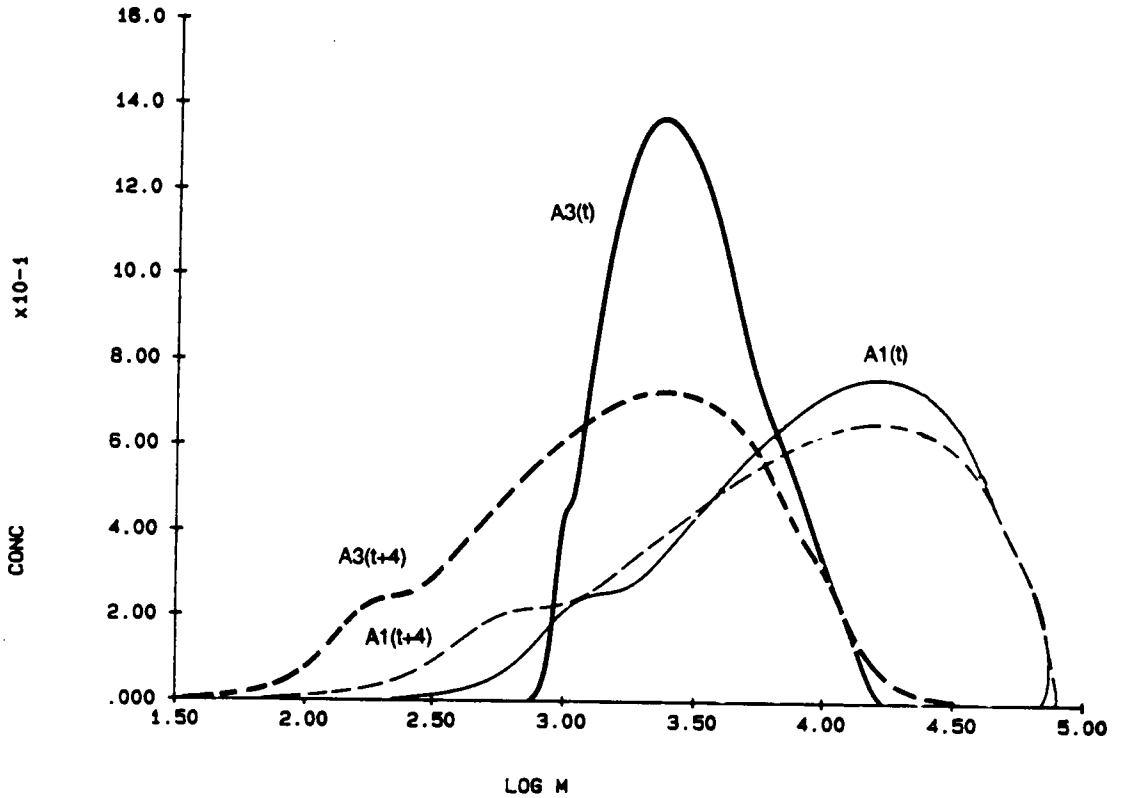

Figure 3.22: Absolute molecular weight distributions for aspen A.

The molecular weight values in Table 3.5 show that for the solutions in set A, the molecular weights on the third day were lower than those on the first day. Within the first day, the molecular weight increase was significant. For experiments B, the trends were reversed.

3.4.4.4. Westvaco Hardwood Kraft

Figure 3.23 illustrates the molecular weight distributions for the Westvaco HPL's first day and third day investigations. In the case of Westvaco A1(t) and A1(t+4), the distribution has clearly moved to higher molecular weights four hours after sample preparation. On the third day, the distributions indicate an overall decrease of molecular weights upon storage. Sample A3(t+4) had more low molecular weight species than A3(t). A summary of molecular weight data in Table 3.5 shows that for the data in set A, the molecular weights increased on the first day after four hours, then decreased on the third day. Although the distribution showed more low molecular weight species in the later run on the third day, the average molecular weight did not change greatly.

3.4.5. GPC/DV

3.4.5.1. Red Oak

An example of the raw data for red oak is shown in Figure 3.24. Figure 3.24a is the trace of the data for red oak B3(t), while Figure 3.24b is from red oak B3(t+4). The bold trace represents the DRI signal and the finer trace reveals the concurrent viscosity signal. Again, as was the case of the LALLS, the viscosity detector output was noisier than the DRI signal since the molecular weights of the sample were approaching the DV lower detection limit. Later experiments indicated that the noisy signal may be improved by a fourfold increase in the concentration of the solution used. Such a change in procedure resulted in the much cleaner signal shown in Figure 3.24c.

The absolute molecular weight distributions for the red oak B1(t), B1(t+4), B3(t) and B3(t+4) are overlaid in Figure 3.25. The distributions of red oak B1(t) and B1(t+4) appear to form the boundaries for low and high molecular weight materials present. Although the distributions changed in three days as seen in the results for B3(t) and B3(t+4), the shifts occurred within these boundaries.

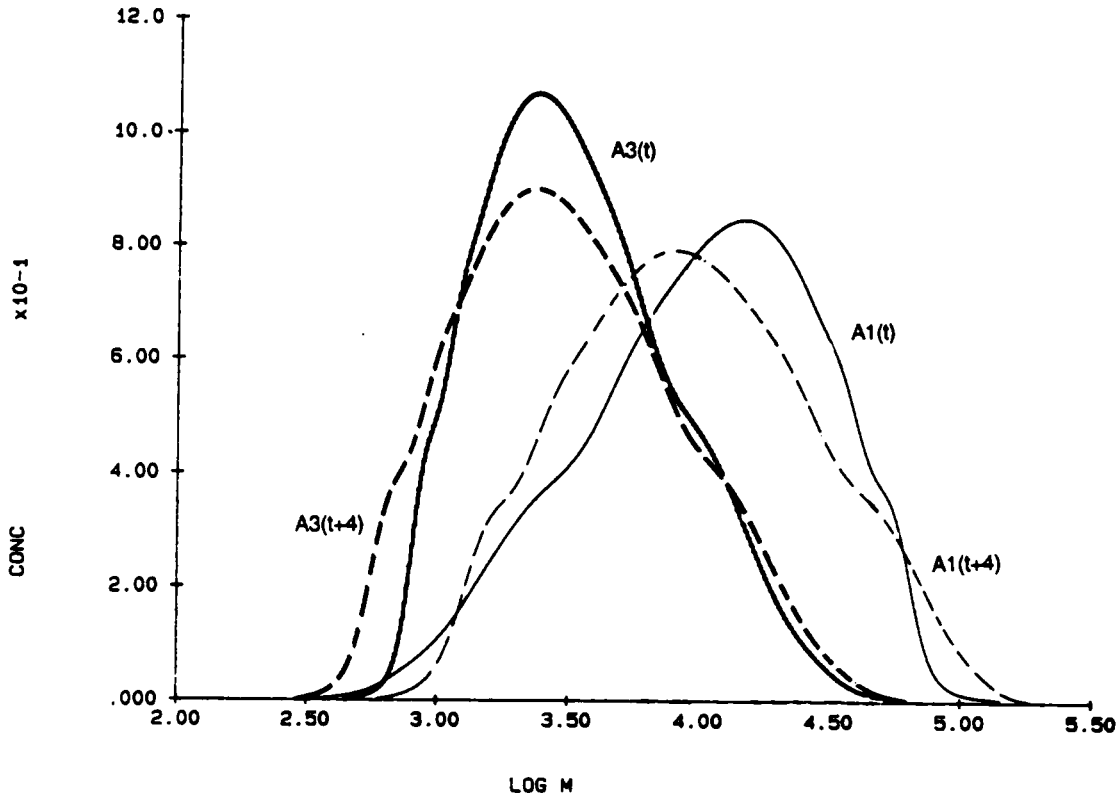

Figure 3.23: Absolute molecular weight distributions for Westvaco A.

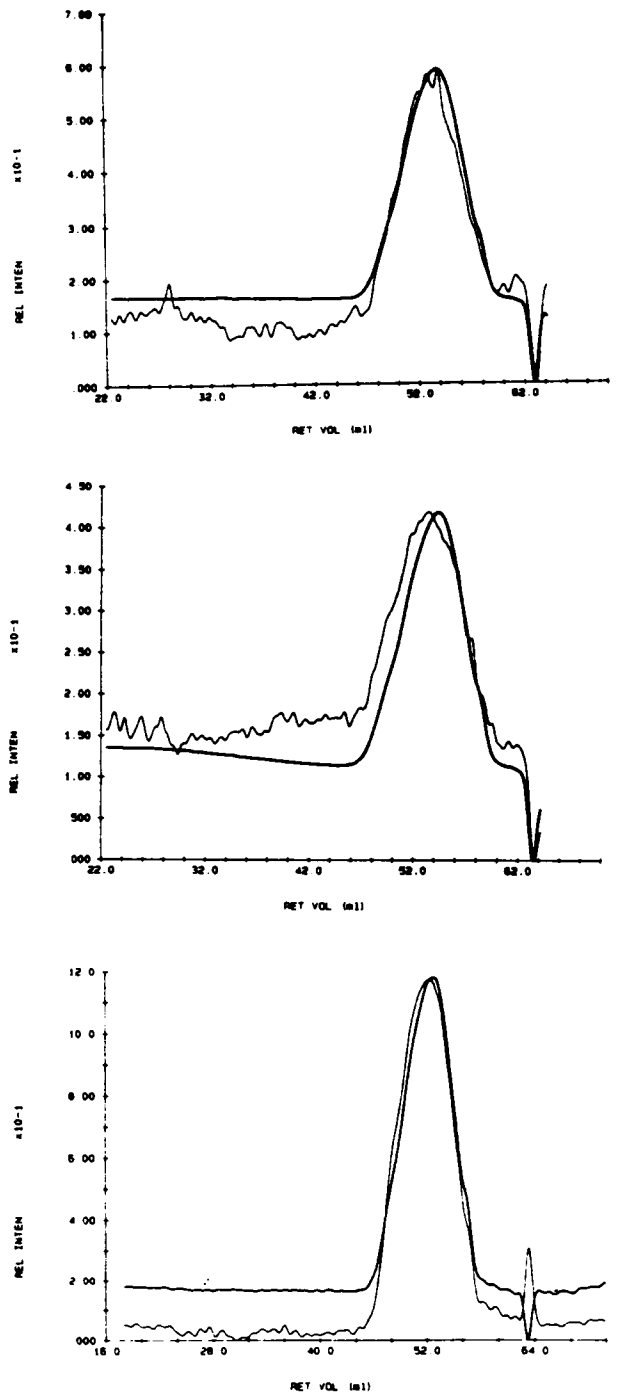

Figure 3.24: GPC/DV dual chromatogram for a) red oak B3(t) b) red oak B3(t+4) c) red oak with fourfold increase in concentration.

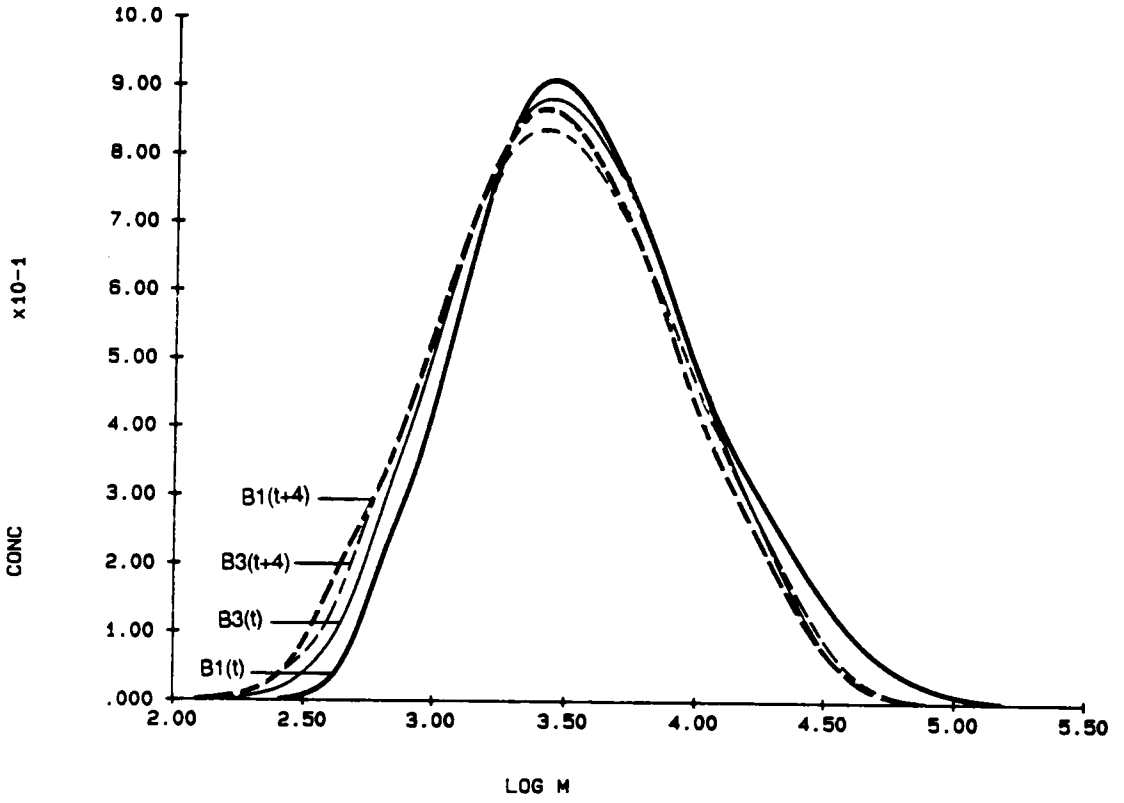

Figure 3.25: Absolute molecular weight distributions for red oak B.

A summary of the results from GPC/DV is given in Table 3.6. For the data set A, the molecular weights increased on the first day, in a span of four hours. Storage for a couple of days resulted in a slight decrease initially before another increase. For duplicate sample set B, the molecular weights continuously decreased from the first to the third day. It should be emphasized that the DV results are in substantial agreement with those of the VPO for $\overline{M}_n$ and the changes in $\overline{M}_n$ with time. Furthermore, the noisy signal from the DV did not significantly alter the results obtained. The $\overline{M}_n$ calculated from the improved chromatogram was 1478 g/mole, clearly within error of the values obtained from the noisy DV signal.

3.4.5.2. RO:PO

The absolute molecular weight distribution for this set of samples is shown in Figure 3.26. There is an obvious shift towards lower molecular weights after a standing time of four hours subsequent to the mixing of the sample with the solvent. Again, the shift in the distributions on the first day constituted the major change. The changes in the distributions for samples B3(t) and B3(t+4) occurred within the high and low molecular weight boundaries set by samples B1(t) and B1(t+4).

An examination of the results in Table 3.8 reveals that while the values of molecular weights obtained for two sets of identical samples (A, B) were not exactly reproducible the agreement was certainly satisfactory, in agreement with the VPO and yielded information on the absolute molecular weight distribution quickly and conveniently.

3.4.5.3. Aspen

Some of the difficulties in analyzing lignins are once again demonstrated in Figure 3.27 where the molecular weight distributions for aspen A1(t), A1(t+4), A3(t) and A3(t+4) are overlaid. Initially, there was a shift of the distribution to lower molecular weights as shown by solutions A1(t) to A1(t+4). However, storage for two days resulted in an increase in the proportion of high molecular weight species. The distribution then remained relatively constant as evidenced by the almost identical distributions for A3(t) and A3(t+4).

TABLE 3.6
Summary of GPC/DV Results

SAMPLE	SET	DAY	TIME	[η] (dl/g)	$\overline{M}_n$ (g/mole)	$\overline{M}_w$ (g/mole)	POLYDISPERSITY
Red Oak	A	1	t	0.041	1535	3852	2.51
	B	1	t	0.040	2388	5704	2.39
	A	1	t+4	0.039	1732	4109	2.37
	B	1	t+4	0.037	1971	4945	2.51
	A	3	t	0.045	1433	4335	3.03
	B	3	t	0.043	2013	5091	2.53
	A	3	t+4	0.036	2080	5111	2.46
	B	3	t+4	0.041	1676	5045	3.01
RO:PO	A	1	t	0.032	1567	4971	3.17
	B	1	t	0.036	2132	5036	2.36
	A	1	t+4	0.045	1367	2741	2.00
	B	1	t+4	0.041	1701	3899	2.29
	A	3	t	0.041	1473	3541	2.40
	B	3	t	0.035	1935	5355	2.77
	A	3	t+4	0.039	1701	3607	2.12
	B	3	t+4	0.038	1628	4752	2.92
Aspen	A	1	t	0.044	1591	4783	3.01
	B	1	t	0.045	1889	4825	2.55
	A	1	t+4	0.051	1471	3583	2.44
	B	1	t+4	0.045	2174	5655	2.60
	A	3	t	0.045	1924	4615	2.40
	B	3	t	0.042	2385	6555	2.75
	A	3	t+4	0.047	1846	4630	2.51
	B	3	t+4	0.046	1258	3958	3.14
Westvaco	A	1	t	0.047	1597	4589	2.87
	B	1	t	0.043	1515	6254	4.13
	A	1	t+4	0.046	1858	6333	3.41
	B	1	t+4	0.046	2014	6524	3.24
	A	3	t	0.044	1951	6190	3.17
	B	3	t	0.045	1711	7166	4.19
	A	3	t+4	0.048	1518	5580	3.68
	B	3	t+4	0.043	897	3982	4.44

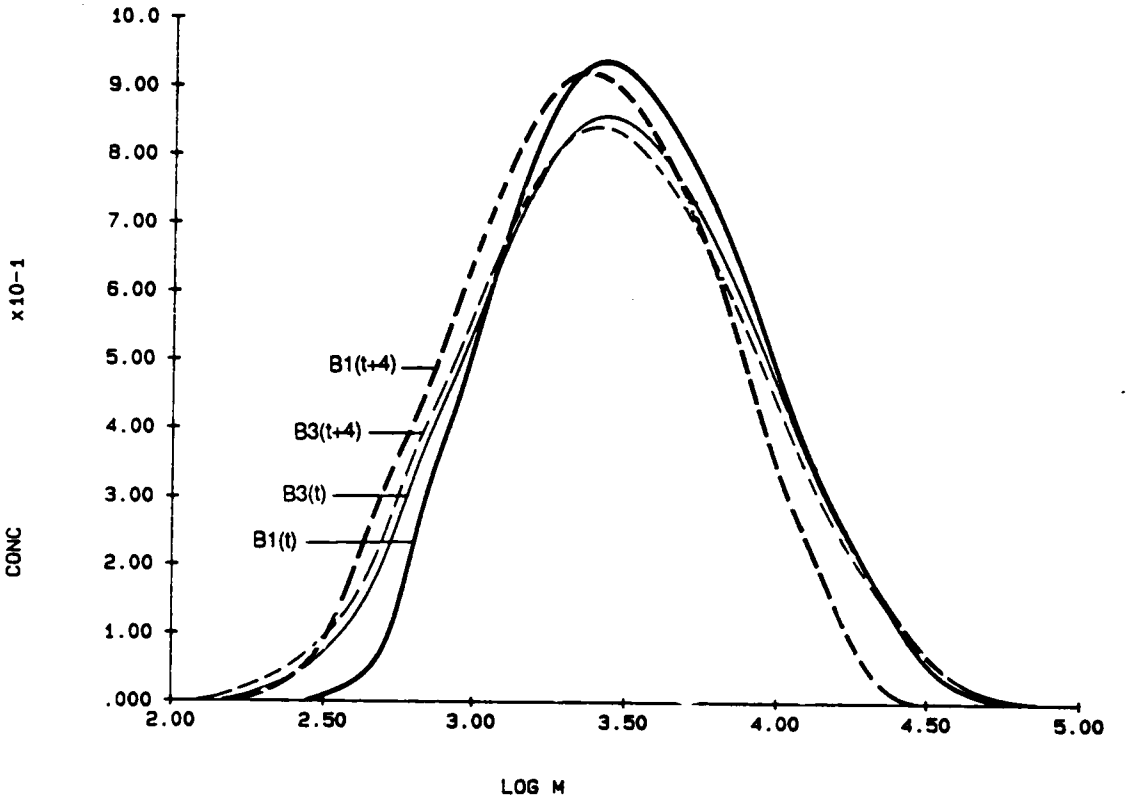

Figure 3.26: Absolute molecular weight distributions for RO:PO B.

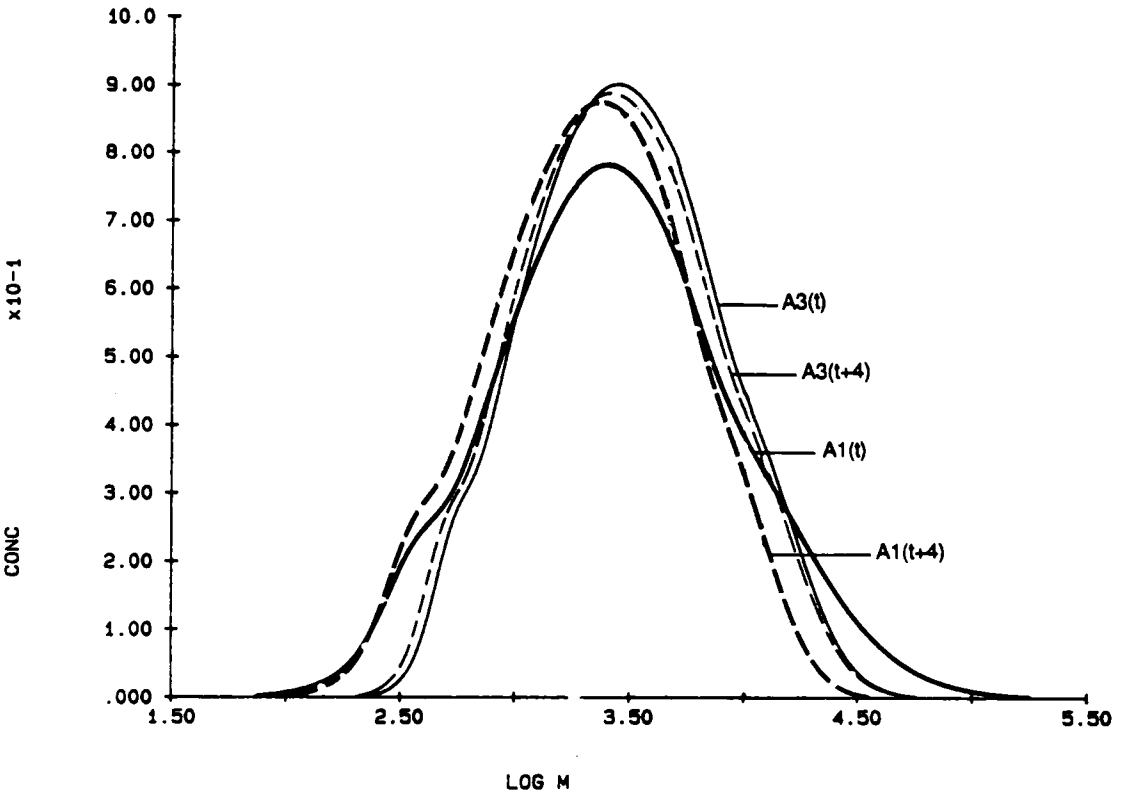

Figure 3.27: Absolute molecular weight distributions for aspen A.

A duplicate experiment was run for verification purposes. The molecular weight distributions are shown in Figure 3.28 as overlays for aspen B1(t), B1(t+4), B3(t), and B3(t+4). The agreement was quite close overall. There was a continuous increase of high molecular weight species from B1(t), B1(t+4), to B3(t), then a decrease was seen in B3(t+4).

An examination of Table 3.6 reveals that the molecular weights were between 1500 to 2000 on the first day for the various times that the samples were run. They were generally higher on the third day.

3.4.5.4. Westvaco Hardwood Kraft

The absolute molecular weight distributions for set B of samples is shown in Figure 3.29. The molecular weights clearly increased within four hours of sample preparation as seen from the shift in distribution from Westvaco A1(t) to A1(t+4). After storage for a couple of days, the distributions did not seem to be altered significantly from its state in A3(t) to A3(t+4).

A look at the results in Table 3.6 reveals that for this sample, the trends, as well as the values of molecular weights were reproducible between experiments A and B and were supported by the VPO analyses.

3.4.6. GPC/DV/LALLS

A summary of the results from the GPC and VPO are given in Table 3.7. The values of number average molecular weights chosen for comparison were those obtained immediately after initial sample preparation since this was the state of the solutions for the VPO experiment. If the $\overline{M}_n$ obtained by VPO were used as the "correct" value, then the contents of Table 3.7 suggest that GPC/DV yielded results that were consistently closer to this number than did those from GPC/LALLS. The LALLS detector generally produced higher values. This indicates that there was a need to do the LALLS experiment with the beam polarization correction which reportedly brings the numerical values down by 30-40% (76,77).

3.5. SUMMARY AND CONCLUSIONS

The work presented above has shown that VPO can be used to very reliably obtain number average molecular weights for the HPL lignin derivatives if a multiple standard calibration scheme is employed. In

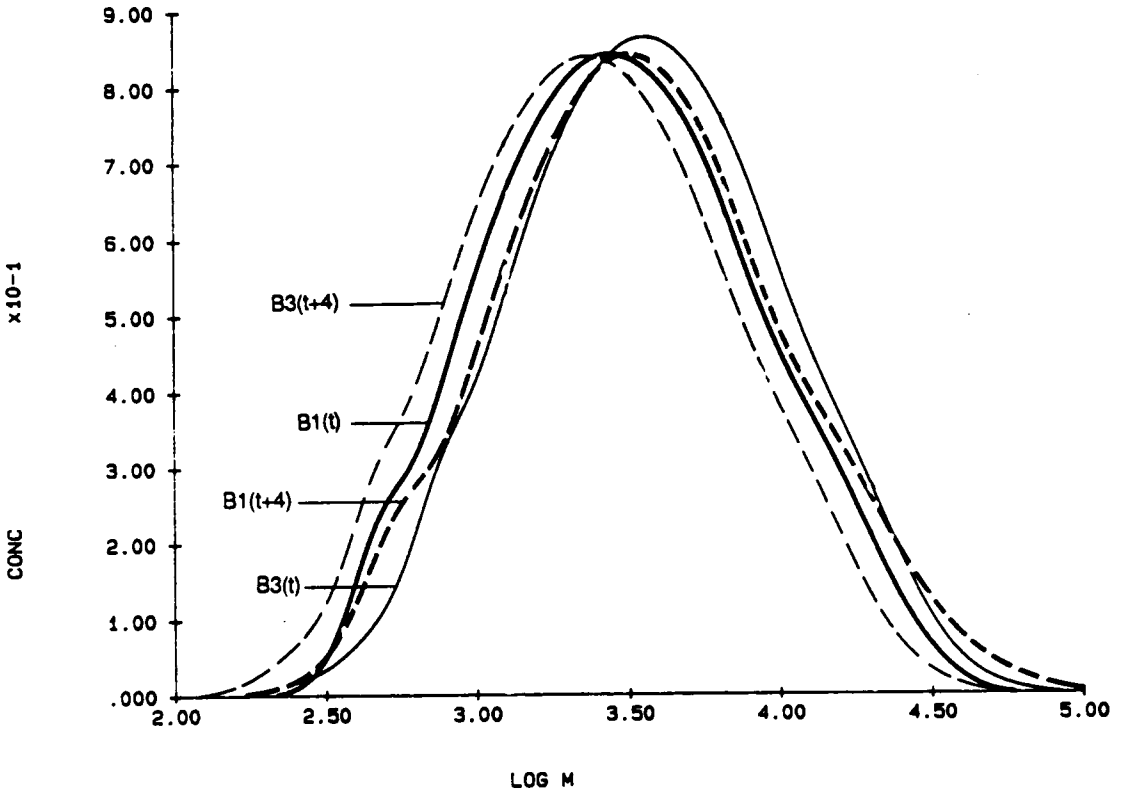

Figure 3.28: Absolute molecular weight distributions for aspen B.

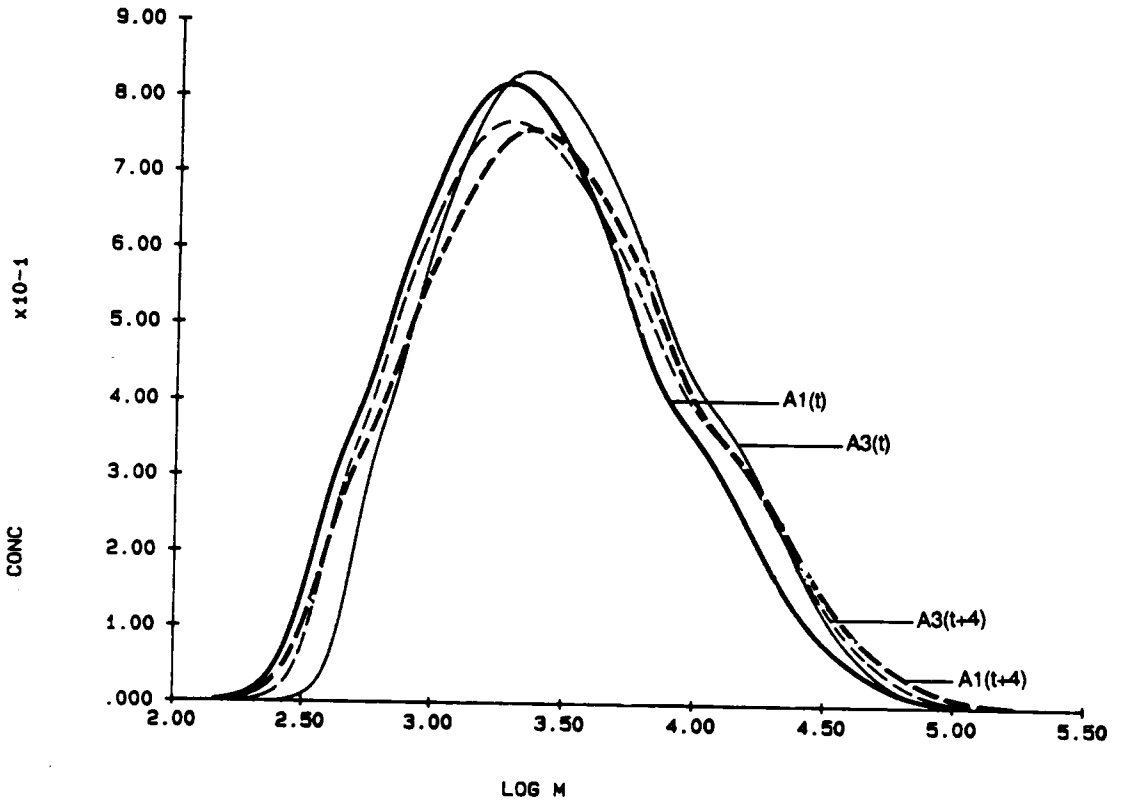

Figure 3.29: Absolute molecular weight distributions for Westvaco A.

TABLE 3.7
Comparison of M_n from VPO, GPC/LALLS and GPC/DV

			$\overline{M}_n$ (g/mole)	
SAMPLE	DAY	VPO	GPC/LALLS	GPC/DV
Red Oak	1	1416	6708	1535
	1		9441	2388
	3	1684	1701	1433
	3		4906	2013
RO:PO	1	1108	5433	1567
	1		9326	2132
	3	1348	2459	1473
	3		1578	1935
Aspen	1	1393	4004	1591
	1		6470	1889
	3	1691	2205	1924
	3		2190	2385
Westvaco	1	1499	3711	1597
	1		12430	1515
	3	1850	2386	1951
	3		858	1711

addition, a time study revealed that number average molecular weights by VPO increased over time as a result of association.

Results obtained by GPC showed that in order to use the LALLS detector, one has to consider not only the influence of sample absorbance and fluorescence on molecular weight determination, but also the effect of beam polarization. Without the polarizer correction (which requires 0° and 90° measurements), the LALLS gave erroneously high molecular weights when compared to the VPO. Furthermore, static LALLS measurements were complicated by association which brought about irreproducible surges in scattered intensity. This lack of consistency did not permit the calculation of second virial coefficients from LALLS. The VPO proved to be a valuable source of the second virial coefficient for the GPC/LALLS calculations.

The results obtained by GPC/DV proved that the viscosity detector is a quite acceptable and convenient instrument for obtaining absolute molecular weights and molecular weight distributions for these polydisperse low molecular weight HPL lignin derivatives. In spite of some noise in the raw data that were a consequence of signals close to the lower detection limit of the detector, very good results were obtained. This strongly indicates that the lignins studied could be analyzed by a universal calibration GPC procedure. Hence, the viscosity detector provides a means of obtaining absolute molecular weights and molecular weight distributions reliably, quickly and easily.

The changes in absolute molecular weight distributions obtained here in ***all*** experiments confirms that a time dependent association does occur in lignin derivatives. In addition, there was positive evidence for McCarthy's postulate that association in lignins occurs by the specific interaction between high and low molecular weight species. This was illustrated by the shift of the molecular weight distribution towards higher molecular weights over time as the smaller species are "consumed" through association to form larger molecules.

REFERENCES

1. Glasser, W. G., Kelley, S. S., in *Encyclopedia of Polymer Science and Engineering* Kroschwitz, J. I., (ed.) Wiley, New York, 1984, Vol. 8, pp. 795.

2. Soni, P. L., Gaur, B., J. Sci. Ind. Res., **43**, 589 (1984).

3. Kolpak, F. J., Cietek, D. J., Fookes, W., Cael, J. J., Appl. Polym. Symp., **37**, 491 (1983).

4. Grubisic, Z., Rempp, P., Benoit, H., J. Polym. Sci., Polym. Lett., **5**, 753 (1967).

5. Trowbridge, P., Brower, L., Seeger, R., McIntyre, D., Polym. Mater. Sci. Eng., **54**, 85 (1986).

6. Styring, M., Polym. Mater. Sci. Eng., **54**, 88 (1986).

7. Kuo, C., Provder, T., Koehler, M. E., Kah, A. F., Polym. Mater. Sci. Eng., **54**, 80 (1986).

8. Haney, M. A., Armonas, J. A., Rosen, L., Polym. Mater. Sci. Eng., **54**, 75 (1986).

9. Yau, W. W., Polym. Mater. Sci. Eng., **54**, 74 (1986).

10. Tinland, B., Mazet, J., Rinaudo, M., Makromol. Chem., Rapid Commun., **9**, 69 (1988).

11. Letot, L., Lesec, J., Quivoron, C., J. Liq. Chrom., **3**, 427 (1980).

12. Lecacheux, P., Lesec, J., Quivoron, C., J. Appl. Polym. Sci., **27**, 4867 (1982).

13. Malihi, F. B., Kuo, C., Koehler, M. E., Provder, T., Kah, A. F., in *ACS Symp. Ser. 245* Provder, T., (ed.) ACS, Washington, D. C., 1984, pp. 281.

14. Hamielec, A. E., Meyer, H., in *Developments in Polymer Characterisation -- 5* Dawkins, J. V., (ed.) Elsevier, London, 1986, pp. 95.

15. Haney, M. A., J. Appl. Polym. Sci., **30**, 3023 (1985).

16. Haney, M. A., J. Appl. Polym. Sci., **30**, 3037 (1985).

17. Lindstrom, T., Coll. Polym. Sci., **257**, 277 (1979).

18. Benko, J., Tappi, **47**, 508 (1964).

19. Brown, W., J. Appl. Polym. Sci., **11**, 2381 (1967).

20. Connors, W. J., Sarkanen, S., McCarthy, J. L., Holzforschung, **34**, 80 (1980).

21. Sarkanen, S., Teller, D. C., Hall, J., McCarthy, J. L., Macromolecules, **14**, 426 (1981).

22. Sarkanen, S., Teller, D. C., Stevens, C. R., McCarthy, J. L., Macromolecules, **17**, 2588 (1984).

23. Garver, T. M., Jr., Sarkanen, S., in *Renewable Resource Materials, New Polymer Sources* Carraher, C. E., Jr., Sperling, L. H., (eds.) Plenum Press, New York, 1986, pp. 287.

24. Garver, T. M., Jr., Sarkanen, S., Polym. Mater. Sci. Eng., **52**, 224 (1985).

25. Feldman, D., Lacasse, M., Beznaczuk, L. M., Prog. Polym. Sci., **12**, 271 (1986).

26. Gray, R. L., Parham, R. A., Chemtech, **12**, 232 (1982).

27. Meister, J. J., in *Renewable Resource Materials, New Polymer Materials* Carraher, C. E., Jr., Sperling, L. H., (ed.) Plenum Press, New York, 1986, pp. 305.

28. Wilson, J. D., Hamilton, J. K., J. Chem. Ed., **63**, 49 (1986).

29. Glasser, W. G., in *Pulp and Paper Chemistry and Chemical Technology* Casey, J. P., (ed.) Wiley, New York, 1980, pp. 39.

30. El-Saied, H., Nada, A. M., Ibrahem, A. A., Yousef, M. A., Die Angew. Makromol. Chem., **122**, 168 (1984).

31. Glasser, W. G., Barnett, C. A., Sano, Y., Appl. Polym. Symp., **37**, 441 (1983).

32. Glasser, W. G., Barnett, C. A., Muller, P. C., Sarkanen, K. V., J. Agric. Food Chem., **31**, 921 (1983).

33. Wu, C. F. L., Glasser, W. G., J. Appl. Polym. Sci., **29**, 1111 (1984).

34. Saraf, V. P., Glasser, W. G., Wilkes, G. L., J. Appl. Polym. Sci., **30**, 3809 (1985).

35. Rials, T. G., Glasser, W. G., Holzforschung, **40**, 353 (1986).

36. Mansour, O., Nagaty, A., Beshay, A. D., Nosseir, M. H., Cellulose Chem. Technol., **20**, 59 (1986).

37. Himmel, M. E., Oh, K. K., Sopher, D. W., Chum, H. L., J. Chromatogr., **267**, 249 (1983).

38. Falkehag, S. I., Appl. Polym. Symp., **28**, 247 (1975).

39. Goldstein, I. S., Appl. Polym. Symp., **28**, 289 (1975).

40. Lindberg, H. H., Gra, V. A., Jauhiainen, T. P., Appl. Polym. Symp., **28**, 269 (1975).

41. Tsao, G. T., in *Progress in Biotechnology* Hill, R. D., Munck, L., (eds.) Elsevier, Netherlands, 1985, pp. 297.

42. Glasser, W. G., Barnett, C. A., Rials, T. G., Saraf, V. P., J. Appl. Polym. Sci., **29**, 1815 (1984).

43. Hsu, O. H., Glasser, W. G., Appl. Polym. Symp., **28**, 297 (1975).

44. Feldman, D., Lacasse, M., J. Appl. Polym. Sci., **35**, 247 (1988).

45. Meister, J. J., Patil, D. R., Channell, H., Ind. Eng. Chem. Prod. Res. Dev., **24**, 306 (1985).

46. Meister, J. J., Nicholson, J. C., Patil, D. R., Field, L. R., Polym. Mater. Sci. Eng., **55**, 679 (1986).

47. Sakakibara, A., Wood Sci. Technol., **14**, 89 (1980).

48. Glasser, W. G., Glasser, H. R., Nimz, H. H., Macromolecules, **9**, 866 (1976).

49. Lundquist, K., Appl. Polym. Symp., **28**, 1393 (1976).

50. Morck, R., Yoshida, H., Kringstad, K. P., Hatakeyama, H., Holzforschung, **40**(Suppl.), 51 (1986).

51. Isogai, A., Ishizu, A., Nakano, J., J. Wood Chem. Technol., **7**, 311 (1987).

52. Pla, F., Yan, J. F., J. Wood. Chem. Technol., **4**, 285 (1984).

53. Pla, F., Robert, A., Holzforschung, **38**, 37 (1984).

54. Favis, B. D., Yean, W. Q., Goring, D. A. I., J. Wood Chem. Technol., **4**, 313 (1984).

55. Sarkanen, S., Teller, D. C., Abramowski, E., McCarthy, J. L., Macromolecules, **15**, 1098 (1982).

56. Goring, D. A. I., Gancet, R. V., Chanzy, H., J. Appl. Polym. Sci., **24**, 931 (1979).

57. Gravitis, J., Erins, P., Appl. Polym. Symp., **37**, 421 (1983).

58. Goring, D. A. I., in *Lignins Occurrence, Formation, Structure and Reactions* Sarkanen, K. V., Ludwig, C. H., (eds.) Wiley, New York, 1971, pp. Ch. 17.

59. Yoshida, H., Morck, R., Kringstad, K. P., Holzforschung, **41**, 171 (1987).

60. Obiaga, T. I., Wayman, M., J. Appl. Polym. Sci., **18**, 1943 (1974).

61. Kondo, R., McCarthy, J. L., Holzforschung, **39**, 231 (1985).

62. Huttermann, A., Holzforschung, **32**, 108 (1978).

63. Forss, K. G., Stenlund, B. G., Sågfors, P. E., Appl. Polym. Symp., **28**, 1185 (1976).

64. Kristersson, P., Lundquist, K., Simonson, R., Tingsvik, K., Holzforschung, **37**, 51 (1983).

65. Nicholson, J. C., Meister, J. J., Patil, D. R., Field, L. R., Anal. Chem., **56**, 2447 (1984).

66. Pellinen, J., Salkinoja-Salonen, M., J. Chromatogr., **322**, 129 (1985).

67. Fiserova, M., Polcin, J., Opalena, E., Masarykova, M., Cellulose Chem. Technol., **19**, 185 (1985).

68. Pellinen, J., Salkinoja-Salonen, M., J. Chromatogr., **328**, 299 (1985).

69. Connors, W. J., Lorenz, L. F., Kirk, T. K., Holzforschung, **32**, 106 (1978).

70. Connors, W. J., Holzforschung, **32**, 145 (1978).

71. Concin, R., Burtscher, E., Bobleter, O., J. Chromatogr., **198**, 131 (1980).

72. Faix, O., Lange, W., Salud, E. C., Holzforschung, **35**, 3 (1981).

73. Meier, V. D., Faix, O., Lange, W., Holzforschung, **35**, 247 (1981).

74. Concin, R., Burtscher, E., Bobleter, O., Holzforschung, **35**, 279 (1981).

75. Faix, O., Lange, W., Beinhoff, O., Holzforschung, **34**, 174 (1980).

76. Pla, F., Private communicaton, 1988.

77. Pla, F., in *Lignin: Properties and Materials* Glasser, W. G., Sarkanen, S., (eds.) ACS, Washington, D. C., 1989.

78. Elias, H. G., in *Order in Polymer Solutions* Solc, K., (eds.) Gordon & Breach, London, 1976, pp. 209.

79. Elias, H. G., in *Light Scattering of Polymer Solutions* Huglin, M. B., (eds.) Academic Press, New York, 1972, pp. 397.

80. Elias, H. G., *Macromolecules 1 Structure and Properties,* Plenum Press, New York, 1984.

81. Morck, R., Reimann, A., Kringstad, K. P., Holzforschung, **42**, 111 (1988).

CHAPTER 4

DILUTE SOLUTION PROPERTIES OF PMMA-g-PMMA's

4.1. INTRODUCTION

A detailed description of polymer characteristics may be given by several polymer parameters which affect their properties. Foremost of these parameters is chemical composition. This is dictated by the chemistry of the atoms that comprise the polymer chain. Secondly, physical properties of polymers are affected by their molecular weights and the distribution of molecular weights. It is not possible to synthesize macromolecules so that they have a singular molecular weight. Instead, there is always a distribution of polymer chain sizes, the polydispersity of which is determined by the mode of synthesis. The third major polymer parameter is morphology -- the features of the polymer in the solid state that result from the various levels of molecular and macroscopic organization. The polymer may be amorphous when the chains are not ordered, in which case, they can be characterized by a glass transition temperature. Or they can be ordered and thus be semicrystalline. Due to the size of polymer chains, it is not possible to attain the organization in the solid state to yield a perfectly crystalline polymer; instead, amorphous and crystalline regions coexist, thus the term semicrystalline. These polymers possess both a glass transition temperature and a melting temperature. The different levels of organization in a molecule may be affected by two other polymer parameters, the stereochemistry and the topology. Stereochemistry may be of the geometrical cis/trans variety encountered in the chemistry of small molecules or brought about by stereoregularity along the polymer backbone. This regularity is referred to as tacticity and is illustrated in Figure 4.1. Tacticity can be classified into three categories. Isotactic polymers contain repeat units of the same chirality, syndiotactic polymers have substituents which fall in meso and racemic forms, finally, atactic polymers contain a more or less random combination of alternating isotactic and syndiotactic sequences. The last major polymer parameter is topology. Polymer chains can have different architectures, the simplest of which is the linear polymer chain. Synthetic routes taken to make polymers sometimes result in random branching along the chain. These branches may be short (the order of five or six carbon

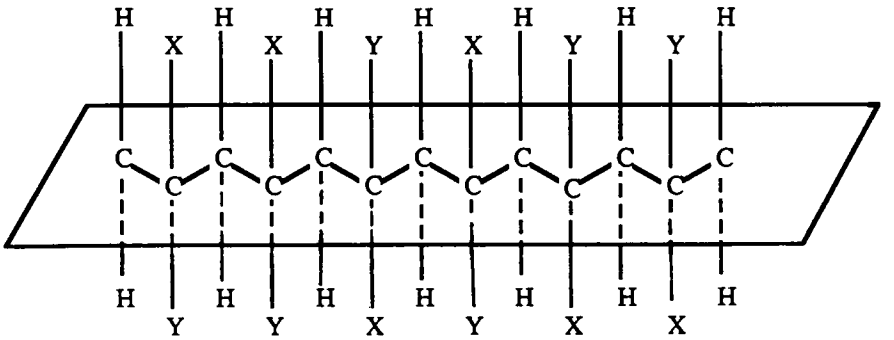

a

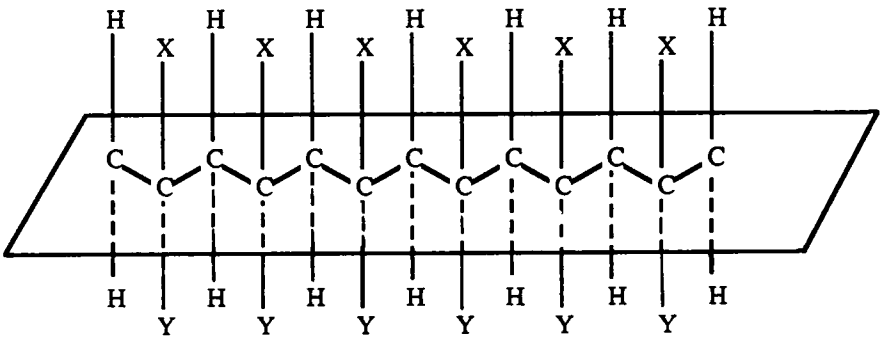

b

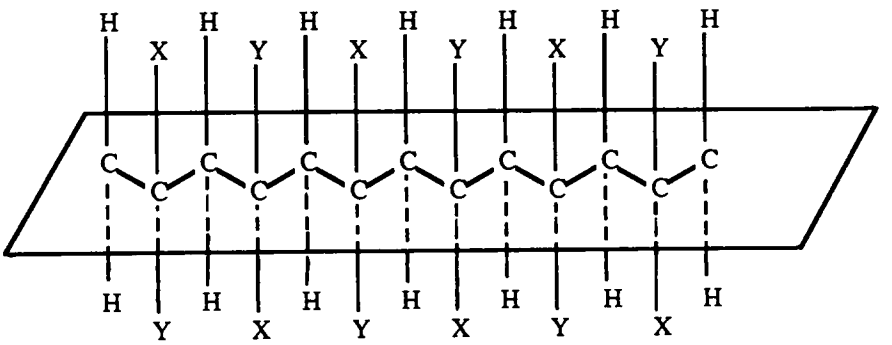

c

Figure 4.1: Diagrams showing tacticity of polymers a: Atactic b: Isotactic c: Syndiotactic configurations.

units) or long -- branches having molecular weights of the same order as the backbone. Short chain branches affect solid state properties, while long chain branches influence solution and melt properties. Two special types of long chain branching are shown in Figure 4.2. The first one is a radial star branched polymer, where the branching results from arms emanating from a central point. The second type of branching shown is the comb where long chains are attached along the backbone and each branch point can have a functionality of three or four. The most widely studied branched polymers are polyethylene, poly(vinyl acetate), polystyrene, polydienes, poly(vinyl chloride) and polyamides (1-9).

Investigations of polymer properties usually fall under one of the polymer parameters described above. The objective of the work in this chapter was to investigate the effect of long chain branching on dilute solution properties. Specifically, the system of interest is the graft or comb poly(methyl methacrylate) homopolymer (PMMA-g-PMMA). PMMA is a high volume commercial plastic produced in the United States under trade names such as Lucite, Plexiglas and Perspex (10,11). The PMMA-g-PMMA's used here were synthesized with the goal of obtaining polymers with differing levels of branching while maintaining relatively constant overall molecular weights. It thus follows that the effect of branching on the conformational behavior of the polymer chain in dilute solution could be isolated. The expected result of keeping the molecular weight constant would be to increase the coil density and decrease the hydrodynamic size of the polymer chains.

Two main goals in this study are: to determine whether universal calibration is an appropriate way to obtain accurate results from GPC, and to study the effect of branching on the hydrodynamic behavior of polymers having about the same molecular weights. The first goal was approached by doing gel permeation chromatography (GPC) with the differential viscosity detector (DV) and low angle laser light scattering detector (LALLS), on-line. GPC/LALLS is a fairly established molecular weight determination technique widely regarded as yielding absolute molecular weights since it does not require calibration with an external standard. GPC/DV on the other hand, is a new technique based on universal calibration. The values obtained using these two detectors were compared. In addition, separate experiments were conducted

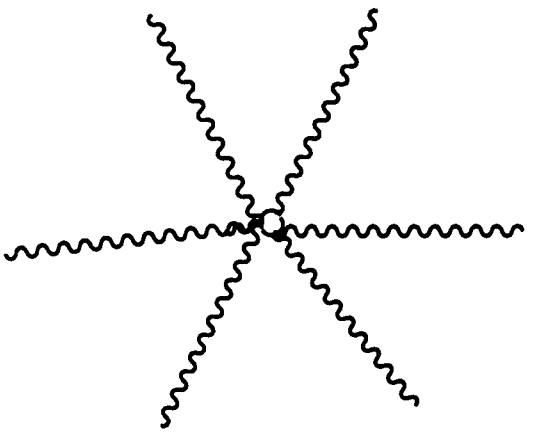

a

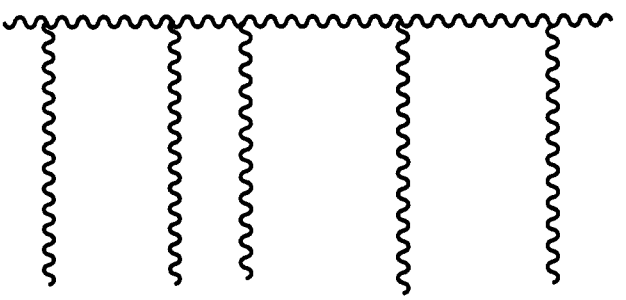

b

Figure 4.2: Examples of a: star branching and b: comb with f = 4.

to get the absolute molecular weights by membrane osmometry and static LALLS to provide reference values for the GPC experiments.

The hydrodynamic behavior of the branched polymers was investigated by doing intrinsic viscosity experiments at various temperatures to examine possible changes in conformation brought about by the increase in temperature. Again the results were compared to the ones obtained from the GPC/DV. The data generated from the GPC/DV will provide unperturbed dimensions of the branched molecules by extrapolating the results obtained with good solvents to theta conditions.

Finally, branching information such as number of branches and distribution of branching usually obtained by GPC/LALLS was determined by GPC/DV.

4.2. LITERATURE REVIEW

In this section, the theories and methods currently used to study branching in polymers will be presented. The emphasis of this review will be on the application of the theories and methods to long chain branching and where appropriate, to comb architectures specifically.

4.2.1. Dilute Solution Theory

The molecular weight of polymer molecules preclude their existence in the gaseous state where they might be studied in isolation from other molecules. It is therefore possible to study single polymer chains only in dilute solutions where they are separated from one another. Dilute solution properties of polymers include average molecular dimensions, second virial coefficients and intrinsic viscosities. On one level, these dilute solution properties may be treated in a two parameter theory where the relationships among the three quantities are formulated in terms of the mean square end-to-end distance $\langle r_\theta^2 \rangle$ of a chain in the theta state and z which is proportional to the effective excluded volume of a pair of chain elements at infinite dilution. These properties are considered in conjunction with the chain structure at the atomic or subchain level. In this respect, the focus is on the effect of architecture on the dilute solution properties. The two levels are closely related and are essential to the understanding of polymer solution characterization (12).

4.2.1.1. Average Molecular Dimensions

In solution, a polymer may assume several shapes as a result of rotations about single bonds on the chain brought about by random thermal fluctuations. These shapes are referred to as conformations, not to be confused with configuration, which pertains to the stereoregularity of the molecule which can be altered only with the breaking of chemical bonds.

The average dimensions of linear chains in solution are given by the average end-to-end distance which is illustrated in Figure 4.3. The end-to-end distance, r, is defined as the vectorial distance between the ends of the polymer molecule. The simplest calculation of r assumes that the polymer is comprised of n segments with length l joined linearly without any angular restrictions. With these assumptions, the result is

$$\langle r^2 \rangle = nl^2 \qquad [4\text{-}1]$$

The average end-to-end distance is expressed as the mean square end-to-end distance since the end-to-end vector can go in either the positive or negative direction, ensemble averaging to zero. Thus the square of the r is more meaningful. It is shown to be proportional to the number of segments present in the chain. This result seriously underestimates the true dimension of the chain because real polymer chains are restricted in their rotation by the valence angle. When this constraint is taken into account, the resulting molecular dimensions are expanded as follows:

$$\left\langle r^2 \right\rangle = nl^2 \left[\frac{1 - \cos\theta}{1 + \cos\theta} \right] \qquad [4\text{-}2]$$

where θ is the valence angle, equal to 109.5° for carbon to carbon linkages. The chain dimensions are further expanded when certain conformations are preferred over others as a result of potential energy considerations as shown in Figure 4.4. When this restriction is considered, the following expression results:

$$\left\langle r^2 \right\rangle = nl^2 \left[\frac{1 - \cos\theta}{1 + \cos\theta} \right] \left[\frac{1 + \langle \cos\phi \rangle}{1 - \langle \cos\phi \rangle} \right] \qquad [4\text{-}3]$$

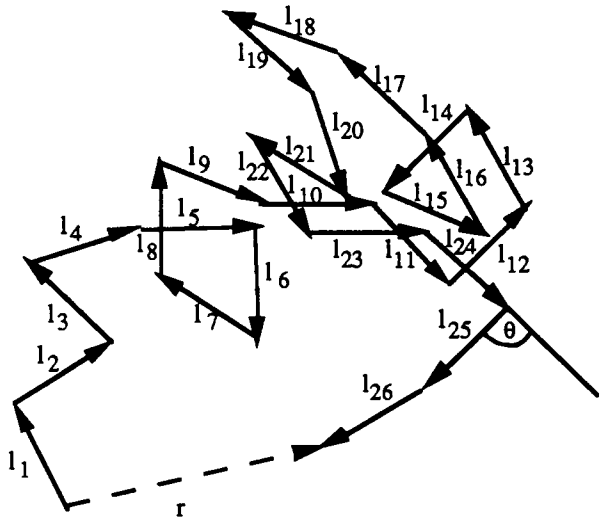

Figure 4.3: An unrestricted macromolecule. Bond lengths li are fixed and equal and there no preferred angles θ.

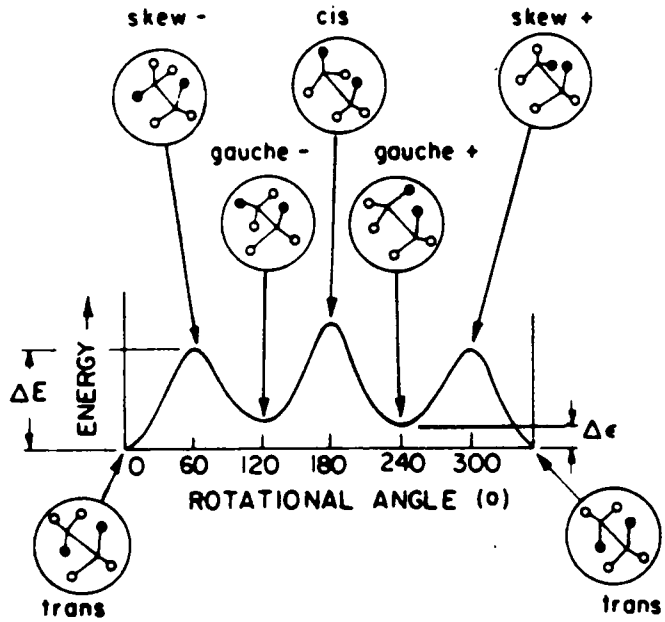

Figure 4.4: Torsional potentials about adjacent atoms in the polyethylene chain. The white circles represent H's and the black circles represent segments of the polymer chain (13).

where <cos ϕ> is the average value of the cosine of the rotation angle ϕ. When all values of ϕ are equally probable as in the case of free rotation, then cos ϕ is zero and equation [4-3] reduces to equation [4-2]. The model breaks down at the limit where ϕ is equal to 0 and cos ϕ =1. This occurs in a completely planar zigzag conformation where all rotamers are trans. Nevertheless, the equation does show that the chain becomes more extended when the rotation angle is close to zero .

Equation [4-3] defines the unperturbed mean square end-to-end distance of a polymer chain. This implies that the chain dimensions are affected only by molecular characteristics. When the chain exists in the dilute solution, the polymer coil is swollen by solvent and the actual coil dimensions as given below

$$\left\langle r^2 \right\rangle^{1/2} = \left\langle r_0^2 \right\rangle^{1/2} \alpha \qquad [4\text{-}4]$$

are expanded by α. The subscript o refers to unperturbed dimensions. The magnitude of α depends on the "goodness" of solvent-polymer interaction. When the random polymer coil is strongly solvated α will be large. When the polymer is in a poor solvent, then α is close to one. This is the theta condition where, theoretically, the end-to-end distance of the polymer chain in the solution is the same as that in the bulk polymer at the same temperature (8,13-15).

While root mean square end-to-end distance may describe linear chains having only two ends, it does not correctly describe branched molecules which contain more than two chain ends. The more appropriate term to use is the radius of gyration expressed as

$$r_g = \left(\frac{\Sigma_i m_i r_i^2}{\Sigma_i m_i} \right)^{1/2} \qquad [4\text{-}5]$$

where r_g is the radius of gyration, m_i is the mass of an element on the chain and r_i is the distance of the element from the center of mass. Radius of gyration is defined as the root mean square distance of the elements in a chain from the center of gravity. For a linear molecule, provided it is a flexible coil,

$$\langle r_g^2 \rangle = \frac{1}{6} \langle r^2 \rangle \qquad [4\text{-}6]$$

This is a useful relationship since the radius of gyration is a more accessible parameter which can be measured directly by light scattering and viscosity experiments.

For a branched molecule, the equation corresponding to equation [4-4] is:

$$\langle r_g^2 \rangle^{1/2} = \langle r_g^2 \rangle_0^{1/2} \alpha \qquad [4\text{-}7]$$

where the actual radius of gyration of a polymer chain in solution is the unperturbed dimension expanded by a factor α. For a molecule containing long chain branching, α_b is typically larger than α_l for its linear analog of the same molecular weight. This implies that the increased degree of branching results in greater polymer-solvent interaction thus causing greater expansion of the molecule (1,10,16).

For a polymer chain containing branches but having no loops, one can define a factor g which is the ratio of the mean square radius of gyration of a branched molecule to that of a linear molecule containing the same number of segments, n:

$$\langle r_g^2 \rangle_b = g \langle r_g^2 \rangle_l = \frac{1}{6} n a^2 g \qquad [4\text{-}8]$$

where the subscripts b and l refer to branched and linear chains respectively and a is the unperturbed effective length (12,17).

Expressions for g may be derived for different chain architectures (12). As visualized in Figure 4.5, a branched molecule will have some segments attached to three or more branches. These segments are the branch points and have a functionality f, which indicates the number of branches emanating from it. A subchain is defined as the portion of the molecule between two junction points or between a junction point and the unit on a free, dangling end. A molecule is assumed to have m branch points and p subchains. If n_λ is the number of segments in the λth subchain then

$$n = \sum_{\lambda=1}^{p} n_\lambda \qquad [4\text{-}9]$$

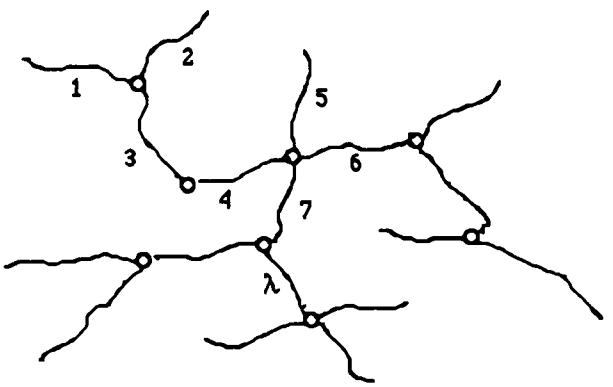

Figure 4.5: Branched molecule with branching terminology defined.

and $\langle r_g^2 \rangle_b$ may be written as

$$\langle r_g^2 \rangle_b = \frac{1}{n^2} \sum_{(i_\lambda, j_\mu)} \langle r_{i_\lambda j_\mu}^2 \rangle \qquad [4\text{-}10]$$

where $r_{i_\lambda j_\mu}$ is the distance between the ith segment in the λth subchain and the jth segment in the μth subchain. The summation is carried out over all i_λ, j_μ pairs. the sum in equation [4-10] may be evaluated to yield expressions of g for different types of branch architectures. Assuming fixed n and m and that all branch points have the same functionality, the following relationship may be obtained.

$$p = (f - 1)m + 1 \qquad [4\text{-}11]$$

The number of segments n_λ may have either a uniform distribution of subchain lengths or a random distribution. For a uniform distribution, all λ's have $n_\lambda = n/p$. Given that $\upsilon_{\lambda\mu}$ is the number of subchains between the λth and the μth subchains, then $n_{\lambda\mu} = \upsilon_{\lambda\mu} n/p$. In a random distribution, the distribution of chain lengths may be described by an average value which allows for the equal probability of the occurrence of a set of $n_1, n_2, \ldots, n_p$ values. The relatively simple expressions of g for star and comb type branching are given below for both uniform and random distributions of subchain lengths. For a star branched chain, m=1 and $\upsilon_{\lambda\mu} = 0$ so that

$$g_u(\text{star}) = \frac{3f - 2}{f^2} \qquad [4\text{-}12]$$

$$g_r(\text{star}) = \frac{6f}{(f + 1)(f + 2)} \qquad [4\text{-}13]$$

From these expressions, the functionality, or number of arms in a star may be obtained once g is determined.

For comb type branching the following two expressions for g may be derived for uniform and random distributions of subchains:

$$g_u(\text{comb}) = \frac{3p - 2}{p^2} + \frac{1}{3}\frac{(f - 1)^2 m \left(m^2 - 1\right)}{p} \qquad [4\text{-}14]$$

$$g_r(\text{comb}) = \frac{6}{p(p+1)(p+2)}\left[p^2 + \frac{1}{6}(f-1)^2 m(m^2-1)\right] \qquad [4\text{-}15]$$

Since p can be expressed in terms of f and m as given in equation [4-11], equations [4-14] and [4-15] can be written in terms of f and m and the number of branch points in a comb may be determined by assuming that all these points have the same functionality.

The numerical values of g have been calculated and in all cases, they have a value less than 1 (12). Since g is defined as the ratio of the radius of gyration of a branched molecule to a linear molecule of the same molecular weight, these results indicate that the average chain dimensions of a branched molecule will always be smaller than that of its linear counterpart having the same degree of polymerization.

4.2.1.2. Second Virial Coefficient

The second virial coefficient, A_2, is a parameter that measures polymer solvent compatibility. A large positive A_2 indicates good solvent polymer interaction. A small value is a sign of a poor solvent. A_2 can also be negative, in which case it indicates the presence of association of the molecules in solution. At the Θ temperature, A_2 is zero. Under this condition, there is no interaction between the solute and the solvent. The solvent is there merely to support the polymer chains and the chains are in a state near precipitation although they remain in solution. This is the point at which unperturbed chain dimensions are measured (8,13-15). It was found that the Θ temperature of branched polymers is less than that of linear molecules of equivalent molecular weight (18).

Aside from solvent power, other factors affect the second virial coefficient. These factors include chain architecture, temperature and molecular weight. For branched molecules, A_2 may be expressed as follows:

$$A_2 = (N_A n^2 \beta / 2M^2)(1 - Cz + \ldots) \qquad [4\text{-}16]$$

where N_A is Avogadro's number, β is the binary cluster integral for a pair of segments and represents the effective excluded volume for one segment due to the presence of another segment in that space. β is generally larger in good solvents where good polymer/solvent interaction exists. It is zero or negative in poor solvent systems. M is the polymer molecular weight, C is a constant which is a function of chain

structure. For a comb branched molecule with branch functionality of three, C increases with increasing number of branches, resulting in a decreasing second virial coefficient (12,16,19).

When the temperature of a solution is increased, this energy input usually causes an increase in A_2 by increasing chain flexibility and effecting an increase in polymer-solvent interaction. For branched polystyrenes, the rate of increase in A_2 as a function of temperature decreases as the temperature is increased until the value observed approaches that of the linear analog (16,20).

Lastly, A_2 is dependent on molecular weight. In a good solvent, this dependence is given as

$$A_2 = kM^{-\gamma} \qquad [4\text{-}17]$$

where k is a constant and the exponent γ varies from 0.2 to 0.3. This relationship is influenced by both the solvent power and the temperature. An increase in solvent power reduces the molecular weight dependence of A_2. Likewise, below the Θ temperature, A_2 is virtually independent of M (14,17,21,22).

4.2.1.3. Intrinsic Viscosity

The average molecular dimensions of a branched chain may be obtained directly by light scattering experiments if the molecular weight is high enough to scatter light asymmetrically. Otherwise, this information may be calculated indirectly by doing intrinsic viscosity experiments which are relatively inexpensive and simple. Intrinsic viscosity, $[\eta]$, is defined as

$$[\eta] = \left(\frac{\eta_{sp}}{c}\right)_{c \to 0} \qquad [4\text{-}18]$$

where η_{sp} is the specific viscosity defined below and c is the concentration typically given in terms of g/dl or g/ml. The ratio of specific viscosity to concentration is the reduced viscosity.

$$\eta_{sp} = \frac{t - t_0}{t_0} \qquad [4\text{-}19]$$

where t is the efflux time of the solution in a viscometer and t_0 is that of the solvent. Alternatively, intrinsic viscosities can be expressed in terms of relative viscosity as

$$[\eta] = \left(\frac{\ln \eta_r}{c}\right)_{c \to 0} \qquad [4\text{-}20]$$

where relative viscosity is the ratio of the solution flow time to the solvent flow time. The quantity in parenthesis is the inherent viscosity. Very often, data are plotted both in terms of reduced viscosity and inherent viscosity and $[\eta]$ is obtained by taking the intercept at c=0. Where the intercepts do not coincide, the average value of the two quantities is considered the $[\eta]$.

From theories of the frictional properties of polymer molecules, it can be shown that the intrinsic viscosity is proportional to the ratio of the effective hydrodynamic volume of a polymer molecule in solution to its molecular weight. For a random, flexible coil, the hydrodynamic volume is taken to be the cube of the root mean square end-to-end distance $\langle r_2 \rangle^{1/2}$ so that one may write at Θ conditions

$$[\eta] = \frac{\Phi \langle r^2 \rangle^{3/2}}{M} \qquad [4\text{-}21]$$

where Φ was postulated by Flory to be a universal constant and is equal to 2.5×10^{23} for flexible random coils when r is expressed in cm, M in g/mole and $[\eta]$ in ml/g. Equation [4-21] holds for linear molecules. For application to non-linear molecules, the equation must be expressed in terms of radius of gyration as follows:

$$[\eta] = \frac{\Phi' \langle r_g^2 \rangle^{3/2}}{M} \qquad [4\text{-}22]$$

Here, $\Phi' = 6^{3/2}\Phi$ due to the relationship between radius of gyration and end-to-end distance for a flexible linear chain given in equation [4-6]. Equation [4-21] is often used to obtain the unperturbed chain dimensions by using the relationship in equation [4-4] to generate the equation

$$[\eta] = \Phi \left(\frac{\langle r_0^2 \rangle}{M}\right)^{3/2} M^{1/2} \alpha^3 = K M^{1/2} \alpha^3 \qquad [4\text{-}23]$$

where

$$K = \Phi \left(\frac{r_0^2}{M} \right)^{3/2} \qquad [4\text{-}24]$$

is a constant for a given polymer independent of solvent and molecular weight. Since $\alpha = 1$ under Θ conditions, the measurement of intrinsic viscosities under this constraint should yield the unperturbed chain dimensions of a polymer molecule (7,12,13,15,23,24). However, to do the experiment under these conditions is not an easy task. The usual practice therefore is to use good solvents and extrapolate to theta conditions. Several investigators have proposed equations for this purpose. The simplest of these which has been found to be adequately accurate is the one proposed by Stockmayer and Fixman:

$$\frac{[\eta]}{M^{1/2}} = K + 0.51\, \Phi\, B\, M^{1/2} \qquad [4\text{-}25]$$

where B is a constant dependent on the molecular weight of the chain segments and is an indication of long range interaction (2,23,25-28). The intercept of a plot of $[\eta]/M^{1/2}$ against $M^{1/2}$ should then yield an intercept of K from which the unperturbed chain dimensions may be calculated. If $\Phi = \Phi'$ is used, then the unperturbed dimension obtained here is the radius of gyration.

Intrinsic viscosity values are dependent not only on the solvent used in the experiment but also on the temperature of the measurements. The temperature coefficient of intrinsic viscosity is in fact related to the changes in unperturbed chain dimensions and expansion factor as a function of temperature in the following manner:

$$\frac{d \ln [\eta]}{dT} = \frac{d \ln K_\theta}{dT} + 3 \frac{d \ln \alpha}{dT} \qquad [4\text{-}26]$$

From the variation of intrinsic viscosity with temperature, it is then possible to detect any conformational changes in the polymer. In fact, PMMA has been documented to exhibit conformational transformations in various solvents. When the experiment is conducted over a sufficiently wide range of temperatures, the results show that for some polymer/solvent systems, there is a temperature at which $[\eta]$ is maximum.

Recently, it has been reported that there are also transitions in $[\eta]$ near the Θ temperature which cannot be attributed to conformational transitions. Instead, it was proposed that while the conformational transitions are brought about by side group effects, the transitions near the Θ temperature are due to chain backbone effects. Both types of phenomena affect only short range interactions (25,29-41).

4.2.2. Determination of Long Chain Branching in Polymers

The g factor defined in equation [4-8] can be used to determine the amount of branching present in a polymer. The procedure requires the measurement of the radius of gyration of a branched molecule and its linear analog having the same molecular weight; however, this necessitates the use of expensive light scattering equipment since the experiment has to be conducted through several angles to provide the data points for a Zimm plot. The relationship more commonly employed for this study is :

$$g^{x} = \frac{[\eta]_b}{[\eta]_l} \qquad [4\text{-}27]$$

The equation can be used to obtain branching information if the intrinsic viscosity experiment can be conducted on both the branched and linear polymers of the same molecular weight in the the same solvent and temperature. When it is not possible to obtain the linear analog, one can then use the knowledge of molecular weight and its relationship to intrinsic viscosity given by the Mark-Houwink equation:

$$[\eta] = KM^{a} \qquad [4\text{-}28]$$

K and a being the Mark-Houwink constants. This route is contingent on the availability of the Mark-Houwink constants for the polymer/solvent/temperature combination of interest.

The expression for g^x is useful for the investigation of branching only if the architecture is known since both the exponent x and the final equation for g required are dependent on the type of branching present in the polymer (1,18,42-47). Values for x range from 0.5 to 1.5. For star branched polymers, it has been established that x = 0.5. For combs with many short branches x approaches 1.5. When the comb

has a low branching frequency, then x is closer to 0.5. For randomly branched polymers, x ranges from 0.7 to 1.3 depending on the degree of branching present (1,5,16,43,48).

With the advent of gel permeation chromatography (GPC), which can conveniently and rapidly fractionate whole polymers, the task of studying long chain branching has been eased, when the proper detectors are employed. In the following sections, the use of the differential viscosity (DV) and low angle laser light scattering (LALLS) in the study of branching will be described.

4.2.2.1. GPC/DV

Operation of the GPC with a differential viscosity detector is based on the universal calibration curve developed by Benoit. This calibration technique was already discussed in Chapter 2 (49,50). Its validity has been reiterated by theoretical studies that demonstrate that solute shape and its interaction with the pores of the GPC column packing determine the separation of the molecules (51,52). Although universal calibration has been shown to have some shortcomings, it gives far superior results when compared to quantities obtained from calibrations based on molecular weights, the calibration curve of which changes as a function of the conformation of the standards used (29,51,53,54).

Based on the universal calibration technique, one may use GPC to determine not only the number average molecular weight $\overline{M}_n$, and weight average molecular weight $\overline{M}_w$, but other ratios of moments of the molecular weight distribution as well. It has been demonstrated by Hamielec and Ouano that the appropriate molecular weight for the universal calibration relationship is $\overline{M}_n$ (not $\overline{M}_w$, which was instinctively used by many initially due to its proximity in value to the viscosity average molecular weight (19,55)). The conclusion of this proof was that the viscosity detector can only reliably yield $\overline{M}_n$.

GPC coupled with a viscosity detector is the most direct method of obtaining the branching factor g^x since the intrinsic viscosity is the quantity measured by the detector (18). The importance of the information obtained by the coupling of GPC with intrinsic viscosity experiments in branching studies is demonstrated by the fact that before on-line viscosity detectors were devised, the study of branching via GPC was conducted through the tedious collection of effluent fractions as they eluted from the columns into

microviscometers for the measurement of intrinsic viscosities of these monodisperse fractions. With the improvement in chromatographic efficiency however, the amount of sample injected has dramatically decreased in volume so that the earlier procedure was dropped (56-60). More recently, universal calibration was used as the basis for obtaining the molecular weight and branching distribution without the use of an on-line viscometer (5,48,61,62).

Several viscosity detectors have been developed for use on the GPC in conjunction with a concentration sensitive detector (63-75). However, only one design is currently available commercially. This detector obtains specific viscosity on-line based on a differential pressure measurement (72-74). Measurement of the change in pressure that results from the presence of a solute in the mobile phase in this way eliminates the noisy baseline that plagues the other detectors (76).

Park and Graessley have used an on-line viscometer that measures flow times of the eluents from the GPC to determine intrinsic viscosities. This experiment was utilized in the study of branched polystyrenes having a functionality of 4 and poly(vinyl acetate)s having a branch functionality of 3. They found that the technique was satisfactory for specimens having only moderate branching frequency. Where there was a large branching frequency, both this characteristic as well as the molecular weight obtained were underestimated. It was also discovered that very small amounts of branching were difficult to detect due to the insensitivity of the concentration detector at the portion of the elution curves where the effect of the branching would be visible (44).

As for the Viscotek differential viscosity detector, which is currently the only commercially available viscosity detector , Hamielec et al. have tested its accuracy in the molecular weight determination of some linear as well as branched polymers. It was found that the weight average molecular weights were in good agreement with the values quoted for the materials used. Number average molecular weights however varied. It was postulated that the deviation in molecular weights from their "true" value was due to peak broadening. Although the molecular weights of branched poly(vinyl acetates) were measured, no attempt was made to look into the branching characteristics of these materials (77).

Although the differential viscosity detector does yield the intrinsic viscosities, an analysis of the separation mechanism reveals that g^x is not the quantity that one obtains directly. As Jordan and McConnell pointed out, g^x is the ratio of intrinsic viscosities for a branched and linear molecule having the same molecular weight. GPC however, does not separate based on molecular weight but on hydrodynamic volume -- molecules having the same hydrodynamic volume elute at the same retention volume, so the g obtained here is actually

$$g_v = \left(\frac{[\eta]_b}{[\eta]_l}\right)_v \qquad [4\text{-}29]$$

where v here stands for elution volume. The relationship between g^x and g_v can be derived with the use of equation [4-28]. It was shown to be

$$g^x = g_v^{a+1} \qquad [4\text{-}30]$$

where the "a" was the Mark-Houwink constant. Obtaining the Mark-Houwink constants requires fractionation of a polymer and the determination of the intrinsic viscosities and molecular weights of each of these fractions. All these are achieved by the GPC/DV system thus making it the ideal method for investigating branching in polymers (2,78,79).

4.2.2.2. GPC/LALLS

In contrast to GPC/DV, light scattering has been around for a long time. In fact, the first light scattering photometer was introduced at the beginning of this century. The theory relating light scattering intensity to molecular weight and size and its application to polymers specifically was developed in the 1940's (2). It is no surprise therefore, that the use of light scattering to characterize polymer molecular weights and dimensions is fairly well entrenched. Light scattering experiments typically entail the measurement of light scattered from polymer solutions of a range of concentrations at various scattering angles. These data are then used to construct a Zimm plot from which double extrapolation to

concentration and scattering angle equal zero yields the weight average molecular weight and the radius of gyration. A comprehensive treatment of this subject may be found in the text by Huglin (80).

Although, a sensitive on-line light scattering detector was developed twenty years after the first photometer, the most successful molecular weight detector was available only twelve years ago (2). The design of this detector is based on the measurement of the light scattered at very low angles so that only a single extrapolation to zero concentration is necessary to obtain molecular weight. In addition, the second virial coefficient for any polymer solvent pair can be obtained (81-84). The procedure to do this experiment on a LALLS is detailed in Chapter 2.

With very slight variations in the experimental set-up the LALLS can be used as an on-line molecular weight detector for the GPC. The equation used for static LALLS is given as

$$\frac{Kc}{R_\theta} = \frac{1}{\overline{M}_w} + 2A_2c \qquad [4\text{-}31]$$

Definitions for all the terms in this equation have been given in Chapter 2 and will not be repeated here. Suffice it to say that with this equation a plot of Kc/R_θ against concentration should yield weight average molecular weight, $\overline{M}_w$, from the inverse of the intercept and the second virial coefficient from the slope. When the LALLS is used as a molecular weight detector, equation [4-31] is modified slightly to

$$\frac{Kc}{R_{\theta i}} = \frac{1}{\overline{M}_i} + 2A_{2,i}c_i \qquad [4\text{-}32]$$

where the i's in the subscript refer to a slice of the chromatogram (2,81). In theory, the GPC can separate whole polymers into monodisperse fractions so that $\overline{M}_i = \overline{M}_n = \overline{M}_w$. However, some mixing does occur in the detector so that it contains a broader than ideal dispersion of molecular weights at any one time and $\overline{M}_i$ is really $\overline{M}_w$. For this reason, many investigators believe that GPC/LALLS can only give accurate $\overline{M}_w$'s while the other moments of molecular weight distribution that GPC is supposed to supply are unreliable except for polymers having a small polydispersity (4,19,81,85-88).

The above equation requires that the specific refractive index increment which goes into the calculation of K and the second virial coefficient be accurately determined separately for the polymer/solvent system and temperature used and assumes that these two quantities remain constant throughout the molecular weight distribution. This causes pitfalls when the technique is applied to copolymers which may have an inhomogeneous chemical composition distribution. The dn/dc is particularly sensitive to temperature. Although its dependence on temperature is linear, the relationship could be positive, negative or, rarely, zero (20,89-92). The error brought about by using the wrong dn/dc is more significant since it is squared in the calculation. A 5% error in dn/dc can lead to a 10% error in the K and $\overline{M}_w$. On the other hand, the results from the GPC/LALLS experiment are not as severely affected by A_2. In fact, it was demonstrated that a fourfold increase in A_2 resulted in only a 2% increase in $\overline{M}_w$ and a 1-4% increase in the $\overline{M}_n$ (86).

In its application to branching investigations, the relationship used is not that given in equation [4-8] since the low angles accessible to this instrument prevents the determination of radius of gyration. For the study of branched molecules, the only relevant parameter that may be obtained is the molecular weight. Therefore, equation [4-27] together with the relationship for universal calibration given in equation [2-2] are used to obtain:

$$g^x = \frac{[\eta]_b}{[\eta]_l} = \frac{M_l}{M_b} \qquad [4\text{-}33]$$

As discussed in the section on the application of GPC/DV to branching studies, the branching factor g^x here is actually that which obtains at a constant elution volume rather than a constant molecular weight. Equation [4-30] will thus be correct with the exception that g is now couched in terms of molecular weights instead of intrinsic viscosities. Again the Mark-Houwink constant "a" is required (2,4,42,43,47,78,79, 93,94). However, the use of GPC/LALLS data necessitates a more complex route to obtain a. Iterative methods based on a log normal distribution have been suggested (95). Another method proposed the use of equations giving the relatively complicated dependence of hydrodynamic volume on Mark-Houwink

constants. This requires picking a pair of points in the regions of the concentration and LALLS chromatogram having high intensities and using a pair of equations to solve for the two constants (43,96).

While GPC/LALLS offers useful information, its use in conjunction with a concentration sensitive differential refractive index (DRI) detector has accompanying problems. The LALLS detector is sensitive to high molecular weight materials and lacks sensitivity at the low molecular weight end of the chromatogram. The DRI detector on the other hand lacks sensitivity on both peripheries of the chromatogram. The decreased resolution on both ends of the chromatogram affect the $\overline{M}_w$ if error occurs in the lower elution volumes where the large species elute and causes an error in the calculated $\overline{M}_n$ where the error is on the low molecular weight end of the chromatogram. A solution suggested for this problem is to electronically enhance the signal to noise ratio where needed to increase the accuracy of the data obtained (19,21,78,86,97).

In the case of both GPC/DV and GPC/LALLS, axial dispersion is a pertinent factor. It is postulated that the mixing of monodisperse fractions of polymers in the detector cells result in an error in the calculated molecular weight distribution so that each detector can only reliably give one moment of the distribution. In addition, whenever two detectors are used in tandem, caution should be exercised in the determination of the dead volume in between the detectors. Calculation of the lag times between detector cells may be in error due to band distortion caused by tubing connections (55,75,86,98,99). In spite of these problems, variations in the molecular weights determined by GPC/LALLS are less than previously obtained by other methods (100). In addition, unlike conventional GPC, GPC/LALLS is applicable to linear as well as branched polymers (101).

4.2.2.3. Multidetection GPC

From the discussion on GPC above, it may be concluded that in order to have complete information on the molecular weight distribution of a polymer, not only dual detection but multidetection is required. This may be achieved by separately running GPC/LALLS and GPC/DV experiments. The ideal instrument would have three detectors -- concentration, viscosity and light scattering -- in tandem on a GPC. Although

this arrangement should yield the maximum information in the most efficient manner, one has to be careful about the dead volume and axial dispersion problems of such a configuration (2,5,75,79,98,99,102). So far, there has only been one such combined instrument reported in the literature (103).

For branching studies, a pair of detectors should suffice, with the GPC/DV being the ideal choice (87). A recent suggestion for another possible pair is GPC with sedimentation velocity determination. This method was proposed by Tung. His application of this system to some comb polystyrenes yielded an underestimation of the branching level and branching frequency. It was suggested that perhaps universal calibration, which he invoked in the investigation, may not have been appropriate for the highly branched polymers under examination, and is a major subject of the present work.

4.3. EXPERIMENTAL

In this section the procedures used in this investigation of the graft PMMA homopolymers will be detailed.

4.3.1. Materials

The synthesis of the materials required for this study was carried out by Joe DeSimone and Ann Hellstern in the laboratory of Dr. James E. McGrath at Virginia Tech. This investigation required the synthesis of model branched homopolymers having a well defined molecular weight distribution as well as branching level. This was achieved by the synthesis of PMMA-g-PMMA using the macromonomer technique (104,105). The macromonomer was synthesized via group transfer polymerization which yields products having a narrow distribution of molecular weights. These macromonomers will make up the graft part of the polymer thus resulting in a narrow distribution of branch lengths for the PMMA-g-PMMA's made. The backbone was synthesized via anionic polymerization which also yields a narrow molecular weight distribution due to its "living" nature. This combination of synthetic methods should therefore produce extremely well defined model branched homopolymers having controlled molecular weight and branch length distributions. The final step of the synthetic procedure is shown in Figure 4.6. The finer

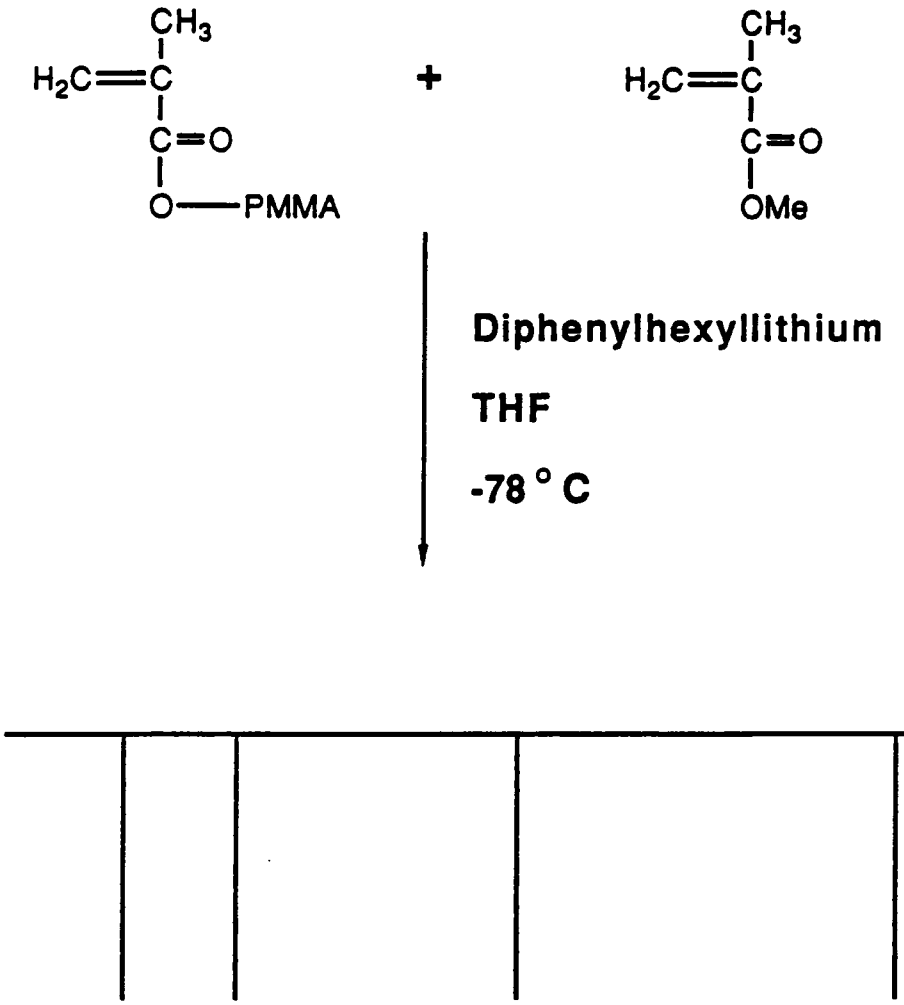

Figure 4.6: Synthesis of PMMA-g-PMMA.

points of the synthesis are detailed elsewhere (106,107). Three samples of PMMA-g-PMMA's with different levels of branching obtained in the above manner will be used in this study.

In order to determine branching, a linear analog of the polymer having the same molecular weight was needed. A PMMA narrow distribution GPC standard was obtained from American Polymer Standards Corp. for this purpose. The specifications from the source indicated that the standard had a $\overline{M}_w$ of 251,000 and a $\overline{M}_n$ of 239,100. The intrinsic viscosity at 30°C in THF was given as 0.7 g/dl and the Mark-Houwink constant "a" was 0.69.

4.3.2. Extraction of Unincorporated Macromonomer

The graft polymers obtained after synthesis contained a small amount of unincorporated macromonomer which does not significantly affect GPC analysis since the signal due to the unincorporated material and its concentration may be eliminated in the data processing step of the experiment. For the rest of the investigation however, the instrumentation applied could not separate the effect caused by the presence of the linear macromonomers having a much smaller molecular weight than the graft polymer. It was therefore necessary to remove the unincorporated material. This was achieved using steps based on fractional precipitation (108). The most effective way of doing this involved making a ca. 1% solution of the polymer in tetrahydrofuran (THF). Nonsolvent was slowly added to this solution with agitation. Either methanol or hexane was the nonsolvent, with hexane being more effective. Nonsolvent addition was terminated before the turbidity endpoint which was indicated by difficulty in dissipating the cloudiness of the solution following nonsolvent addition. At this point, the solution was allowed to ripen for several hours. More nonsolvent was subsequently added until precipitates were visible. The solution was then left to stand at room temperature in order to allow sedimentation of the precipitate. When methanol was utilized as the nonsolvent, twenty minutes of centrifuging were necessary to facilitate the separation of the precipitate from the supernatant liquid. This method yielded a thick film of the graft PMMA. In order to ensure the absence of solvent in the graft PMMA's, it was necessary to reprecipitate the PMMA film. This was achieved by making up a 5% solution of the material in THF and slowly adding this solution to

approximately ten times its volume of hexane in a Waring blender set at a moderate blending speed. The resulting flakes were dried at about 40°C under vacuum for at least six hours. After the drying step, no smell of the solvents used in the extraction was detectable. The procedure detailed above can be used to fractionate large quantities of polymer at one time so that the sample to be used in the whole study did not have to be pooled from several fractionations, as would be the case if preparative scale GPC were utilized. For this investigation, approximately 10 grams of polymer was fractionated and the yield at the end was roughly 75%. The procedure was completed for one batch of polymer within a couple of days. All the experiments conducted below, except for the determination of the number of branches utilized the PMMA's from which the unincorporated macromonomer had been extracted.

4.3.3. Vapor Phase Osmometry (VPO)

The absolute number average molecular weight of the macromonomer was determined using a Wescan model 233 vapor phase osmometer before it was used in the synthesis of the various graft polymers. The experiment was conducted in HPLC grade, unstabilized THF at 30°C and in HPLC grade toluene at 63°C. Molecular weight was obtained using the multistandard calibration explained in Chapter 3. The standards used were sucrose octaacetate and polystyrene standards with narrow polydispersities and having molecular weights of 1250, 2150, 2950, 5050 and 9200 g/mole. In addition, for toluene, polystyrene with a molecular weight of 19,000 g/mole and PMMA with a molecular weight of 13,000 g/mole were also used. For each experiment, four solutions were used. The concentrations of these solutions ranged from 1 to 7 g/L for the macromonomer and the standards having molecular weights of up to 5050 g/mole. The other standards required higher concentrations to compensate for the decreased sensitivity of the instrument due to their higher molecular weights. For those materials the solutions used ranged in concentration from 2 to 9 g/L.

4.3.4. Membrane Osmometry (MO)

The absolute number average molecular weights of the PMMA-g-PMMA's were measured using the Wescan model 231 membrane osmometer. The measurements were done with RC 52 and RC 51

regenerated cellulose membranes which have lower molecular weight cut-off limits of 20,000 and 10,000 g/mole respectively. Experiments were conducted at 30°C in HPLC grade toluene. Seven solutions with concentrations ranging from 2 to 8 g/L were used. They were filtered through MSI teflon membrane filters having pore diameters of 0.5 μm prior to the measurements. When the filtering step was bypassed, erroneous results were obtained.

4.3.5. Static Low Angle Laser Light Scattering (LALLS)

The weight average molecular weights and second virial coefficients of the PMMA-g-PMMA's were measured using the Chromatix KMX-6 LALLS photometer in the static mode. The experiments were conducted in unstabilized, HPLC grade THF using solutions ranging in concentration from 1 to 5 mg/ml. The measurements were done at room temperature. The solutions were filtered through an Acrodisc CR 0.2 μm filter as it was pumped at about 0.2 ml/min by a Sage syringe pump through the 15 mm teflon sample cell.

4.3.6. Specific Refractive Index Increments (dn/dc)

The dn/dc's required for both the static LALLS experiments and GPC/LALLS measurements were obtained by using the Chromatix KMX-16 laser differential refractometer having a He-Ne laser operating at 633 nm. Experiments were conducted at 25°C and 45°C in unstabilized, HPLC grade THF for the PMMA-g-PMMA's and the linear PMMA standard. The solutions used ranged in concentration from 4 to 10 mg/ml. At 45°C, the solutions were made in a water bath set at the temperature of the experiments. The solutions used were immersed in this bath for about 30 minutes to assure that there was no temperature gradient in the contents of the volumetric flask. They were then made up to correct volume by the addition of solvent that had also been kept in the bath. These precautions were taken to assure that the concentration used in the calculations was that which obtained at the temperature of the experiment. It was crucial that the solvent used in the reference cell be as close in temperature to that of the solution. A big thermal gradient between the sample and the reference cell results in extra long equilibration times and yields the wrong results. Symptomatic of the error caused by the thermal gradient in the sample cell is the constant

decrease in readings and inability to obtain reproducible data despite hours of equilibration. The experiment for each concentration should be completed within 30 to 40 minutes if sample evaporation is to be kept at a minimum. An indication of solvent evaporation, which would cause an error in the concentration, was a constant increase in dn/dc taken at one to two minute intervals. Ideally, the sample should be allowed to equilibrate for 15 - 20 minutes after the temperature has been reached. Readings reproducible to ± 5 units could then be obtained at the time intervals recommended above.

The cell constant used in the calculation of dn/dc was measured using NaCl solutions at 25°C. This calibration constant is supposed to be valid even at elevated temperatures and remains relatively unchanged over a long period of time. When elevated temperature operations are undertaken however, it is recommended that the cell constant be evaluated more often. Over a period of three months when the temperature of sample cell was raised and lowered in the experiments done, the cell constant changed by a mere 0.05%. The dn/dc's calculated using the cell constant obtained at the beginning of this series of studies were thus considered reliable.

4.3.7. Gel Permeation Chromatography (GPC)

GPC was performed on both the extracted and unextracted form of the polymer. Analysis was conducted on a Waters 150C ALC/GPC which was equipped with a differential refractive index detector, Viscotek model 100 differential viscosity detector and the Chromatix KMX-6 LALLS. The configuration used is the same as the one shown in Figure 3.7. Experiments using the GPC/DV were conducted in two modes, one where the LALLS was off-line and one with the LALLS on-line. This way the effect of multidetection could be studied.

Five Column Resolution repacked Permagel columns ranging in pore diameters from 100 Å to 10^5 Å were connected in series to an Ultrastyragel® column having a pore diameter of 10^6Å. The polymer standards used to construct the universal calibration curve were Polymer Laboratories narrow distribution polystyrene standards having molecular weights of 1250, 2150, 2950, 5000, 9200, 22000, 34500, 52000, 68000, 120000, 170000, 500000 and 1130000 g/mole. Approximately 2 mg/ml of unstabilized, degassed

THF solutions of the branched and linear PMMA's were used. They were filtered through MSI teflon membrane filters having pore diameters of 0.5 μm prior to injection. An injection volume of 300 μl was found to offset the effect of the small difference in refractive indices of PMMA from THF to yield a stable baseline. The flow rate used was 0.9 ml/min. The parameters on the GPC were set as follows: sensitivity -64, scale factor 10 and run time was 80 minutes with 2 minute equilibration periods between samples. The gain on the computer was set at 1. Experiments were conducted at 30°C, 35°C, 40°C and 45°C, with a calibration curve generated and detector lag times calculated at each temperature.

At temperatures above 30°C, the viscometer and the LALLS were heated. Aside from the heaters available on the LALLS which were connected to the sample flow cell alone, an auxiliary heater was made by attaching a 1" x 5" 25W strip heater on each side of the sample holder that were controlled by an Omega model CN9111 temperature controller. This was to ensure the heating of the quartz glass windows that were holding the sample cell thus preventing thermal gradients in the cell.

At elevated temperatures, solution preparation was completed in the heated injection compartment to ensure the correct concentration at the higher temperature.

4.3.8. Intrinsic Viscosity [η]

Intrinsic viscosity experiments were carried out in Cannon CUU 50 Ubbelohde capillary viscometers. THF solution flow times of greater than 100 seconds were obtained and eliminated the need to do kinetic energy corrections. Measurements were done for the linear and branched PMMA's at temperatures from 25°C to 45°C at 5° intervals. The flow times of the solutions were measured until five consecutive readings that vary by less than 0.1% were obtained. The temperature of the bath was controlled to within ± 0.02 °C. Four to seven concentrations ranging from 0.2 g/dl to 0.8 g/dl were used in the experiments.

4.4. RESULTS AND DISCUSSION

4.4.1. Vapor Phase Osmometry

The calibration curves used for the molecular weight determination of the macromonomer are overlaid in Figure 4.7. A wider range of molecular weights can be measured using toluene which has a lower vapor

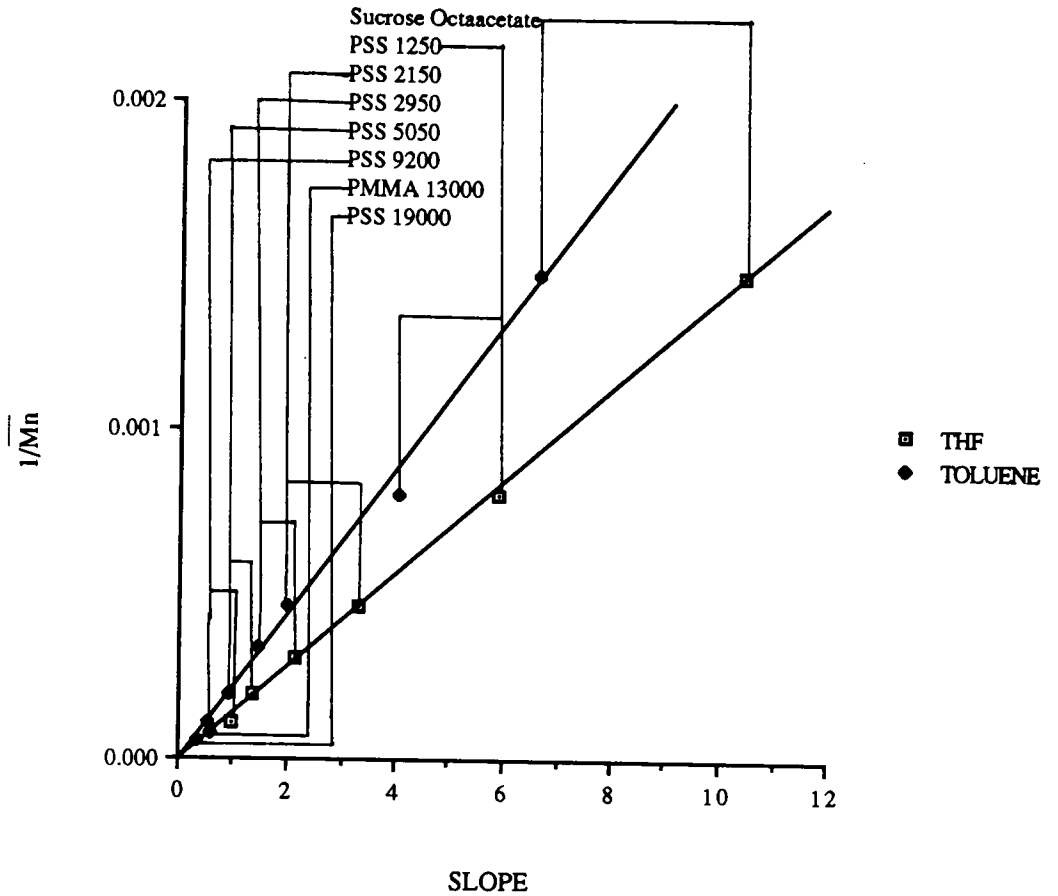

Figure 4.7: VPO calibration curves.

pressure than THF. The molecular weight for the macromonomer when the experiment was done in THF was 6922 g/mole. In toluene at the higher temperature, the values obtained were 7011 and 7127 g/mole from two separate experiments. The proximity in results in the different solvents is expected for samples in which no anomalous behavior such as association exists. For calculations where the molecular weight of the macromonomer is needed an average value of 7020 g/mole was used.

4.4.2. Stoichiometric Determination of Branching

The number of grafts on the comb PMMA's synthesized were determined stoichiometrically by combining information from synthesis, GPC and the VPO. The assumption made here was that all of the macromonomer charged in the synthesis was recovered either as free, unincorporated macromonomer or as grafts on the PMMA-g-PMMA that resulted. A diagram of the algorithm used in the branching calculations is shown in Figure 4.8. The right hand portion shows the final step in the reaction where a known amount of macromonomer and MMA monomer were combined in a reactor to get the graft PMMA. The resulting product is a mixture of the unincorporated macromonomer and the PMMA-g-PMMA. In Figure 4.9, the GPC chromatogram of the macromonomer, the thin trace, was overlaid on the chromatogram of the product of the synthesis, shown as the bolder trace. The small peak is due to the unincorporated graft as evidenced by having the same retention volume as the macromonomer.

As shown in the left hand side of Figure 4.8, the next step was to use the molecular weight distributions from the GPC to determine the proportion of graft PMMA and free macromonomer in the product. The GPC/DV was used to obtain the cumulative molecular weight and molecular weight distribution of the unextracted material as shown in Figure 4.10. The molecular weight distribution was used to determine the molecular weight of the unincorporated macromonomer. The corresponding molecular weight on the cumulative distribution was picked out by aligning the abscissas of both plots -- they have the same scale. The percentage of macromonomer was then read directly off the ordinate of the cumulative distribution plot in terms of percent. The resolution of the scale on the computer screen where this procedure was accomplished was accurate to the nearest whole number. For this part of the study, the

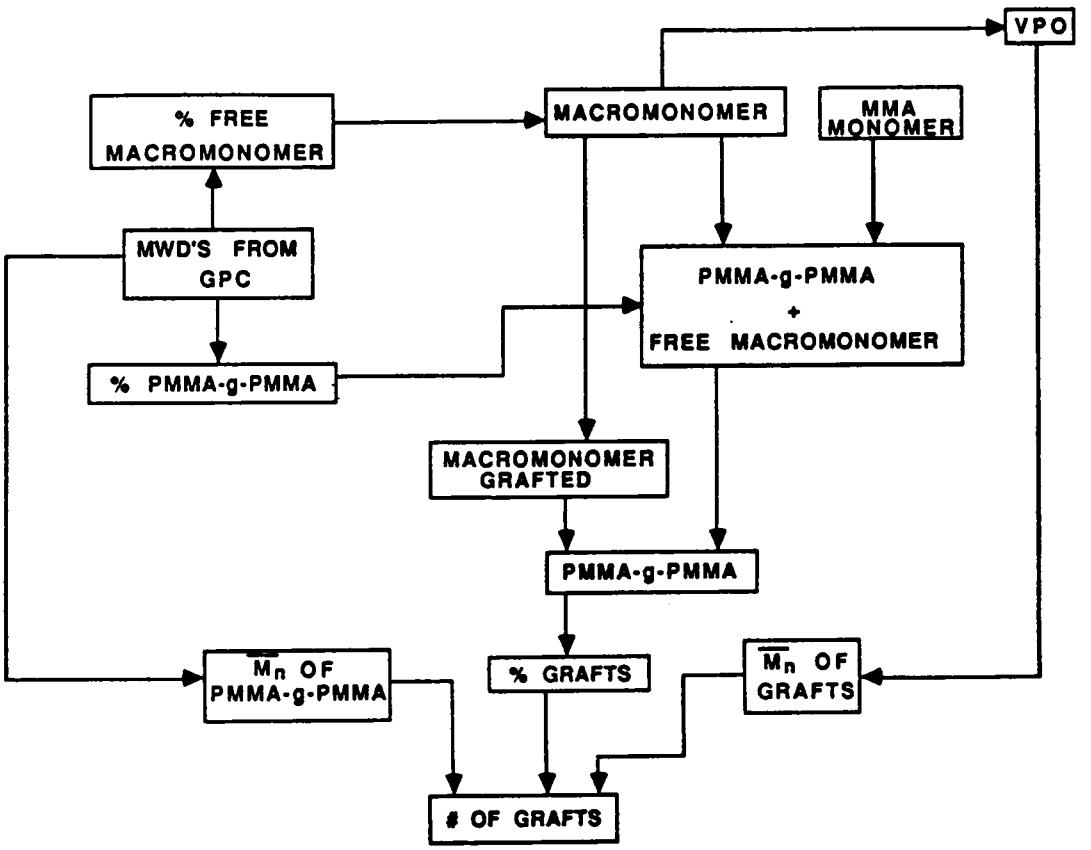

Figure 4.8: Algorithm for stoichiometric branching calculation.

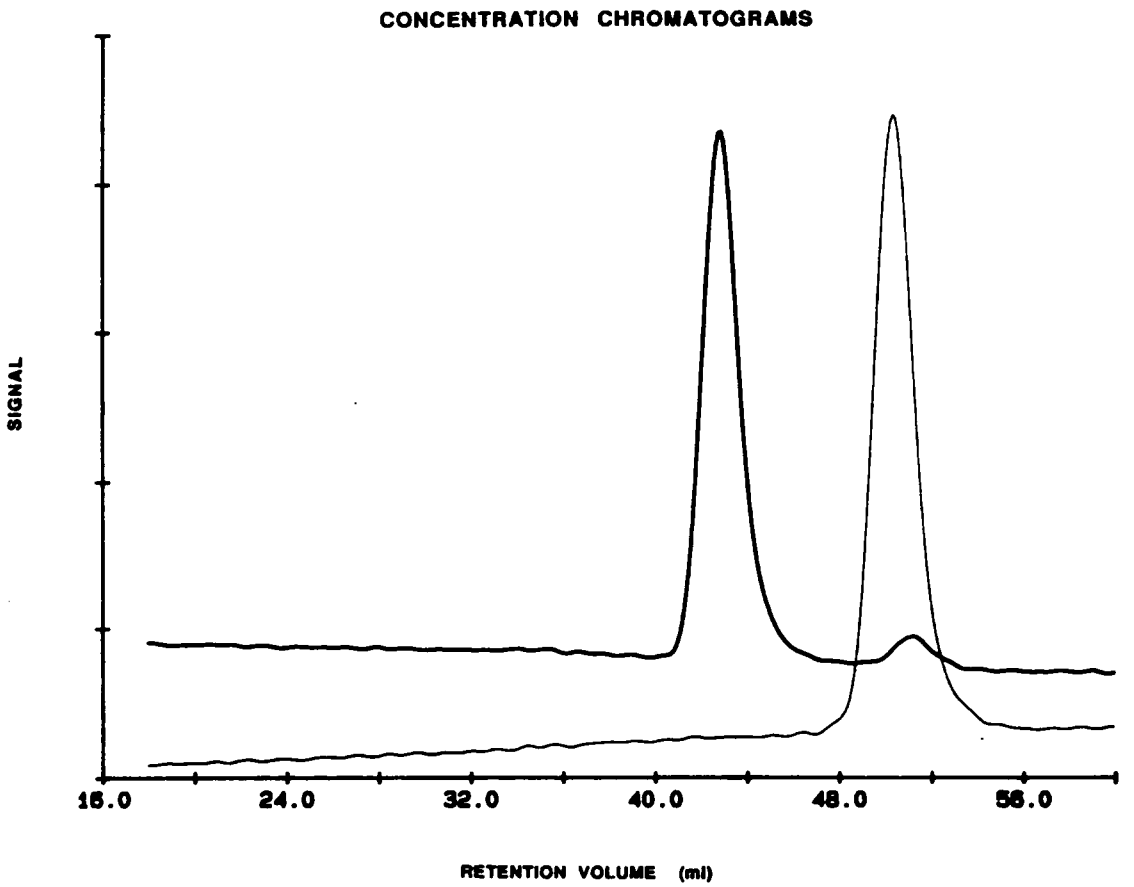

Figure 4.9: GPC chromatograms of PMMA macromonomer overlayed on PMMA-g-PMMA.

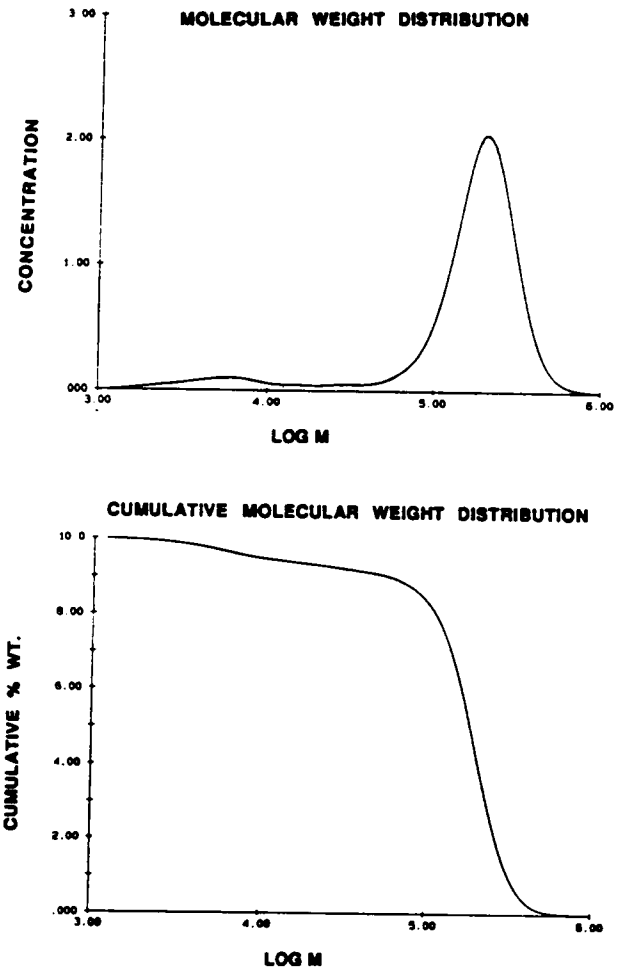

Figure 4.10: Molecular weight distributions used for branching calculations.

experiments were conducted three times so the results were an average of these three runs. It was determined that the residual macromonomer was of the order of 3%, 5% and 6% ± 1% for the three samples which will be designated A, B and C respectively.

Since the amount of reactants and the yield from the synthesis were known and the percentage of the graft polymer and free macromonomer present in the yield had been obtained, it was possible to calculate the amounts of graft polymer and unincorporated macromonomer in the product. The amount of macromonomer grafted was thus the difference between the amount charged and the amount recovered as unincorporated macromonomer. This step is shown in the middle of Figure 4.8. The percentage of the comb polymer comprised of these grafts resulted from ratioing of the amount of incorporated grafts to the amount of PMMA-g-PMMA. The number average molecular weight of the PMMA-g-PMMA was also obtained from the molecular weight distribution. This together with the number average molecular weight of the macromonomer obtained by VPO and the percentage of grafts present in the polymer was used to calculate the number of branches:

$$\text{\# of branches} = \frac{\left\{\%\text{ grafts in PMMA-g-PMMA}\right\}\left\{\overline{M}_n \text{ of PMMA-g-PMMA}\right\}}{\overline{M}_n \text{ of graft}} \qquad [4\text{-}34]$$

The results are given in Table 4.1.

4.4.3. Extraction of Unincorporated Macromonomer

All experiments beyond this section were conducted on the PMMA-g-PMMA's from which the unincorporated grafts had been extracted. Since branching results will be compared between those from stoichiometric experiments and those obtained from other experiments, it was important to make sure that the PMMA-g-PMMA was modified only by the removal of the unincorporated macromonomer during extraction. It would be undesirable to have the distribution of molecular weights shift after this process. The success of the procedure is demonstrated in Figure 4.11 where the concentration chromatogram of the extracted PMMA, in the bold trace, was overlaid on the chromatogram of the unextracted graft polymer, shown in the finer trace. The signals were not normalized so the intensities were different due to the

TABLE 4.1
Number of Branches Calculated Stoichiometrically

Sample	Number of Branches	% Graft/Molecule
A	2	5.4
B	7	24.0
C	13	39.9

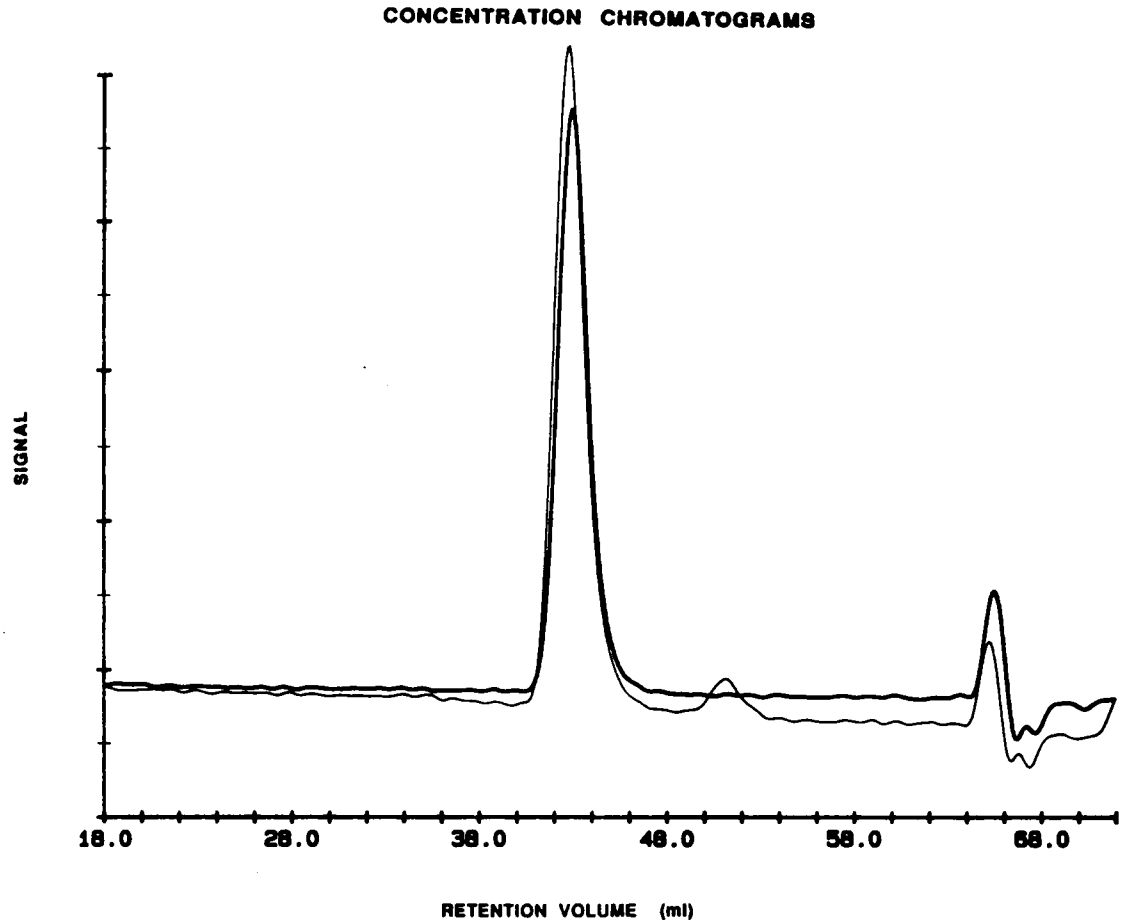

Figure 4.11: Chromatograms of extracted and unextracted PMMA-g-PMMA's.

difference in the concentration of solution injected. However, as evidence that the molecular weight distribution had not been disturbed by the extraction, the peak positions of the chromatograms are essentially identical.

4.4.4. Membrane Osmometry

The results from membrane osmometry are given in Table 4.2. These results are absolute molecular weights and will be used to compare the GPC results with. Considering that the molecular weight aimed for in the synthesis was about 250,000 g/mole, these numbers show that indeed there was very good control of the molecular weight.

4.4.5. Low Angle Laser Light Scattering

The results obtained from static LALLS are shown in Table 4.3. These weight average molecular weights are regarded as the most accurate molecular weights and will be used as the reference values to compare with GPC numbers. Combining results obtained here and those from the MO experiment, the polydispersity of these samples may be calculated and are listed in the table as well. Results indicate a small polydispersity, as expected from the synthetic route used. In addition to molecular weights, LALLS also yielded second virial coefficients, A_2, in THF. The parameter decreases in value as one moves towards polymers with more branching. This is in line with theory which predicted a decrease in polymer-solvent interaction as the density of segments within polymer molecules increased (12).

4.4.6. Specific Refractive Index Increment

Specific refractive index increments have to be measured at the same wavelength and temperature as that at which the LALLS experiment is to be conducted. Because GPC/LALLS was run at 30 to 45°C, dn/dc's for these temperatures were needed. The dn/dc's were measured only at two temperatures, 25°C and 45°C. Based on the linear dn/dc relationship with temperature in the literature, values for intermediate temperatures were interpolated. The dn/dc's obtained at the two temperatures where experiments were conducted is given in Table 4.4. The value of the temperature coefficient was of the magnitude expected -- of the order of 10^{-4} to 10^{-5} ml/g/°C (92).

TABLE 4.2
Results from Membrane Osmometry

Sample	$\overline{M}_n$ (g/mole)
A	281,200
B	215,400
C	248,600

TABLE 4.3
Results from Static LALLS

Sample	$\overline{M}_w$ (g/mole)	$A_2 \times 10^4$ (mole cm^3/g^2)	$\overline{M}_w//\overline{M}_n$
A	294,600	3.135	1.05
B	233,000	2.894	1.08
C	265,600	2.407	1.06

TABLE 4.4
dn/dc's Used in LALLS Calculations

Sample	Temperature (°C)				
	25	30	35	40	45
A	0.0820	0.0835	0.0850	0.0866	0.0881
B	0.0811	0.0808	0.0805	0.0803	0.0800
C	0.0791	0.0794	0.0796	0.0799	0.0801

The optical constant K needed in the LALLS experiment was calculated using these dn/dc's and the solvent refractive indices at the various temperatures. The refractive index for THF used here is the one obtained by interpolation of the data from two other wavelengths. This linear relationship between the refractive index and the square of the inverse of the wavelength at which it was measured has been established and is given by the Couchy formula:

$$n_0 = \zeta_1 + \frac{\zeta_2}{\lambda_0^2} \qquad [4\text{-}36]$$

where n is the refractive index, the ζ's are empirical constants and λ is the wavelength in the experiment (109). The change in refractive index with temperature also had to be considered and the temperature coefficient for this change was taken to be -0.0004/°C (110).

4.4.7. Molecular Weights from Gel Permeation Chromatography

As discussed in the Section 4.2, GPC with dual detectors can be used to obtain absolute molecular weight distributions which are inaccessible by conventional GPC. Results obtained from the GPC/DV and GPC/LALLS shall be evaluated by comparing them with the numbers measured separately on the MO and on the LALLS.

4.4.7.1. GPC/DV

GPC/DV was run in two modes as indicated above. In the first mode, the LALLS was on-line and in the second, the LALLS was removed. The molecular weights at 30°C obtained in these two modes are shown in Table 4.5 together with the $\overline{M}_n$ obtained on the GPC in other experiments where no viscosity detector was used, and whose calibration was based on the molecular weight of linear PMMA standards. These numbers are given in the first column. The results from the first mode of configuration where the LALLS was on-line are indicated by GPC/DV(LALLS). The results obtained for the second series are given in the column GPC/DV. These values from the GPC/DV experiment are averages of two experiments. The numbers are usually reproducible to within 2%. A survey of the numbers and comparison with the results obtained by the absolute molecular weights in Table 4.2 and 4.3 indicate that calibration based on

TABLE 4.5
Molecular Weights from GPC/DV

Sample	GPC		GPC/DV(LALLS)		GPC/DV	
	$\overline{M}_n$	$\overline{M}_w$	$\overline{M}_n$	$\overline{M}_w$	$\overline{M}_n$	$\overline{M}_w$
A	181,000	229,900	214,500	259,600	236,900	283,600
B	152,000	176,300	178,700	205,200	203,000	232,700
C	167,000	195,400	194,600	224,200	214,700	252,300

linear molecular weight standards was ***not*** suitable for ***branched*** polymers. The molecular weights obtained in this way underestimate the true values by 30-35%. For the GPC/DV with the LALLS on-line, the $\overline{M}_n$'s still underestimated the value provided by the membrane osmometer, although there was about a 10% improvement in the accuracy compared to that obtained by calibration with molecular weights. The best results were obtained by doing the experiment without the LALLS connected, in which case the values were underestimated by anywhere from 5-15%. This is discussed below.

Weight average molecular weights gathered from the GPC experiment using calibration with linear PMMA standards deviated from the absolute values by about 25%. An examination of the $\overline{M}_w$'s obtained by GPC/DV show that with the LALLS on-line, the deviations of the measured values from the absolute $\overline{M}_w$'s from static LALLS experiments were about 12-15%. When the LALLS was absent from the detector chain, results were in excellent agreement with static LALLS numbers, with deviations being less than 4%, well within the limits of experimental error. Again, these findings confirm the unsuitability of using linear standards to calibrate a GPC when branched samples are investigated. The larger deviation in results from the absolute values in both the $\overline{M}_n$'s and the $\overline{M}_w$'s when the LALLS was on-line may be due to the problem of dead volume in the connections between the detectors. This was apparently affecting the data at the longer elution volumes thus causing a bigger error in the $\overline{M}_n$'s than in the $\overline{M}_w$'s. Although the software that came with the DV detector provided for dead volume correction, this problem warrants more attention.

The molecular weights determined here using GPC/DV demonstrate the same trends as those seen by Hamielec et al. where it was found that the use of the Viscotek detector led to an underestimation of the $\overline{M}_n$ while giving the correct $\overline{M}_w$. (77). This is surprising; theoretically, the viscosity detector should yield the correct $\overline{M}_n$ and not $\overline{M}_w$ since its operation is based on universal calibration from which $\overline{M}_n$ is the quantity that is obtained directly.

The GPC/DV experiments were also conducted at elevated temperatures. The main purpose of raising the temperature was to investigate the change in hydrodynamic behavior of the polymers with the infusion

of thermal energy into the system. This change should be indicated by the variation in intrinsic viscosities. The molecular weights calculated at these higher temperatures should not deviate from those obtained at lower temperatures. Indeed, the results in Table 4.6 (taken with the LALLS on-line) indicate that this is so as the variation in molecular weights at the different temperatures were within 5%. These calculations provided a check on the proper functioning of the system.

4.4.7.2. GPC/LALLS

Results for the GPC/LALLS experiments are shown in Table 4.7 for all the temperatures at which measurements were conducted. Again, the numbers given in the table are averages of duplicate runs and were reproducible to within 2% between runs. As expected, the molecular weights did not vary significantly with temperature. They were also in excellent agreement with the absolute molecular weights obtained from MO and static LALLS. Compared to the results obtained from GPC/DV, GPC/LALLS appears to be more a more accurate means of obtaining both the $\overline{M}_n$ and the $\overline{M}_w$ of branched polymers.

While the GPC/LALLS afford more accurate molecular weights, its use requires more experiments and more care in conducting the experiments when compared to the GPC/DV. This is because one needs to measure A_2 separately on static LALLS if the system under investigation is one that involves a new polymer-solvent combination for which no literature values are available. One also needs to measure dn/dc accurately at the same temperature and wavelength at which the LALLS experiment is to be conducted. Of the two constants, GPC/LALLS is more sensitive to errors in dn/dc. As a test, different A_2's were entered as constants in the data processing of these data. It was found that a fourfold increase in A_2 resulted in a 3% increase in the $\overline{M}_n$ and a 2% increase in the $\overline{M}_w$. These differences are within the limits of experimental error of the instrument. In fact, results were reproducible to these limits. On the other hand, slight errors in dn/dc could produce large errors in the molecular weights obtained. As an example, when the dn/dc was in error by 15%, the $\overline{M}_w$ obtained was higher by 40%. The fact that the molecular weights shown in Table 4.7 are reproducible shows that the dn/dc's obtained by measurement on the differential refractometer and the

TABLE 4.6
Results from Variable Temperature GPC/DV(LALLS)

$M \times 10^{-5}$ (g/mole)

Sample	30°C		35°C		40°C		45°C	
	$\overline{M}_n$	$\overline{M}_w$	$\overline{M}_n$	$\overline{M}_w$	$\overline{M}_n$	$\overline{M}_w$	$\overline{M}_n$	$\overline{M}_w$
A	2.144	2.596	2.077	2.542	2.072	2.518	2.170	2.658
B	1.786	2.052	1.726	2.007	1.780	2.021	1.902	2.237
C	1.946	2.242	1.837	2.171	1.920	2.160	2.051	2.407

TABLE 4.7
Results from Variable Temperature GPC/LALLS

$M \times 10^{-5}$ (g/mole)

Sample	30°C		35°C		40°C		45°C	
	$\overline{M}_n$	$\overline{M}_w$	$\overline{M}_n$	$\overline{M}_w$	$\overline{M}_n$	$\overline{M}_w$	$\overline{M}_n$	$\overline{M}_w$
A	2.593	2.828	2.694	2.930	2.840	3.031	2.910	3.048
B	2.162	2.287	2.159	2.303	2.196	2.318	2.271	2.438
C	2.544	2.656	2.486	2.637	2.484	2.670	2.460	2.618

interpolation done to obtain the constants for the temperatures at which the dn/dc's were not measured were correct.

4.4.8. Intrinsic Viscosities

Intrinsic viscosities were obtained using capillary viscometers as well as GPC/DV. Here the values obtained from GPC/DV will be compared with the numbers from capillary viscometry which will be considered the true values.

4.4.8.1. Capillary Viscometry

The results of viscometry for the linear PMMA and the PMMA-g-PMMA's at the different temperatures are shown in Table 4.8. These values were obtained by taking the average of the [η] results from the double extrapolation of reduced viscosity and inherent viscosity. In all cases, there was little if any discrepancy in the two values. The information from this table was plotted out in Figure 4.12 where one can clearly see the difference in hydrodynamic behavior of linear and branched PMMA's. The linear PMMA had a higher intrinsic viscosity than any of the three branched polymers, even where some of the PMMA-g-PMMA's actually have higher molecular weights. PMMA-g-PMMA C had slightly higher [η]'s than PMMA-g-PMMA B even if it has about twice the number of branches. This probably was a reflection of the higher molecular weight of C compared to B which counterbalanced the effects of higher coil density in C.

The temperature coefficients of the intrinsic viscosities are given in Table 4.9. Results show how the intrinsic viscosities, hence hydrodynamic volumes, shift as temperature was increased in relatively small increments. It may be gleaned that for the more highly branched PMMA's the biggest change in conformation occurred when the temperature was increased from 25 to 30°C. For PMMA-g-PMMA A, this transformation did not occur until 40°C while for the linear PMMA, the biggest jump was from 30 to 35°C.

In order to more closely examine the effect of temperature on changes in hydrodynamic behavior brought about by the introduction of branching, the hydrodynamic volumes of the polymers were

TABLE 4.8
Intrinsic Viscosity Results

	[η] (dl/g)				
Sample	25°C	30°C	35°C	40°C	45°C
Linear	0.711	0.707	0.730	0.732	0.737
A	0.613	0.615	0.631	0.628	0.660
B	0.514	0.543	0.532	0.538	0.565
C	0.537	0.575	0.573	0.579	0.586

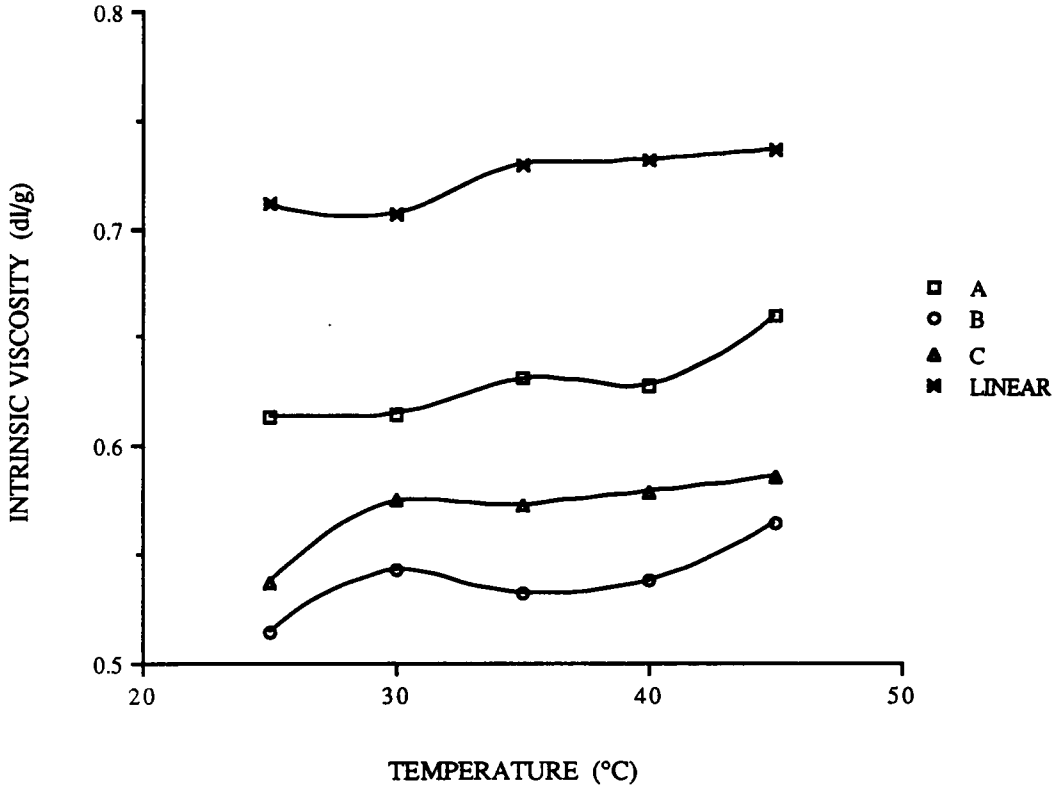

Figure 4.12: Temperature dependence of intrinsic viscosities for linear and branched PMMA's.

TABLE 4.9
Temperature Coefficients of Intrinsic Viscosity

	$d\ln[\eta]/dT \times 10^3$			
Sample	25°C-30°C	30°C-35°C	35°C-40°C	40°C-45°C
Linear	-1.13	6.4	0.40	1.0
A	0.66	5.1	-0.76	9.9
B	10.9	-4.1	2.3	9.7
C	13.9	-0.84	2.2	2.4

independently determined at the temperatures where they had the smallest [η]'s and at the temperatures at which these viscosities were at the maximum. The results, together with the temperatures at which these calculations were done are shown in Table 4.10. It is interesting to note that the maximum changes in hydrodynamic volumes were significantly higher in the branched systems compared to those of the linear PMMA. With the addition of two branches, the change in hydrodynamic volume almost doubled in a 20° span of temperature. These results are in agreement with theories where it has been proposed that an increase in branching encourages greater polymer/solvent interaction -- thus causing greater expansion of the molecule -- which is in turn is reflected in bigger hydrodynamic volumes (1,16).

4.4.8.2. GPC/DV

Intrinsic viscosities may be determined by the differential viscosity detector. Below are results obtained from such calculations and comments on their agreement with values obtained with the capillary viscometer.

Initial GPC based calculations of the intrinsic viscosities are given in Table 4.11. The numbers were consistently higher than those obtained with glass capillaries, whether the LALLS was on-line or not. A graph that illustrates this deviation is typical of the results for all three graft polymers and is shown in Figure 4.13. On the average, the results differed by 10% from the values obtained using capillary viscometry.

The same data may be processed to obtain different results. One of the parameters in the DV software may be changed to obtain more accurate [η]'s. This is the DPT (differential pressure transducer) sensitivity. If the transducer were properly calibrated, the factor should be equal to 1.000, which is what was used to calculate the viscosities in Table 4.11. As a check of the accuracy of this parameter, the results obtained for the linear PMMA, which should coincide with those obtained by glass capillaries, were compared. It was found that at 30°C, there was about a 10% discrepancy between the two values, the ones from the GPC being higher. To correct for this error, the DPT sensitivity was changed by taking the ratio of the [η] from the GPC and the one obtained manually. This factor was used as the DPT sensitivity and was calculated for

TABLE 4.10
Changes in Hydrodynamic Volume with Temperature

	$[\eta]M \times 10^{-5}$ (dl/mole)			
Sample	Minimum	Maximum	% Change	Temperature (°C)
Linear	1.69	1.76	4.2	30-45
A	1.72	1.86	7.7	25-45
B	1.11	1.22	9.9	25-45
C	1.33	1.46	9.1	25-45

TABLE 4.11
Uncorrected [η] Results from GPC/DV(LALLS)

	[η] (dl/g)			
Sample	30°C	35°C	40°C	45°C
Linear	0.774	0.768	0.759	0.766
A	0.680	0.685	0.698	0.726
B	0.579	0.587	0.589	0.606
C	0.622	0.630	0.632	0.645

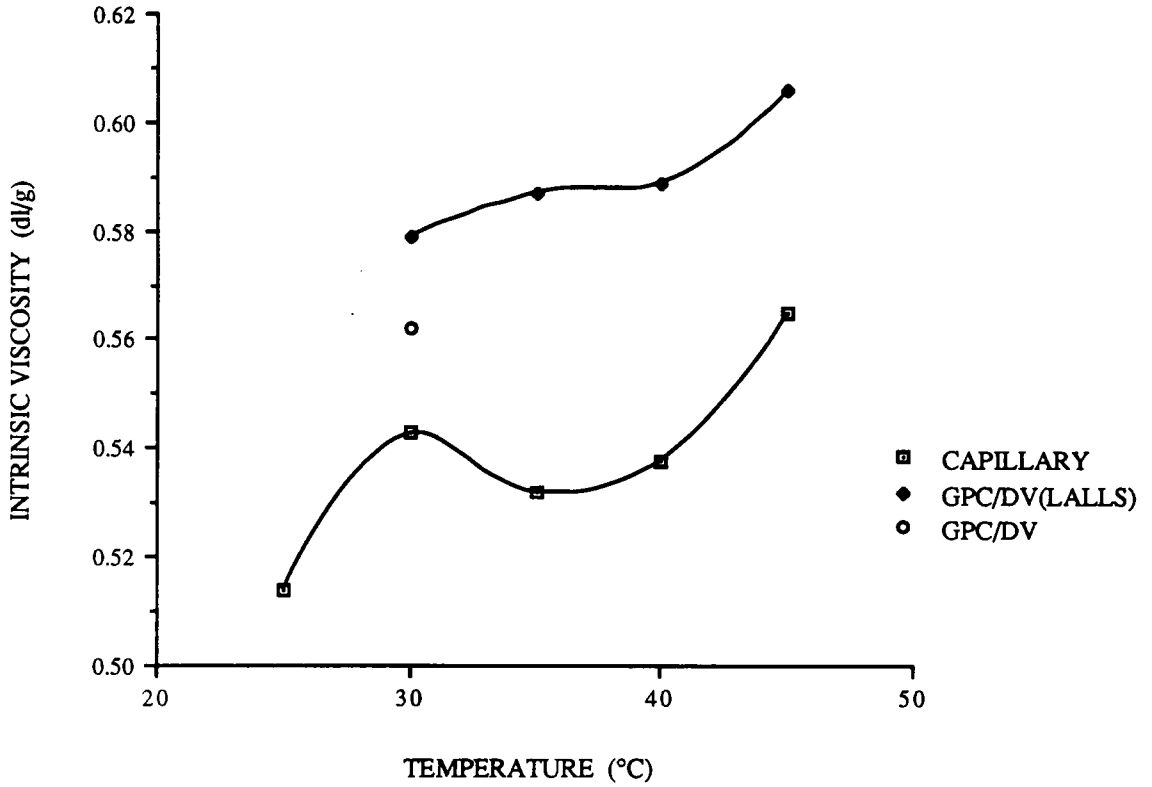

Figure 4.13: Uncorrected intrinsic viscosities from GPC/DV.

all the temperatures at which the GPC experiments were run. The values obtained are given in Table 4.12 and show slight changes as a function of temperature. The calibration curves as well as the data from from all the samples were recalculated to reflect this change. The new results which were calculated with the corrected DPT sensitivity are now shown in Table 4.13. For the linear PMMA's, this change resulted in a five to tenfold decrease in the deviation from the "true" value indicating that with a properly calibrated DPT, obtaining accurate [η]'s via GPC/DV presents no problem. For the branched systems, the values from the GPC/DV are now much closer to those from capillary viscometry, with differences of only 3% on the average. Graphs showing the comparison of results from the GPC/DV and capillary viscometry are shown in Figure 4.14 for the linear PMMA and in Figure 4.15 for PMMA-g-PMMA B. The trends in Figure 4.15 are representative of those seen for all three branched systems. For reasons that are not clear at this point, the deviations at 40°C for all three branched PMMA's were the greatest.

4.4.9. Universal Calibration

Considering the underestimation of molecular weights obtained on the GPC/DV through universal calibration, some investigators have suggested that this calibration breaks down for some branched systems. This assertion was checked using the accumulated data. The intrinsic viscosities obtained from capillary viscometry and the number average molecular weight obtained by MO were multiplied to get hydrodynamic volume which is the ordinate of the universal calibration curve. The abscissa of the calibration curve is retention volume. This was obtained for the graft PMMA's by picking out the retention volume at the peak of the GPC chromatogram. The results are shown in Figure 4.16 as well as the universal calibration curve that was obtained at the same temperature. Excellent agreement is shown, ***especially considering that the plot was made with data points from three independent sources.*** This shows that the universal calibration does work for these branched systems, a major finding. The fact that the molecular weights obtained were not as accurate as they should be may be due to a limitation in hardware sensitivity rather than a shortcoming in the theory.

TABLE 4.12
DPT Sensitivity Dependence on Temperature

DPT Sensitivity (mV/Pa)	Temperature (°C)
1.089	30
1.063	35
1.035	40
1.040	45

TABLE 4.13
Corrected [η] Results from GPC/DV(LALLS)

	[η] (dl/g)			
Sample	30°C	35°C	40°C	45°C
Linear	0.698	0.720	0.734	0.733
A	0.614	0.644	0.675	0.652
B	0.530	0.552	0.566	0.562
C	0.570	0.588	0.610	0.608

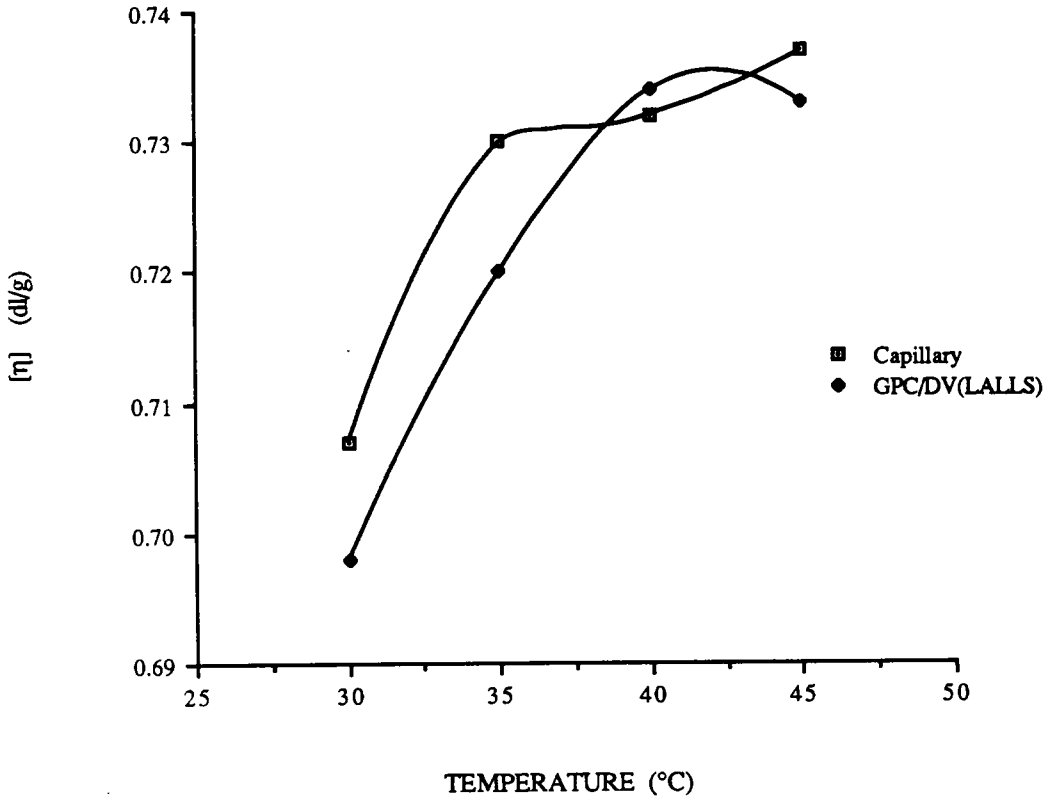

Figure 4.14: Comparison of intrinsic viscosities from capillary viscometry and GPC/DV for linear PMMA.

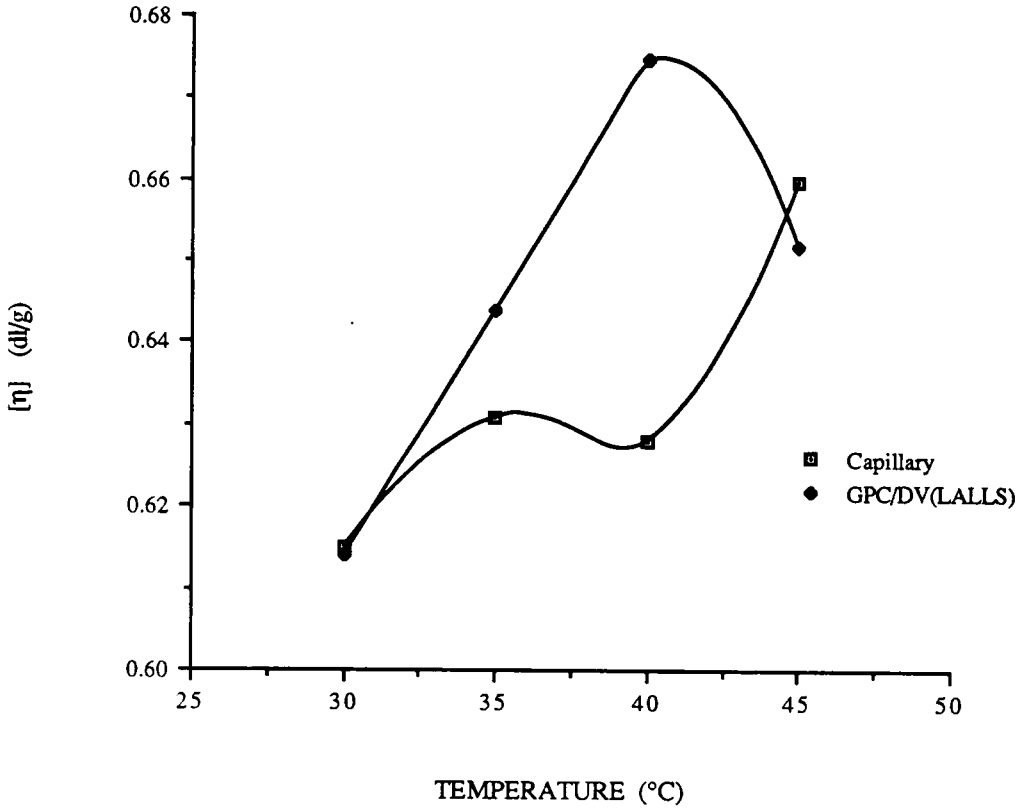

Figure 4.15: Corrected intrinsic viscosities for PMMA-g-PMMA B from GPC/DV.

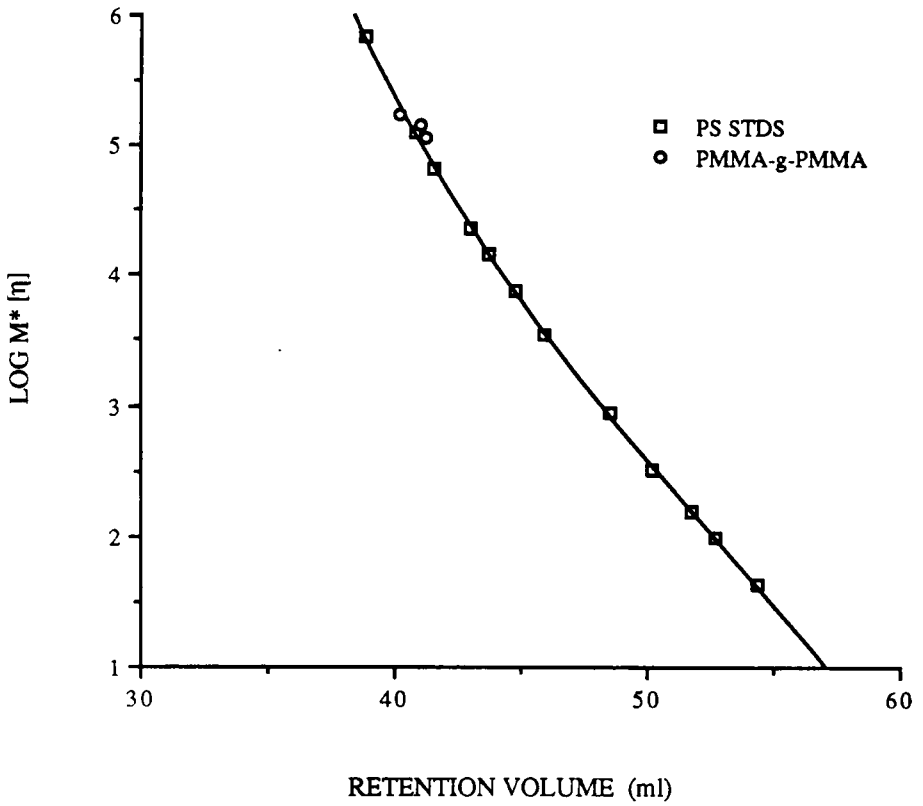

Figure 4.16: Overlay of universal calibration curve from GPC/DV and data points obtained independently.

4.4.10. Mark-Houwink Constants

The Mark-Houwink equation given in Equation [4-28] can be rewritten as:

$$\log [\eta] = \log k + a \log M \qquad [4\text{-}37]$$

If one can fractionate a polymer into monodisperse portions and obtain the intrinsic viscosity and molecular weight of each of these fractions, then it is possible to get the Mark-Houwink constants by plotting the log of $[\eta]$ against the log of the molecular weight for each fraction. The intercept of such a plot is log k and the slope is a, With the GPC/DV system, the GPC was used to fractionate the whole polymers and the DRI and DV detector together provided the information needed to make the Mark-Houwink plot. The results obtained for the three graft PMMA's are given in Table 4.14 for the four temperatures at which experiments were conducted. The Mark-Houwink constant a is a reflection of the chain conformation in solution and the fluctuations with temperature are an indication of the slight changes the polymer chains underwent as the temperature of their environment was changed. Values of a that are about 0.5 are indicative of random coils (24). These constants were necessary for the determination of branching in the PMMA-g-PMMA's by GPC.

4.4.11. Unperturbed Chain Dimensions

The ability of the GPC/DV system to fractionate the polymer and provide the intrinsic viscosity and molecular weight of each fraction was used in order to get unperturbed chain dimensions at conditions away from the Θ condition. The Stockmayer-Fixman equation given in Section 2 of this chapter as equation [4-25] will be used due to its simplicity. The value of Φ used was 3.7×10^{24} for $[\eta]$'s in terms of ml/g. This value was arrived at by multiplying the Φ given by Yamakawa (12) by $6^{3/2}$ so that the unperturbed dimension obtained is radius of gyration, which is more meaningful for the branched polymers here than end-to-end distance. Flory has indicated that the constant K in the Stockmayer-Fixman equation may be applied to non-linear polymers if couched in terms of radius of gyration instead of unperturbed end-to-end distance (7).

TABLE 4.14
Mark-Houwink Constants from GPC/DV(LALLS)

Sample	30°C		35°C		40°C		45°C	
	-log k	a	-log k	a	-log k	a	-log k	a
Linear	0.300	1.742	0.352	2.012	0.370	2.205	0.397	2.244
A	0.579	3.311	0.516	2.954	0.600	3.380	0.620	3.505
B	0.621	3.546	0.571	3.267	0.650	3.686	0.611	3.464
C	0.574	3.287	0.556	3.182	0.639	3.606	0.611	3.429

Using the calculated data for intrinsic viscosities and molecular weights from GPC/DV at four temperatures, the ratio of intrinsic viscosity to the square root of molecular weight was plotted against the square root of molecular weight. The Stockmayer-Fixman equation predicts that a straight line will result with an intercept equal to K as defined by equation [4-24]. To convert equation [4.24] from one based on the unperturbed end-to-end distance to one that is a function of radius of gyration, the following relationship was used:

$$K = 6^{3/2}\Phi\left(\frac{\overline{r_g^2}}{M}\right)^{3/2} \qquad [4\text{-}38]$$

where M ideally should be the absolute weight average molecular weight of the polymer.

When every other data point shown in the results of the GPC/DV was used, a graph that was typical of the results appears as in Figure 4.17. It contains a linear region at the lower molecular weight portion and deviates from linearity at the higher molecular weights. This behavior has been observed by others in similar measurements done with good solvents. In such circumstances, the unperturbed dimensions are overestimated (12,24). This being so, only data in the linear region of the graph were used in the determination of the unperturbed radius of gyration. This was done by taking about a dozen points at the lower portion of the molecular weight distribution for the calculation where the line generated was definitely linear. An example of results obtained when the calculations were done in this manner is shown in Figure 4.18. The numerical results are given in Table 4.15. The calculations were done for duplicate runs on the GPC. No attempt was made to take average values which would obscure the fact that the results were not very reproducible. In addition to the lack of reproducibility, there are three blank spaces in the table where negative values were obtained. However, the scale of the results are in the right order of magnitude and indicate that this technique may be viable but fails due to the insensitivity of the detectors used at the low molecular weight end of the distribution where the data was needed. Perhaps better reproducibility and

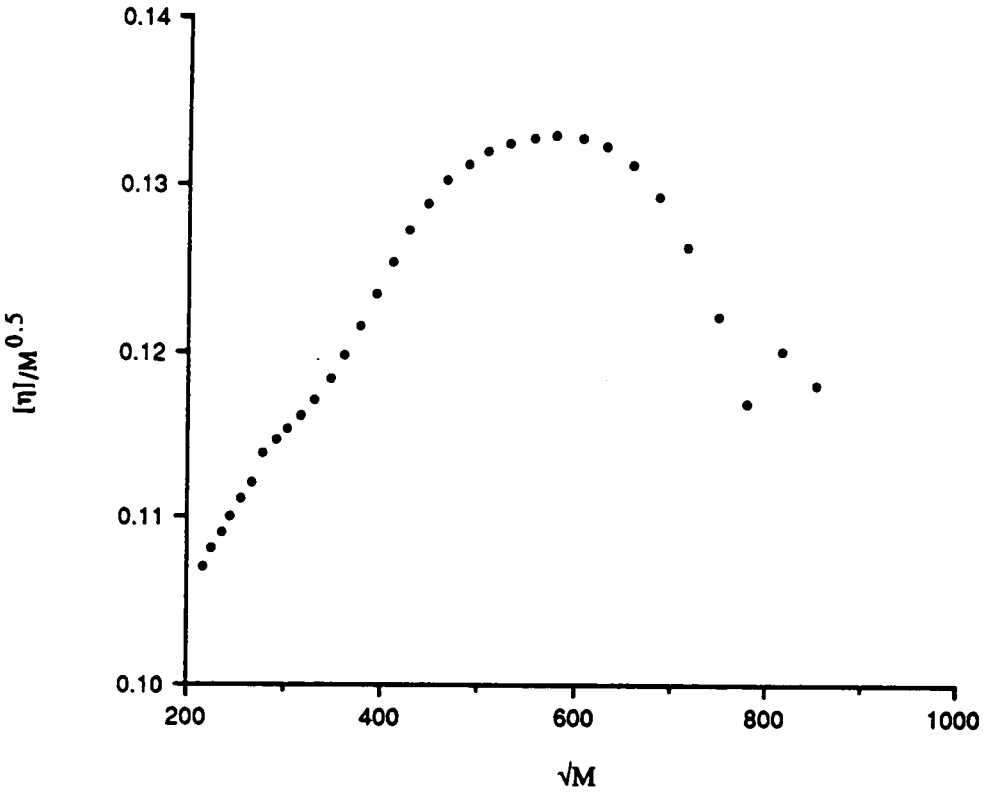

Figure 4.17: Stockmayer-Fixman plot obtained from GPC/DV.

TABLE 4.15

$\langle r_g^2 \rangle$ from Stockmayer-Fixman Plot

	$\langle r_g^2 \rangle \times 10^{12}$ cm^2			
Sample	30°C	35°C	40°C	45°C
A	2.41	1.62	1.51	0.65
	1.67	-	1.88	0.42
B	1.41	0.49	0.27	1.87
	2.01	1.58	1.13	1.77
C	1.65	0.51	-	1.32
	2.30	1.20	-	0.56

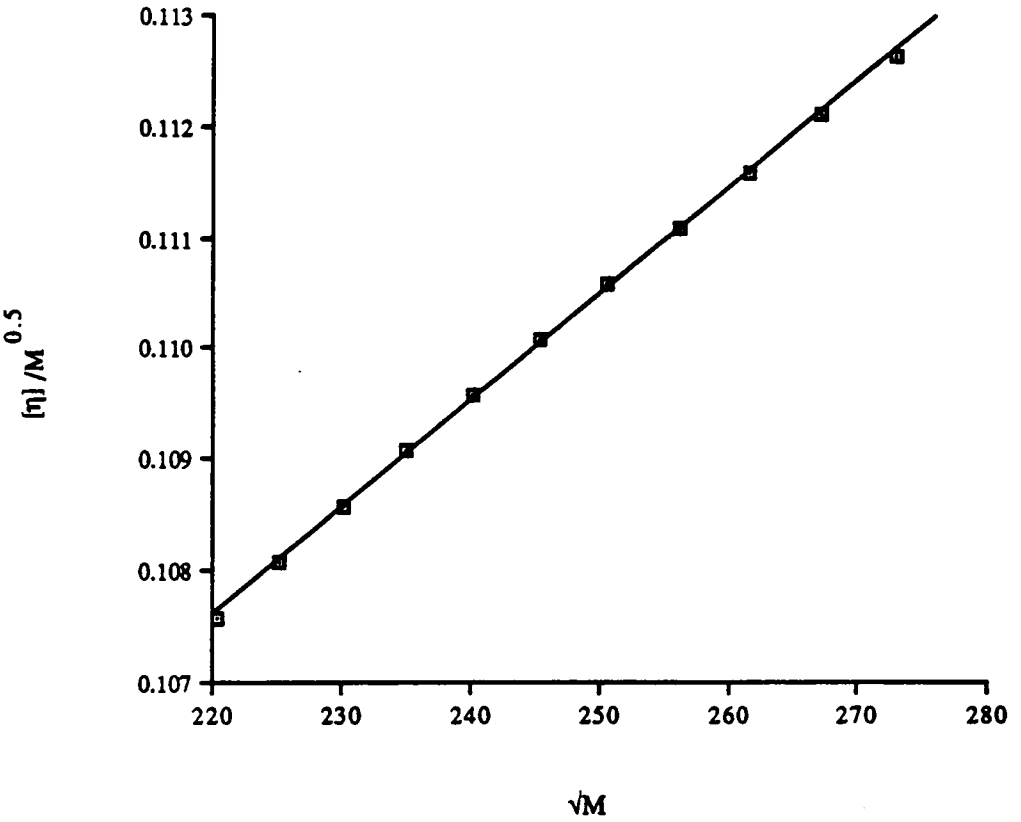

Figure 4.18: Portion of Stockmayer-Fixman plot used in unperturbed dimension calculation.

accuracy can be obtained if the signal at this end of the distribution could be selectively enhanced electronically as was done by Hamielec et al. for GPC/LALLS (19).

Because the results here do not appear to be reliable under the conditions where they were obtained, an attempt to calculate their temperature coefficients was not made. Had the results been more reasonable, it would have been possible to combine results here with those in Table 4.9 for use in Equation [4-26] to calculate the temperature coefficients of the expansion factors.

4.4.12. Branching Factors

The branching factor g^x may be calculated from the intrinsic viscosity experiments done in capillary viscometers, the GPC/DV experiments and indirectly through the GPC/LALLS experiments. The table of g values for a given number of grafts which are randomly placed along the backbone is generated in Table 4.16 by putting p in terms of f and m and using f=3. Different m's were substituted into the equation and the g calculated. This equation was chosen because although the lengths of the grafts of the samples used here were fairly uniform, their placement on the backbone was not, therefore, the subchain lengths as defined in Section 2 of this chapter were not uniform. Also shown in the same table are the g factors calculated with the most commonly used x's.

4.4.12.1. Capillary Viscometry

The g^x factors based on results from capillary viscometry for the three graft PMMA's at the different temperatures are given in Table 4.17. These were generated by taking the ratio of the intrinsic viscosity of the branched PMMA's to that of the linear PMMA standard. The data used are the ones shown in Table 4.8. Since the number of branches remains constant even with a change in temperature, it was logical to take the average values the g factors at all the temperatures and to use the average value to check for branching. The small spread in the numbers is shown in the column of standard deviation provides support for this argument.

To determine the average number of branches the closest match to a g factor in Table 4.16 was used. For PMMA-g-PMMA A, the closest match is in the column with x = 0.7 and number of branches of about

TABLE 4.16
g Factors Calculated for Randomly Branched Combs

m	$g^{0.5}$	$g^{0.7}$	$g^{0.8}$	g	$g^{1.3}$	$g^{1.5}$
2	0.910	0.877	0.861	0.829	0.784	0.755
3	0.880	0.836	0.815	0.774	0.717	0.681
4	0.856	0.805	0.780	0.733	0.668	0.628
5	0.838	0.781	0.754	0.703	0.632	0.589
6	0.824	0.763	0.734	0.679	0.605	0.560
7	0.812	0.748	0.717	0.660	0.583	0.536
8	0.803	0.736	0.704	0.645	0.565	0.518
9	0.795	0.725	0.693	0.632	0.551	0.502
10	0.789	0.717	0.684	0.622	0.539	0.491
11	0.783	0.710	0.676	0.613	0.529	0.480
12	0.778	0.703	0.669	0.605	0.520	0.471
13	0.773	0.698	0.663	0.598	0.513	0.462
14	0.769	0.693	0.657	0.592	0.506	0.455
15	0.766	0.689	0.653	0.587	0.500	0.450
20	0.753	0.672	0.635	0.567	0.478	0.427
25	0.745	0.662	0.624	0.555	0.465	0.413

TABLE 4.17
$g^{X'}$s from Capillary Viscometry

Sample	25°C	30°C	35°C	40°C	45°C	Average
A	0.862	0.870	0.864	0.858	0.896	0.870
B	0.723	0.768	0.729	0.735	0.767	0.744
C	0.755	0.813	0.785	0.791	0.795	0.788

2. This is in excellent agreement with the stoichiometrically determined number. In the column where x = 0.5, there is also a good match at between three and four branches. The exponent x = 0.5 is usually recommended for stars, and 0.7 for combs, although it has been suggested that 0.5 may be appropriate for low degrees of branching (1,5). It appears here that x = 0.7 should be the value chosen. For PMMA-g-PMMA B, there are two possible matches as well. These can be found at seven branches when x = 0.7 is used and at 25 branches when x = 0.5 is chosen. For this degree of branching, x = 0.5 is not usually recommended. In addition, with x = 0.7, the level of branching also agrees with the stoichiometrically calculated value. The best match for PMMA-g-PMMA C is ten branches as shown under the x = 0.5 column. Although this value is close to what was calculated based on stoichiometry, theoretically the 0.5 exponent is inconsistent.

The almost arbitrary way by which the number of branches is commonly determined may be a reflection of the uncertainty in the method. In the literature, there is no agreement as to which exponent has to be used with certain polymer architectures. Perhaps a study using g (with no exponent) from the ratio of radii of gyration of branched and linear polymer should be used to establish the rules for the use of exponents to obtain branching through intrinsic viscosities, which is more accessible experimentally. On the other hand, the difficulty encountered here may also be an indication of the sensitivity of the method in the sense that the molecular weights of the linear and branched analogs should be closer than they were. When they are not exactly right, the g^x could be underestimated or overestimated just enough so that the results are ambiguous as was found.

4.4.12.2. GPC/DV

GPC/DV can be used to provide not only the average number of branches in graft polymers by taking the intrinsic viscosities of linear and branched polymers. One can take advantage of the fractionation that the GPC performed to compare intrinsic viscosities of the branched and linear analogs at the same elution volume. This then leads to a representation of the branching frequency throughout the molecular weight distribution of the graft polymers. These results will be discussed below.

4.4.12.2.1. Average Branching Factors

As already given above one of the results obtained from GPC/DV was the intrinsic viscosity. This being so, the average g factor may also be calculated from these findings to give the average number of branches present in the graft polymers by trying to find the best match with the numbers tabulated in Table 4.16. The g^x quantities for the three graft PMMA's are given in Table 4.18 for data taken at 30°C. An average g^x taken across the temperature range utilized was obtained and tabulated in the last column of the table. For PMMA-g-PMMA A the closest match is found at between two and three branches with x = 0.5. For PMMA-g-PMMA B, the nearest value was found under the column of x = 0.7 with six branches. These findings coincide with those obtained from capillary viscometry. Again, the results for PMMA-g-PMMA C were nebulous.

4.4.12.2.2. Branching Distribution

The branching distribution will be obtained following a suggestion of Jordan and McConnell. Using GPC data, they caution that while the g factor is the definition based on taking the ratio of intrinsic viscosities of a linear and branched polymer of the same chemical composition and molecular weight, GPC does not separate by molecular weight. One is actually looking at the intrinsic viscosities of the two polymers at the same elution volume whose ratio they defined as g_v. The conversion of g_v to g^x simply involves raising g_v to one plus the Mark-Houwink constant "a" of the linear polymer (78)

These results are shown in Tables 4.19-4.24 for the duplicate runs on each of the three graft polymers at 30°C. The elution volume at which the calculations were commenced was dictated by the match in elution volume found in the results from the linear PMMA. With the elution volumes were rounded off to the second decimal point a difference of ±0.02 was considered to be equal elution volumes. The data start out at about 40.26 ml. A check on the sample chromatogram shown in Figure 4.19 reveals that this is in the region on the high molecular weight end where the intensities of both the viscosity and concentration signals are fairly intense. The calculations were stopped at a comparably lower intensity on the lower molecular weight end. The fact that the whole chromatogram was not used does not detract from the

TABLE 4.18
g^X's from GPC/DV(LALLS)

Sample	30°C	35°C	40°C	45°C	Average
A	0.880	0.894	0.920	0.889	0.896
B	0.759	0.767	0.771	0.767	0.766
C	0.817	0.817	0.831	0.829	0.824

TABLE 4.19
g^x Distribution of PMMA-g-PMMA A from GPC/DV(LALLS)

$V_{el\ (br)}$ (ml)	[η] (dl/g)	log M	$V_{el\ (lin)}$ (ml)	[η] (dl/g)	$g^{1.69}$
40.26	0.688	5.431	40.25	1.143	0.424
40.34	0.672	5.412	40.36	1.116	0.425
40.68	0.608	5.338	40.68	1.037	0.406
41.02	0.545	5.263	41.00	0.965	0.381
41.10	0.530	5.245	41.11	0.941	0.379
41.35	0.486	5.189	41.33	0.897	0.355
41.44	0.472	5.170	41.44	0.875	0.352
41.52	0.458	5.152	41.54	0.854	0.349
41.77	0.421	5.096	41.76	0.814	0.328
41.86	0.409	5.077	41.87	0.794	0.326
42.19	0.369	5.002	42.19	0.739	0.309
42.28	0.360	4.984	42.30	0.721	0.309
42.53	0.334	4.928	42.52	0.687	0.296
42.61	0.326	4.909	42.62	0.67021	0.296
42.86	0.300	4.853	42.84	0.638	0.279
42.95	0.292	4.835	42.95	0.623	0.278
43.28	0.263	4.760	43.27	0.579	0.264
43.37	0.256	4.742	43.38	0.565	0.263
43.62	0.237	4.686	43.60	0.539	0.250
43.70	0.231	4.667	43.70	0.526	0.249
43.79	0.225	4.649	43.81	0.514	0.248

TABLE 4.20
g^x Distribution of PMMA-g-PMMA A from GPC/DV(LALLS)

$V_{el\ (br)}$ (ml)	[η] (dl/g)	log M	$V_{el\ (lin)}$ (ml)	[η] (dl/g)	$g^{1.69}$
40.26	0.688	5.430	40.25	1.143	0.424
40.34	0.671	5.412	40.36	1.116	0.424
40.68	0.608	5.339	40.68	1.037	0.405
41.02	0.546	5.266	41.00	0.965	0.382
41.10	0.530	5.248	41.11	0.941	0.379
41.35	0.484	5.194	41.33	0.897	0.353
41.44	0.469	5.175	41.44	0.875	0.348
41.52	0.454	5.175	41.54	0.854	0.343
41.77	0.411	5.102	41.76	0.814	0.315
41.86	0.397	5.084	41.87	0.794	0.310
42.10	0.362	5.030	42.08	0.757	0.288
42.19	0.352	5.011	42.19	0.739	0.285
42.28	0.342	4.993	42.30	0.721	0.283
42.53	0.313	4.939	42.52	0.687	0.265
42.61	0.303	4.920	42.62	0.670	0.262
42.86	0.275	4.866	42.84	0.638	0.240
42.95	0.266	4.847	42.95	0.623	0.237
43.28	0.235	4.775	43.27	0.579	0.218
43.37	0.228	4.756	43.38	0.565	0.215
43.62	0.208	4.702	43.60	0.539	0.200
43.70	0.201	4.683	43.70	0.526	0.197
43.79	0.195	4.663	43.81	0.513	0.195

TABLE 4.21
g^x Distribution of PMMA-g-PMMA B from GPC/DV(LALLS)

$V_{el\ (br)}$ (ml)	[η] (dl/g)	log M	$V_{el\ (lin)}$ (ml)	[η] (dl/g)	$g^{1.69}$
40.26	0.677	5.421	40.25	1.14	0.413
40.34	0.663	5.409	40.36	1.116	0.415
40.68	0.604	5.338	40.68	1.037	0.401
41.02	0.546	5.268	41.00	0.965	0.383
41.10	0.532	5.250	41.11	0.941	0.381
41.35	0.491	5.197	41.33	0.897	0.361
41.44	0.478	5.180	41.44	0.875	0.359
41.52	0.464	5.162	41.54	0.854	0.357
41.77	0.426	5.109	41.76	0.814	0.335
41.86	0.414	5.091	41.87	0.794	0.332
42.19	0.367	5.021	42.19	0.739	0.307
42.28	0.356	5.003	42.30	0.721	0.304
42.53	0.326	4.950	42.52	0.687	0.284
42.61	0.317	4.933	42.62	0.670	0.282
42.86	0.293	4.880	42.84	0.638	0.268
42.95	0.285	4.862	42.95	0.623	0.267
43.37	0.245	4.774	43.38	0.565	0.244
43.62	0.225	4.721	43.60	0.539	0.228
43.70	0.219	4.703	43.70	0.526	0.227
43.79	0.212	4.686	43.81	0.513	0.225
44.04	0.195	4.633	44.03	0.489	0.211
44.12	0.189	4.615	44.14	0.477	0.209

TABLE 4.22
g^x Distribution of PMMA-g-PMMA B from GPC/DV(LALLS)

$V_{el\ (br)}$ (ml)	[η] (dl/g)	log M	$V_{el\ (lin)}$ (ml)	[η] (dl/g)	$g^{1.69}$
40.26	0.665	5.434	40.25	1.143	0.400
40.34	0.649	5.416	40.36	1.116	0.400
40.68	0.587	5.346	40.68	1.037	0.382
41.10	0.518	5.259	41.11	0.941	0.364
41.35	0.479	5.207	41.33	0.897	0.346
41.44	0.466	5.189	41.436	0.875	0.345
41.52	0.454	5.172	41.54	0.854	0.343
41.77	0.417	5.120	41.76	0.814	0.323
41.86	0.405	5.102	41.87	0.794	0.321
42.19	0.362	5.032	42.19	0.739	0.299
42.28	0.352	5.015	42.30	0.721	0.298
42.53	0.330	4.963	42.52	0.687	0.289
42.61	0.324	4.945	42.62	0.670	0.292
42.86	0.308	4.893	42.84	0.638	0.292
42.95	0.303	4.875	42.95	0.623	0.295
43.28	0.271	4.806	43.27	0.579	0.277
43.37	0.265	4.788	43.38	0.565	0.278
43.70	0.243	4.718	43.704	0.526	0.271
44.04	0.222	4.648	44.03	0.489	0.263
44.12	0.217	4.631	44.14	0.477	0.264

TABLE 4.23
g^x Distribution of PMMA-g-PMMA C from GPC/DV(LALLS)

$V_{el\ (br)}$ (ml)	[η] (dl/g)	log M	$V_{el\ (lin)}$ (ml)	[η] (dl/g)	$g^{1.69}$
40.26	0.688	5.425	40.25	1.143	0.424
40.34	0.673	5.407	40.36	1.116	0.425
40.68	0.611	5.334	40.68	1.037	0.409
41.02	0.553	5.261	41.00	0.965	0.391
41.10	0.539	5.243	41.11	0.941	0.390
41.35	0.498	5.188	41.33	0.897	0.370
41.44	0.484	5.170	41.44	0.875	0.367
41.52	0.470	5.152	41.54	0.854	0.365
41.77	0.431	5.097	41.76	0.814	0.341
41.86	0.418	5.078	41.87	0.794	0.338
42.19	0.370	5.005	42.19	0.739	0.311
42.28	0.359	4.987	42.30	0.721	0.308
42.53	0.330	4.932	42.52	0.687	0.289
42.61	0.321	4.914	42.62	0.670	0.288
42.86	0.296	4.859	42.84	0.639	0.272
42.95	0.284	4.841	42.95	0.623	0.265
43.28	0.252	4.768	43.27	0.579	0.245
43.37	0.245	4.750	43.38	0.565	0.243
43.62	0.224	4.695	43.60	0.539	0.244
43.70	0.217	4.677	43.70	0.526	0.224
43.79	0.211	4.658	43.81	0.513	0.222

TABLE 4.24
g^x Distribution of PMMA-g-PMMA C from GPC/DV(LALLS)

$V_{el\ (br)}$ (ml)	[η] (dl/g)	log M	$V_{el\ (lin)}$ (ml)	[η] (dl/g)	$g^{1.69}$
40.26	0.674	5.434	40.25	1.143	0.410
40.34	0.659	5.415	40.36	1.116	0.411
40.68	0.598	5.342	40.68	1.037	0.395
41.02	0.540	5.269	41.00	0.965	0.375
41.10	0.526	5.250	41.11	0.941	0.373
41.35	0.485	5.195	41.33	0.897	0.354
41.44	0.473	5.177	41.44	0.875	0.353
41.52	0.461	5.159	41.54	0.854	0.352
41.77	0.426	5.104	41.77	0.814	0.335
41.86	0.415	5.086	41.87	0.794	0.334
42.19	0.375	5.012	42.19	0.739	0.318
42.28	0.366	4.994	42.30	0.721	0.318
42.53	0.342	4.939	42.52	0.687	0..308
42.61	0.336	4.921	42.62	0.670	0.311
42.86	0.322	4.866	42.84	0.638	0.314
42.95	0.303	4.847	42.95	0.623	0.296
43.28	0.275	4.774	43.27	0.579	0.284
43.37	0.269	4.756	43.38	0.565	0.284
43.62	0.250	4.701	43.60	0.539	0.273
43.70	0.244	4.682	43.70	0.526	0.273
43.79	0.238	4.664	43.81	0.513	0.273

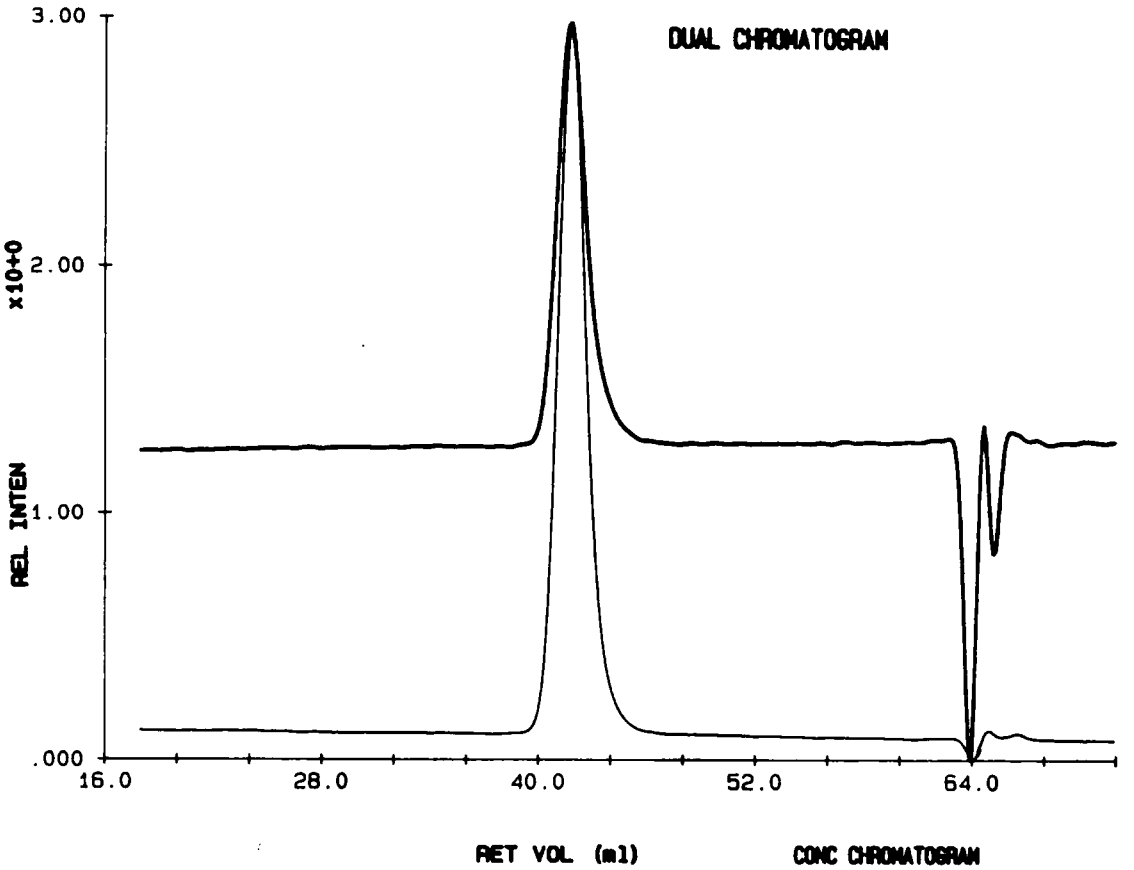

Figure 4.19: GPC chromatogram of PMMA-g-PMMA A.

purpose of determining the branching distribution which was to give an idea of how the frequency of branching changed as the molecular weight varied across the distribution..

The distributions of branching for the three polymers are shown in Figures 4.20 to 4.22 in which each graph shows duplicate experiments. It is clear that as the molecular weight increased across the distribution, branching frequency decreased. This observation stresses the fact that the number of branches calculated using the intrinsic viscosities were the average values for the particular molecular weight distribution. The gaps in the plot are due to the fact that matches in the elution volumes of the linear and branched polymers were not always found. However, the trend is still clear.

4.5. SUMMARY AND CONCLUSIONS

In summary, it was shown that GPC/DV is an appropriate way to determine absolute molecular weights and molecular weight distributions for branched systems. The universal calibration approach was shown to be valid for graft homopolymers containing up to 40% long chain branching. However, the multidetector instrumentation appears to require more hardware and software refinements to eliminate errors caused by dead volume between detectors and axial dispersion both of which led to the underestimation of molecular weights. With these problems eliminated, GPC/DV offers a favorable alternative to the more tedious and error prone GPC/LALLS.

The other branching parameters such as the g factor and branching frequency may be obtained directly from data provided by GPC/DV. The accuracy of these characteristics also depend on the software and hardware improvements. Moreover, the area of branching theory can bear more exploration to yield more definite foundations for experimental findings.

The intrinsic viscosities obtained at each increment of the elution volume may also be used to calculate unperturbed chain dimensions with the accuracy dependent on the sensitivity of both the DRI and DV detectors.

The variable temperature capability of the GPC was taken advantage of to yield information on the temperature coefficient of intrinsic viscosities. With some refinement, it may be possible to obtain the

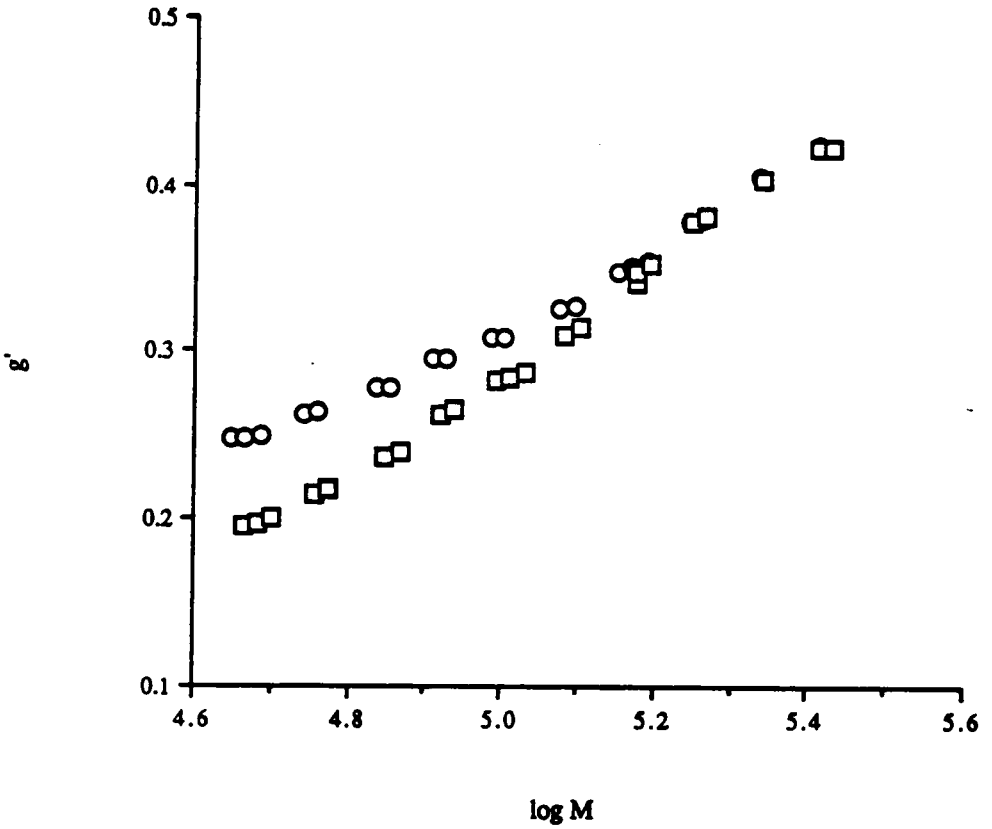

Figure 4.20: Branching distribution for PMMA-g-PMMA A from GPC/DV.

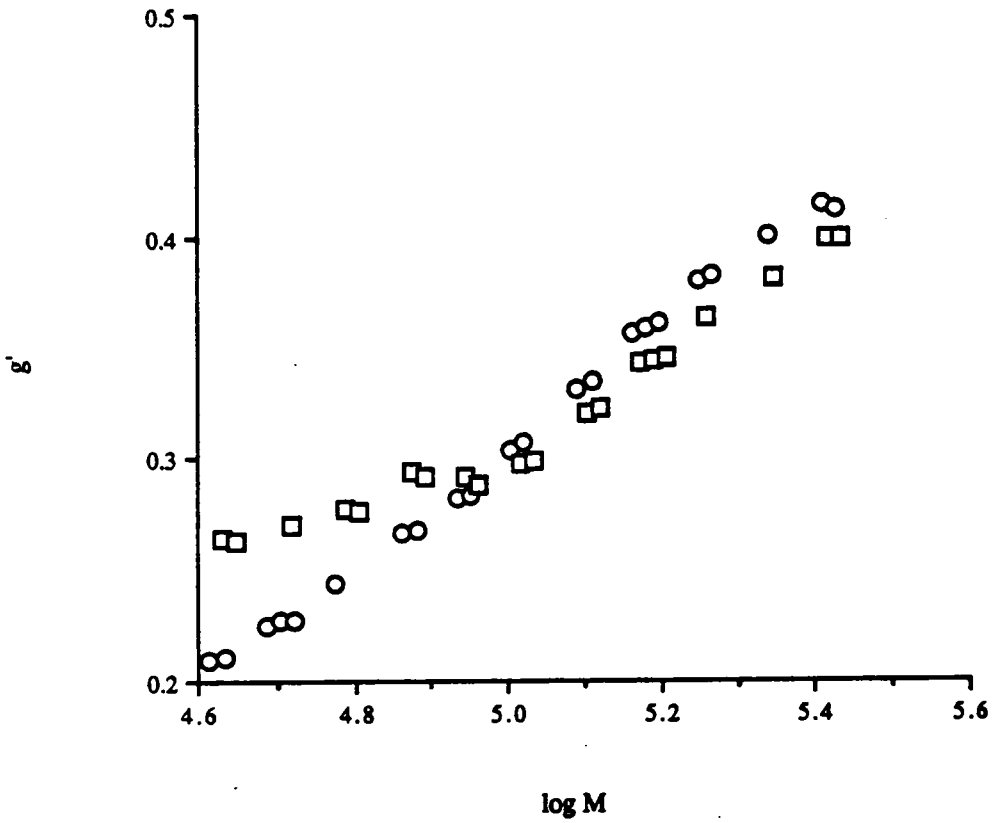

Figure 4.21: Branching distribution for PMMA-g-PMMA B from GPC/DV.

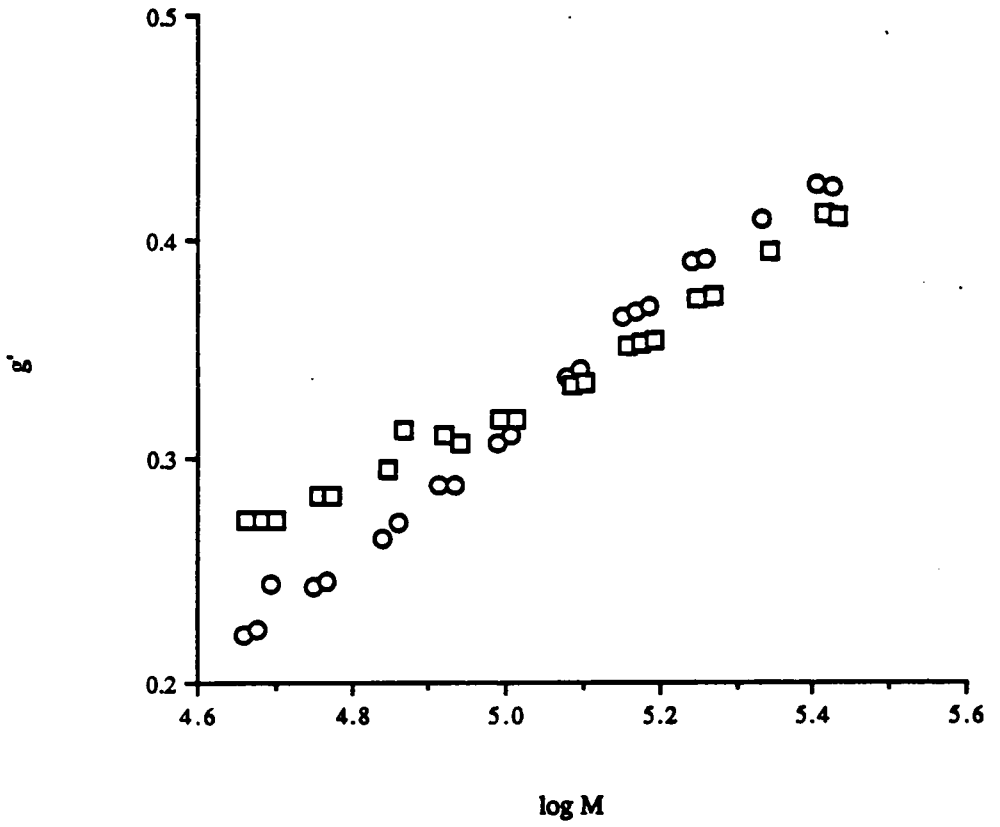

Figure 4.22: Branching distribution for PMMA-g-PMMA C from GPC/DV.

temperature coefficients of the unperturbed chain dimensions thus leading to the temperature coefficient of the expansion factor.

REFERENCES

1. Scholte, T. G., in *Developments in Polymer Characterization -- 4* Dawkins, J. V., (ed.) Applied Science, New York, 1983, pp. 1.

2. Hamielec, A. W., Meyer, H., in *Developments in Polymer Characterization -- 5* Dawkins, J. V., (ed.) Elsevier, New York, 1986, pp. 95.

3. Matthews, G. P., J. Chem. Educ., **61**, 552 (1984).

4. Quivoron, C., in *Steric Exclusion Liquid Chromatography of Polymers* Janca, J., (ed.) Marcel Dekker, New York, 1984,

5. Foster, G. N., Hamielec, A. E., MacRury, T. B., in *Size Exclusion Chromatography (GPC)* Provder, T., (ed.) ACS, Washington, D. C., 1980, pp. 131.

6. Ward, T. C., Notes, Physical Chemistry of High Polymers, Virginia Polytechnic Institute & State University, Fall 1985

7. Flory, P. J., *Principles of Polymer Chemistry*, Cornell University Press, New York, 1953.

8. Hiemenz, P. C., *Polymer Chemistry, The Basic Concepts*, Marcel Dekker, New York, 1984.

9. Koenig, J. L., *Chemical Microstructure of Polymer Chains*, Wiley, New York, 1980.

10. Das, P. K., Ph. D. Dissertation, Virginia Polytechnic Institute & State University, 1984.

11. Odian, G., *Principles of Polymerization*, Wiley, New York, 1981.

12. Yamakawa, H., *Modern Theory of Polymer Solutions*, Harper & Row, New York, 1971.

13. Rudin, A., *The Elements of Polymer Science and Engineering*, Academic Press, New York, 1982.

14. Cowie, J. M. G., *Polymers: Chemistry & Physics of Modern Materials*, International Book Co., Ltd., London, 1973.

15. Billmeyer, F. W., Jr., *Textbook of Polymer Science*, Wiley, New York, 1984.

16. Berry, G. C., J. Polym. Sci. A-2, **9**, 687 (1971).

17. Berry, G. C., Casassa, E. F., Macromol. Rev., **4**, 1 (1970).

18. Small, P. A., in *Adv. Polym. Sci.* Verlag, New York, 1975, pp. 1.

19. Hamielec, A. E., Ouano, A. C., Nebenzahl, L. L., J. Liq. Chromatogr., **1**, 527 (1978).

20. Dondos, A., Rempp, P., Benoit, H., Makromol. Chem., **171**, 135 (1973).

21. Hunkeler, D., Hamielec, A. E., J. Appl. Polym. Sci., **35**, 1603 (1988).

22. Fujita, H., Macromolecules, **21**, 179 (1988).

23. Berry, G. C., J. Polym. Sci., Polym. Phys. Ed., **26**, 1137 (1988).

24. Elias, H. G., *Macromolecules I Structure and Properties*, Plenum Press, New York, 1984.

25. Katime, I., Vera, C. R., Figueruelo, J. E., Eur. Polym. J., **13**, 451 (1977).

26. Vasudevan, P., Santappa, M., J. Polym. Sci. A-2, **9**, 483 (1971).

27. Khan, H. U., Kumar, K., J. Macromol. Sci., Chem., **A21**, 757 (1984).

28. Das, P. K., Allen, R. D., Ward, T. C., McGrath, J. E., Dodson, R. J., Polym. Pre., **25**(1), 185 (1984).

29. Mori, S., Suzuki, M., J. Liq. Chromatogr., **7**, 1841 (1984).

30. Tsitsilianis, Dondos, A., Makromol. Chem., Rapid, Commun., **5**, 625 (1984).

31. Tsitsilianis, C., Polym. Bull., **18**, 183 (1987).

32. Tsitsilianis, C., Dondos, A., Macromolecules, **10**, 658 (1987).

33. Moore, W. R., in *Progress In Polymer Science* Jenkins, A. D., (ed.) Pergamon, New York, 1967, pp. 1.

34. Gargallo, L., Mendez, I., Radic, D., Makromol. Chem., **184**, 1053 (1983).

35. Katime, I., Roig, A., Cabanas, P. G., Eur. Polym. J., **10**, 897 (1974).

36. Katime, I., Vera, C. R., Eur. Polym. J., **13**, 783 (1977).

37. Katime, I., Ibarra, X., Garay, M., Valenciano, R., Eur. Polym. J., **17**, 509 (1981).

38. Herold, H. K., Wolf, B. A., J. Mater. Chem. Phys., **14**, 311 (1986).

39. Katime, I. A., Garay, M. T., J. Chem. Soc. Faraday Trans., **81**, 705 (1985).

40. Katime, I., Pereg, M. G., Bri. Polym. J., **15**, 117 (1983).

41. Katime, I., Garay, M. T., Polym. Commun., **27**, 74 (1986).

42. Shiga, S., Kato, E., Rubber Chem. Technol., **59**, 693 (1986).

43. Grinshpun, V., Rudin, A., Potter, D., Polym. Bull., **13**, 71 (1985).

44. Park, W. S., Graessley, W. W., J. Polym. Sci., Polym. Phys. Ed., **15**, 85 (1977).

45. Kim, J. R., Ree, T., J. Polym. Sci., Polym. Chem. Ed., **23**, 119 (1985).

46. Dobkowski, K., J. Appl. Polym. Sci., **30**, 355 (1985).

47. Lang, P., Burchard, W., Makromol. Chem., Rapid Commun., **8**, 451 (1987).

48. Drott, E., A., M. R., J. Polym. Sci. A-2, **8**, 1361 (1970).

49. Grubisic, Z., Rempp, P., Benoit, H., J. Polym. Sci., Polym. Lett., **5**, 753 (1967).

50. Benoit, H., Grubisic, Z., Rempp, P., Decker, D., Zilliox, J. G., J. Chim. Phys., **63**, 1507 (1966).

51. Yau, W. W., Bly, D. D., in *Size Exclusion Chromatography (GPC)* Provder, T., (ed.) ACS, Washington, D. C., 1980, pp. 197.

52. Casassa, E. F., Tagami, Y., Macromolecules, **2**, 14 (1969).

53. Hester, R. D., Mitchell, P. H., J. Polym. Sci., Polym. Chem. Ed., **18**, 1727 (1980).

54. Pannell, J., Polymer, **13**, 277 (1972).

55. Hamielec, A. E., C., O. A., J. Liq. Chromatogr., **1**, 111 (1978).

56. Meyerhoff, G., Makromol. Chem., **118**, 265 (1968).

57. Meyerhoff, G., Sep. Sci., **6**, 239 (1971).

58. Goedhart, D., Opschoor, A., J. Polym. Sci. A-2, **8**, 1227 (1970).

59. Grubisic-Gallot, Z., Picot, M., Gramain, P. H., Benoit, H., J. Appl. Polym. Sci., **16**, 2931 (1972).

60. Coleman, T. A., Dawkins, J. V., J. Liq. Chromatog., **9**, 1191 (1986).

61. Foster, G. N., MacRury, T. B., Hamielec, A. E., in *Liquid Chromatography of Polymers & Related Materials II* Cazes, J., Delamare, X., (eds.) Marcel Dekker, New York, 1980, pp. 143.

62. Yau, W. W., Jones, M. E., Ginnard, C. R., Bly, D. D., in *Size Exclusion Chromatography (GPC)* Provder, T., (ed.) ACS, Washington, D. C., 1980, pp. 91.

63. Trowbridge, P., Brower, L., Seeger, R., McIntyre, D., Polym. Mater. Sci. Eng., **54**, 85 (1986).

64. Styring, M., Polym. Mater. Sci. Eng., **54**, 88 (1986).

65. Kuo, C., Provder, T., Koehler, M. E., Kah, A. F., Polym. Mater. Sci. Eng., **54**, 80 (1986).

66. Haney, M. A., Armonas, J. A., Rosen, L., Polym. Mater. Sci. Eng., **54**, 75 (1986).

67. Yau, W. W., Polym. Mater. Sci. Eng., **54**, 74 (1986).

68. Tinland, B., Mazet, J., Rinaudo, M., Makromol. Chem., Rapid Commun., **9**, 69 (1988).

69. Letot, L., Lesec, J., Quivoron, C., J. Liq. Chromatogr., **3**, 427 (1980).

70. Lecacheux, P., Lesec, J., Quivoron, C., J. Appl. Polym. Sci., **27**, 4867 (1982).

71. Malihi, F. B., Kuo, C., Koehler, M. G., Provder, T., Kah, A. F., in *SEC: Methodology & Characterization of Polymers & Related Materials* Provder, T., (ed.) ACS, Washington, D. C., 1984, pp. 281.

72. Haney, M. A., J. Appl. Polym. Sci., **30**, 3023 (1985).

73. Haney, M. A., J. Appl. Polym. Sci., **30**, 3037 (1985).

74. Haney, M. A., Am. Lab., **17**, 116 (1985).

75. Gallot, Z., in *Liquid Chromatography of Polymers & Related Materials II* Cazes, J., Delamare, X., (eds.) Marcel Dekker, New York, 1980, pp. 113.

76. Malihi, F. B., Kuo, C., Koehler, M. E., Provder, T., Kah, A. F., Org. Coat. Appl. Polym. Sci., **48**, 760 (1983).

77. Styring, M. G., Armonas, J. E., Hamielec, A. E., J. Liq. Chromatogr., **10**, 783 (1987).

78. Jordan, R. C., McConnell, M. L., in *Size Exclusion Chromatography (GPC)* Provder, T., (ed.) ACS, Washington, D. C., 1980, pp. 107.

79. Hamielec, A. E., Styring, M., Pure Appl. Chem., **57**, 955 (1985).

80. Huglin, M. B., *Light Scattering from Polymer Solutions*, Academic Press, New York, 1972.

81. Chromatix Application Note, LS-2, 1977.

82. Chromatix Application Note, LS-1, 1977.

83. Kaye, W., McDaniel, J. B., Appl. Opt., **13**, 1934 (1974).

84. Kaye, W., Havlik, A. J., Appl. Opt., **12**, 541 (1973).

85. Kato, T., Kanda, A., Takahashi, A., Noda, I., Maki, S., Nagasawa, M., Polymer J., **11**, 575 (1979).

86. Froment, P., Revillon, A., J. Liq. Chromatog., **10**, 1383 (1987).

87. Kratochvil, P., Pure Appl. Chem., **54**, 379 (1982).

88. Beltzung, L., Strazielle, C., Makromol. Chem., **185**, 1145 (1984).

89. Chromatix KMX-16 Application Note, LS-7, 1978.

90. Hadjichristidis, N., Fetters, J., J. Polym. Sci., Polym. Phys. Ed., **20**, 2163 (1982).

91. Huglin, M. B., J. Appl. Polym. Sci., **9**, 4003 (1965).

92. Huglin, M. B., in *Light Scattering from Polymer Solutions* Huglin, M. B., (ed.) Academic Press, New York, 1972, pp. 165.

93. Beltzung, L., Strazielle, C., Makromol. Chem., **185**, 1155 (1984).

94. Yu, L. P., Rollings, J. E., J. Appl. Polym. Sci., **35**, 1085 (1988).

95. Bo, S. Q., Cheng, R. S., J. Liq. Chromatogr., **5**, 1405 (1982).

96. Grinshpun, V., Rudin, A., Makromol. Chem., Rapid Commun., **6**, 219 (1985).

97. Prochazka, O., Kratochvil, P., J. Appl. Polym. Sci., **31**, 919 (1986).

98. Bressau, R., in *Liquid Chromatography of Polymers & Related Materials II* Cazes, J., Delamare, X., (ed.) Marcel Dekker, New York, 1980, pp. 73.

99. Lesec, J., in *Liquid Chromatography of Polymers & Related Materials II* Cazes, J., Delamare, X., (ed.) Marcel Dekker, New York, 1980, pp. 1.

100. Dumelow, T., Holding, S. R., Maisey, L. J., Polym. Commun., **24**, 307 (1983).

101. McConnell, M. L., Am. Lab., **10**, (1978).

102. Lecacheux, D., Lesec, J., Quivoron, C., J. Liq. Chromatogr., **5**, 217 (1982).

103. Pang, S., Pronovost, J., Rudin, A., Polym. Mater. Sci. Eng., **58**, 474 (1988).

104. Rempp, P., Lutz, P., Masson, P., Franta, E., Makromol. Chem., **8**, 13 (1984).

105. Schulz, G. O., Milkovich, R., J. Appl. Polym. Sci., **27**, 4773 (1982).

106. DeSimone, J. M., Hellstern, A. M., Siochi, E. J., Ward, T. C., McGrath, J. E., Polym. Pre., **30**(1), 137 (1989).

107. Hellstern, A. M., Ph. D. Dissertation, Virginia Polytechnic Institute & State University, 1989.

108. Akira, K., in *Polymer Fractionation* Cantow, M. J. R., (ed.) Academic Press, New York, 1967, pp. 43.

109. Johnson, B. L., Smith, J., in *Light Scattering from Polymer Solutions* Huglin, M. B., (ed.) Academic Press, New York, 1972, pp. 27.

110. *Lange's Handbook of Chemistry*, McGraw-Hill, New York, 1979.

CHAPTER 5

SUMMARY

In this work, the GPC was used to examine absolute molecular weight distributions (MWD's) and hydrodynamic behavior of three systems having various architectures. Nitrocellulose is a linear material shown to have a semiflexible random coil conformation, low molecular weight hydroxypropylated lignins have a three dimensional network architecture and high molecular weight graft PMMA's contained long chain branching (LCB). For these three types of materials, there has been hesitance in the polymer community in applying universal calibration procedures based on hydrodynamic volume to obtain absolute MWD's. By using GPC/DV which operates on the basis of universal calibration, these materials were studied and all these were confirmed to obey universal calibration.

In Chapter 2, GPC/DV was used to study time dependent changes in the MWD's. A battery of other experiments -- infrared spectroscopy, intrinsic viscosities and low angle laser light scattering lent support to the postulate that the change in MWD was not due to degradation but to gradual dissociation of large aggregates. Especially significant were the intrinsic viscosity results obtained from samples that were aged in solution, dried and redissolved. It was shown that the decrease in viscosity of the NC samples could be reversed by slow drying and redissolving. This provided conclusive evidence, never before forwarded, that NC underwent slow dissociation in short term storage -- three to four weeks. In the long term (six months) however, it undoubtedly degraded. A two step mechanism for aging was proposed.

In Chapter 3, the study of MWD's of hydroxypropylated lignins by GPC/DV confirmed previous work that this family of materials tended to associate in solution. More importantly however, it was shown that when this characteristic was taken into account, procedures may be undertaken to obtain accurate MWD's using GPC/DV. Universal calibration was shown to be valid for these highly branched polymers. The main contribution of this work to the lignin community was the evidence that a convenient, rapid and reliable MWD method is now available through the GPC/DV This would make the current practice of tedious fractionation of lignins to obtain MWD information obsolete.

Finally, in Chapter 4, work on branched systems was extended to model high molecular weight PMMA's containing long chain branching. These well defined polymers with systematically varied branching content were used to provide unequivocal proof of the validity of universal calibration for systems of this architecture. As more branched polymers are being developed as a means of varying material properties, the necessity of finding a reliable characterization method has become more urgent. In dilute solution studies of long chain branching, universal calibration has often been thought to be invalid. This work has shown that the theoretical validity of universal calibration applies more widely than prior literature would indicate.

Different parts of this work showed the power of GPC/DV. But, efforts should be focussed on honing instrumentation toward greater efficiency. This was especially obvious in the multidetection system employed here. While still in its infancy, multidetection will be the way of the future due to the wealth of information that may be obtained in a few, simple experiments.By taking advantage of the fractionating capability of the GPC in combination with the absolute molecular weight information available through the DV detector, it was possible not only to study association by following changes in hydrodynamic volume but also to obtain such fundamental characteristics as average chain dimensions and branching parameters. Average chain dimensions have been obtained before only by tedious fractionation and subsequent molecular weight determination experiments. GPC/DV has made it possible for the first time to obtain these quantities quickly and easily. Branching parameters have previously been obtained only indirectly with the more established and tedious GPC/LALLS. Now, GPC/DV has been shown to be capable of obtaining this information directly.

It is hoped that with these findings, a method of studying dilute solution behavior has now been established so that investigators need not be burdened by the lack of reliable theory and instrumentation but can surge forth and open new frontiers in knowledge of dilute solution properties.

APPENDIX

ERROR ANALYSIS

A.1. CONCENTRATION

The error in concentration stemmed from the accuracy of the weighing balance -- 0.0001 g. Since the weight of the solute was obtained as a difference between the weighing paper and the weighing paper with the sample, the error in the weight of the sample was twice the absolute error of 0.0001. The reasoning for the determination of the error in the weight of the solvent was the same. Since concentration was in the units of g/ml and this quantity was calculated by taking the ratio of weight of sample to volume of solvent, the relative error was used as the uncertainty i. e. the percentages in the error of the weight and volume were added yielding the error in the concentration. The absolute error may then be calculated by multiplying the relative error by the concentration.

A.2. SPECIFIC REFRACTIVE INDEX INCREMENT

Specific refractive index increment, dn/dc, was a result of taking the average $\Delta n/c$ for five different concentrations. Δn is the differential refractive index and is given by

$$\Delta n = k\Delta x \qquad [A\text{-}1]$$

where k is the instrument calibration constant and Δx is the deflection measured on the KMX-16 differential refractometer. The error for Δn thus came from two sources. The first and simpler error was merely the standard deviation of five repetitions in the Δx measurements. The second source of uncertainty was in the k. Rearrangement of equation [A-1] yields

$$k = \Delta n/\Delta x \qquad [A\text{-}2]$$

k was obtained by measuring Δx and Δn for NaCl solutions at 25°C. Under this condition, it is known that (110):

$$\Delta n = \{1740.0 + (1.63c - 30.85)c\}c \qquad [A\text{-}3]$$

where c is the concentration. Since concentrations were multiplied and appeared three times in the equation, the error in Δn for the salt solutions was merely three times the relative error in concentration. Again, the

error in Δx was due to the standard deviation in the reproducibility of measuring Δx. Since k was the ratio of Δn and Δx, the error in k was the sum of the relative errors in Δn and Δx of the salt solutions.

Knowing the error in k, the error in Δn of the sample may then be calculated. It was equal to the sum of the relative errors in k and in Δx for the sample. Similarly, the error in $\Delta n/c$ was the sum of the relative errors in Δn and concentration.

Finally, the dn/dc was calculated by taking the average value of the five $\Delta n/c$ measured. The error in dn/dc was the average of the uncertainties of the five $\Delta n/c$'s. In some cases, dn/dc values would have been skewed by anomalous $\Delta n/c$ for certain concentrations. In these instances, the data for one $\Delta n/c$ value was rejected based on the following criterion. The average deviation d was determined by (105):

$$d = 1/N * \Sigma|x_i - x| \qquad [A\text{-}4]$$

where N is the number of data points, x is the mean and x_i is the datum point. The average deviation for $\Delta n/c$ was calculated without including the datum that was to be rejected. The anomalous point eliminated only if its deviation from the mean of the four other data points was four times greater than the average deviation.

A.3. RESULTS FROM LALLS

The LALLS experiment yielded the weight average molecular weight and second virial coefficient. This was obtained by plotting Kc/R_θ against concentration, where K was defined in equation [3-1], and then taking the intercept and slope of the graph. The weight average molecular weight is the inverse of the intercept and the the second virial coefficient is half the value of the slope .

Error analysis had to be broken down into several components. The sources of error for Kc/R_θ were in the optical constant K, concentration and R_θ. Since K is a product of three terms, two of which do not have an error associated with them, the sole source of uncertainty in this quantity is the error from the dn/dc. The term was squared, therefore, the error in K was twice the relative error of dn/dc. The uncertainty in R_θ was the sum of the absolute errors in the Rayleigh scattering of the solution and of the solvent. The errors in the Rayleigh scattering in turn arose from the standard deviation of five measurements. Therefore,

the error in Kc/R_θ was the sum of the relative errors of dn/dc, concentration and R_θ. To determine the slope and intercept of the plot, the following equations were used:

$$m = \frac{n\Sigma xy - \Sigma x\Sigma y}{n\Sigma x^2 - (\Sigma x)^2} \qquad [A\text{-}5]$$

$$b = \frac{1}{n}[\Sigma y - m\Sigma x] \qquad [A\text{-}6]$$

where m is the slope and b is the intercept. x was substituted by concentration and y by Kc/R_θ. This would yield

$$m = \frac{n\Sigma\frac{Kc}{R_\theta}^2 - \Sigma c\Sigma\frac{Kc}{R_\theta}}{n\Sigma c^2 - \Sigma(c)^2} \qquad [A\text{-}7]$$

$$b = \frac{1}{n}\left[\Sigma\frac{Kc}{R_\theta} - m\Sigma c\right] \qquad [A\text{-}8]$$

The errors in the slope and the intercept were calculated from

$$dm = \sum\left|\left(\frac{dm}{dx_i}\right)_{y,\,x=x_i}\right| dx_i + \sum\left|\left(\frac{dm}{dy_i}\right)_{x,\,y=y_i}\right| dy_i \qquad [A\text{-}9]$$

$$db = \sum\left|\left(\frac{db}{dx_i}\right)_{y,\,x=x_i}\right| dx_i + \sum\left|\left(\frac{db}{dy_i}\right)_{x,\,y=y_i}\right| dy_i \qquad [A\text{-}10]$$

After taking the derivatives of the slope and the intercept, the following equations result:

$$dm = \sum\left(\left|\frac{n\left(\frac{Kc}{R_\theta}\right)_i - \Sigma\frac{Kc}{R_\theta} - 2m(nc_i - \Sigma c)}{n\Sigma c^2 - (\Sigma c)^2}\right| dc_i\right) + \sum\left(\left|\frac{nc_i - \Sigma c}{n\Sigma c^2 - (\Sigma c)^2}\right| d\left(\frac{Kc}{R_\theta}\right)_i\right) \qquad [A\text{-}11]$$

$$db = \sum \left(\frac{1}{n} \left| \frac{\Sigma c \left(2\Sigma \frac{Kc}{R_\theta} - n\left(\frac{Kc}{R_\theta} \right)_i \right) - n\Sigma \frac{Kc}{R_\theta}^2}{n\Sigma c^2 - (\Sigma c)^2} \right| dc_i \right) + \sum \left(\frac{1}{n} \left| 1 - \frac{(nc_i - \Sigma c)\,\Sigma c}{n\Sigma c^2 - (\Sigma c)^2} \right| d\left(\frac{Kc}{R_\theta} \right)_i \right) \quad [A\text{-}12]$$

The uncertainty in molecular weight was obtained by taking the relative error in the intercept and the error in the second virial coefficient was the relative error of the slope.

The vita has been removed from the scanned document